

AN ABSTRACT OF THE DISSERTATION OF

Francisco Jose Guerrero Bolaño for the degree of Doctor of Philosophy in Sustainable Forest Management and Water Resources Science presented on November 7, 2018.

Title: Biogeochemical Signals of Mountainous Forested Watersheds' Response to Disturbance

Abstract approved:

Jeff A. Hatten

Small mountainous watersheds are disproportionate sources of land-derived particulate organic matter (POM) to long-term sinks like lake bottoms and the ocean. As such, these ecosystems are an essential component of the global carbon cycle. The burial of POM in lacustrine and marine sediments contributes to the drawdown of atmospheric CO₂ and therefore provides a mechanism of negative feedback for climate change.

POM export in mountainous landscapes is thought to be driven by a natural disturbance regime that, in the Pacific Northwest, historically have included both tectonic (i.e., earthquakes) and climatic (e.g., fires, storms, and flooding) forcings. After World War II, a dramatic increase in timber harvesting and road building resulted in the intensification of an additional anthropogenic forcing with unknown biogeochemical consequences.

In this dissertation, we studied patterns of POM mobilization, transport, and deposition to understand better how fundamental biogeochemical processes in forested mountainous watersheds respond to disturbances triggered by natural and human forcings. We approached our analysis from the paradigm of biogeochemical signals.

A biogeochemical signal is a relative change in POM chemistry correlated with watershed ecosystem processes involving nutrient exports. Here, we examined changes in elemental composition (%C, %N N:C ratios), stable isotopic composition ($\delta^{13}\text{C}$ and $\delta^{15}\text{N}$), and terrestrial biomarkers (e.g., lignin-derived compounds) to characterize different pools of particles moving from headwaters to lake bottoms.

We used categories like carbon-rich/carbon-depleted particles (H.J. Andrews study); colloids, aggregates, fine particulate organic matter, and vascular plant detritus (Alsea study). In the Loon Lake study, we used a Generalized Least Squares regression model to test for significant correlations between specific particle size classes and the bulk chemical characteristics of deposited sediment layers. Based on the regression model, we introduced the concept of pseudo-property-property plots to delineate a general correspondence between particle size classes like colloids, aggregates, clays, and sands with elemental and isotopic composition of Loon Lake sediments.

Our results suggest that the superposition of disturbance forcings (both natural and anthropogenic) modulates the quantity and quality of POM exported from headwater streams and that changes in channel structure could be inferred from changes in variability of the probability distribution of discharge and sediment yields. We used elemental composition data to illuminate how sediment routing and other stream channel processes could affect the source/sink behavior of headwater ecosystems in the context of POM exports.

Along the steep channel of the Alsea River, characterized by high attrition rates and relatively simple geomorphology, we were able to obtain evidence of the role of physical instream processing of organic matter in the export of POM from a small mountainous river system in the Oregon Coast Range. We provide evidence that extensive physical fragmentation of the coarse organic matter transported in the suspended load was a significant source of fine particulate organic matter in the river during this storm. Our data suggest that physical processing during floods, associated with particle delivery and transport must be a driving force behind the imprinting of biogeochemical signatures in sedimentary records.

Lastly, we calculated spectral entropies and the information content of particle size spectra from a high resolution sedimentary archive from a lacustrine sink spanning more than 1500-years of natural history. These metrics, derived from Shannon's information theory, constitute a distribution-free approach to analyze changes in variability. We found that particle size variability not only contains information about specific depositional processes, but also it has the potential to record climatic changes.

An overarching conclusion from this dissertation is the extraordinary heterogeneity that characterizes the biogeochemical signals of watershed's response to disturbances which is in startling contrast with the availability of conceptual approaches to understanding such a heterogeneity. Our results suggest that generalized metrics of signal variability are central for translating between historical structural changes in natural patterns, and their timing and relevance in watershed history. Therefore, a more robust reconstruction of watershed history and a better identification of drivers for pressing environmental issues seems possible under the framework of Shannon's information theory.

©Copyright by Francisco Jose Guerrero Bolaño
November 7, 2018
All Rights Reserved

Biogeochemical Signals of Mountainous Forested Watersheds' Response to
Disturbance

by
Francisco Jose Guerrero Bolaño

A DISSERTATION

submitted to

Oregon State University

in partial fulfillment of
the requirements for the
degree of

Doctor of Philosophy

Presented November 7, 2018

Commencement June 2019

Doctor of Philosophy dissertation of Francisco Jose Guerrero Bolaño presented on
November 7, 2018

APPROVED:

Major professor, representing Sustainable Forest Management and Water
Resources Science

Head of the Department of Forest Engineering, Resources, and Management

Director of the Water Resources Science Program

Dean of the Graduate School

I understand that my dissertation will become part of the permanent collection of Oregon State University libraries. My signature below authorizes release of my dissertation to any reader upon request.

Francisco Jose Guerrero Bolaño, Author

ACKNOWLEDGEMENTS

Somebody once told me that for being a scientist, I work with the pace of an artist. Including myself, up until that moment few people in my life had been able to see that about me, though. I have come to believe that Jeff Hatten, my advisor, is one of those people. Thus, I want to express my acknowledgments to him for being so welcoming and encouraging all these years. In hindsight, I can understand now why his advising style matched my needs so well. It makes a lot of sense now why the most important lesson I've learned from Jeff is that, although we need good science urgently, good science cannot be rushed. Good science should be produced by good people, and good people should have a life balance. That is something that I will carry with me for the rest of my professional life. Thank you, Jeff, for that.

I would also like to thank my committee members, Alba Argerich, Miguel Goni, Roy Haggerty, and Jeff Morrell for their always kind, yet critical feedback. I still remember our first discussion about this dissertation gravitating too much around information theory. Back then, going in that direction seemed to be like approaching a black hole. Nobody knew what we could find on the other side, and you wanted to make sure that I would find my way out. At the same time, you were always open and encouraging towards any original approach I could follow in my research.

Thanks to the Administrative Department of Science, Technology and Innovation from Colombia (Colciencias) for financial support throughout the program. I also give thanks to the College of Forestry, the Department of Forest Engineering, Resources, and Management, and the Office of International Affairs for awarding me with fellowships to support my academic progress.

Thanks to Victor Peñaranda for such a productive exchange of ideas while visiting OSU in 2015. I was expecting to meet my old good friend and you turned into an amazing colleague in deciphering the mysteries of Shannon's entropy.

I had the fortune of having an extraordinary lab team. Kris Richardson, Adrian Gallo, Lauren Matosziuk, Dave Frey, and Yvan Alleau. Kris' dedicated work to the study of Loon Lake core made of that sedimentary record a small museum of natural

history. Adrian let me borrow his family for two consecutive Christmases in 2014 and 2015. And Dave and Lauren, thanks for your productive and always positive feedback on my writing. Lastly, thanks to Yvan for your impeccable commitment to the lab and the generation of high-quality data.

I'm also grateful for those who became my second family in Corvallis, especially Rene Zamora and his wife Ingrid for having the doors of their home always open. Nick Houtman, who also has believed in me as a science communicator from the beginning. Pablo Romero, Maria Lopez, June Marion, and Andre Faria, thank you for your extraordinary support throughout that complicated summer in 2014.

Thanks to Diego Zarrate, Bharat Rastogi and Paulo Murillo for all those productive discussions about our experience as international students. Thanks also to the ALAS family for all these years of encouragement and good memories.

Thanks to my health support team, Dr. Aura Puentes, Dr. Douglas Aukerman and Linda Zang. I would not have been able to walk through this process without your help.

My sincerest thanks to Donna and Fritz Batson for their warmth, generosity, and support during the final stages of my Ph.D. program and my science communication training at CNN Español.

Thanks to my family Silvia, Johanna and Edwin for their unconditional love and support.

Danielle Batson, thank you for never stop believing in me, for your patience, and for your wonderful love.

TABLE OF CONTENTS

	<u>Page</u>
Chapter 1 Introduction: Disturbances and watershed biogeochemistry.....	1
Significance.....	1
Background.....	1
Research goal and questions.....	5
Methodology.....	7
Bibliography.....	9
Chapter 2 A 30-year Record of Particulate Organic Carbon (POC) Exports from Headwater Streams of the Oregon Cascades: A Biogeochemical Signal of Response to Disturbances.....	13
Introduction.....	13
Methods.....	15
Site description.....	15
Disturbance history.....	16
Data preparation and analysis.....	17
Predicting carbon content in suspended sediments and reconstructing historical POC yields.....	19
Results.....	20
Elemental composition of suspended sediments.....	20
Proxies for particulate matter inputs to the study sites.....	21
Predicting the carbon content of suspended sediments.....	21
Long-term trends of POC yields.....	23
Changes in variability of POC yields.....	24
Discussion.....	26

TABLE OF CONTENTS (Continued)

Timber harvesting caused a significant reduction in particulate organic matter (POM) supply to the stream channel	26
A debris flow occurring 12 years after the logging treatment resulted in an unstable detrital pool at the LG site	27
Channel structure modulates variability in quantity and quality of POC yields (and hence biogeochemical responses to disturbances)	28
Conclusions.....	33
Bibliography	33
Figures and tables.....	37
Supplementary methods: Estimation of Kullback-Liebler's Divergence (Divergence _{KL}).....	58
 Chapter 3 Event-associated Overbank Deposits as Testimonies of Particulate Organic Carbon Mobilized along a Small Mountainous River during a Large Flood Event. ...	59
Introduction	59
Methods	60
Study area	60
Sampling.....	62
Particle size distribution and Cesium 137	64
Specific Surface Area.....	64
Carbon, Nitrogen, C/N ratios	64
Stable Isotopes and Lignin Biomarkers	65
Results.....	66
Textural changes and mean particle size along overbank deposits	66
Organic matter distribution along overbank deposits	67
POM sources to overbank deposits.....	71
Discussion.....	74

TABLE OF CONTENTS (Continued)

Deposit layers were texturally heterogeneous due to the influences of an erosion-deposition gradient along the river and local hydrodynamics at the boat ramps.	75
<i>Particle sorting strongly influenced the deposition of organic matter across overbank deposits.</i>	76
The biogeochemical signature of the GCG-2007.....	79
Conclusions.....	81
Bibliography	81
Figures and tables.....	85
Chapter 4 Disentangling signals of watershed responses to disturbance from the information content of particle size spectra: An analysis of a 1500-year sedimentary archive from Loon Lake, Umpqua River Basin, Oregon.	108
Introduction	108
Background: Entropy and the analysis of particle size spectra	110
The concept of entropy in Shannon's information theory.....	110
Entropy of particle size spectra	111
Materials and Methods	113
Setting.....	113
Core 02aN	114
Entropy analysis of particle size spectra.....	115
Results.....	117
Long-term depositional processes.....	117
Entropy analysis of particle size spectra.....	118
Discussion.....	124
Synthesis of the approach.....	124
Modeling particle size variability with Entropy.....	125

TABLE OF CONTENTS (Continued)

Disentangling signals of watershed response to disturbance	127
Conclusions.....	128
Bibliography	128
Figures and tables.....	132
Supplementary method: building “pseudo-property-property” plots.....	148
Chapter 5 . Conclusions	150
Bibliography	152

LIST OF FIGURES

<u>Figure</u>	<u>Page</u>
Figure 1.1. Research project structure. Our research questions address the origin, transport and interpretation of biogeochemical signals of disturbance in FW ecosystems.....	12
Figure 2.1. Watershed 10 prior and after harvesting in 1975..	37
Figure 2.2. Suspended sediment samples collected from two headwater streams draining an old-growth forest (WS09-OG site) and a 100%-logged watershed (WS10-LG site) in the H. J. Andrews Experimental Forest..	38
Figure 2.3. Comparison of the carbon content (%TC) and TN:C ratios of sediments from two headwater streams draining an old-growth forest (WS09-OG site) and a 100%-logged watershed (WS10-LG site) in the H. J. Andrews Experimental Forest.....	39
Figure 2.4. Seasonal patterns of different types of particulate material found at the automatic sampling stations (deposited in the bottom of collection basins) from different experimental watersheds (including our study sites) within the H. J. Andrews Experimental Forests	40
Figure 2.5. Reconstruction of the carbon content (%TC) of suspended sediments by using a multiple regression model for two headwater streams draining an old-growth forest (WS09-OG site) and a 100%-logged watershed (WS10-LG site) in the H. J. Andrews Experimental Forest.....	41
Figure 2.6. Particulate organic carbon exports (POC yields) from two headwater streams draining an old-growth forest (WS09-OG site) and a 100%-logged watershed (WS10-LG site) in the H. J. Andrews Experimental Forest.	42
Figure 2.7. Particulate organic carbon (POC) yields and their average carbon content from two headwater streams draining an old-growth forest (WS09-OG site) and a 100%-logged watershed (WS10-LG site) in the H. J. Andrews Experimental Forest.....	43
Figure 2.8. Long-term (1984-2015) seasonality (A) and elemental composition (B) of particulate organic carbon (POC) exported from two headwater streams draining an old-growth forest (WS09-OG site) and a 100%-logged watershed (WS10-LG site) in the H. J. Andrews Experimental Forest.	44

LIST OF FIGURES (Continued)

<u>Figure</u>	<u>Page</u>
Figure 2.9. Long-term (1984-2015) frequency distribution of particulate organic carbon (POC) yields and their average carbon content from two headwater streams draining an old-growth forest (WS09-OG site) and a 100%-logged watershed (WS10-LG site) in the H. J. Andrews Experimental Forest..	45
Figure 2.10. 5-year window histograms of particulate organic carbon (POC) loads and their average carbon content from two headwater streams draining an old-growth forest (WS09-OG site) and a 100%-logged watershed (WS10-LG site) in the H. J. Andrews Experimental Forest..	46
Figure 2.11. Divergence analysis of long-term trends of discharge and suspended sediments from two headwater streams draining an old-growth forest (WS09-OG site) and a 100%-logged watershed (WS10-LG site) in the H. J. Andrews Experimental Forest.....	47
Figure 2.12. Whole-stream channel responses to disturbances measured as divergence in different components between two headwater streams draining an old-growth forest (WS09-OG site) and a 100%-logged watershed (WS10-LG site) in the H. J. Andrews Experimental Forest.....	48
Figure 3.1. Study Area and sampling locations. Samples were collected along the main channel of the Alsea River, in the Oregon Coast Range, from headwaters to the estuary..	85
Figure 3.2. Contrasting characteristics between flood deposits sampling locations along the Alsea River. I.	86
Figure 3.3. Deposit layers as sample units. Surficial samples were collected from all deposits (0-1cm)..	87
Figure 3.4. Physical properties of overbank deposits along the Alsea River after a flood event in December 2007. fraction..	88
Figure 3.5. A. Longitudinal profiles of organic carbon concentrations (OC_{bulk} , $OC_{coarse} >63\mu m$, and $OC_{fine} <63\mu m$) in overbank deposits along the Alsea River after a flood in December 2007.	89
Figure 3.6. Total organic carbon content ($OC_{bulk} = *OC_{coarse} + *OC_{fine}$) and OC loaded to fine sediments in overbank deposits along the Alsea River after a flood in December 2007.....	90
Figure 3.7. Elemental (A) and isotopic (B) composition of organic matter in sediments and soils in the Alsea River basin.....	91

LIST OF FIGURES (Continued)

<u>Figure</u>	<u>Page</u>
Figure 3.8. Lignin phenols, N/OC ratios (A) and $\delta^{13}\text{C}$ (B) composition of organic matter in sediments and soils in the Alsea River basin and its relationship with OC_{fine} loaded to overbank deposits along the river channel after a flood in 2007..	92
Figure 3.9. $\text{OC}_{\text{coarse}}$ as a proximal source of OC_{fine} in overbank deposits along the Alsea River after a storm in 2007.	93
Figure 3.10. Chemical characteristics of overbank sediments deposited after the GCG-2007 along the Alsea River as compared to suspended sediments from the Alsea ¹⁰ and Umpqua ⁵⁶ Rivers.	94
Figure 4.1. Conceptual model. Disturbance signals propagate like ripples across the bio-geophysical fabric that connect forests soils, through rivers and sediments, to lake bottoms.....	132
Figure 4.2. Study area. A. Loon Lake catchment location within the Umpqua River basin.	133
Figure 4.3. An information theory approach to the analysis of particle size spectra (PSS)..	134
Figure 4.4. Disturbance history of Loon Lake’s catchment as recorded by sediment core 02aN..	135
Figure 4.5. The diversity of particle sizes shows the extremely dynamic deposition that takes place in Loon Lake in response to disturbances (forcings as in Figure 4.4).....	136
Figure 4.6. Information spectra for a “Noisy” core (simulation) and a real sediment core (Loon Lake, 02aN).....	137
Figure 4.7. Effects of data aggregation on the characteristics of the entropy signal derived from particle size spectra from Loon Lake core 02aN.....	138
Figure 4.8. Long-term trends of Modal-Peak equivalents (MP_{eq}) along the sediment core 02aN (Loon Lake, Oregon)..	139
Figure 4.9. Elemental composition of organic matter deposited within selected event layers from Loon Lake sediment core 02aN.....	140
Figure 4.10. Long-term trends of residual Mode-Peak equivalents (rMP_{eq}) along the sediment core 02aN (Loon Lake, Oregon).....	141

LIST OF FIGURES (Continued)

<u>Figure</u>	<u>Page</u>
Figure 4.11. Pseudo-property-property plots using $rMP_{eq}(s)$ from Loon Lake sediment core 02aN..	142
Figure 4.12. Climatic variability in the last 1500 years and as potentially recorded by the textural characteristics of the sediments in the core 02aN, Loon Lake (OCR)..	143
Figure 4.13. Proxies for sediment accumulation rates and their relationship with long-term trends in regional climate in the Pacific Northwest..	144

LIST OF TABLES

<u>Table</u>	<u>Page</u>
Table 2-1. Major disturbances impacting the study sites (WS09-Old growth; WS10-Logged) in the H. J. Andrews Experimental Forest. Compilation from several data sources ^{7,30,35}	49
Table 2-2. Summary of elemental composition of suspended sediments from two headwater streams draining an old-growth forest (WS09) and 100%-logged watershed (WS10) in the H. J. Andrews Experimental Forest. Overall and seasonal averages covering water years from 1980-2014.....	50
Table 2-3. Coefficients from a multiple regression model for %TC. Full model had an R ² of 0.5225 and a p-value <0.0001	51
Table 3-1. Locations for the collection of overbank deposit samples along the Alsea River, Oregon Coast Range, after the Great Coastal Gale (December 2007). (*) Measurements from Google earth pro V 7.3.1.4507 (December 13, 2015)-eye alt:220; provided for relative comparison only.	95
Table 3-2. Textural characteristics of samples from overbank deposits after The Great Coastal Gale (December 2007) along the Alsea River, Oregon Coast Range.	96
Table 3-3. Organic carbon, nitrogen to carbon ratio, specific surface area, and organic carbon loading ([OC:SSA]) in overbank deposits along the Alsea River, Oregon Coast Range. Samples were collected after the Great Coastal Gale (December 2007). The fraction of the sample analyzed is indicated by a subscript (Coarse >63 µm; fine <63 µm). Percentages were calculated over the total mass sediment for that fraction. (*) Loadings calculated over corrected SSA values (see text for details).	97
Table 3-4. δ ¹³ C ratios and Carbon-normalized yields (mg 100 mg OC ⁻¹) of CuO product classes in fine <63 µm and coarse >63 µm particles overbank deposits along the Alsea River, Oregon Coast Range. VP vanillyl phenols, SP syringyl phenols, CP lignin-derived cinnamyl phenols, 3,5-Bd 3,5-Dihydroxybenzoic acid	98
Table 1-1. General Least Squares Regression of biogeochemical proxies on modal peak equivalents (MP _{eq}) for Loon Lake sediment core 02aN.	145

Chapter 1 Introduction: Disturbances and watershed biogeochemistry

Significance

Tectonic, climatic, and human forcings drive a dynamic disturbance regime in forested watersheds (FW) of the Pacific Northwest. In the last 1500 years, these landscapes have been affected by earthquakes, fires, and large storms. During the 20th century, old growth forests were intensively harvested and dissected by road networks. Nonetheless, little is known about the long-term consequences these disturbances have on fundamental ecosystem processes, like nutrient export. More importantly, it is unclear how much biogeochemical resilience FW ecosystems exhibit under a changing disturbance regime. Understanding the mechanisms behind biogeochemical resilience in FW is essential for the development of adaptive management schemes that not only help us to maintain these ecosystems but also to sustain the provision of valuable goods and services like timber and high-quality water.

Background

Many forested watershed (FW) ecosystems function far from steady-state conditions because of disturbances¹⁻³. A variety of events ranging from stand-replacing fires to earthquakes or massive landslides not only change species composition and forest physical attributes, they also disrupt nutrient cycling via biomass removal and increased nutrient export^{4,5}. Changes in runoff patterns, soil erosion rates, and even basin structure can result from these disturbances. Decades or even centuries might pass before the ecosystem recovers its original structure, and very often during that recovery period other disturbances occur to alter the recovery process and to set a new baseline for ecosystem's structure⁶. Since an increase in the frequency and magnitude of disturbances impacting FW is expected; understanding ecosystem resilience becomes a pressing need if we want to maintain these ecosystems as well as their provisions of goods and services, like timber and high-quality water. However, an ecosystem's resilience is the result of past interactions with disturbance, and our current knowledge still has fundamental gaps about FW responses to disturbances in the context of their natural history^{7,8}.

Historical records of ecosystem change are available as human-made, long-term datasets and as natural archives. High-resolution time series of FW responses to disturbances are currently produced and maintained by researchers at Long Term Ecological Research (LTER) sites. The temporal scale for most of the long-term research is, however, still short in comparison with FW natural dynamics. While many of the longest studies in LTER sites were established in the 1950's, forest ecosystem processes span over centuries and millennia. Hence, natural archives are an essential complementary source for understanding FW historical responses to disturbances.

Natural historical records are available in the form of chronosequences, tree rings, and sediment cores^{8,9}. Among these records, sediments have a pivotal importance in historical reconstruction in FW because sediments have the potential to preserve integrated watershed responses for longer timescales^{8,10}. Chronosequences provide a more general understanding of the impacts of disturbances on nutrient cycling because they are assembled from large-scale spatial patterns⁹. However, chronosequences lack the temporal resolution provided by well-laminated lake sediments, which we used in this dissertation. Tree rings can be used to reconstruct watershed hydrology¹¹; yet, the evidence they can provide about other watershed-scale processes like erosion and nutrient export is mostly indirect and depending on models of runoff effects on sediment transport. Sediment cores, on the other hand, provide evidence for time-resolved reconstructions of historical events. Sedimentary records can be used to reconstruct multi-centennial to millennial time series of proxies derived from sediment chemical characteristics.

Long-term time series of sediment chemistry are referred as to geochemical signals¹². When the chemical analyses are done on the biogenic organic matter stored in those sediments, a more direct link between sediment chemical properties and processes involving ecosystem nutrient cycling can be established. Thus, long-term time series of chemical proxies including elemental composition (%C, %N, N:C ratios), stable isotopic composition ($\delta^{13}\text{C}$ and $\delta^{15}\text{N}$), and terrestrial

plant-derived biomarkers (e.g. lignin phenols) are referred as to **biogeochemical signals**^{5,8,10}. Biogeochemical signals not only carry information about the occurrence of disturbances, observed as discrete peaks (or drawdowns) in the time series, but could also contain information about disturbance impacts and trajectories of ecosystem recovery⁸. Despite the central role of biogeochemical signals in reconstructing FW history, just recently have scientists formulated conceptual models to interpret these long-term records in the context of ecosystem functioning^{5,8,13,14}. These models of ecosystem's biogeochemical responses to disturbance can be grouped into two broad categories depending on the spatial scale that is encompassed in the analysis: small basin scale models and source-to-sink models. The spatial scope of these conceptual models also determines the type of historical reconstruction that could be achieved from the interpretation of the biogeochemical signals obtained from sedimentary records.

Small basin scale models of biogeochemical responses to disturbance are developed by ecologists. These small-scale models focus on alterations in nutrient cycling within the terrestrial portion of a watershed ecosystem (i.e., forests) after specific and localized disturbances, like insect outbreaks or fires^{5,8,10}. The disturbance regime is discrete (events occur with a probability of 0 or 1) and is reconstructed directly from the record by analyzing changes in the accumulation of pollen and charcoal among other indicators. Thus, variability in the accumulation of biogeochemical proxies can be translated into metrics of disturbance magnitude¹⁰. Because of the small size of the basin analyzed, the propagation of biogeochemical signals is mostly mediated by surface erosion and aeolian transport. The fundamental limitation of these small-scale models is the temporal resolution at which the sedimentary record can be analyzed⁵, which in turn depends not only on sampling effort (i.e. spatial separation between sedimentary layers being analyzed) but also on higher sedimentation rates.

Source-to-sink models¹³ are strongly influenced by hydrological and geomorphological concepts¹⁴ related to sediment transport and their application to reconstruct biogeochemical responses to disturbances is even more incipient¹³. Source-to-sink models focus on alterations in nutrient export, as a part of larger biogeochemical cycles that includes both the terrestrial sources (e.g. forests, floodplains, fluvial channels) and aquatic sinks (e.g. lakes and oceans). In a source-to-sink approach, the disturbance regime is continuous, as forcings (e.g. earthquakes, fires, floods) can exhibit spatiotemporal gradients. Because source-to-sink models describe processes at the watershed scale, the propagation of biogeochemical signals of response to disturbance is mediated by factors that modulate responses at the landscape scale like mass wasting and fluvial transport. Thus, leveraging watershed's responses to disturbance in source-to-sink systems is challenging because biogeochemical signals can be highly entangled and even "shredded" by internal watershed processes^{15,16}.

The information contained in biogeochemical signals is produced by the sequential deposition of sediment layers in lake bottoms; each depositional event resulting from complex interactions between physical and biological processes within the watershed. Such interactions make difficult to establish direct links between disturbances and watershed responses as recorded in sedimentary archives. In the physical domain, *erosion and sediment transport* modulate the intensity of biogeochemical signals by controlling the amount of POM exported from watersheds¹⁷. In the biological domain, *POM production, and stabilization within the soil* modulate the content of biogeochemical signals by controlling OM chemical composition at the source¹⁸. Physical and biological processes also interact to modulate biogeochemical signals. For instance, when intense erosion excavates deep soil horizons, it exposes POM that is highly decomposed, with lower C and N contents, and more enriched in ¹³C (ref.^{19,20}). In some cases, deep eroded POM is mostly petrogenic¹³. In contrast, in highly productive forests occurring on thick soils, POM is mainly derived from surficial erosion and carries chemical characteristics typical of recent biogenic

material (e.g., less decomposed, higher C and N contents, ^{13}C depleted)^{13,21}. Further modulation of POM chemistry in bulk sediment mixtures is exerted by hydrodynamic sorting of grain sizes during sediment transport²²⁻²⁴. For example, Bergamaschi et al.²² found that different biomarker signals could be obtained from different grain size fractions (e.g. silt, clays, sands) in coastal sediments in Peru. Similar evidence related to the transport of POM has been found in coastal deposits created by small mountainous river systems in the Pacific Northwest²⁵.

Transport of POM through fluvial networks involve an even more complex set of biogeochemical transformations (i.e. biological degradation)^{26,27} coupled with continuous deposition and resuspension of particles along the channels²⁸. In mountainous rivers, most of the sediments are exported during large storms and floods¹³, and the particles mobilized from different source areas across the watershed can cover a wide spectrum of ages and in-channel residence times^{29,30}. Much of the POM has been likely biologically pre-processed in soils as well as in headwater channels^{31,32} before becoming part of the suspended load. Once deposited in lake bottoms, POM can undergo further degradation if enough oxygen is available for aerobic decomposition or being preserved by efficient burial at high sedimentation rates³³.

Thus, a more precise interpretation of sedimentary records relies on disentangling biogeochemical signals of response to disturbance from other signals produced by watershed processes.

Research goal and questions

The **overarching goal** of this project is to *understand the long-term interactions between watershed processes, nutrient export and disturbances in FW ecosystems in the Pacific Northwest by the analysis of their biogeochemical signals of response to disturbance*. We study biogeochemical signals starting at headwaters, where nutrient cycling and export are tightly coupled with water flow (figure 1). These fundamental functional units in the watershed are highly

sensitive to disturbances because of their small size. Biogeochemical signals produced in headwaters are communicated along the main fluvial corridor. Then, the longitudinal evolution of the suspended load determines which signals are replaced and which signals are eventually imprinted in sedimentary records stored in lake bottoms. Finally, to interpret these records it is necessary to integrate all the available information related to POM provenance, transport and preservation that can be extracted from the sedimentary archive and compare this information with known patterns of POM dynamics in the watershed or in similar systems. Following this description, we formulate our **research question** as follows:

What modulates the content of biogeochemical signals of forested watershed response to disturbances?

Our **general objective** is to disentangle the role of erosion, sediment transport and soil organic matter dynamics in modulating the content of biogeochemical signals of forested watershed response to disturbance. Since this modulation occurs from headwaters to final sinks (e.g. lake bottoms) we study the processes affecting biogeochemical signals during its origin, transport and recording in sedimentary archives. Thus, our initial question is further decomposed into the following (figure 1):

1. *Signal Origin: Do logging and other disturbances produce a recognizable biogeochemical signature in small mountainous watersheds?*
2. *Signal Transport: What kind of biogeochemical signatures can be produced by Small Mountainous River Systems during floods?*
3. *Signal recording: What kind of signals of watershed response to disturbance can we identify from the information content of a sedimentary record?*

These three overarching questions guide specific chapters along this dissertation. To understand the origin of biogeochemical signals in headwaters, in chapter 2, “A 30-year Record of Particulate Organic Carbon (POC) Exports from Headwater Streams of the Oregon Cascades: A Biogeochemical Signal of Response to Disturbances”, we compare the chemical characteristics of suspended POM between two watersheds during the last 3 decades. In chapter 3, “Event-associated Overbank Deposits as Testimonies of Particulate Organic Carbon Mobilized along a Small Mountainous River during a Large Flood Event.”, we analyze longitudinal trends of geochemical properties of flood deposits as surrogates of an evolving suspended load along the fluvial corridor. We compare these longitudinal trends with erosional/depositional processes measured with radio nuclides. We also investigate the role of particle size distributions, as indicators of sediment transport processes, on the geochemical properties of flood deposits. In chapter 4, “Disentangling signals of watershed responses to disturbance from the information content of particle size spectra: An analysis of a 1500-year sedimentary archive from Loon Lake, Umpqua River Basin, Oregon.”, we develop an information-theory based approach to analyze a sedimentary archive containing 1500 years of natural history of a small mountainous watershed impacted a variety of disturbances including at least 4 high magnitude (>8.5) earthquakes, a stand replacing forest fire in the early 1800’s, and intensive logging during the first part of the 20th century.

Methodology

Fluvial sediments are composed of a diverse array of particles encompassing a wide range of chemical characteristics³⁴. Direct characterization of these particles requires laborious microscopic techniques (Scanning Electron Microscopy, micro CT scan) with laboratory protocols that span several weeks for sample preparation and analysis^{35,36}. Here, we combined variables related to sediment mobilization and export (suspended sediment concentrations, export rates, particle size spectra) with elemental, isotopic, and biomarker chemical composition to characterize different pools of particles moving from headwaters to lake bottoms.

Different sampling protocols were used to characterize the particulate load/deposits in our study sites. In the H.J. Andrews study auto-samplers target suspended Fine Particulate Organic Matter ($0.7 \mu\text{m} < \text{FPOM} < 1\text{mm}$)³⁷. In the Alsea study, we used a $63 \mu\text{m}$ screen to separate the coarse and fine fractions of the overbank sediments. Such particle size threshold differs from that commonly used by stream ecologists to separate Coarse Particulate Organic Matter (CPOM) from FPOM i.e., 1 mm. For this reason, we labeled the size fractions recovered from Alsea's overbank sediments as OCcoarse ($>63 \mu\text{m}$) and OCfine ($<63 \mu\text{m}$) instead of CPOM and FPOM. In the Loon Lake study, we analyzed the bulk chemical properties of sediment layers after freeze-drying raw samples. Since freeze-drying preserves sediment's interstitial water³⁵, the chemical characteristics of Loon Lake sediments might reflect the composition of both POM and interstitial DOM. Accordingly, we measured total carbon (%TC or TOC, given the almost negligible contribution of carbonates ($<5\%$) found in these samples)³⁸. However, we found significant correlations between the bulk chemical composition of Loon Lake sediments and different particle size classes within each layer. Thus, our data suggest that part of the chemical variability observed along the sedimentary record is explained by the behavior of the particulate load.

We used categories like carbon-rich/carbon-depleted particles (H.J. Andrews study); colloids, aggregates, fine particulate organic matter, and vascular plant detritus (Alsea study). In the Loon Lake study, we used a Generalized Least Squares regression model to test for significant correlations between specific particle size classes and the bulk chemical characteristics of deposited sediment layers. Based on the regression model, we introduced the concept of pseudo-property-property plots to delineate a general correspondence between particle size classes like colloids, aggregates, clays, and sands with elemental and isotopic composition of Loon Lake sediments.

We use the definition of Particulate Organic Matter (POM) in its more general sense to describe the continuum of particle types collected with the different sampling protocols used in this dissertation. Our focus was to understand watershed's response to disturbance as represented in relative changes of POM chemistry (i.e. biogeochemical signals) and not a direct comparison between study sites in terms of their particulate loads within a specific range of particle size (e.g., FPOM or CPOM or OCcoarse, etc.). Such a strict comparison would be highly valuable if all the samples would have been taken within the same watershed. Instead, we exploit the flexibility in the treatment of POM to build a more integrated view of particulate nutrient export combining the information obtained from our study sites.

Bibliography

1. Vitousek, P. M. & Matson, P. A. Disturbance, Nitrogen Availability, and Nitrogen Losses in an Intensively Managed Loblolly Pine Plantation. *Ecology* 66, 1360–1376 (1985).
2. Bormann, F. H. & Likens, G. E. Ecosystem Development and the Steady State. in *Pattern and Process in a Forested Ecosystem* 164–191 (Springer New York, 1994). doi:10.1007/978-1-4612-6232-9_6
3. Smithwick, E. A. H. Pyrogeography and Biogeochemical Resilience. in *The Landscape Ecology of Fire* (eds. McKenzie, D., Miller, C. & Falk, D. A.) 143–163 (Springer Netherlands, 2011).
4. Pickett, S. T. & P. S. White. *The ecology of natural disturbance and patch dynamics*. (Academic Press, 1985).
5. Morris, J. L., McLauchlan, K. K. & Higuera, P. E. Sensitivity and complacency of sedimentary biogeochemical records to climate-mediated forest disturbances. *Earth-Sci. Rev.* 148, 121–133 (2015).
6. Buma, B. Disturbance interactions: characterization, prediction, and the potential for cascading effects. *Ecosphere* 6, art70 (2015).
7. Landres, P. B., Morgan, P. & Swanson, F. J. Overview of the Use of Natural Variability Concepts in Managing Ecological Systems. *Ecol. Appl.* 9, 1179–1188 (1999).
8. McLauchlan, K. K. *et al.* Reconstructing Disturbances and Their Biogeochemical Consequences over Multiple Timescales. *BioScience* 64, 105–116 (2014).
9. Perakis, S. S., Tepley, A. J. & Compton, J. E. Disturbance and Topography Shape Nitrogen Availability and $\delta^{15}\text{N}$ over Long-Term Forest Succession. *Ecosystems* 18, 573–588 (2015).
10. Dunnette, P. V. *et al.* Biogeochemical impacts of wildfires over four millennia in a Rocky Mountain subalpine watershed. *New Phytol.* 203, 900–912 (2014).
11. MacDonald, G. M. Variations in the Pacific Decadal Oscillation over the past millennium. *Geophys. Res. Lett.* 32, (2005).
12. Bloemsmma, M. R. *et al.* Modelling the joint variability of grain size and chemical composition in sediments. *Sediment. Geol.* 280, 135–148 (2012).
13. Leithold, E. L., Blair, N. E. & Wegmann, K. W. Source-to-sink sedimentary systems and global carbon burial: A river runs through it. *Earth-Sci. Rev.* 153, 30–42 (2016).
14. Romans, B. W., Castellort, S., Covault, J. A., Fildani, A. & Walsh, J. P. Environmental signal propagation in sedimentary systems across timescales. *Earth-Sci. Rev.* 153, 7–29 (2016).

15. Jerolmack, D. J. & Paola, C. Shredding of environmental signals by sediment transport. *Geophys. Res. Lett.* 37, (2010).
16. Phillips, C. B. & Jerolmack, D. J. Self-organization of river channels as a critical filter on climate signals. *Science* 352, 694–697 (2016).
17. Galy, V., Peucker-Ehrenbrink, B. & Eglinton, T. Global carbon export from the terrestrial biosphere controlled by erosion. *Nature* 521, 204–207 (2015).
18. Schmidt, M. W. I. *et al.* Persistence of soil organic matter as an ecosystem property. *Nature* 478, 49–56 (2011).
19. Acton, P., Fox, J., Campbell, E., Rowe, H. & Wilkinson, M. Carbon isotopes for estimating soil decomposition and physical mixing in well-drained forest soils: CARBON ISOTOPES FOR FOREST SOILS. *J. Geophys. Res. Biogeosciences* 118, 1532–1545 (2013).
20. Guillaume, T., Damris, M. & Kuzyakov, Y. Losses of soil carbon by converting tropical forest to plantations: erosion and decomposition estimated by $\delta^{13}\text{C}$. *Glob. Change Biol.* 21, 3548–3560 (2015).
21. Hatten, J. A., Goñi, M. A. & Wheatcroft, R. A. Chemical characteristics of particulate organic matter from a small, mountainous river system in the Oregon Coast Range, USA. *Biogeochemistry* 107, 43–66 (2012).
22. Bergamaschi, B. A. *et al.* The effect of grain size and surface area on organic matter, lignin and carbohydrate concentration, and molecular compositions in Peru Margin sediments. *Geochim. Cosmochim. Acta* 61, 1247–1260 (1997).
23. Bianchi, T. S., Galler, J. J. & Allison, M. A. Hydrodynamic sorting and transport of terrestrially derived organic carbon in sediments of the Mississippi and Atchafalaya Rivers. *Estuar. Coast. Shelf Sci.* 73, 211–222 (2007).
24. Wakeham, S. G. *et al.* Partitioning of organic matter in continental margin sediments among density fractions. *Mar. Chem.* 115, 211–225 (2009).
25. Roy, M. *et al.* Reactive iron and manganese distributions in seabed sediments near small mountainous rivers off Oregon and California (USA). *Cont. Shelf Res.* 54, 67–79 (2013).
26. Marín-Spiotta, E. *et al.* Paradigm shifts in soil organic matter research affect interpretations of aquatic carbon cycling: transcending disciplinary and ecosystem boundaries. *Biogeochemistry* 117, 279–297 (2014).
27. Aufdenkampe, A. K. *et al.* Riverine coupling of biogeochemical cycles between land, oceans, and atmosphere. *Front. Ecol. Environ.* 9, 53–60 (2011).
28. Battin, T. J. *et al.* Biophysical controls on organic carbon fluxes in fluvial networks. *Nat. Geosci.* 1, 95–100 (2008).
29. Blair, N. E. *et al.* The persistence of memory: the fate of ancient sedimentary organic carbon in a modern sedimentary system. *Geochim. Cosmochim. Acta* 67, 63–73 (2003).
30. Rosenheim, B. E. & Galy, V. Direct measurement of riverine particulate organic carbon age structure. *Geophys. Res. Lett.* 39, L19703 (2012).
31. Naiman, R. J. & Sedell, J. R. Characterization of Particulate Organic Matter Transported by Some Cascade Mountain Streams. *J. Fish. Res. Board Can.* 36, 17–31 (1979).
32. Vannote, R. L., Minshall, G. W., Cummins, K. W., Sedell, J. R. & Cushing, C. E. The river continuum concept. *Can J Fish Aquat Sci* 37, 130–137 (1982).
33. Meyers, P. A. Organic geochemical proxies of paleoceanographic, paleolimnologic, and paleoclimatic processes. *Org. Geochem.* 27, 213–250 (1997).
34. Droppo, I. G. Rethinking what constitutes suspended sediment. *Hydrol. Process.* 15, 1551–1564 (2001).
35. Uramoto, G.-I., Morono, Y., Uematsu, K. & Inagaki, F. An improved sample preparation method for imaging microstructures of fine-grained marine sediment using microfocuss X-ray computed tomography and scanning electron microscopy: Sample prep for microstructure observation. *Limnol. Oceanogr. Methods* 12, 469–483 (2014).

36. Bendle, J. M., Palmer, A. P. & Carr, S. J. A comparison of micro-CT and thin section analysis of Lateglacial glaciolacustrine varves from Glen Roy, Scotland. *Quat. Sci. Rev.* 114, 61–77 (2015).
37. Yoshimura, C., Gessner, M. O., Tockner, K. & Furumai, H. Chemical properties, microbial respiration, and decomposition of coarse and fine particulate organic matter. *J. North Am. Benthol. Soc.* 27, 664–673 (2008).
38. Richardson, K. N. D., Hatten, J. A. & Wheatcroft, R. A. 1500 years of lake sedimentation due to fire, earthquakes, floods and land clearance in the Oregon Coast Range: geomorphic sensitivity to floods during timber harvest period. *Earth Surf. Process. Landf.* 43, 1496–1517 (2018).

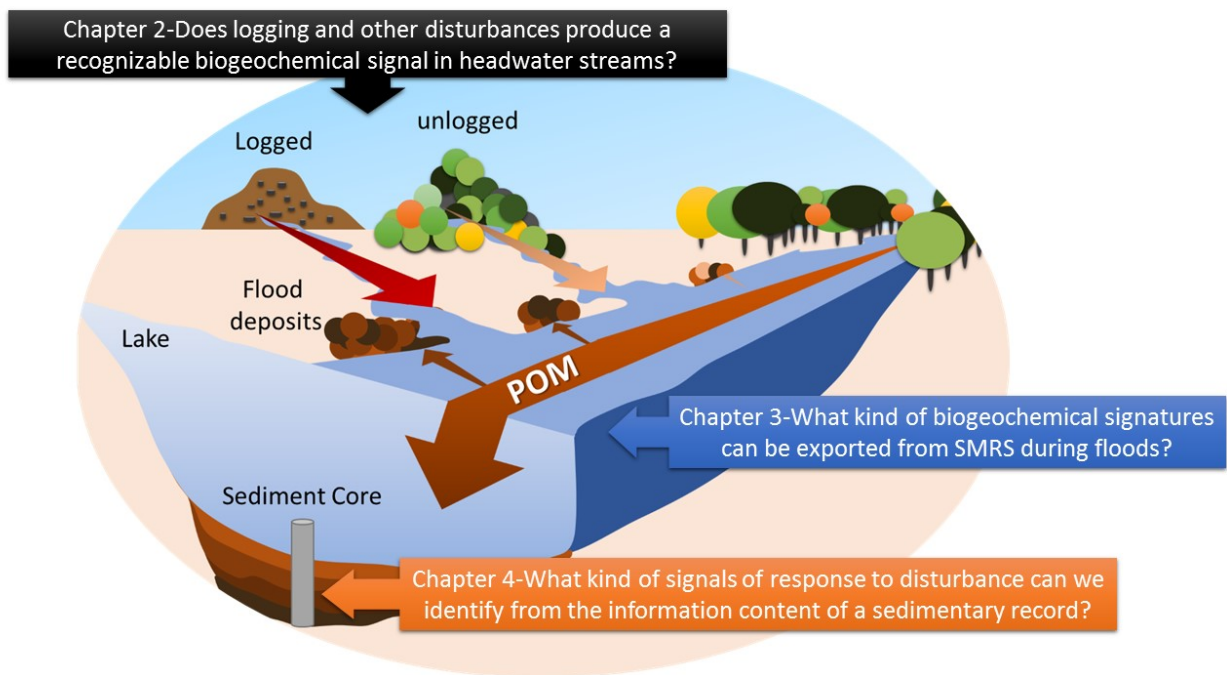


Figure 1.1. Research project structure. Our research questions address the origin, transport and interpretation of biogeochemical signals of disturbance in FW ecosystems. We hypothesize that headwaters produce different POM signatures because of disturbances, in this case logging in WS-9 and WS-10 in the H.J. Andrews experimental forest (chapter 2). These signals are further integrated along the main fluvial corridor. Because of the longitudinal changes in biophysical features along small mountainous river systems, there is also a longitudinal evolution of the biogeochemical signatures. We hypothesize that this longitudinal evolution can be analyzed from flood deposits along the main channel (e.g. Alesa River study, chapter 3). Lastly, these signals are recorded in lake bottoms where the superposition of all the above-mentioned processes can be disentangled by assessing the information content of sedimentary records (e.g. Loon Lake study, chapter 4).

Chapter 2 A 30-year Record of Particulate Organic Carbon (POC) Exports from Headwater Streams of the Oregon Cascades: A Biogeochemical Signal of Response to Disturbances

Introduction

Approximately 90% of the global river length is represented by first-order streams¹. Thus, ecological processes in headwater ecosystems can influence global dynamics², including carbon cycling³⁻⁵. Theoretically, the role of headwater streams in the global carbon cycle should be determined by the balance between storage, export, and decomposition of the organic matter imported from the watershed³. However, such a view requires a steady-state framework for different components of the organic carbon budget (i.e. dissolved, gaseous and particulate)⁴. For particulate organic carbon (POC) at least, this framework is in startling contrast with the dynamic regime of particulate material transfer that characterizes headwater ecosystems.

First order streams are extremely sensitive to mass wasting processes that physically erode significant amounts of particulate material from their hillslopes^{6,7}, including POC^{5,8,9}. Because of their small size, these streams lack the capacity to transport large sediment inputs and they become part of the channel structure^{6,7,10}. The longitudinal profile of first order streams is typically composed by a mosaic of small and large sediment accumulations held in between the junctions of fallen trees and crossing roots. In the short term, headwater channels function as traps for sediments and organic matter¹¹. In the long term, headwater catchments are sources of large amounts of organic matter that is exported episodically in response to disturbances such as large floods or debris flows^{5,8,9}.

The disturbance regime in headwater streams is not only driven by natural forcings such as climate and tectonics, but also by human forcings related to the extraction of natural resources¹². Timber harvesting has been one of the most common activities threatening the integrity of headwater ecosystems in the last century¹³. The traditional assessment of the impacts of logging practices has been focused on short-term alterations (<10 years) in the magnitude of water, nutrient, and sediment fluxes resulting from forest harvesting. However, these types of assessments overlook the role of the disturbance regime on material fluxes.

During the last 40 years, paired watershed studies in headwaters have provided insights about the impacts of human activities as well as natural disturbances on watershed biogeochemistry^{14,15,16}. Many of these studies have been carried out at Long-Term Ecological

Research (LTER) sites where records of streamflow, water chemistry, and sediment transport are available for several decades¹⁷. However, initial research projects at LTER sites were mainly focused on dissolved nutrient export (nitrogen and phosphorous) and suspended sediments and less attention was dedicated to particulate forms of elements such as carbon (i.e. POC) with some exceptions^{18,19}. More importantly, despite the episodic and disturbance-driven character of POC export in headwater streams, long-term records of changes in POC concentrations and associated constituents (i.e. N) in response to a variety of disturbances are lacking in the literature. Understanding POC dynamics is important not only to constrain nutrient balances in biogeochemical models but also to gain mechanistic insights into the generation of biogeochemical signals that will eventually be stored in sedimentary records. In this chapter, we study long-term biogeochemical responses of two small headwater streams draining an old growth forest and a 100% clear cut watershed (1975) in the H. J. Andrews experimental forest, an LTER site located in the Western Oregon Cascades. Besides analyzing the impacts of logging 5 years after treatment application, we study POC elemental composition in sediments exported after several disturbances including storms, landslides, and debris flows in the post-harvest succession period between 1980 and 2015.

The general research questions to be addressed in this chapter are:

Does logging produce a recognizable biogeochemical signature in small mountainous watersheds?

What is the biogeochemical signature of post-harvest succession?

Do logged and unlogged watersheds produce different biogeochemical signals in response to other disturbances?

To answer these questions, we formulate the following objectives:

- *To compare the carbon content of suspended sediments exported from a 100% logged watershed and an old-growth forested watershed by means of a multiple regression model, after accounting for potential differences in particulate export, dissolved nutrients, wetting regime, and seasonality.*
- *To reconstruct a 30 year-long time series to examine POC dynamics 10 years after treatment application.*
- *To examine the recovery path after two debris flows occurring post-treatment application (1986 and 1996).*

Methods

Site description

The study watersheds are located within the H.J. Andrews Experimental Forest in the Willamette National Forest in the Cascade Mountain Range of western Oregon. These watersheds were part of a paired study in 1975 (WS09, old-growth (**OG site**), and WS10, 100% logged (**LG site**), Figure 2.1). The underlying geology consists of highly weathered volcanoclastics deposited on steep slopes (>60%) prone to mass movements. The soils are loamy, permeable, well-drained, and with depths between <1m up to 3m. The elevation range for both catchments is between 400-700m and catchment areas are 8.5 ha (OG site) and 10 ha (LG site). Despite these similarities, the LG site is more prone to debris flows and other processes of sediment production due to its steeper hillslopes and channel (Swanson, unpublished manuscript).

Climate is characterized by dry summers and wet winters. Mean annual temperature is 8.5°C with daily extremes of 39°C in summer and -20°C in winter. Mean annual precipitation is 2300 mm of which ~98% is rain falling between October and May. Winter snow packs in these watersheds are small and short-lived (1-2 weeks). Based on the long-term records from the H. J. Andrews Experimental Forest (1969-2013), mean daily discharge is 3.11 and 4.81 l s⁻¹ at the OG and LG sites respectively. Mean annual sediment yields are 49 and 91.8 Kg ha⁻¹ (OG and LG sites respectively). These estimates exclude the high sediment yields recorded in 1996 in the Old growth (3058 kg ha⁻¹) and logged watershed (1185 kg ha⁻¹), and do not account for the high volume of sediments exported from the logged watershed after a debris flow in 1986 (~700 m³ mobilized as bedload).

The hydrological regime is event-dominated due to high discharge storms during the winter (Figure 2.2). Suspended sediment concentrations lack a clear seasonal trend and sediment inputs to the channel can be highly stochastic. Relatively high concentrations of suspended sediments are likely any day during the water year (Figure 2.2). Therefore, the characterization of sediment loads is difficult to predict from hydrological data and requires continuous monitoring.

Prior to the clear cut in 1975, vegetation in both watersheds consisted of old-growth forests (>450 -year-old) regenerated after stand replacing fires in the early 1500's. Dominant species were Douglas-fir (*Pseudotsuga menziesii*), western hemlock (*Tsuga heterophylla*), and western red cedar (*Thuja plicata*) overshadowing most of the stream length. Today, vegetation in WS10 consists of replanted Douglas-fir and western hemlock of ~40 years old. Because hillslopes issue

directly into the streams, there is no riparian vegetation bordering the streams channels in our study sites²⁰.

Each study watershed has a continuous record of streamflow and water quality starting in November 1968²². Daily streamflow is measured using trapezoidal flumes and water quality is analyzed from three-week composite samples. Water quality data include inorganic compounds, dissolved nutrients and suspended sediments. An autosampler collected water aliquots at varying frequencies depending on flow stage to account for changes in concentration with discharge. These flow-weighted samples are recovered every week, refrigerated, and every three weeks combined into a large sample for chemical analysis. Additionally, each watershed has a bedload collection basin downstream the gauging station. The material accumulated in the bedload basins is measured on an annual basis.

Disturbance history

Besides the logging treatment on the LG site, disturbance history (Table 1-1) in the study area includes the passing of several record storms (1964-65, 1986, 1996)^{6,21} and droughts (1977, 2001). Mass movements are frequent in the region and more than 30 landslides were triggered in the area including the Lookout Creek watershed (H.J. Andrews) by the storms in 1964 and 1965²¹. Although there is no evidence of mass movements from 1964 and 1965 affecting our study sites, the impacts of these flooding events could not be estimated due to the lack of data (gauging stations were installed in 1968).

The immediate impacts (~ first 3 years) of the clear-cut treatment on the stream channel structure at the LG site were described by Cromack et al²². Here, we use available historical data of bedload from our study sites to update these former descriptions.

In the spring of 1975, a 100% removal of tree biomass was completed at the LG site (high-level cable-yarded)¹⁷ (Figure 2.1A and B). About 8.8×10^2 Mg ha⁻¹ of organic matter from the watershed were extracted from the watershed (>60% of the original biomass stock)²². Logging activities also redistributed the mass of coarse debris around the stream channel and across the hillslopes. While the standing crop of down logs in the stream area was reduced to 22% of the pre-logging level (Figure 2.1C), slashed material accumulated substantially on the stream banks (with increases between 30-95%) despite the efforts to prevent coarse debris loading into the stream corridor²². Also, due to the steepness of the terrain many logs were dragged along the surface

exposing mineral soils and uprooting stumps. These impacts were particularly notorious on the southeast hillslope of the watershed at the LG site.

Most of the coarse woody debris accumulated on the stream channel after the logging were flushed out from the LG site as bedload by winter storms in 1976 and 1978²². Four winter storms in 1976 accounted for the removal of 1.7 Mg ha⁻¹ of particulate matter from the channel of which 0.7 Mg ha⁻¹ were organic matter (~0.35 MgC ha⁻¹)²². The total bedload during the first year following clearcutting (4.8 Mg ha⁻¹) was 40 times greater than the 30-year average bedload export from the OG site (0.15 Mg ha⁻¹). 1977 was the second driest year in the record (surpassed only by droughts in 2001) and winter storms in 1978 accounted for additional 3.4 Mg ha⁻¹ of bedload export. By assuming that bedload was 20% organic material, between 1976 and 1978, the LG site exported about 1 MgC ha⁻¹.

The soils and the woody debris that accumulated from yarding in 1975 on the southeast slope of the LG site failed after a major storm in February 1986²³. This debris flow resulted in the scouring of 220 m of the stream channel down to bedrock with an average width of 8m (Figure 2.1D)²³. About 659 m³ of debris accumulated in the basin downstream the gauging station (which was destroyed by the passage of the colluvium). It was estimated that 50% of the volume deposited at the collection basin was organic (F. Swanson, unpublished manuscript). By assuming a density of 450 kg m⁻³ for coniferous woody material²⁴, the debris flow in 1986 exported ~6.8 MgC ha⁻¹ from the LG site.

Although no debris flow has affected the OG site in the last 50 years, a storm in 1996, the largest on the record, mobilized significant amounts of woody material from the watershed. Bedload transport accounted for 1.6 Mg ha⁻¹ of particulate material exported from the OG site. By assuming a bedload composition equal to that exported from the LG site in 1986, the storm in 1996 would have exported 0.07 MgC ha⁻¹. In the logged watershed the same event mobilized 13.6 Mg ha⁻¹ of particulate material as bedload due to a minor debris flow²¹. Since the availability of woody material along the stream channel at the LG site changed so dramatically after 1986²¹, it is difficult to estimate the carbon content of those sediments.

Data preparation and analysis

For POC analysis, we measured the elemental composition (%TC, %TN, TN:C ratios) from suspended sediment samples collected between 1979 and 2014 (Our statistical analysis only

considered filters starting on 1984 though, see below). We took advantage of a well-preserved archive of glass fiber filters (GFF-F, 0.7 μm) containing suspended sediments from the OG and LG sites. These filters have been stored in dry conditions within paper envelopes since their collection. Prior to chemical analysis, filters containing enough suspended sediments were pulverized in a KLECO ball mill to reduce the samples to a fine homogeneous powder. This procedure allowed us to reduce sample losses due to excessive manipulation or transfers between containers required by manual grinding. Homogenization also prevented bias introduced by surficial scraping against smaller sediment particles embedded in the fiber matrix within the filters. A previous study²⁵ detected no significant short-term effects of the storage conditions on the integrity of the samples (i.e. no contamination from the envelopes or changes in the chemical composition of the sediments after six months of storage). The same study showed that the contribution from the filters to the carbon and nitrogen signals was within the range of analytical error or below detection levels respectively.

Elemental composition was determined by high-temperature combustion on a Flash EA1112 Elemental Analyzer. Based on replicate analyses of selected samples, the precision of these measurements was better than 5% of the measured values and analyses of reference materials showed they were within 2% accuracy. We used the elemental TN:C ratios to characterize our samples since TC:N ratios tend to underestimate land-derived contributions to aquatic sediments^{26,27}. Due to the relatively low concentration of suspended sediments in the study watersheds, many samples did not have enough material to produce signals above detection limits. Thus, only samples containing more than 8 mg of suspended sediments per filter were analyzed. Because of this analytical constraint we measured elemental composition on 301 samples out of >1200. Yet, these samples were representative of a typical water year and encompassed all water years in between 1980 and 2014 (Figure 2.2).

We report our results as particulate organic carbon (POC) even though we did not pre-acidify our samples before elemental analysis. This choice was based on the following reasons. First, due to the volcanic origin of the soils in the study area, carbonate concentrations are not expected to significantly influence %TC. Second, previous studies have shown that most of the carbon in the suspended sediments in rivers of the Pacific Northwest is from top soil layers (not bedrock), organic, and biospheric^{5,25,28,29}. Lastly, most samples contained less than 50 mg of suspended sediments and Smith (ref²⁵) reported that carbonate removal via acidification resulted in up to 50% losses of carbon content in samples with less than 200 mg of suspended sediments.

Furthermore, these losses were selective for the labile OC fraction. Thus, acidification of the samples could have resulted in a higher bias on the estimation of POC content from our study sites than non-acidification.

Predicting carbon content in suspended sediments and reconstructing historical POC yields

To identify the controls on POC exports from our study sites we used multiple linear regression. Our model structure allowed us not only to compare the carbon content (%TC) of the suspended sediments (TSS) exported from the old growth and logged watersheds (WS), but also to account for the role of other influential factors on POC dynamics in the studied headwater streams. These factors included water year (WY), maximum precipitation (P_{max} ; over the three weeks prior to sample collection and compositing), discharge (Q), dissolved organic nitrogen (DON; as a proxy for particulate organic nitrogen), dissolved silica (S; as a proxy for soil wetting regime), and seasonality (SSN; to account for potential temporal correlation within each season). We excluded the 1996 event from model fitting as TSS concentrations exhibited outlying values (> 600 mg/l) and we had no interests in predicting %TC of these sediments since we had direct measurements of them. We checked for serial correlation in the model residuals using semi-variograms since autosampler measurements are not exactly spaced at three weeks intervals. All variables were log-transformed before parameter estimation (except for WS and WY). %TC was predicted according to the following equation:

$$\%TC = \beta_0 + \beta_1(WS) + \beta_2(WY) + \beta_3(P_{max}) + \beta_4(Q) + \beta_5(TSS) + \beta_6(TSS)^2 + \beta_7(DON) + \beta_8(S) + \beta_9(SSN) + \beta_{10}(WS*DON)$$

A similar model was used to compare the old growth and logged watersheds in terms of the %TN and TN:C ratios.

Our exploratory data analysis suggested a correlation between %TC, %TN and particulate organic nitrogen (PON). Although PON data are available in the H. J. Andrews database, we used DON data in our model because PON values are calculated as the difference of DON, nitrate, and total N. DON concentrations are typically low in forested ecosystems in the Pacific Northwest, and many samples are close to detection limits. Thus, in many cases, low DON concentrations render missing values for PON. In our model, dissolved silica accounted for changes in underground wetting regimes. Much of the water that feeds small streams in the study area moves

vertically through the permeable soils. Since soil saturation conditions could be also related to sediment inputs to these streams (i.e. wet heavy soils might be more prone to vertical collapse), we assume that dissolved silica might behave as an indicator of hydraulic control of sediment supply.

Changes in filtering techniques and analytical inconsistencies prevented us from using data before 1984 in our statistical analysis. Although suspended sediment data are consistent through time, the effects that changes in filtering techniques could have on the retention of different types of organic particles is difficult to constrain. Also, dissolved silica data before March 1983 are marked as questionable in the H.J. Andrews database due to an unforeseen impact of sample refrigeration on dissolved silica reactivity. Thus, our regression model predicted %TC starting on 1984.

We used the calibrated multiple linear regression model to reconstruct a time series of POC concentrations at the three-week time scale using the available long-term database of water chemistry. We replaced a small percentage of missing values in the long-term time series of predictors (1134 data points) using linear interpolation (1.0, 0.5, and 3.5 % of the time series were missing for suspended sediments, dissolved silica, and dissolved organic nitrogen, respectively). These interpolated datasets were used mostly in the reconstruction of the POC time series. Interpolation played a negligible role in model's parameter estimation because we had only three missing data points (out of >200) of DON in the calibration dataset.

Predicted %TC values were corrected from bias resulting from log-log relationships. This correction consisted in regressing predicted values against untransformed observed data and multiplying the former by the resulting slope ($m=0.937$). Corrected %TC were multiplied by TSS to obtain POC concentrations in mg l^{-1} and POC concentrations were multiplied by discharge and divided by watershed area to obtain POC yields (kg ha^{-1}).

Results

Elemental composition of suspended sediments

Raw data suggested differences in the elemental composition and the seasonal behavior of the particulate organic matter exported from our study sites (Figure 2.3). The average %TC of sediments from the OG site ($19.20\pm 8.9\%$) was higher than that observed at the LG site ($13.91\pm 7.5\%$) (Table 2-2). Suspended sediments from the OG site also had higher nitrogen content and lower TN:C ratios than sediments from the LG site ($1.50\pm 0.66\%$ vs. $1.24\pm 0.69\%$ TN;

0.072±0.02 vs. 0.079±0.02 TN:C) (Table 2-2, Figure 2.3). The highest carbon contents were typically observed during the summer season in the OG site (23.99±7.4%); while suspended sediments had the lowest carbon content during the winter season in the same location (14.13±7.5%). In the LG site, sediments had the highest carbon content in the fall (16.11±8.2%) and the lowest carbon content in winter (10.94±5.5%). Seasonal trends were less evident in TN:C ratios. Yet, in the OG site, the lowest TN:C ratios were observed in summer (0.066±0.02) while in the LG site TN:C ratios were higher in summer and fall (>0.08) and lower in winter and spring (0.075±0.02) (Table 2-2, Figure 2.3).

On a multiannual basis, the largest carbon content was 49.16% (1986) in the OG site and 50.80% (2013) in the LG site (Table 2-2, Figure 2.3). The carbon content in the LG site in 1986 was the second largest (48.62%). The highest TN:C ratio was 0.143 (1982) in the old-growth site and 0.148 (2007) in the LG site. The TN:C ratio in the LG site in 1982 was 0.140 (second largest) (Table 2-2, Figure 2.3).

Overall, the old-growth site exported sediments enriched in carbon with lower TN:C ratios and exhibited a stronger seasonal behavior compared to the logged sites. These differences were more accentuated after 1986 (Figure 2.3).

Proxies for particulate matter inputs to the study sites

As a proxy for inputs of particulate material to our study sites, we used a compilation of field notes documenting findings of leaves, needles, insects, etc., in the collection basins surrounding the autosamplers. These data are shown in Figure 2.4. The open canopy in the LG site resulted in a lower occurrence of leaves and needles compared to the OG site. Also, these data suggest two seasonal peaks of litter input to stream draining the OG site (Figure 2.4). Fines and particulates tend to accumulate towards the end of the spring and during summer low flows in the OG site, while the same materials tend to accumulate in November in the LG site (despite relatively high flows). The LG site has also the lower occurrence of ants and other insects and higher occurrence of algae and lichen, as expected from a channel receiving more solar irradiation due to the lack of a conspicuous riparian vegetation (Figure 2.4).

Predicting the carbon content of suspended sediments

We found strong evidence for differences in the elemental composition of suspended sediments exported from our study sites in response to logging. %TC was higher at the OG site than at the

LG site; although the evidence was moderate in the full model shown Table 2-3 ($p=0.019$), when we dropped the non-significant interaction between WS and $\log[\text{DON}]$ from the model, the p -value for the effects associated with WS type was <0.0001 . We also found strong evidence that the TN:C ratios were significantly lower in the OG site compared to the LG site ($p=0.009$) and very strong evidence for an overall increase of the TN:C ratio over time ($p<0.0001$). The evidence for the effects of dissolved organic nitrogen, dissolved silica, winter season, and suspended sediments on %TC was strong ($p<0.01$; Table 2-3). While %TC was positively correlated with DON and dissolved silica, %TC decreased significantly during winters and with increases in suspended sediment concentrations.

In terms of predictive capabilities, the model explained $>54\%$ of the variability in %TC across both study sites (Figure 2.5). We observed a good agreement between predicted and observed %TC with just a few samples significantly departing from the 1:1 line (Figure 2.5A). These samples had the highest carbon contents and corresponded to water years 1986 (OG site) and 2013 (LG site). A full comparison of the model outputs with the raw data is shown in the Supplementary Figure 1. The calibrated model captured the most important trends observed in the raw data including the contrasting impact of the 1986's debris flow on the carbon content of suspended sediments at the LG site as well as the marked seasonal behavior of %TC (Supplementary Figure 1).

To reconstruct long-term trends of %TC in our study sites we combined model predictions with our observations into a single time series (our measurements accounted for more than 75% of the sediment load exported from both watersheds between 1984-2014). The reconstructed time series of %TC are shown in Figure 2.5 B-D). On a multiannual scale, the OG site showed the impacts of the storms of 1989, 1996, and 2009, with reductions in the carbon content of the exported sediments. On average, %TC dropped between 4 to 6% compared with the pre-storm conditions and then returned to values within the long-term average $\sim 20\text{-}25\%$ (Figure 2.5B). In contrast, the LG site showed a significant impact after the debris flow in 1986 with the average carbon content of the suspended sediments decreasing, on average, from 20% to 12%. There is no evidence of complete recovery of %TC to pre-1986 levels in the sediments exported from the LG site; %TC has remained below 17% since 1990 (Figure 2.5B). At the annual scale, %TC showed a unimodal behavior with maximum values around summer and fall and minimum values in winter (Figure 2.5C). Although %TC was significantly higher in the OG site compared to the LG site along the year, such a difference is more pronounced in the summer season. This strong seasonal contrast is also evident at the three-week sampling timescale (Figure 2.5D). The

reconstructed long-term time series of %TC in the study sites reveals the superposition of different processes driving changes in %TC at different temporal scales: disturbances driving multiannual changes in %TC and seasonality driving changes in %TC at the annual scale.

Long-term trends of POC yields

We used the reconstructed %TC time series to calculate POC yields and to examine watershed responses to disturbance in terms of POC exports. The multiannual total POC yield was 0.28 Mg C ha⁻¹ for the OG site and 0.30 Mg C ha⁻¹ for the LG site (Figure 2.6A). The events of 1996 and 2009 represented about 17 and 4% (respectively) of the total POC yield at the OG site, while the events of 1996 and 1989 represented about 14 and 3% of the total POC yield at the LG site (Figure 2.6A). Since each event had a duration > 1 week, the storms mentioned above contributed with more than 17% of the total yield in less than 0.4% of the time, highlighting the episodic character of POC export from these small watersheds. Yet, when compared to the POC yield resulting from the channel-scouring debris flow in 1986 at the LG site, 6.8 Mg C ha⁻¹, the values above represent only a small fraction of the total POC exported during the 30 years covered by our analysis (Figure 2.6A). Note that suspended yield from the LG site did not capture the magnitude of 1986 event because all the particulate material was exported as bedload. Furthermore, due to the destruction of the gauging station, grab samples were collected until the beginning of the 1987 water year. At any rate, if we include our estimate for carbon exported as bedload in 1996 from the OG site (~0.07 Mg C ha⁻¹) (Figure 2.6A), the LG site exported at least 20 times more POC than the OG site between 1984 and 2015.

Such a dramatic difference in POC yields between our study sites is not evident in the long-term trends of total and average (suspended) POC yields (Figure 2.6B-D). Despite the episodic increases in POC yields in response to storm events and debris flows, the long-term trends of total annual POC yields are similar between the OG and LG sites (Figure 2.6B). The interannual rate of change of POC exports is mostly negative between 1984 and 1995 and mostly positive between 2001 and 2012 in both watersheds. The multiannual average POC yield for the OG site was 5.12±3.4 kg C ha⁻¹ and 7.16±4.4 kg C ha⁻¹ for the LG site. These estimates excluded the POC yields from 1986 (16.6 and 11.2 kg C ha⁻¹; OG and LG respectively), 1996 (96.7 and 80.4 kg C ha⁻¹; OG, LG), and 2009 (22.19 and 10.25 kg C ha⁻¹; OG, LG) (Figure 2.6C and D).

Changes in variability of POC yields

A closer look at the variability of POC yields in our study sites suggests different responses to disturbances between the OG site and the LG site (Figure 2.6C and D). At the OG site variability in POC yields increased noticeably after 1996, mostly due to an increase in the frequency of low POC yields ($< 10^{-2} \text{ kg ha}^{-1}$) (Figure 2.6C). At the LG site, POC yield variability is larger (spanning about 4 orders of magnitude) compared to that observed at the OG site for almost the entire period analyzed (Figure 2.6D).

We examined changes in variability of POC yields at the three-week sampling scale. We observed that the range of variability increased from 1 to 2 and then to 3 orders of magnitude in the OG site after the storms in 1986 and 1996 respectively (Figure 2.7). At the LG site, the range of variability of POC yields increased from 2 to almost 4 orders of magnitude after the debris flow in 1986. Widening of the variability ranges persisted for several years (>5) and consisted mostly of an increase in the frequency of low POC yields (Figure 2.7). These observations suggest that changes in variability in POC yields in our study sites could depend on the interaction between disturbance and land-use history.

Changes in variability of POC yields were also linked to qualitative changes of the carbon content of the suspended sediments. In both sites, the highest POC yields were characterized by carbon-depleted sediments ($>5\% \text{TC}$) and the lowest yields by carbon-enriched sediments (Figure 2.7). Low POC yields were typically more enriched in carbon at the OG site ($>20\% \text{TC}$) than at the LG site ($<20\% \text{TC}$) (Figure 2.7).

Since POC yields integrate the seasonality already present in the discharge signal, the chemical composition of the particulate matter exported from our study sites reflects the superposition of opposite seasonal trends (Figure 2.8A). Carbon-depleted sediments were more frequent during the winter season in both watersheds (as shown by the negative correlation between $\% \text{TC}$ and winter season in our regression model), coinciding with high flows due to winter rainfall. Carbon-enriched sediments were more frequent during the summer season, coinciding with low flows and increased litterfall from conifer trees (Figure 2.4). Despite these similarities, carbon-depleted sediments were more readily entrained into the suspended load at the LG site than at the OG site (Figure 2.8A). Higher abundance of carbon-depleted sediments in the suspended load during winters could either represent contributions from deeper soil horizons in the watershed (i.e.

deeper erosion) or increases in stream transport capacity to mobilize carbon depleted sediments already available in the channel.

We used elemental composition (%TC vs TN:C ratios) as a proxy for potential sources of POC within the watersheds (Figure 2.8B). At the OG site, carbon-depleted sediments have higher TN:C ratios (>0.075) than carbon-enriched sediments (TN:C ratios as low as 0.03) suggesting contributions from distinct sources (e.g. soil organic matter vs. plant litter) (Figure 2.8B). In contrast, at the LG site, we found no relationship between carbon content and TN:C ratios; both carbon-depleted and carbon-enriched sediments exhibited TN:C ratios as low as 0.045 or as high as 0.12 (Figure 2.8B), suggesting no systematic contribution of specific sources to the observed POC yields. However, seasonal changes of contributing sources alone could not explain the widening of POC yield variability ranges in either watershed.

To better understand how long-term changes in the variability of POC yields influenced the carbon content of the sediments exported from our study sites, we analyzed the frequency distributions of POC yields (Figure 2.9). Due to the stochastic character of the sediment transport in our study sites, histograms of POC yields integrated over long periods of time could represent the material that was available for transport inside the stream channel over such a time. Besides the overall difference in variability observed between our study sites as described in previous sections, the histograms covering the entire period of analysis (1984-2015) showed that each category (or bin) of POC yield had a more heterogeneous composition at the OG site than at the LG site. Within the POC yield category with the highest frequency at both sites ($\sim 0.14 \text{ kg ha}^{-1}$), we observed contributions from sediments with carbon contents covering the entire range of %TC at the OG site; at the LG site the same POC yield category was mostly dominated by sediments with carbon contents between 12-17% (Figure 2.9). Contrasting patterns of POC yield compositions between the OG and LG sites were also observed at other yields either above or below the modal POC yield in the frequency distributions (Figure 2.9).

We also observed differences in POC yield composition for a given magnitude of POC export at shorter temporal scale (~ 5 years; Figure 2.10). Despite such differences, we observed that the shapes of the frequency distributions from our study sites became more similar after 1996. By separating the variables involved in the calculation of the POC yields, we found that frequency distributions of discharge calculated using the same time window followed a similar trend of convergent shapes for the OG and LG sites after 1996 (Supplementary Figure 2).

Discussion

Timber harvesting caused a significant reduction in particulate organic matter (POM) supply to the stream channel

Sediments exported from the OG site were more carbon-enriched and had a lower TN:C ratio than sediments from the LG site. Raw data also showed that these differences were more pronounced after the channel-scouring debris flow in 1986. Differences in the elemental composition of the POC exported from our study sites were significant even after accounting for the role of other influential variables like the concentration of suspended sediments or season. These results suggest a long-term effect of logging on the amount and type of the organic matter supplied to the stream channels.

Vegetation removal during timber harvesting results in significant reductions of litter inputs to the stream channel^{15,30}, and in a shift in the type and timing of these inputs going from a conifer-dominated to a riparian-dominated litterfall^{12,15,30}. In the Oregon Cascades region, red Alder (*Alnus rubra*) dominates the riparian zones of many small streams with disturbed channels and its litterfall peaks in the Fall. In contrast, in many old-growth forested streams, litterfall is dominated by conifer inputs (needles and cones) which are continuous throughout the year and exhibits peaks throughout the summer^{30,31}. Accordingly, we observed marked seasonality in the carbon content of sediments exported from the OG site (Figure 2.5D) and also fall and summer peaks in litterfall inputs (Figure 2.4), indicating that these changes in %TC were potentially signaling litter input dynamics.

Reduction in litter inputs can deplete channel POM stocks in less than 1 year and therefore the carbon concentration of exported sediments can be reduced as well³². Although in some streams, the recovery of riparian vegetation can be relatively rapid (<5 years)⁸, litter input from the re-established riparian fringe can take years to decades to refill in-stream POM pools³². In our study sites, the steep hillslopes merge directly into the channel providing no suitable habitat for riparian vegetation. Thus, the opportunity for a fast recovery of OM inputs is minimal and the duration of logging impacts on POC exports can persist for decades.

It is important to note that although our suspended sediment samples could carry a signal related to litter inputs into the streams, our measurements are indirect and at best indicative of temporal trends of coarse OM inputs. This is because particles larger than 1 mm were sieved in the

laboratory before filtering the water for suspended sediment analysis. On the other hand, particulate export from headwater streams in the study area is composed mostly of very fine POM (<53 μm)³¹ and the organic content of these sediments can be influenced by changes in the concentration of dissolved organic matter through flocculation or sorption^{18,33}. Furthermore, in the H.J. Andrews, DOM concentrations are significantly higher in streams draining old-growth forests than in those draining logged watersheds (including our study sites)¹⁷, and we found that DON was a significant predictor of %TC. However, the differences in carbon concentration in the sediments exported from our study sites remained even after accounting for the influence of DON, suggesting that they might be reflecting the overall reduction in particulate organic matter inputs to the streams resulting from logging.

A debris flow occurring 12 years after the logging treatment resulted in an unstable detrital pool at the LG site

Besides the differences in the amount of carbon associated to the sediments exported from our study sites, we also found significant differences in the TN:C ratios of these sediments, suggesting that the contributing sources of POC are different between the OG and LG site. Although elemental ratios by themselves cannot provide enough resolution into specific sediment sources, our observations strongly suggest that POC from the LG site might be derived from a mixed detrital pool characteristic of channels disturbed by debris flows³⁴ (i.e. the contribution of multiple sources typically carbon-depleted and with high TN:C ratios, Figure 2.8B).

At the LG site, significant export of wood residues from the logging treatment has occurred at the expense of the scouring of the stream channel^{22,35}. The rapid reduction of the woody detrital pool at the LG site provides a sense of the impact that these bedload pulses had on the stream channel between 1976 and the early 2000's. Timber harvesting reduced the amount of carbon stored in logs, snags, and stumps more than 50% (from 97 to 46 MgC ha^{-1})²². In the early 2000's this detrital pool was even smaller (21 MgC ha^{-1})¹⁷, most likely due to mobilization and decomposition^{21,36}. Terrestrial decomposition of coarse woody debris in the Pacific Northwest could account for up to 1% of losses from the woody detrital pool over the period of time considered here³⁷. In contrast, at least 7.8 MgC ha^{-1} were exported as bedload between 1976 and 1986. Furthermore, by assuming a 20% organic matter content in the minor debris flow of 1996, an additional of ~ 1.4 MgC ha^{-1} would have abandoned the basin as bedload. These estimations of carbon export are based on the material deposited in the collection basin downstream the gauging station at the LG site and do not account for the material that could have been flushed farther away or exported as

part of the coarse fraction of the suspended load. Yet, carbon exported as bedload represented at least ~37% of the total carbon lost from the detrital pool highlighting the extraordinary role of woody debris fluxes in the depletion of ecosystem carbon storage. The passage of debris flows through these small streams typically results in disordered channel units with lower retention of particulate organic matter, unstable soils on hillslopes, redistribution and exposure of old-decomposed detritus along the banks, and the accrual of benthic algae^{6,34}.

Channel structure modulates variability in quantity and quality of POC yields (and hence biogeochemical responses to disturbances)

Sediment routing processes had a significant effect on the quality of suspended sediments

The statistical significance of TSS as a predictor of %TC suggest a physical modulation of the quality of the sediments exported from our study sites. TSS was negatively related to %TC even after accounting for a potential dilution of the organic load during the winter. In larger streams or small mountainous river systems suspended sediments and POC concentrations are controlled by hydrology³⁸. Thus, in those fluvial environments, a dilution of the organic load with increasing discharge would be expected. However, researchers have found that the reduction of the organic content of suspended sediments during winters is most likely due to a replacement of sediment sources, from surficial to deep soil horizons or stream banks^{28,39}. Moreover, since suspended sediment concentrations in our study sites lack seasonal trends (Figure 2.2), the negative correlation between TSS and %TC points towards an influence of the stochastic sediment routing processes occurring at our study sites on the elemental composition of the POC yields.

Intra-annual variability of the carbon content of suspended sediments result from the superposition of stochastic sediment supply, seasonal litter inputs, and bank erosion.

In small headwater streams, sediment availability is governed by stochastic inputs of particulate material associated with natural and anthropogenic disturbances forcings like storms, floods, and timber harvesting. Large inputs of particulate material due to debris flows become the dominant mechanisms of sediment supply in the long term³². In the short-term, and in the absence of inputs from mass wasting processes, sediments might be readily supplied by immediate and unstable sediment sources (e.g. stream banks or stream bed)³⁹. It would be expected that the particles supplied to the channel from these sources would be typically carbon-depleted, while the carbon-enriched particles would be supplied by litterfall. Indeed, we found that suspended sediment concentrations were good predictors of carbon-depleted particles (%TC>20) while carbon-enriched particles were better predicted by variables with strong seasonal behavior (e.g. dissolved

silica). These results stress the importance of litterfall inputs during low flow conditions and of bank/channel erosion processes at high flow conditions on regulating the chemical composition of POC yields on an annual basis. Yet, headwater ecosystems also store sediments from previous mass wasting processes which³⁵, depending on their proximity to the stream can become significant sources of sediments or even overwhelm streamflow by literally burying a portion of the channel³⁴. However, the effect of these interactions on regulating the variability of POC yields, transcend the annual scale. In the case of our study sites, a long-term perspective is required to explain the observed widening of POC yield variability ranges observed at the multiannual scale, particularly after disturbances.

Long-term variability in POC yields reveal contrasting channel features between the OG and LG sites

To understand long-term changes in POC yield variability, we also explored a probabilistic representation of the yields (Figure 2.9). We assumed that under that over longer periods of time, frequency distributions of POC exports and their associated carbon content would capture channel processes related to the overall availability of particulate material and its contribution to the suspended load. If so, differences in POC yield frequency distributions could be indicative of the dominance of different processes regulating POC yields at our study sites. For instance, the suspended load exported from a retentive channel would be more heterogeneous in terms of its elemental composition than sediments exported from a channel dominated by erosional processes. This is because in retentive channels structures like debris dams, would accumulate a higher diversity of organic matter particles that would be carried in suspension as the transport capacity of the stream increases³². In contrast, in a channel where the banks are more heavily eroded, or where carbon-depleted particles are more available due to previous mass wasting processes, particle entrainment should be more abrupt and leading rapidly towards an increase in carbon-depleted particles in the suspended sediments³⁹. In other words, in an erosion-driven channel, we would expect a more predictable decrease in carbon content with increases in POC yields.

After examining the long-term frequency distributions of POC yields from our study sites we found that at the OG site a wider variety of particles were available to be exported at a given range of POC yields (bin) (Figure 2.9). At the LG site, almost specific categories of C-depleted particles become available with increasing POC yields. Also, at the LG site, the entrainment of those C-depleted particles occurred at a faster rate than at the OG site during the fall season (Figure

2.8A). Overall, these results confirmed our assumption about using POC yields frequency distributions to explore changes in stream channel dynamics as connected to the export of POC.

The frequency distributions of POC yields and other fluxes diverged between our study sites in response to disturbances

To gain insights into the mechanisms behind the observed changes in POC export variability, we compare POC yield frequency distributions at a higher temporal resolution (~5 years) by means of a divergence analysis (see supplementary methods: Estimation of Kullback-Liebler's Divergence ($Divergence_{KL}$)). Briefly, divergence analysis compares two frequency distributions on a bin by bin basis. It measures the goodness of fit between those distributions by literally superimposing their shapes and estimating the amount of information lost after approximating one distribution by another. This analysis was motivated originally by the failure of certain statistical tests to meet the Fisher's information sufficiency criterion: "that the statistic chosen should summarize the whole of the relevant information supplied by the sample"⁴⁰. This is particularly the case of standard statistical tests that assume variance homogeneity when the populations examined are heteroscedastic⁴¹. We observed that changes in variability of POC yields were linked to changes in variability in the variables used for its calculation, particularly discharge (Supplementary Figure 2). Thus, we started our divergence analysis by using discharge and suspended sediment data as shown in Figure 2.11.

The frequency distributions of discharge and suspended sediments diverged between our study sites after 1975 in response to the logging treatment. Hydrologic divergence (Q-Divergence) was relatively small while divergence in terms of suspended sediments (TSS-Divergence) was quite large in comparison to pre-logging conditions (Figure 2.11). In both cases, this period of coupled divergence in discharge and suspended sediments ended around 1982. A 5-year period of noticeable impacts of timber harvesting on water quantity and quality are commonly reported in the literature⁴².

After 1982, and contrary to what could be expected from previous findings, both Q-and TSS-Divergences between the LG site and the OG site increased dramatically and abruptly over alternating periods of time (Figure 2.11). Between 1982 and 1987, Q-Divergence was ~2 orders of magnitude higher than during pre-logging conditions. Then, it decreased between 1987 and 1992 and increased again, up to ~2.5 orders of magnitude, between 1992 and 1996. TSS-Divergence followed an opposite pattern to that of Q-Divergence by decreasing between two

alternated periods 1982-1987 and 1992-1996. TSS-Divergence increased between 1987 and 1992 and after 1996 until 2003. Q-Divergence was sensitive to increases in summer streamflow deficits⁴¹ (Figure 2.11) while TSS-Divergence was sensitive to high sediment pulses (data not shown). Summer streamflow deficits were more frequent at the LG site than at the OG site. However, the increase in TSS-Divergence after 1996 was due to higher concentrations of suspended sediments at the OG site (Figure 2.11, Supplementary Figure 2). Moreover, our data suggest that after the record flooding event in 1996 both the entrainment of sediment particles during the fall (Supplementary Figure 3) and the frequency of summer streamflow deficits increased at the OG site.

We extended the divergence analysis to other variables involved in particulate fluxes including POC yields. Surprisingly, we observed a strong episode of convergence between our study sites after 1996. This convergence episode involved not only discharge and particulate exports (sediment and POC yields) but also the carbon content of the suspended sediments (Figure 2.12). Although particulate fluxes depend directly on discharge, divergence in sediment and POC yields do not follow Q-Divergence due to the contrasting pattern of its temporal changes compared to those of TSS-Divergence. Nonetheless, all frequency distributions (except for TSS) strongly converge after 1996's flooding event (Figure 2.12).

The divergent and convergent behavior of the different fluxes between our study sites reveal a complex structure behind the responses to disturbance from these headwater ecosystems. A more detailed analysis of the discharge and sediment transport signals falls out of the scope of this chapter. However, we advance a preliminary hypothesis linking the changes in variability of the different signals included in the divergence analysis. Our data suggest, that disturbances induced changes in stream channel structure via enhanced supply of sediments from the hillslope that were linked to further alterations in streamflow. The most noticeable consequence of these alterations was an increase in the frequency of summer streamflow deficits⁴¹. We observed that summer stream flow deficits increased after disturbances in both watersheds, but they were overall more frequent at the LG site. During periods of increased summer streamflow deficits, carbon supplied by litterfall becomes the "active" sediment in the channel, resulting in higher C contents in extremely low POC yields.

Temporal changes in divergence suggest that variability in water and particle fluxes from our study sites was highly sensitive to disturbances and responded differently to similar forcings depending

on previous land use history (i.e. Old-growth vs. logged) (Figure 2.12). Since material fluxes encompass interactions between discharge, sediment transport, and organic matter dynamics within the stream channel, changes in stream channel structure might modulate the magnitude of responses to disturbance in these headwater ecosystems. Also, changes in variability were still evident when integrated over a multiannual temporal scale, as illustrated by the episode of strong convergence in 1996. Therefore, the stream channel might also behave as a source of biogeochemical signals of response to disturbance.

In his conceptual model about process-domains⁴³, D. Montgomery had already proposed that at headwater locations, the physical structure of the stream channel is more sensitive and responsive to disturbance than the actual sediment yields. The process-domains model has been the basis for the formulation of new conceptual models in stream ecology (e.g. the concept of riverscapes)⁴⁴. But the predictions from these models as related to headwater ecosystems functioning have remained largely untested due to the lack of empirical data. Recent support to those hydro-geomorphic descriptions of headwater streams have come from short-term paired watershed experiments in the Oregon Coast Range. These recent findings have shown that geomorphology could modulate the suspended sediment signal in small headwater ecosystems and that because such a modulation the impacts of logging on watersheds that are more vulnerable to clear-cutting³⁵ might be more difficult to detect. Yet, to reveal the specific mechanisms of stream channel response to the interactions between geomorphology and climate in the context of disturbances, long term records of biogeochemical signals are critical but unfortunately rare. Here, we have illuminated some physical processes modulating the export of particulate material by analyzing a unique reconstruction of 30-years of particulate organic carbon yields from headwater streams in the Oregon Cascades.

We found that the superposition of stochastic sediment inputs, driven by either natural or anthropogenic disturbance forcings, seasonal litterfall, and sediment routing processes result in complex biogeochemical signals or response to disturbance from headwater streams ecosystems. The effects of such a superposition on stream channel functioning are highly dynamic and depend on the temporal scale of the analysis. From a short-term perspective, channel structure modulates the production of response signals to minor disturbances like annual floods. Yet, depending on previous land-use history, a stream channel might behave as an erosion-dominated (e.g. LG site) or as more retentive element of the landscape (e.g. OG site). Thus, under quiescent conditions, headwater streams function as sinks of particulate organic

carbon⁴⁵. From a long-term perspective, major disturbances dramatically re-structure the stream channel to facilitate the massive export of particulate materials. Under such a scenario headwater streams function as sources of particulate organic carbon¹⁵.

Conclusions

The primary impact of logging on POC dynamics was an overall reduction in the organic matter supply to the stream channel, as in many other logged headwater streams^{12,15,46}. The lack of riparian vegetation that could temporarily supply the stream with allochthonous material enhanced this type of impact in our study sites. On the other hand, a more complex impact seems to have resulted from the interaction of the legacies of the logging treatment and the natural disturbance regime (e.g. storms, floods). A debris flow mobilizing logging residues just 12 years after the treatment application severely scoured the stream channel and apparently remodeled the structure of the detrital pool at the LG site, altering the elemental composition of the suspended sediments (e.g. significant differences in TN:C ratios). Our analysis suggests that channel structure modulates the quantity and quality of POC exported from these headwater stream and that changes in channel structure could be inferred from changes in variability of probability distribution of discharge and sediment yields. We used elemental composition data to illuminate sediment routing and other stream channel processes could affect the source/sink behavior of headwater ecosystems in the context of POC exports. Yet, but more detailed analyses are needed to gain further insights in the ecological implications of such a dynamic behavior and to link it to other components of the aquatic-terrestrial carbon cycle (e.g. CO₂ evasion, DOC dynamics, total C exports, etc.)⁴⁰. Previous studies have provided evidence that geology and geomorphology could modulate responses to timber harvesting. Now, we have evidence that in the short-term channel structure modulates responses to logging and other disturbances by changes in the availability of particles that could be exported. In the long-term, disturbances modulate channel structure and changes in variability in particulate matter export becomes the biogeochemical signal of response to those disturbances.

Bibliography

1. Downing, J. A. *et al.* Global abundance and size distribution of streams and rivers. *Inland Waters* **2**, 229–236 (2012).
2. Freeman, M. C., Pringle, C. M. & Jackson, C. R. Hydrologic Connectivity and the Contribution of Stream Headwaters to Ecological Integrity at Regional Scales¹. *JAWRA Journal of the American Water Resources Association* **43**, 5–14 (2007).
3. Aufdenkampe, A. K. *et al.* Riverine coupling of biogeochemical cycles between land, oceans, and atmosphere. *Frontiers in Ecology and the Environment* **9**, 53–60 (2011).
4. Argerich, A. *et al.* Comprehensive multiyear carbon budget of a temperate headwater stream. *J. Geophys. Res. Biogeosci.* **121**, 2015JG003050 (2016).

5. Hilton, R. G. Climate regulates the erosional carbon export from the terrestrial biosphere. *Geomorphology* **277**, 118–132 (2017).
6. Swanson, F. J., Johnson, S. L., Gregory, S. V. & Acker, S. A. Flood Disturbance in a Forested Mountain Landscape. *BioScience* **48**, 681–689 (1998).
7. Swanson, F. J., Fredricksen, R. L. & McCorison, F. M. Material transfer in a Western Oregon forested watershed. in *Analysis of coniferous forest ecosystems in the western United States*. 233–266 (Hutchinson Ross Publishing Company, 1982).
8. Hilton, R. G., Galy, A. & Hovius, N. Riverine particulate organic carbon from an active mountain belt: Importance of landslides. *Global Biogeochem. Cycles* **22**, GB1017 (2008).
9. Clark, K. E. *et al.* Storm-triggered landslides in the Peruvian Andes and implications for topography, carbon cycles, and biodiversity. *Earth Surface Dynamics* **4**, 47–70 (2016).
10. Bywater-Reyes, S., Segura, C. & Bladon, K. D. Geology and geomorphology control suspended sediment yield and modulate increases following timber harvest in temperate headwater streams. *Journal of Hydrology* **548**, 754–769 (2017).
11. Wondzell, S. M. & Swanson, F. J. Floods, channel change, and the hyporheic zone. *Water Resources Research* **35**, 555–567 (1999).
12. Webster, J., Benfield, E. J., Golladay, S. W. & McTammany, M. E. Recovery of particulate organic matter dynamics in a stream draining a logged watershed. In: *Swank, Wayne T.; Webster, Jackson R., comps., eds. Long-term response of a forest watershed ecosystem. Clearcutting in the southern Appalachian*. Oxford University Press: 156-176. 156–176 (2014).
13. Zhang, M. *et al.* A global review on hydrological responses to forest change across multiple spatial scales: Importance of scale, climate, forest type and hydrological regime. *Journal of Hydrology* **546**, 44–59 (2017).
14. Lajtha, K. & Jones, J. Forest harvest legacies control dissolved organic carbon export in small watersheds, western Oregon. *Biogeochemistry* (2018). doi:10.1007/s10533-018-0493-3
15. Webster, J. R., Golladay, S. W., Benfield, E. F., D'Angelo, D. J. & Peters, G. T. Effects of Forest Disturbance on Particulate Organic Matter Budgets of Small Streams. *Journal of the North American Benthological Society* **9**, 120–140 (1990).
16. Perry, T. D. & Jones, J. A. Summer streamflow deficits from regenerating Douglas-fir forest in the Pacific Northwest, USA: Summer streamflow deficits from regenerating Douglas-fir forest. *Ecohydrology* **10**, e1790 (2017).
17. Johnson, S. L. *et al.* Stream chemistry concentrations and fluxes using proportional sampling in the Andrews Experimental Forest, 1968 to present. *Andrews Forest* (2018). Available at: <http://andlter.forestry.oregonstate.edu/data/abstract.aspx?dbcode=CF002>. (Accessed: 25th October 2018)
18. Naiman, R. J. & Sedell, J. R. Characterization of Particulate Organic Matter Transported by Some Cascade Mountain Streams. *Journal of the Fisheries Research Board of Canada* **36**, 17–31 (1979).
19. Sedell, J. R., Naiman, R. J., Cummins, K. W., Minshall, G. W. & Vannote, R. L. Transport of particulate organic material in streams as a function of physical processes: With 3 figures and 2 table in the text. *SIL Proceedings, 1922-2010* **20**, 1366–1375 (1978).
20. van Verseveld, W. J., McDonnell, J. J. & Lajtha, K. The role of hillslope hydrology in controlling nutrient loss. *Journal of Hydrology* **367**, 177–187 (2009).
21. Dyrness, T. *et al.* FLOOD OF FEBRUARY 1996 IN THE H. J. ANDREWS EXPERIMENTAL FOREST. 34
22. Cromack Jr., K., Swanson, F. J. & Grier, C. C. A comparison of harvesting methods and their impact on soils and environment in the Pacific Northwest. in *Forest soils and land use* 449-476. (Department of Forest and Wood Sciences, Colorado State University, 1978).
23. Gecy, J. L. & Wilson, M. V. Initial Establishment of Riparian Vegetation after Disturbance by Debris Flows in Oregon. *American Midland Naturalist* **123**, 282 (1990).

24. Means, J. E., MacMillan, P. C. & Cromack Jr., K. Biomass and nutrient content of Douglas-fir logs and other detrital pools in an old-growth forest, Oregon, U.S.A. *Canadian Journal of Forest Research* **22**, 1536–1546 (1992).
25. Smith, J. C. Particulate organic carbon mobilisation and export from temperate forested uplands. (University of Cambridge, 2013).
26. Perdue, E. M. & Koprivnjak, J.-F. Using the C/N ratio to estimate terrigenous inputs of organic matter to aquatic environments. *Estuarine, Coastal and Shelf Science* **73**, 65–72 (2007).
27. Hastings, R. H., Goñi, M. A., Wheatcroft, R. A. & Borgeld, J. C. A terrestrial organic matter depositor on a high-energy margin: The Umpqua River system, Oregon. *Continental Shelf Research* **39**, 78–91 (2012).
28. Hatten, J. A., Goñi, M. A. & Wheatcroft, R. A. Chemical characteristics of particulate organic matter from a small, mountainous river system in the Oregon Coast Range, USA. *Biogeochemistry* **107**, 43–66 (2012).
29. Richardson, K. N. D., Hatten, J. A. & Wheatcroft, R. A. 1500 years of lake sedimentation due to fire, earthquakes, floods and land clearance in the Oregon Coast Range: geomorphic sensitivity to floods during timber harvest period. *Earth Surface Processes and Landforms* **43**, 1496–1517 (2018).
30. Frady, C., Johnson, S. & Li, J. Stream Macroinvertebrate Community Responses as Legacies of Forest Harvest at the H.J. Andrews Experimental Forest, Oregon. *for sci* **53**, 281–293 (2007).
31. Abee, A. Nutrient cycling in throughfall and litterfall in 450-year-old Douglas-fir stands. *Proceedings-Research on coniferous forest ecosystems-A symposium. Bellingham, Washington (March 23-24)* 11 (1972).
32. Eggert, S. L., Wallace, J. B., Meyer, J. L. & Webster, J. R. Storage and export of organic matter in a headwater stream: responses to long-term detrital manipulations. *Ecosphere* **3**, 1–25 (2012).
33. Hernes, P. J., Robinson, A. C. & Aufdenkampe, A. K. Fractionation of lignin during leaching and sorption and implications for organic matter “freshness”. *Geophys. Res. Lett.* **34**, L17401 (2007).
34. Lamberti, G. A., Gregory, S. V., Ashkenas, L. R., Wildman, R. C. & Moore, K. M. S. Stream Ecosystem Recovery Following a Catastrophic Debris Flow. *Canadian Journal of Fisheries and Aquatic Sciences* **48**, 196–208 (1991).
35. Hood, E., Gooseff, M. N. & Johnson, S. L. Changes in the character of stream water dissolved organic carbon during flushing in three small watersheds, Oregon. *Journal of Geophysical Research: Biogeosciences* **111**, (2006).
36. Abdelnour, A., McKane, R., Stieglitz, M., Pan, F. & Cheng, Y. Effects of harvest on carbon and nitrogen dynamics in a Pacific Northwest forest catchment: EFFECTS OF HARVEST ON CARBON AND NITROGEN. *Water Resources Research* **49**, 1292–1313 (2013).
37. Janisch, J. E. & Harmon, M. E. Successional changes in live and dead wood carbon stores: implications for net ecosystem productivity. *Tree Physiol.* **22**, 77–89 (2002).
38. Wheatcroft, R. A., Goñi, M. A., Hatten, J. A., Pasternack, G. B. & Warrick, J. A. The role of effective discharge in the ocean delivery of particulate organic carbon by small, mountainous river systems. *Limnol. Oceanogr.* **55**, 161–171 (2010).
39. Johnson, E. R. Particulate organic matter (POM) composition in stream runoff following large storm events: role of POM sources, particle size, and event characteristics. (University of Delaware, 2017).
40. Kullback, S. & Leibler, R. A. On Information and Sufficiency. *The Annals of Mathematical Statistics* **22**, 79–86 (1951).
41. Alila Younes, Kuraś Piotr K., Schnorbus Markus & Hudson Robert. Forests and floods: A new paradigm sheds light on age-old controversies. *Water Resources Research* **45**, (2009).

42. Moore, R. D. & Wondzell, S. M. Physical Hydrology and the Effects of Forest Harvesting in the Pacific Northwest: A Review¹. *JAWRA Journal of the American Water Resources Association* **41**, 763–784 (2005).
43. Montgomery, D. R. Process Domains and the River Continuum¹. *JAWRA Journal of the American Water Resources Association* **35**, 397–410 (1999).
44. Allan, J. D. Landscapes and Riverscapes: The Influence of Land Use on Stream Ecosystems. *Annual Review of Ecology, Evolution, and Systematics* **35**, 257–284 (2004).
45. Wohl, E., Dwire, K., Sutfin, N., Polvi, L. & Bazan, R. Mechanisms of carbon storage in mountainous headwater rivers. *Nature Communications* **3**, 1263 (2012).
46. Webster, J. R., Meyer, J. L., Wallace, J. B. & Benfield, E. F. Organic Matter Dynamics in Hugh White Creek, Coweeta Hydrologic Laboratory, North Carolina, USA. *Journal of the North American Benthological Society* **16**, 74–78 (1997).
47. Bozdogan, H. Akaike's Information Criterion and Recent Developments in Information Complexity. *Journal of Mathematical Psychology* **44**, 62–91 (2000).
48. Scott, D. W. On Optimal and Data-Based Histograms. *Biometrika* **66**, 605 (1979).

Figures and tables

Figure 2.1. Watershed 10 prior and after harvesting in 1975. A and B are views from Mona Creek Road (East). C. Main channel prior to harvesting in 1975. D. Post debris flow channel (February 22, 1986). Photographs by Fred Swanson-Andrews Forest Image Library (H. J. Andrews Experimental Forest).

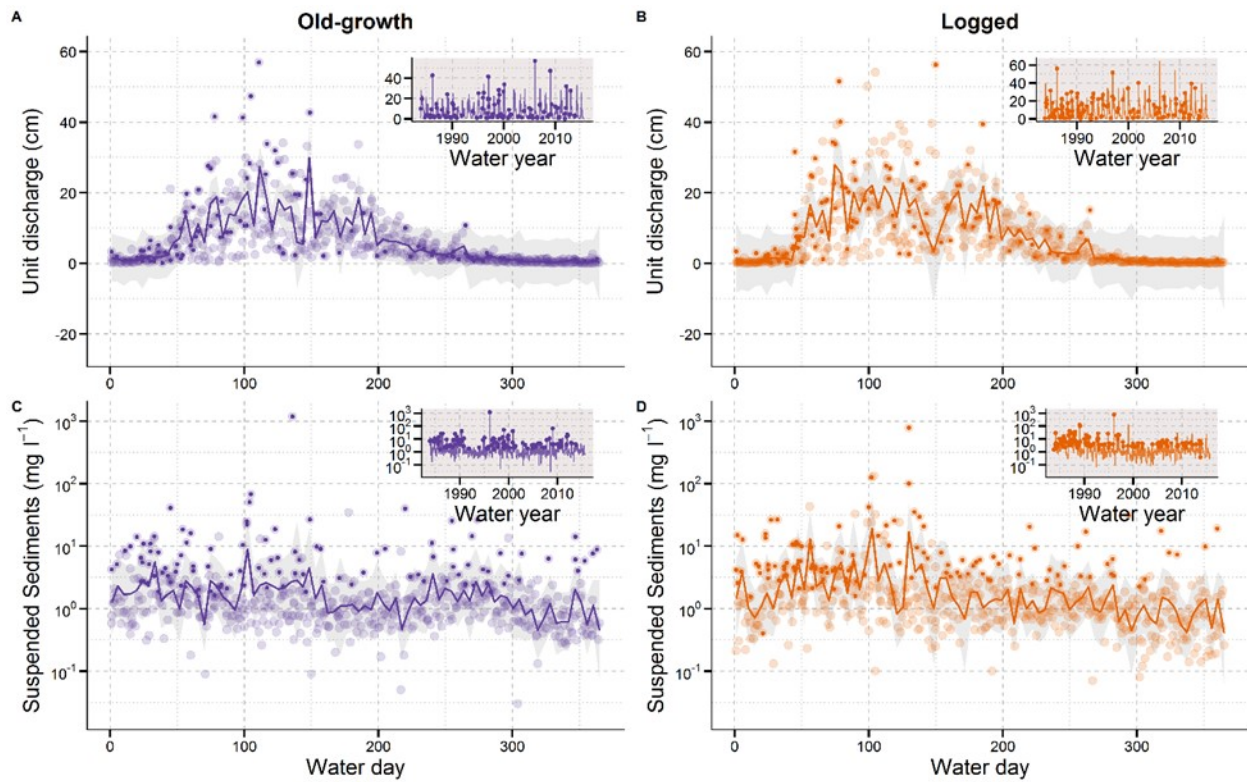


Figure 2.2. Suspended sediment samples collected from two headwater streams draining an old-growth forest (WS09-OG site) and a 100%-logged watershed (WS10-LG site) in the H. J. Andrews Experimental Forest. Sampling points (solid dots) are represented along the population of water days sampled as part of the regular long-term sampling program between 1984 and 2014 (transparent dots). Panels on top depict sampling points along unit discharge data. Panels in the bottom depict sampling points along suspended sediment data. Solid lines represent a smoothed trend estimated with LOESS regression (smoothing parameter (α)=0.02) and the light-shaded region represents 95% confidence intervals. Small inserts inside each panel show the sampling scheme along the entire time series for each corresponding variable.

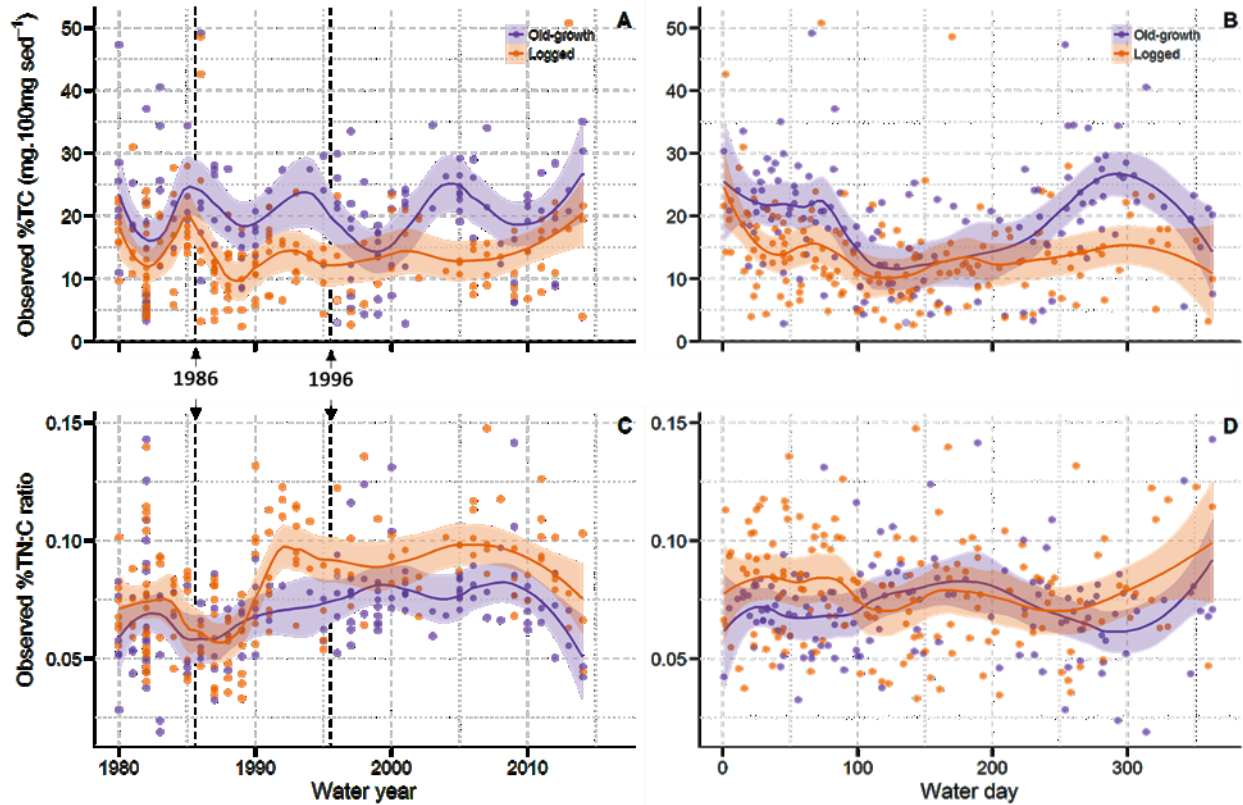


Figure 2.3. Comparison of the carbon content (%TC) and TN:C ratios of sediments from two headwater streams draining an old-growth forest (WS09-OG site) and a 100%-logged watershed (WS10-LG site) in the H. J. Andrews Experimental Forest. Top panels: Annual (A) and seasonal (B) changes in %TC. Bottom panels: Annual and seasonal changes in TN:C ratios (C and D, respectively). Dotted lines on the left of panels A and C separating samples collected before 1986's debris flow at the LG site and 1996's flooding event (affecting both watersheds). Solid-thick lines represent a smoothed trend estimated with LOESS regression (smoothing parameter $\alpha=0.35$, the light-shaded region represents 95% confidence intervals).

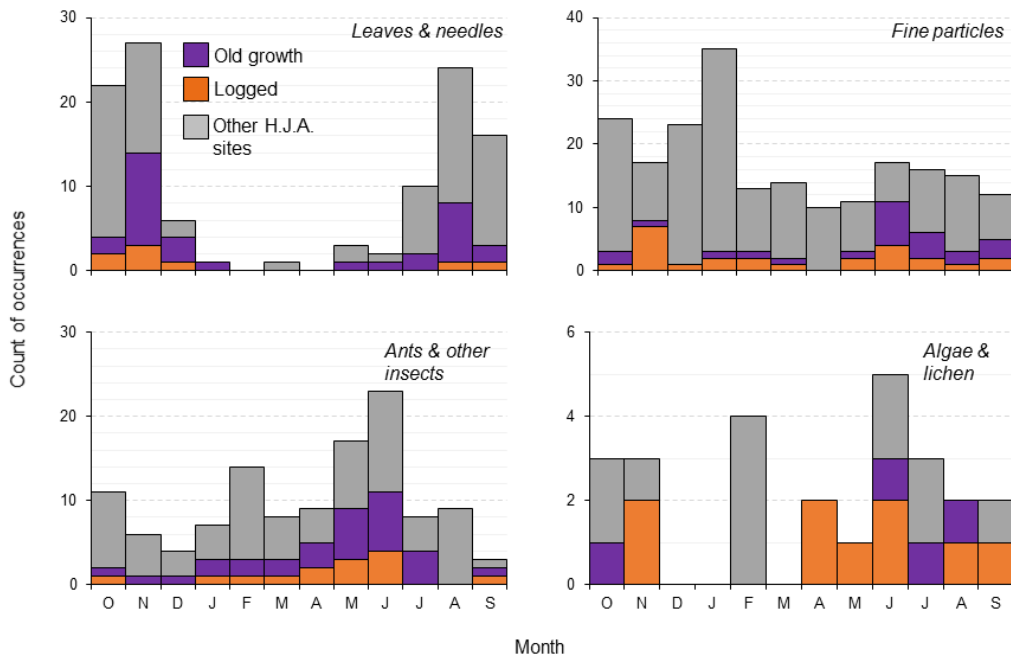


Figure 2.4. Seasonal patterns of different types of particulate material found at the automatic sampling stations (deposited in the bottom of collection basins) from different experimental watersheds (including our study sites) within the H. J. Andrews Experimental Forests. The inventory of occurrences is based on a compilation of 20+ years (1993-2016) of field notes. (Notes supplied by Sherri Johnson, H.J. Andrews Experimental Forest).

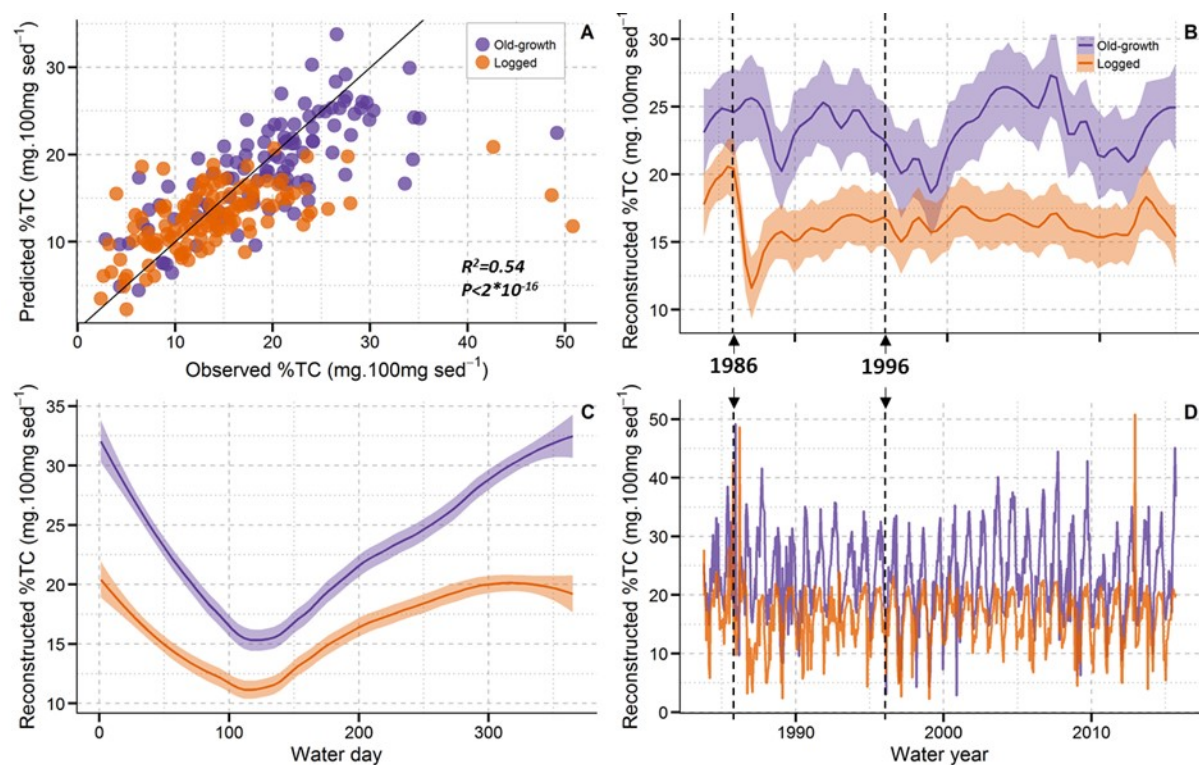


Figure 2.5. Reconstruction of the carbon content (%TC) of suspended sediments by using a multiple regression model for two headwater streams draining an old-growth forest (WS09-OG site) and a 100%-logged watershed (WS10-LG site) in the H. J. Andrews Experimental Forest. (A) predicted vs. observed values. B-D Reconstructed (observed + modeled data) indexed by water year, water day and three-week sampling period respectively. Solid-thick lines in panels B and C represent a smoothed trend estimated with LOESS regression (smoothing parameter (α) = 0.35 (B) and 0.5(C)); the light-shaded region represents 95% confidence intervals). Dotted black lines on panels B and D separating time periods before 1986's debris flow at the LG site and 1996's flooding event (affecting both watersheds).

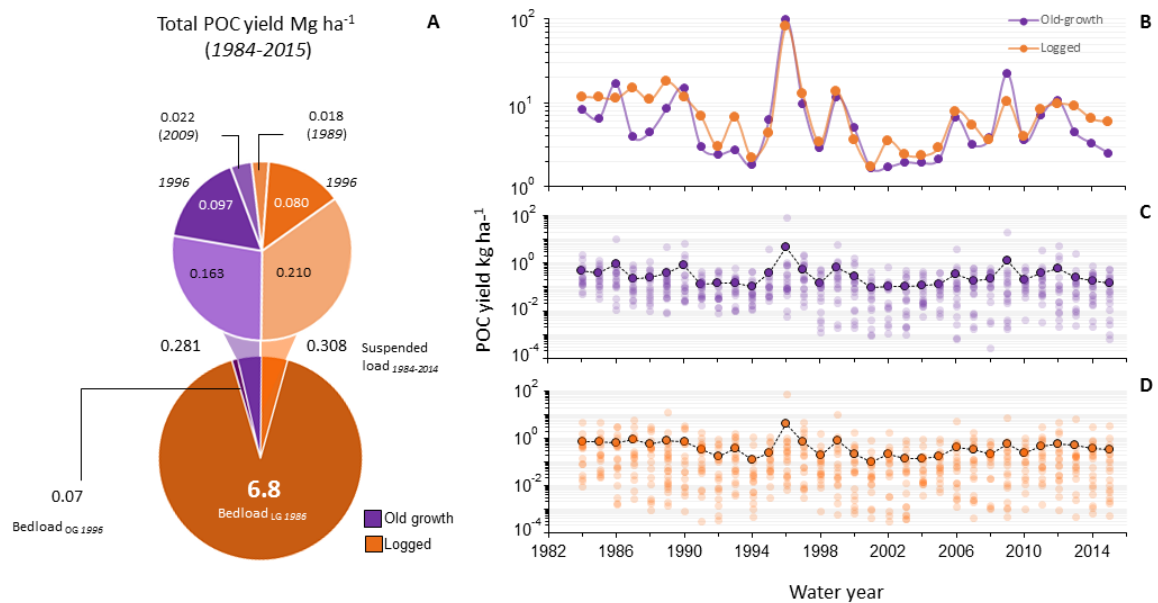


Figure 2.6. Particulate organic carbon exports (POC yields) from two headwater streams draining an old-growth forest (WS09-OG site) and a 100%-logged watershed (WS10-LG site) in the H. J. Andrews Experimental Forest. **A.** Total POC exported between 1984-2015, excluding and including a channel-scouring debris flow affecting the LG site in Feb-1986. **B.** Total annual yields per site. **C -D.** Average annual POC yields (solid points) from the OG and LG sites respectively. Translucent points showing all measurements used in the calculation of the annual average.

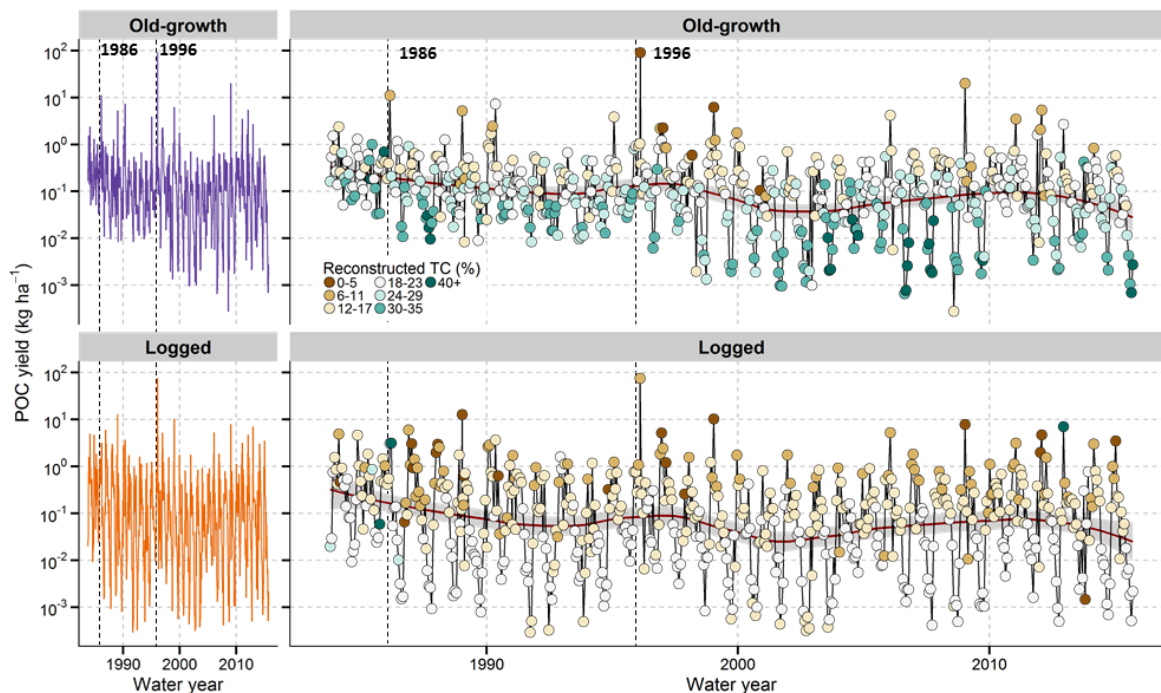


Figure 2.7. Particulate organic carbon (POC) yields and their average carbon content from two headwater streams draining an old-growth forest (WS09-OG site) and a 100%-logged watershed (WS10-LG site) in the H. J. Andrews Experimental Forest. Panels on the left showing yields only. Panels on the right showing the range for the average carbon content used in the calculation of POC yields (color scale). Solid-thick lines in panels on the right represent a smoothed trend estimated with LOESS regression (smoothing parameter (α) = 0.4; the light-shaded region represents 95% confidence intervals). Dashed lines in black separating periods prior to flooding events in 1986 and 1996. The number of categories for %TC was initially calculated as the number of bins required to represent the data in a histogram (following D. W. Scott's formula: $3.49 * SD_{\%TC} * n^{-1/3} = 15$) but it was divided in half for clarity.

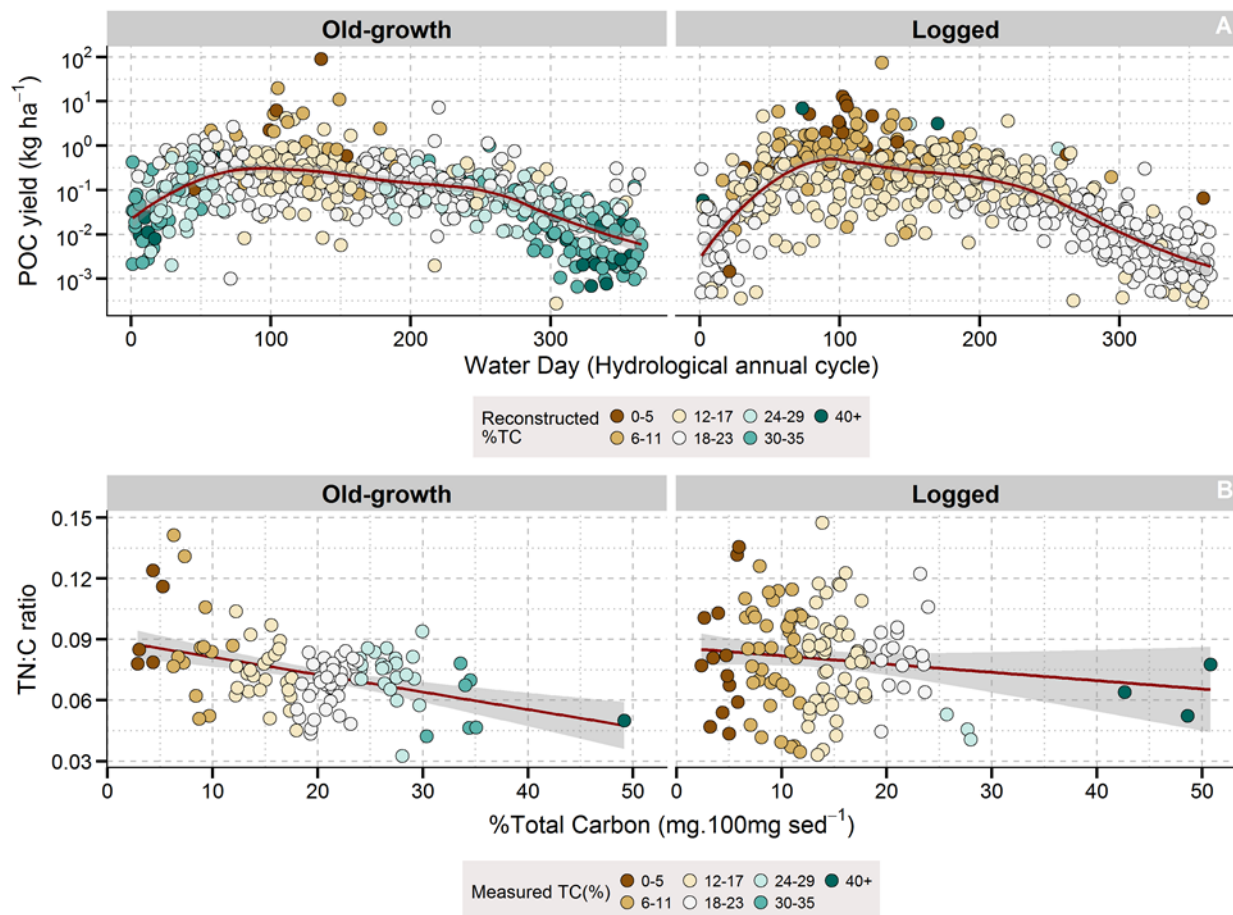


Figure 2.8. Long-term (1984-2015) seasonality (A) and elemental composition (B) of particulate organic carbon (POC) exported from two headwater streams draining an old-growth forest (WS09-OG site) and a 100%-logged watershed (WS10-LG site) in the H. J. Andrews Experimental Forest. Solid, thick, red lines represent smoothed trends estimated with LOESS regression (smoothing parameter (α)=0.5, only for A; the light-shaded region represents 95% confidence intervals). Note that color scales reflecting carbon content use reconstructed and measured %TC in A and B respectively. Qualitative %TC categories were determined as in Figure 2.7.

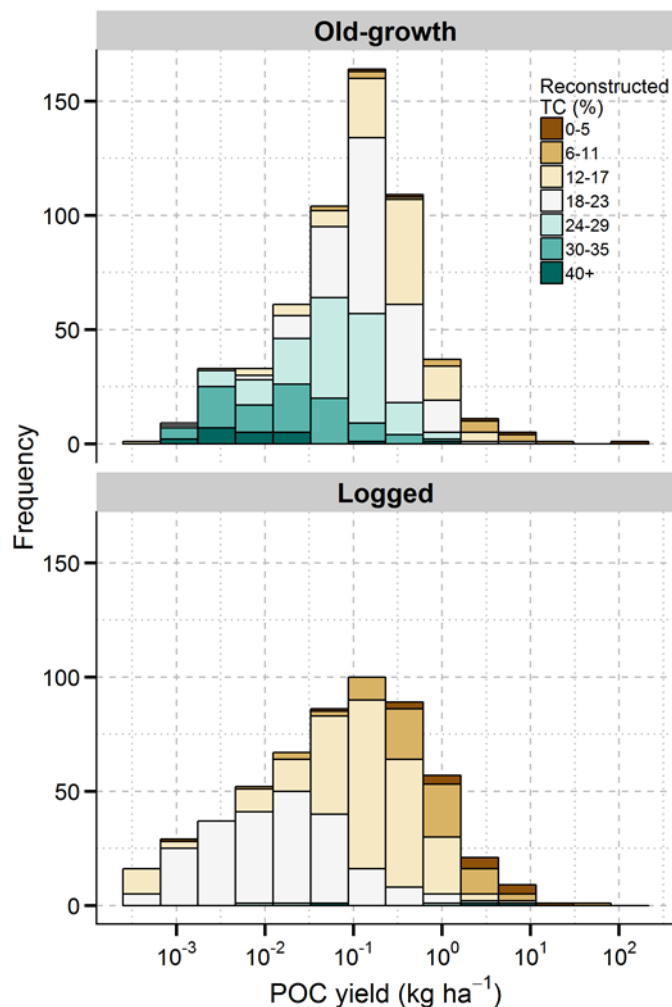


Figure 2.9. Long-term (1984-2015) frequency distribution of particulate organic carbon (POC) yields and their average carbon content from two headwater streams draining an old-growth forest (WS09-OG site) and a 100%-logged watershed (WS10-LG site) in the H. J. Andrews Experimental Forest. The bin width was calculated as: $3.49 * SD_{POC\ yield} * n^{-1/3}$ following to the method described by D. W. Scott. Qualitative %TC categories were determined with the same method and divided in half for clarity (as in Figure 2.7).

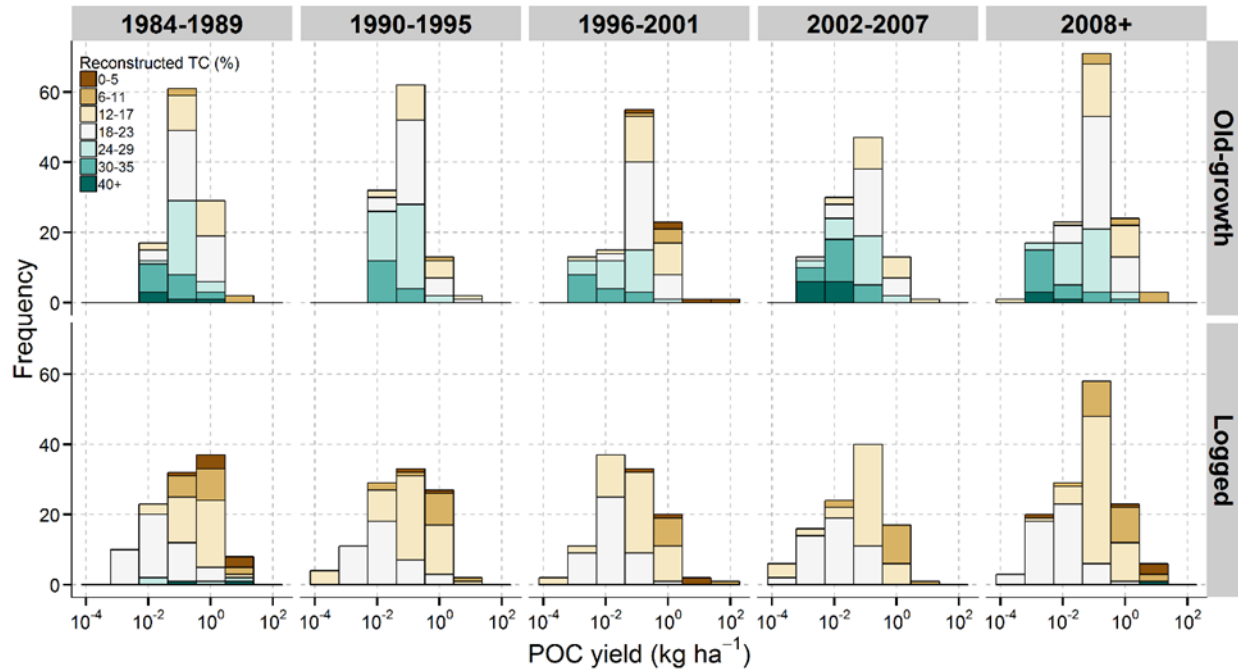


Figure 2.10. 5-year window histograms of particulate organic carbon (POC) loads and their average carbon content from two headwater streams draining an old-growth forest (WS09-OG site) and a 100%-logged watershed (WS10-LG site) in the H. J. Andrews Experimental Forest. The bin width and the qualitative categories for %TC were calculated as in Figure 2.9.

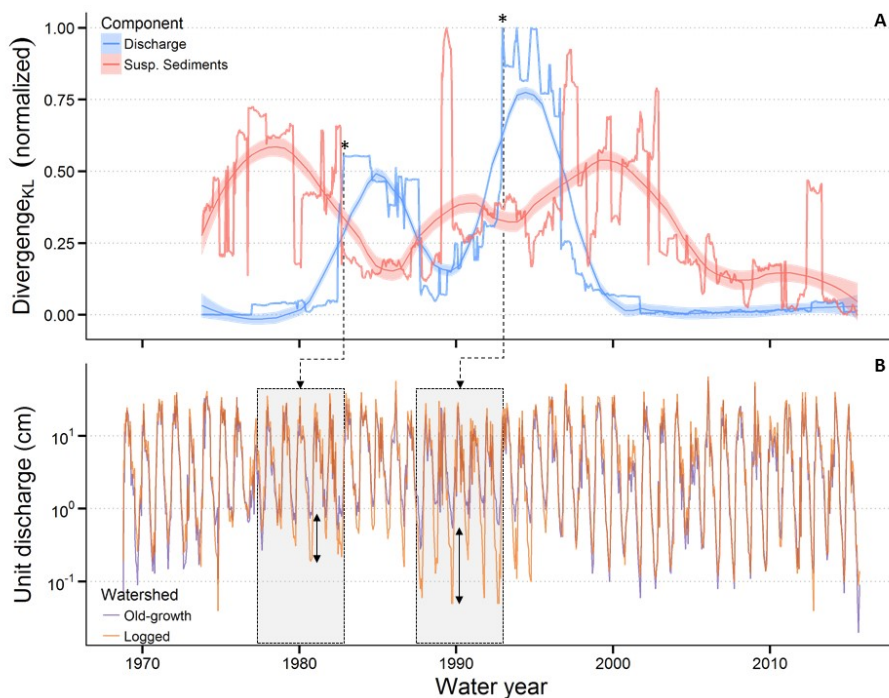


Figure 2.11. Divergence analysis of long-term trends of discharge and suspended sediments from two headwater streams draining an old-growth forest (WS09-OG site) and a 100%-logged watershed (WS10-LG site) in the H. J. Andrews Experimental Forest. A. Kullback-Liebler's Divergence ($Divergence_{KL}$) compares frequency distributions with irregular shapes. Lower divergence values indicate that frequency distributions are more similar in terms of their shapes and mean values. B. We used a running window of 5 years (light gray rectangles) to calculate frequency distributions of discharge and suspended sediments (data not shown) along the 1969-2015 period. Thus, each data point along the $Divergence_{KL}$ time series, represents the divergence between frequency distributions of a given variable over the previous five years (example points marked with stars). Due to the size of the window, the first point in the $Divergence_{KL}$ time series corresponds to the period 1969-1974. Solid-shaded lines represent a smoothed trend of divergence estimated with LOESS regression (smoothing parameter (α) = 0.3 or ~10 years; 95% confidence intervals). Divergence in discharge was sensitive to the increase in the frequency of summer streamflow deficits at the LG site (double headed arrows).

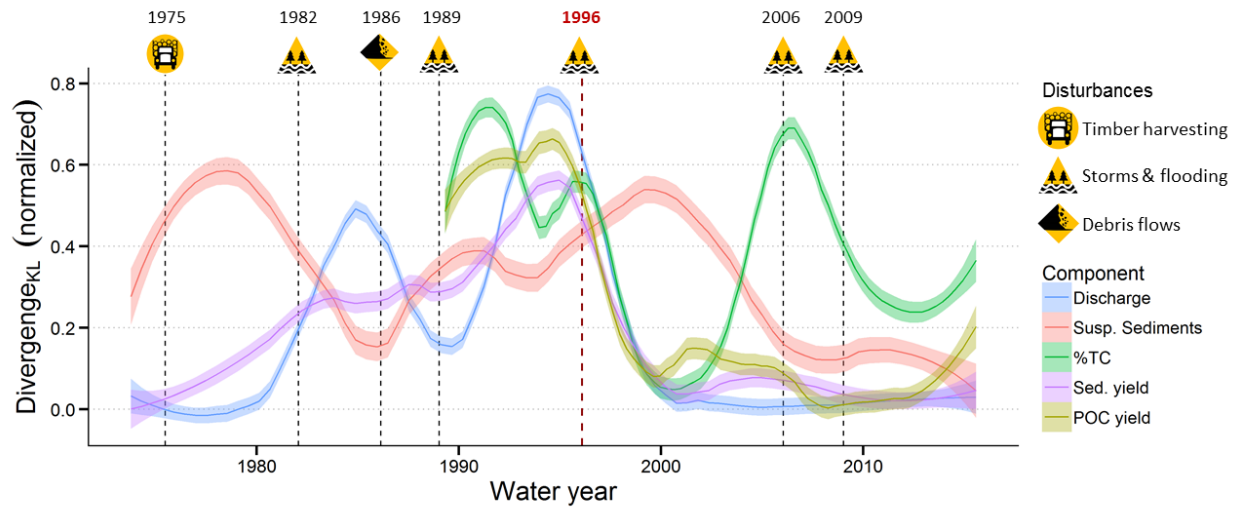


Figure 2.12. Whole-stream channel responses to disturbances measured as divergence in different components between two headwater streams draining an old-growth forest (WS09-OG site) and a 100%-logged watershed (WS10-LG site) in the H. J. Andrews Experimental Forest. Divergence_{KL} was calculated as described in Figure 2.11. Divergence_{KL} temporal trends for carbon related variables starts in 1989 (First window of analysis: 1984-1989). Solid-shaded lines represent a smoothed trend of divergence estimated with LOESS regression (smoothing parameter (α) =0.3 or ~10 years; 95% confidence intervals). A significant reduction in the divergence between our study sites was observed after the flooding in 1996.

Table 2-1. Major disturbances impacting the study sites (WS09-Old growth; WS10-Logged) in the H. J. Andrews Experimental Forest. Compilation from several data sources^{7,30,35}.

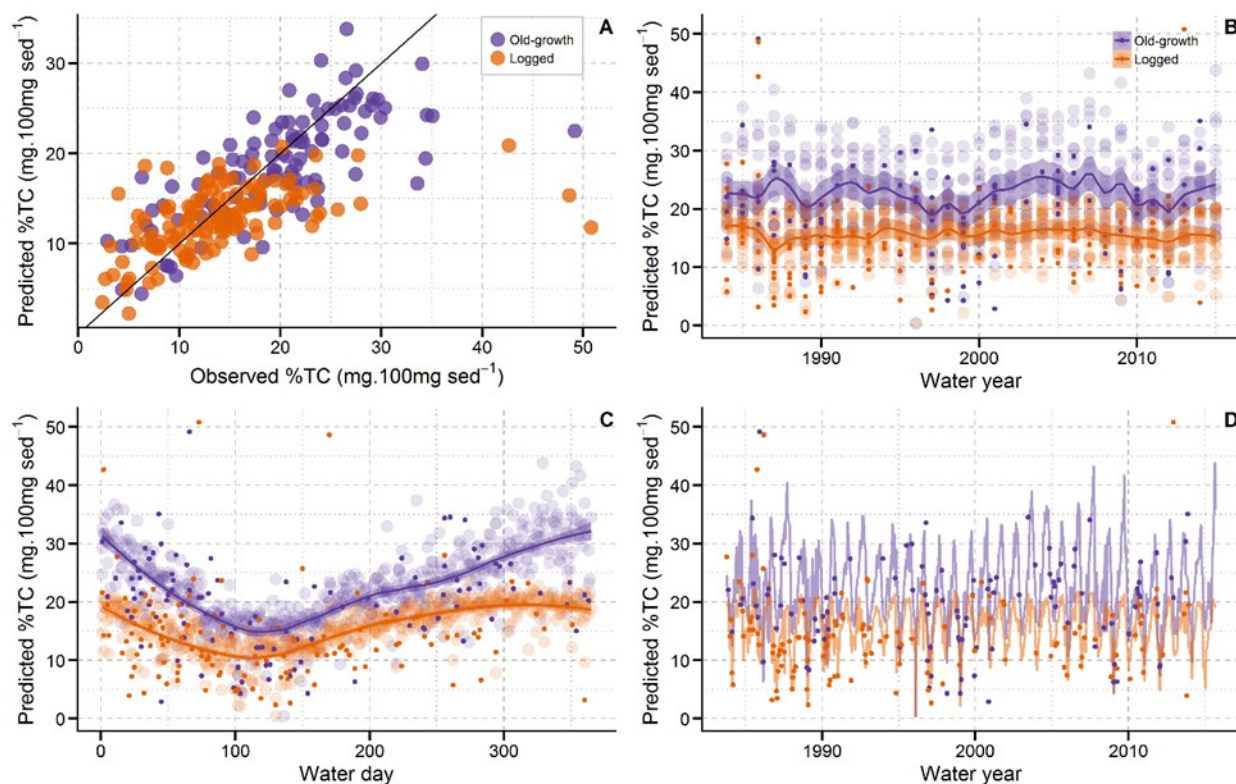
Forcing	Year	Magnitude/type	Return interval (years)*	Old growth	Logged
Natural	c.a. 1525	Stand-replacing fire	200-415	X	X
	Winter 1996	Largest flood on record (1.47 m ³ /s/km ²)	30-100	X	X
	Winter 1986	Large flood (top 10 on record, 1.11 m ³ /s/km ²)	N.A.	X	X
	Winter 1986	Channel-scouring debris flow (700 m ³ ; 220m channel affected)	580		X
Anthropogenic	Spring 1975	100% clear cut (high-level cable-yarded)	100		X

Table 2-2. Summary of elemental composition of suspended sediments from two headwater streams draining an old-growth forest (WS09) and 100%-logged watershed (WS10) in the H. J. Andrews Experimental Forest. Overall and seasonal averages covering water years from 1980-2014.

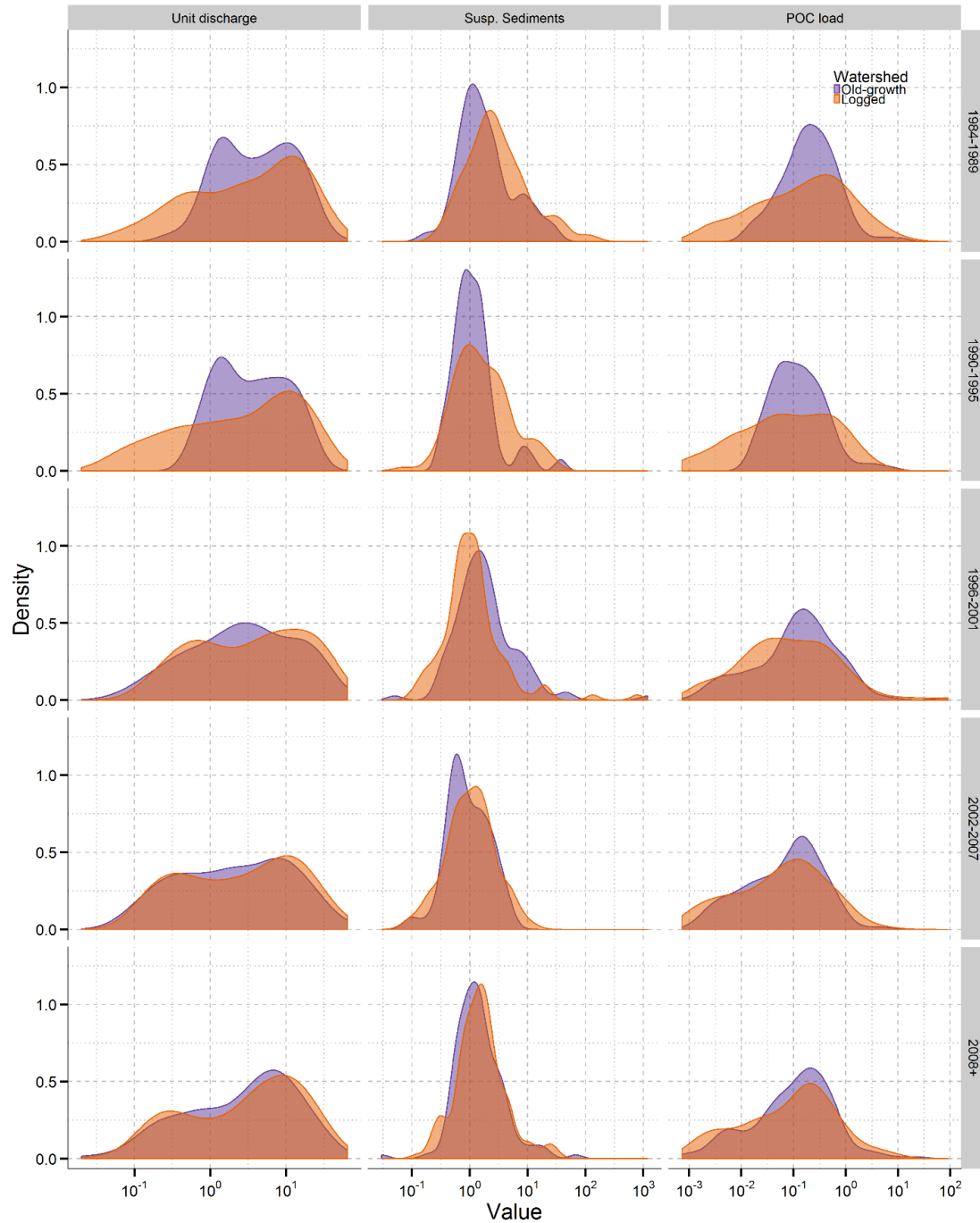
Site	Old-growth			Logged		
	Average	s.d.	n	Average	s.d.	n
%TC						
Overall	19.20	8.97	138	13.91	7.45	162
<i>Fall</i>	21.43	7.87	48	16.11	8.21	59
<i>Winter</i>	14.13	7.54	39	10.94	5.49	47
<i>Spring</i>	17.60	10.66	24	13.74	8.16	37
<i>Summer</i>	23.99	7.37	27	14.72	5.45	19
%TN						
Overall	1.50	0.66	138	1.24	0.69	i.d.
<i>Fall</i>	1.72	0.62	48	1.52	0.77	i.d.
<i>Winter</i>	1.15	0.56	39	0.94	0.52	i.d.
<i>Spring</i>	1.36	0.64	24	1.14	0.57	i.d.
<i>Summer</i>	1.76	0.64	27	1.36	0.67	i.d.
TN:C						
Overall	0.072	0.02	138	0.079	0.02	i.d.
<i>Fall</i>	0.072	0.02	48	0.083	0.02	i.d.
<i>Winter</i>	0.074	0.02	39	0.075	0.02	i.d.
<i>Spring</i>	0.074	0.02	24	0.075	0.02	i.d.
<i>Summer</i>	0.066	0.02	27	0.081	0.03	i.d.

Table 2-3. Coefficients from a multiple regression model for %TC. Full model had an R^2 of 0.5225 and a p -value <0.0001

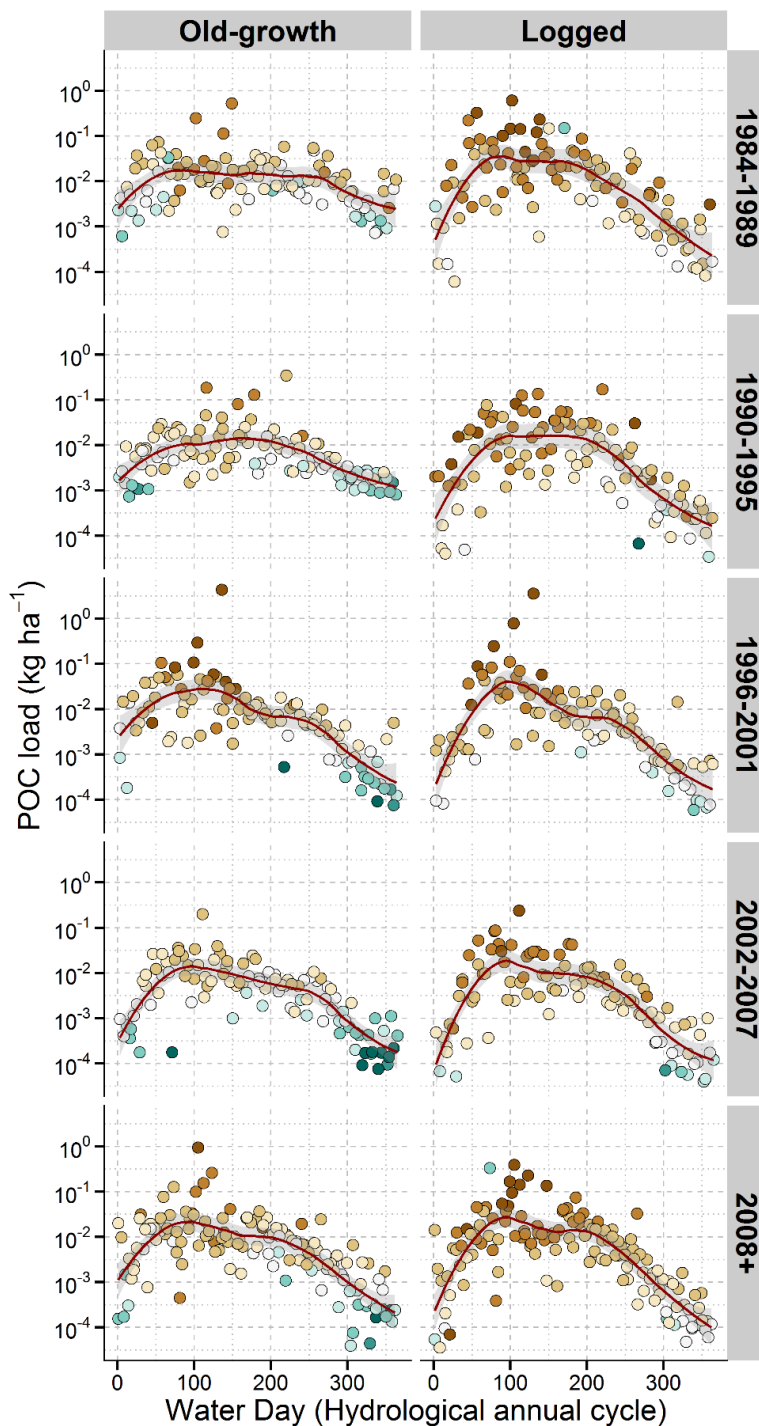
<i>Coefficients:</i>	<i>Estimate</i>	<i>S.E.</i>	<i>p-value</i>
Intercept	10.532	6.244	0.0931
Watershed type (Logged)	-0.856	0.362	0.019
Log [Dissolved organic nitrogen (DON)]	0.240	0.089	0.007
Log [Unit discharge]	-0.032	0.026	0.216
Log [Max. precipitation+1]	0.003	0.032	0.936
Log [Dissolved silica]	1.020	0.349	0.004
Water year	-0.004	0.003	0.148
Spring season	-0.016	0.084	0.852
Summer season	-0.003	0.098	0.974
Winter season	-0.232	0.077	0.003
Log [Susp. Sediments]	-0.020	0.104	0.847
Log [Susp. Sediments]²	-0.068	0.024	0.005
Watershed type: Log [Dissolved organic nitrogen (DON)]	-0.175	0.107	0.105



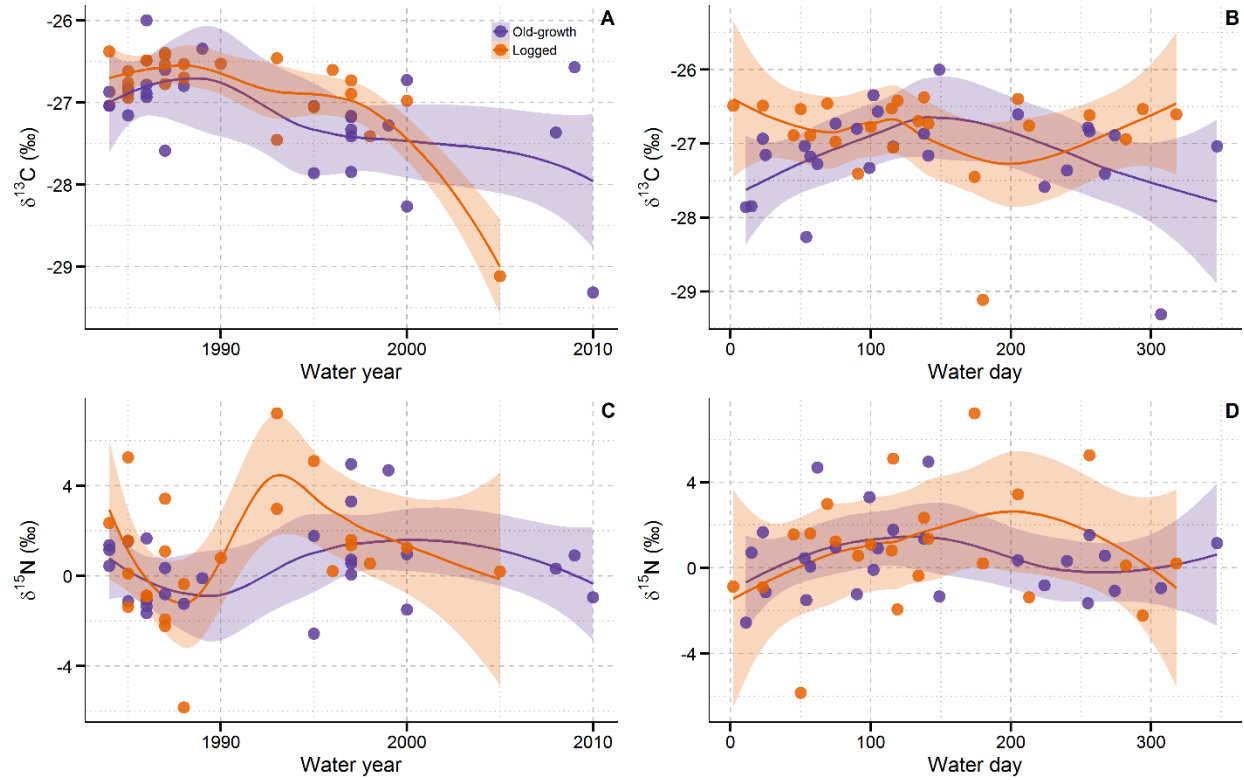
Supplementary Figure 1. Comparison of the carbon content of sediments (%TC) as predicted by a multiple regression model with observed values from headwater streams draining an old-growth forests (WS09) and 100%-logged watershed (WS10) in the H. J. Andrews Experimental Forest. (A) predicted vs. observed values without temporal indexing. B-D Predicted (translucent colors) and observed values (solid colors) indexed by water year, water day and three weeks sampling period respectively. Solid-thick lines represent a smoothed trend estimated with LOESS regression (α -parameter=0.15 (B) and 0.5(C)); the light-shaded region represents 95% confidence intervals).



Supplementary Figure 2. Approximated probability distributions for unit discharge, suspended sediments and particulate organic carbon (POC) load from two headwater streams draining an old-growth forest (WS09) and a 100%-logged (10) watershed in the H. J. Andrews Experimental Forest (Data correspond to a 5-year non-overlapping window ($n \sim 100$)).



Supplementary Figure 3. Seasonality of particulate organic carbon (POC) loads and their average carbon content (range) from two headwater streams draining an old-growth forest (WS09) and 100%-logged watershed (WS10) in the H. J. Andrews Experimental Forest. Solid-thick lines represent a smoothed trend estimated with LOESS regression (α -parameter=0.5; the light-shaded region represents 95% confidence intervals). Data correspond to a 5-year non-overlapping window ($n \sim 100$).



Supplementary Figure 4. Annual and seasonal trends of isotopic composition of sediments exported from two headwater streams draining an old-growth forest (WS09) and 100%-logged watershed (WS10) in the H. J. Andrews Experimental Forest. Solid-thick lines represent a smoothed trend estimated with LOESS regression (the light-shaded region represents 95% confidence intervals).

Supplementary table 1. Coefficients from a multiple regression model for TC: N ratios. Full model had an R^2 of 0.1856 and a p-value <0.0001

Coefficients:	Estimate	S.E.	p-value
Intercept	23.566	4.386	0.000
Watershed type (Logged)	-0.643	0.245	0.009
Log [Dissolved organic nitrogen (DON)]	0.064	0.063	0.313
Unit discharge	-0.001	0.002	0.652
Average precipitation	0.000	0.001	0.534
Log [Dissolved silica]	0.210	0.242	0.386
Water year	-0.011	0.002	0.000
Spring season	-0.021	0.056	0.708
Summer season	-0.078	0.067	0.245
Winter season	-0.001	0.052	0.991
Log [Susp. Sediments]	0.000	0.022	0.988
Watershed type: Log [Dissolved organic nitrogen (DON)]	-0.160	0.073	0.030

Supplementary table 2. Summary of elemental composition of suspended sediments from two headwater streams draining an old-growth forest (WS09) and 100%-logged watershed (WS10) in the H. J. Andrews Experimental Forest. Overall and seasonal averages covering water years from 1980-2014.

Site	Old-growth			Logged		
	Average	s.d.	n	Average	s.d.	n
$\delta^{13}\text{C}$						
Overall	-27.135	0.654	27	-26.808	0.578	24
Fall	-27.364	0.509	9	-26.675	0.231	7
Spring	-27.033	0.419	5	-27.268	1.106	5
Summer	-27.662	1.122	4	-26.693	0.220	3
Winter	-26.729	0.427	9	-26.695	0.360	9
$\delta^{15}\text{N}$						
Overall	0.503	1.811	27	1.212	3.024	24
Fall	0.372	2.099	9	-0.032	2.918	7
Spring	-0.050	1.221	5	2.948	3.536	5
Summer	-0.075	1.111	4	-0.635	1.379	3
Winter	1.199	2.031	9	1.833	2.868	9

Supplementary methods: Estimation of Kullback-Liebler's Divergence ($Divergence_{KL}$)

$Divergence_{KL}$ is a relative measure of goodness of fit between any two probability distributions⁴⁷. Introduced by B. S. Kullback and R. A. Liebler⁴⁰, it estimates the information lost -in bits if Log_2 is used- that results from approximating an observed probability distribution with another. The most common application of this measure is the estimation of the Akaike's Information Criterion (AIC) in statistical model selection. AIC allows for choosing the best approximating model for a given set of observations by minimizing $Divergence_{KL}$ between the model and the data. For a pair of discrete probability distributions, $Divergence_{KL}$ is calculated as:

$$Divergence_{KL}(p||q) = \sum_{i=1}^N p(x_i) * \log \frac{p(x_i)}{q(x_i)}$$

Where p is the observed probability distribution and q is the approximating probability distribution. N is the number of bins used to represent the data in the discrete form and $p(x_i)$ and $q(x_i)$ are the frequencies of the bin i in the observed and approximating probability distributions respectively. From the equation above it follows that $Divergence_{KL}$ will increase monotonically as a function of N and for two distributions to be compared they should have the same number of bins.

Here, we measured the information lost resulting from approximating frequency distributions from the LG (Logged) site by using distributions from the OG (Old-growth) site. In this way, the bin size used for comparisons between our study sites would be predetermined by the characteristics of the control site. All variables were log-transformed prior to the divergence analysis. We calculated bin width as $3.49 * SD * n^{-1/3}$ (SD: standard deviation; n =number of data points) following to the method described by D. W. Scott⁴⁸. Bin size was calculated by dividing the range of the log-transformed variable by the bin width. Although we were more interested in comparing frequency distributions from our study sites at a given point in time, we found that changes of divergence along the time series also captured important aspects of channel dynamics at the OG and LG sites. For this reason, we used a 5-year moving window to calculate a time series of divergences between the OG and LG site. We allowed the bin size to change over time to better capture the differences between our study sites within a given period of analysis. However, bin size did not fluctuate significantly (CVs<21%) nor exhibited temporal trends that could bias out interpretation of the changes in divergence over time.

Chapter 3 Event-associated Overbank Deposits as Testimonies of Particulate Organic Carbon Mobilized along a Small Mountainous River during a Large Flood Event.

Introduction

Floods mobilize most of the particulate organic carbon along small mountainous river systems (SMRS)¹⁻⁴. During floods, a landscape composed of highly heterogeneous patches gets more connected by an expanded fluvial network⁵. Thus, particles of different sizes, origins, and chemical composition are mixed to produce complex biogeochemical signals transported along the fluvial corridor³. These signals and their longitudinal evolution are poorly documented due to logistical difficulties of sampling during large storms².

Because the export of POC from SMRS occurs as fast pulses moving downstream with flooding waters^{3,6}; it is believed that the longitudinal evolution of the organic content of the suspended load is negligible⁴. Furthermore, most of the transformations of the POC mobilized are assumed to occur by means of chemical reactions mediated by microbial metabolism that has little change to operate under fast flood conditions⁶. Therefore, SMRS are assumed to be highly efficient exporters of POC that once buried in the ocean, becomes a long-term carbon sink with implications in climatic regulation⁴.

At the same time, it is well-known that SMRS are characterized by complex geomorphological dynamics that creates opportunities for transient storage of POC across the fluvial network⁷⁻⁹. Even small river channels can accommodate significant amounts of wood on their banks because of the simultaneous bank erosion that occur during the flood⁹. Also, materials coming from debris flows follow complicated paths and might have longer transit times through the fluvial network¹⁰. All those factors contribute to the creation of geophysical opportunities for carbon storage that could either decrease the efficiency of transport or at least increase the interactions between the suspended load and the river channel. These interactions result in successive events of deposition and resuspension that could alter POC chemical composition⁶.

Much of the particulate material carried by rivers during floods is deposited along its floodplains by means of overbank deposition. Thus, overbank deposits have been proposed to be testimonies of the mobilization of sediments through fluvial networks¹¹⁻¹⁵. Although the chemical composition of the POC deposited on the margins of the river could contain information about sediment sources and routing, the chemical characterization of these deposits has been limited to the

analysis of elemental composition (TC, TN)^{16,17} which has limited resolution to separate processes and sources.

Here, we analyze sediment samples from overbank deposits to characterize the diverse array of POM particles mobilized along the Alsea River by the Great Coastal Gale of 2007, hereafter, GCG-2007. Our main objective is to characterize the particles that move along the river, their associated organic load OC loadings and the role of physical and chemical processes in affecting those characteristics, that ultimately constitute a “biogeochemical signature”. We aim for a closer look at particle heterogeneity as an indicator of mobilization and instream processes. The research questions to be addressed in this chapter are:

What kind of biogeochemical signatures can be produced by SMRS during floods?

How does the location along the fluvial corridor influence the biogeochemical signatures produced by SMRS during floods?

What is the role of mineral surfaces, grain size and chemical composition in the imprinting of biogeochemical signatures on sedimentary records?

Our first objective for this study is to analyze the longitudinal evolution of the Great Coastal Gale biogeochemical signal. This signal is decomposed into particulate organic carbon (POC), particulate organic nitrogen (PON), C: N ratios, stable isotopes (¹³C and ¹⁵N) and biomarkers such as lignin-derived phenols.

Our second objective is to identify the controls on the biogeochemical signal of the Great Coastal Gale as related to the effects of erosion, sediment transport, and the contribution from different source areas in a patchily disturbed watershed (i.e. heterogeneous distribution of forest harvesting units).

Methods

Study area

The Alsea River, located in the central Oregon Coast Range (OCR), drains a rugged, forested landscape (basin area 1,220 km²) with a maximal elevation of 1,250 m (Figure 3.1). The lush forests covering the OCR are characterized by relatively high rates of net primary productivity

($0.82\text{--}0.95 * 10^6 \text{ kg C km}^{-2} \text{ year}^{-1}$; Van Tuyl et al. 2005). Vegetation is predominantly coniferous composed mainly by Douglas-fir (*Pseudotsuga menziesii* (Mirb.) Franco), western hemlock (*Tsuga heterophylla* (Raf.) Sarg.), and Sitka spruce (*Picea sitchensis* (Bong.) Carrière). Early successional species such as the nitrogen-fixing Red alder (*Alnus rubra* Bong.) and big-leaf maple (*Acer macrophyllum* Pursh), occur among the dominant vegetation in disturbed areas. These hardwood species dominate riparian fringes. The soils covering the watershed have andic properties (Andisol soil order or Andic sub order), which are derived from the weathering sandstone and siltstone of the Eocene Tye Formation with some intrusive basalt of the Eocene Siletz River and Burpee Formations^{18,19}. Soils in the watershed can be over 2 m deep and contain (Hatten, pers. Comm.), on average, $32 * 10^6 \text{ kg OC km}^{-2}$ (ref¹⁹).

The main channel runs through two distinctive ownership classes along the headwaters-ocean gradient. The headwaters and the area affluent to the Alsea Valley, i.e. the first ~40% of the watershed, are owned by private timber companies. The remaining 60% of the watershed, which drains the area downstream of the Alsea Valley, is under public management by the U.S. Forest Service and the Bureau of Land Management (BLM) for multiple uses (primarily forestry and recreation) (Figure 3.1). The first portion of the watershed is characterized by a distinctive mosaic of land uses including intensive timber management, agriculture, and the small community of Alsea with no more than 250 inhabitants. The second portion of the watershed is characterized by a denser forest cover, particularly within the Siuslaw National Forest (Figure 3.1). Along its course, the Alsea River has a surprising small number of confluences. After the junction of the North and South forks after Mill Creek, the largest contributions of water received from the network occur at Fall Creek, Blackberry (Lobster Creek) and Risley (Canal Creek).

The cool and wet maritime climate of the Pacific Northwest influences the study area and the land use in the watershed encompasses the effects of timber harvest and land sliding. Most of the landslides are shallow and mobilize soil mantle covering unchanneled valleys across the watershed. These shallow landslides dominate sediment inputs to stream channel networks in this region^{20–22}. Discharges of varying magnitudes mobilize these sediments increasing suspended sediment loads²³. Historical discharge data show that the Alsea River is an event-dominated river with the typical hydrograph displaying several high-discharge events per year. These peaks in discharge are associated with the passage of winter storms that last a few days. Based on these records, the Alsea River has a mean discharge of $41.6 \text{ m}^3 \text{ s}^{-1}$ and an annual sediment yield of $75 * 10^3 \text{ kg km}^{-2}$ (ref²⁴).

The Alsea River drains a terrain with underlying marine sediments -the Tyee formation -uplifted more than 50 million years ago to constitute the Coast Range sedimentary province^{25,26}. These sediments have exceptionally low resistance to breakdown and in some areas along the OCR up to 94% of the bed material erodes into sands and finer grains²⁶. Therefore, river channels are typically bounded by bedrock since the attrition of coarser grains transfers bed material into the suspended load. The deposition of these broken sediments promotes flood plain building by enhanced overbank deposition²⁶.

Along with the suspended load, significant amounts of organic matter are transported by the Alsea River during winter storms. In a preliminary characterization of the organic load of the Alsea River, Hatten et al (ref¹⁰) found that a single storm in December 2007 was responsible for exporting c.a. 50% of the annual organic load, which is in the order of $4.6 \cdot 10^6$ kg OC per year (equivalent to ~0.4% of the net primary productivity in the watershed). The chemical composition of the organic matter exported at elevated flows suggested that most of the organic matter mobilized and exported originated from areas affected by shallow landslides as well as from riparian zones, covering a wide range of POM sources. Yet, most of the organic matter exported by the Alsea seems to be of recent origin (~60 years) and produced by the vegetation in the watershed in comparison with other rivers that export organic matter of petrogenic origin eroded from rocks¹⁰. In that sense OM from the Alsea River is considered mostly biospheric¹¹.

Between December 1st and 4th, 2007, the Pacific Northwest was hit by a series of powerful storms named by U.S. meteorologists as the Great Coastal Gale of 2007 (Hereafter GCG-2007). These storms produced widespread record flooding across the states of Oregon and Washington, as well as the Canadian province of British Columbia. The most intense storms and floods were recorded along the coastal range, which is drained by several small mountainous river systems (SMRS) like the Alsea River. The GCG-2007 caused the largest seasonal flood for that year with a peak hourly discharge of $781 \text{ m}^3 \text{ s}^{-1}$ ($Q: Q_{\text{mean}} = 18.8$), which has a return period of 3 years. Several shallow landslides triggered by the intense precipitation during the December 2007 storm were evident when we accessed our sampling locations (e.g. Fall Creek, T6, Figure 3.1).

Sampling

Immediately after the storm (December 5th, 2007), we collected sediment samples from 12 locations distributed along 80 km on the main stem of the Alsea River (Figure 3.1) These locations

encompassed a longitudinal gradient from headwaters to the estuary (Figure 3.1). Most of our sampling locations were camping grounds or day-use parks with access to the river through boat ramps (Table 3-1, Figure 3.2). We collected our samples from these boat ramps and sampling depth was typically limited by a concrete layer that excluded the possibility of collecting sediments from previous storms or the riparian soil (Figure 3.2). We were confident that these concrete surfaces were devoid of previous deposits since they were easily eroded by rainfall. Indeed, we noted many signs of erosion that were removing the deposits when we sampled. Rains that would have fallen prior to the flooding would have “rinsed” the boat ramps clean prior to deposition.

Deposit layers were sampled at the surface and a varying depth depending on the location of the concrete boundary of the boat ramp (typically 0-5 cm) (Figure 3.1)). Only at one location (Clemens) the depth of the deposit allowed us to collect samples from 10 and 15 cm depth (Figure 3.2). In some cases, depending on the size of the deposit, samples were collected from two points at a varying distance from the river channel. A preliminary assessment of the granulometric characteristics of the deposit layers showed significant differences between sampling depths and sampling locations within the boat ramps. Thus, *we analyzed deposit layers separately and we treated them as independent samples*, as they encompassed a wide range of heterogeneous particle sizes and settling conditions (see Supplementary Figure 5).

Size fractionation

Immediately after collection, samples were transported in dark, cool conditions to the laboratory. To reduce the possibility of desorption of OC from the particulate phase we suspended bulk sediments in filtered (0.45 μ m) river water with similar ionic concentrations as the water in the river during the GCG-2007. These slurries were sieved and rinsed (with river water) through a 63 mm stainless steel sieve. Coarse suspended particles > 63 μ m were recovered from the sieve. Fine suspended particles (<63 μ m) were isolated by centrifugation. The coarse and fine suspended materials were oven dried at 60 °C until constant weight was achieved and stored for further analyses. Aliquots of water samples that had undergone the centrifugation step were filtered through pre-weighed, 0.45 μ m glass-fiber filters to determine the fraction of material not isolated with this approach. Overall, the combined coarse and fine fractions accounted for 93.3% of the total mass of sediments collected.

Particle size distribution and Cesium 137

Bulk sediment subsamples were used to determine particle size distribution in the sediments (Figure 3.3). Samples were pretreated with hydrogen peroxide to remove organic constituents and aid deflocculation²⁷. Particle size analysis was performed with a Beckman-Coulter LS 230 (Beckman Coulter Inc., Fullerton, CA, USA) laser diffraction type granulometer, with polarisation intensity differential scattering (PIDS). Due to the presence of several modes in the particle size spectra obtained, we calculated a mean particle size as the arithmetic average of the D_{16} , D_{50} and D_{84} particle diameters for each sample²⁸. Grain size data are presented on the phi (ϕ) scale to facilitate graphical presentation and statistical manipulation²⁹. Along this scale, larger values correspond to finer grains and lower or even negative values correspond to coarse grains. Particle size information was also aggregated and expressed as fractions of sand, silt, and clay for each deposit.

We also measured the activity of Cesium 137 (^{137}Cs) in a selected number of bulk subsamples of overbank sediments by γ -ray spectroscopy²⁴. Specific details of the procedure are specified elsewhere³⁰. ^{137}Cs is commonly used as a tracer of the movement of recently (>1963) deposited sediments and soils^{31,32}. Since this radioactive element is preferentially absorbed onto the surfaces of clay particles, we normalized ^{137}Cs activity by the specific surface area of the bulk samples.

Specific Surface Area

Splits of unground particles were analyzed for specific mineral surface area (SSA) using the Brunauer, Emmett and Teller (BET) technique^{33,34}. Although it is uncommon in practice, we collected SSA data for bulk, fine, and coarse sediments. Samples were combusted at 300°C for 4 h to remove organic matter and degassed under vacuum at 250°C for 1 h to remove adsorbed water prior to the 5-point BET measurement. The precision and accuracy of the technique was monitored by weekly analyses of standard reference materials and replicate analyses of selected samples, which yielded analytical errors of ~5% of measured values.

Carbon, Nitrogen, C/N ratios

To characterize the chemical composition of overbank sediments, we followed the same methodology described by Hatten et al. (ref¹⁰) for suspended sediments. Briefly, weights of bulk, coarse and fine overbank sediments were recorded after oven drying. Organic carbon (OC) and nitrogen (N) contents in all samples were determined by high-temperature combustion after

homogenization and removal of inorganic carbonates. Based on replicate analyses of selected samples, the precision of these measurements was better than 5% of measured value and analyses of reference materials showed they were accurate to within 2%. We used the elemental N:OC ratios to characterize our samples since OC:N ratios tend to underestimate land-derived contribution to aquatic sediments^{35,36}.

Stable Isotopes and Lignin Biomarkers

The stable isotopic composition of OC ($\delta^{13}\text{C}$) in our samples was determined by isotope ratio mass spectrometry after high-temperature combustion of pre-acidified samples. Precision in the $\delta^{13}\text{C}$ measurements was $\sim 0.1\%$, and the analyses of reference materials showed accuracies that were within 5% of measured values. The fine and coarse fractions of overbank sediments were analyzed by alkaline CuO oxidation^{1,37,38} to obtain the yields of a variety of products derived from different biochemical precursors and biological sources. The analytical precision and variability of this technique was evaluated by oxidizing well-characterized standardized materials (vegetation and sediment samples) as well as replicate analyses of selected samples. Overall, the variability in the yield of individual compounds ranged from 5 to 15% of the measured value, with the higher variability associated with compounds with low yields ($<0.05 \text{ mg g}^{-1}$ sediment).

We quantified several classes of reaction products from the CuO oxidation procedure, including vanillyl phenols (VP = vanillin + acetovanillone + vanillic acid), syringyl phenols (SP = syringaldehyde + acetosyringone + syringic acid) and cinnamyl phenols (CP = p-coumaric acid + ferulic acid) that are characteristically derived from different lignin sources³⁹. Because lignin is uniquely synthesized by vascular land plants (i.e., trees, grasses), lignin-derived products have been widely used to trace organic matter derived from terrigenous vegetation in a variety of environments^{40–43}. In addition to these vascular plant biomarkers, we quantified the yields of benzoic acids (BA = benzoic acid + m-hydroxybenzoic acid + 3,5-dihydroxybenzoic acid), which are derived from a variety of sources, including tannins and soil organic matter. These products have been applied in several systems as tracers of organic matter alteration in soils^{41,43}. We use lignin-derived products to trace vegetation-derived contributions to the overbank deposits. We also investigate the diagenetic state of the organic matter using specific markers (e.g., benzoic acids).

We used OC_{coarse} ($>63\mu\text{m}$) and OC_{fine} ($<63\mu\text{m}$) to represent our size fractions to avoid confusions with the size fractions commonly used by stream ecologists, i.e. Coarse Particulate Organic Matter (CPOM $>1\text{mm}$) and Fine Particulate Organic Matter (FPOM $<1\text{mm}$).

Results

Textural changes and mean particle size along overbank deposits

The flood in December 2007 deposited mostly coarse material along the boat ramps. The textural characteristics of these overbank deposits are shown in Table 3-2. Most deposit layers had more than 45% of their volume represented by sands. Deposit layers at headwaters locations had $>93\%$ of their grains represented by sand (Figure 3.4). The exceptions to this compositional pattern were surficial samples from 4 deposits dominated by silts ($\sim 70\%$) and clays ($\sim 30\%$). These mud deposits were located at the confluence with Fall Creek (T6a), a major tributary, and at other downstream locations including the boat ramps at the gauging station at Tidewater (C8a), Risley Park (C11a), and the estuary (RV Park, E12a) (Figure 3.4A). Overall, the proportion of silts increased in the downstream direction, particularly after major confluences, i.e. South Fork (V3a), and Fall Creek (T6a). While deposits collected at headwaters had silt proportions $<11\%$, upland valley deposits, located after South fork (V3-5) confluence had silt proportions between 7-48% (Figure 3.4A).

Evidence of direct sediment inputs to the river channel from a suspected shallow landslide and rocky debris were observed at Fall Creek's confluence (T6a) and at Blackberry park (C7c) respectively (Figure 3.4A, B). Our measurements of ^{137}Cs were consistent with these observations. The highest normalized activity, 0.122 dpm m^{-2} , was found at T6a while the lowest normalized activity was measured at the C7c layer ($2.5 \cdot 10^{-3} \text{ dpm m}^{-2}$). ^{137}Cs normalized activities from other analyzed samples ranged between $9 \cdot 10^{-3} \text{ dpm m}^{-2}$ and $4.2 \cdot 10^{-2} \text{ dpm m}^{-2}$. These range of normalized activities showed a significant increasing trend in the downstream direction ($R^2=0.606$, $p=4 \cdot 10^{-4}$) (Figure 3.4B), suggesting that the samples were collected along an erosion-deposition gradient.

To understand the potential effects of particle sorting on the physical structure of the deposit layers, we calculated the mean grain size of sands, silts, and clays for each deposit. Then, we tested for any longitudinal trend in these fractions separately. We observed significant sorting of sand-sized particles along the river channel (Figure 3.4C). Mean particle diameter in the sand fraction showed a significant decreasing trend along the Alsea's main stem ($R^2= 0.42$; $p=2 \cdot 10^{-4}$).

While mineral grains at headwater locations had an average diameter of 0.57 phi units ($> 600 \mu\text{m}$), corresponding to coarse sands, locations near the estuary had a lower mean grain size, corresponding to very fine sand (3.57 phi units or $\sim 84 \mu\text{m}$). There were no significant longitudinal trends for mean grain size in the silt or clay fraction. Only deposit layers we suspect were derived from landslides had a lower mean particle diameter in the silt fraction (6.93 phi units or $8.2 \mu\text{m}$) than any other sample (average ~ 5.41 phi units or $23.5 \mu\text{m}$; (Figure 3.4C).

In summary, these results suggest that our samples of overbank sediments were collected along a gradient of erosion-deposition from headwaters to the estuary. Along this gradient we observed increased deposition of fine sediments towards the estuary, most likely due to a downstream reduction in transport capacity. The Alsea River's ability to transport and deposit particles larger than 4 phi units ($> 63 \mu\text{m}$) seemed to decrease significantly from our sampling locations at its headwaters compared to those locations near its estuary.

Organic matter distribution along overbank deposits

OC_{bulk}, OC_{coarse} and OC_{fine} along overbank deposits

The organic matter content and the N:OC ratios for the organic matter collected from overbank deposits along the Alsea River are presented in Table 3-3. OC_{bulk} concentrations in overbank deposits increased from headwaters to the ocean along the Alsea River (Figure 3.5). We measured up to 10-fold increases in OC_{bulk} concentration in deposits closer to the estuary compared to those at headwaters. The highest OC concentration was measured at the shallow landslide deposit at the Fall Creek confluence (11.4%). The other three deposits with similar granulometry to that found at Fall Creek had OC concentrations that were among the highest observed within our set of samples (5.8-6.95%). OC_{bulk} concentrations in suspended sediments measured at the gauging station during the storm (Tidewater, 50 km downstream from headwaters) were not only within the range of OC concentrations in overbank deposits, but also fit well within the values expected for that specific location in the downstream direction (Figure 3.5A).

Both OC_{coarse} (%wt) and OC_{fine} (%wt) followed a relatively similar longitudinal trend along the Alsea River to that described for OC_{bulk} (Figure 3.5A). Yet, the amount of variability explained by the position along the river gradient was higher for OC_{fine} than for OC_{coarse}. We measured up to 5-fold increases in OC concentration in the coarse fraction of deposits closer to the estuary compared

to those at headwaters, but regressing these concentrations against distance from headwaters only explained 11% ($p=6.6 \times 10^{-2}$) of the variability in OC_{coarse} concentrations (Figure 3.5A). In contrast, the same gradient explained about 42% ($p=5.2 \times 10^{-4}$) of the variability observed in OC_{fine} concentrations (Figure 3.5A). In both size fractions, exceptionally high OC concentrations were measured at the shallow landslide deposit at the confluence with Fall Creek (17.3 % OC_{coarse} ; 7.4% OC_{fine}); these outlying values were not included in regression analysis. The other three deposits with similar granulometry to that found at Fall Creek had OC concentrations that were among the highest observed within each size fraction (5.9-10.5% OC_{coarse} ; 3.5-4.3% OC_{fine}). OC concentrations in the coarse and fine fractions of the suspended sediments also fell within the longitudinal trends of organic matter content in overbank deposits, this was particularly evident in the fine sediment fraction (Figure 3.5A).

Since a significant amount of variability in the OC_{bulk} concentrations remained unexplained by the longitudinal gradient observed in Figure 3.5A ($OC_{\text{bulk}} \sim \text{Distance from headwaters}$, $R^2=0.26$; $p=7.5 \times 10^{-3}$), we included mean particle diameter of the bulk sample and percentage of clay as predictors in a linear regression model (Figure 3.5A). We found that OC_{bulk} significantly increased towards finer deposits but at the same time, it was inversely related to clay content. After accounting for these grain size effects, which explained $\sim 80\%$ ($p = 1.2 \times 10^{-7}$) of the variability in OC_{bulk} concentrations, no significant changes along the river gradient were observed (i.e. no longitudinal trend in the residuals, data not shown). As part of this exploratory analysis, we also tested for a correlation between the same predictors mentioned above and OC_{coarse} and OC_{fine} concentrations by a multiple linear regression. We found that for both size fractions, mean particle diameter of the bulk mixture was significantly correlated with the concentration of organic matter deposited within each size fraction ($R^2(OC_{\text{coarse}}) = 0.8$, $p(OC_{\text{coarse}}) = 9.2 \times 10^{-8}$, $R^2(OC_{\text{fine}}) = 0.8$, $p(OC_{\text{fine}}) = 1.5 \times 10^{-8}$). Interestingly, while the proportion clay was a significant predictor for organic matter concentrations in the coarse fraction ($p(OC_{\text{coarse}}) = 4 \times 10^{-2}$), it was not significant for OC_{fine} concentrations ($p(OC_{\text{fine}}) = 0.24$). As in the case of OC_{bulk} , no longitudinal trends in OC_{fine} and OC_{coarse} were apparent after accounting for the effects of particle size.

In summary, these results are indicative of a strong influence of particle sorting in the distribution of organic matter across overbank deposits, in both coarse and fine fractions. After accounting for these effects of grain size, no longitudinal trends remained in OC_{coarse} and OC_{fine} concentrations. Yet, when organic matter concentrations in both size fractions were regressed against distance from the headwaters, the relationship was significant and explained different

amounts of variability for OC_{coarse} and OC_{fine} . Furthermore, the downstream increase in OC_{fine} concentrations was inversely proportional to the mean diameter of the coarse mineral grains. These results imply that at least a portion of the particles in the OC_{fine} fraction were more susceptible to increased deposition due to an effect of transport limitation in the downstream direction.

*Availability of coarse and fine organic matter along overbank deposits ($*OC_{coarse}$ vs. $*OC_{fine}$)*

To better understand the differences in the distribution of OC_{fine} and OC_{coarse} along the Alsea River, we compared the total availability of these fractions within each deposit. To do so, we normalized OC concentrations by the total amount of sediment in the sample by multiplying the original concentrations of OC_{coarse} and OC_{fine} by the weight percentage of their corresponding fraction in the bulk sample (% coarse, % fine respectively, Table 3-2). To differentiate these bulk mass-normalized concentrations from OC_{fine} and OC_{coarse} we labeled them as $*OC_{fine}$ and $*OC_{coarse}$. The sum of $*OC_{coarse}$ and $*OC_{fine}$ is equal to the OC_{bulk} content.

We estimated OC_{bulk} from unfractionated sediment samples, and found that our independent calculation of OC_{bulk} was, on average, about a 93% of that estimated from unfractionated samples. We attributed this small discrepancy to minor sample losses during sample size fractionation in the laboratory. The amounts of $*OC_{coarse}$ and $*OC_{fine}$ in Alsea River's overbank deposits are presented in (Figure 3.6A).

The total amounts of $*OC_{coarse}$ were higher than those of $*OC_{fine}$ in all cases. At headwater locations, this difference was about an order of magnitude. For instance, the deposit at H1a had an $*OC_{coarse}$ concentration of 0.72 % and a ten times lower concentration of $*OC_{fine}$ (0.071%) (Figure 3.6A). Likewise, samples collected at H2 had an average $*OC_{coarse}$ concentration of 0.27% and an average $*OC_{fine}$ concentration of 0.036% (Figure 3.6A). The largest $*OC_{coarse}$ concentration was observed in one of the samples collected at the gauging station (C8b) and it was equivalent to 7.8%. The corresponding $*OC_{fine}$ concentration for this sample was 1.42%. Samples collected from suspected landslide deposits were also among the highest across the dataset, particularly in the deposit at the confluence with Fall Creek (T6a), with $*OC_{coarse}$ and $*OC_{fine}$ concentrations of 7.07 and 4.8% respectively (Figure 3.6A). Overall, the variation of $*OC_{coarse}$ and $*OC_{fine}$ across the deposits was almost identical (Figure 3.6A). This pattern suggested a strong correlation between $*OC_{fine}$ and $*OC_{coarse}$ (Figure 3.6C).

Given that larger $*OC_{\text{fine}}$ concentrations were linked to higher inputs of $*OC_{\text{coarse}}$, we consider less likely that changes in organic matter within the fine fraction could be driven by changes in SSA. To rule out any potential impact of varying SSA, we analyzed changes in SSA and OC_{fine} loading (i.e. $[OC: SSA]_{\text{fine}}$), across the deposits.

Mineral particles with SSA of $41 \text{ m}^2/\text{g}$ were found in the H2a-d deposit layers. A significant decreasing trend in SSA values was observed in the downstream direction ($-R^2 = 0.58$, $p = 1.6 \times 10^{-5}$) with SSA reaching values of $14 \text{ m}^2/\text{g}$ at the estuary location (E12) (Table 3-3). These results were unexpected given the reduction in mean particle diameter from headwaters to the estuary. Further analysis of SSA data show that SSA values were affected by a large contribution to overall mineral surface area from very small particles co-deposited along with coarse sands. We suspected these particles were aggregates or flocs retained in the coarse fraction and which were broken down during sample preparation for SSA analysis (see supplementary results about SSA analysis). We confirmed this suspicion with biomarker analysis (see below). We found the contribution of these aggregates to be disproportionate, since these small particles that broke down ($>10 \mu\text{m}$) represented less than 10% of the total volume of the sample. Mineral particles coming from deeper soil horizons with large surface areas ($>100 \text{ m}^2 \text{ g}^{-1}$) could be responsible for such an effect^{44,45}. After correcting for such an effect, by subtracting the amount of SSA that could be contributed to the deposit based on the amount of coarse sediments, SSA was virtually constant across the overbank deposits. Thus, when normalizing OC_{fine} by SSA we found that those deposits located downstream of Fall Creek, i.e. within the confined portion of the Alsea River, had significantly higher OC loadings than deposits located at the headwaters and the upland valley (Figure 3.6A).

Using the criteria of $[OC: SSA]_{\text{fine}} > 1.0 \text{ mg OC}/\text{m}^2$ to define organic-overloaded sediments (following Fisher et al., ref.⁴⁹), we found that OC_{fine} overloading was correlated with the inputs of $*OC_{\text{coarse}}$ to the deposits. In fact, the relationship between $*OC_{\text{coarse}}$, $*OC_{\text{fine}}$, and overloading was almost identical (Figure 3.6B). OC_{fine} loading remains constant within a range of $*OC_{\text{fine}}$ concentrations between 0.02 to 0.5 $\text{mg } OC_{\text{fine}}/\text{mg}$ bulk sediments. For concentrations above 0.5 $\text{mg } OC_{\text{fine}}/\text{mg}$ bulk sediments, we observed direct proportionality between OC_{fine} loading and $*OC_{\text{fine}}$ concentration (Figure 3.6B). Likewise, for $*OC_{\text{coarse}}$ concentrations, the range for which OC_{fine} loading remains unchanged is between 0.17 and 1.29 $\text{mg } OC_{\text{coarse}}/\text{mg}$ bulk sediments. $*OC_{\text{coarse}}$ concentrations above 1.29 $\text{mg } OC_{\text{coarse}}/\text{mg}$ bulk sediments resulted in increased OC_{fine} loadings (Figure 3.6B).

Except for the amount of variability in OC_{coarse} and OC_{fine} explained by the longitudinal gradients along the Alsea River (Figure 3.5A), all the above results suggest that these two organic matter fractions could be strongly correlated. We tested for the correlation between $*OC_{coarse}$ and $*OC_{fine}$ (to avoid confusion resulting from different denominators). Being both $*OC_{coarse}$ and $*OC_{fine}$ a ratio over the total mass of sediments, they are not independent variables and their correlation could be spurious⁴⁶. We ran a Monte Carlo simulation with 10,000 iterations to obtain a distribution of R^2 values for the correlation between $*OC_{fine}$ and $*OC_{coarse}$. We found that the strong positive correlation between those organic matter fractions ($R^2 = 0.89$), had a probability of occurrence $< 5.2 * 10^{-5}$. Thus, we assumed this correlation to be significant and non-spurious (Figure 3.6C). After accounting for changes in $*OC_{coarse}$, neither mean particle size nor distance from headwaters were significant predictors of $*OC_{fine}$. The relationship between $*OC_{coarse}$ and $*OC_{fine}$ was linear on the log-log scale suggesting a power law function as the best fit for the data. The strong correlation between $*OC_{coarse}$ and $*OC_{fine}$ did not explain the distinctive overloading pattern across the samples (Figure 3.6C) nor the apparent longitudinal trend in $*OC_{fine}$ concentrations along the Alsea River ($R^2=0.29$, $p=5*10^{-3}$). We suspected that OC_{fine} overloading was related to a difference in the type of organic particles being deposited along the boat ramps before and after the confluence with Fall Creek (T6a).

*In summary, these results suggest that high concentrations of OC_{fine} in overbank deposits were not due to the deposition of fine particles with large OC_{fine} loadings. Instead, OC_{fine} overloading was predicted by the availability of coarse organic matter in the deposit (i.e. $*OC_{coarse}$). Furthermore, $*OC_{coarse}$ was an overarching predictor for $*OC_{fine}$ over other variables like mean grain size or percentage clay. Nonetheless, this correlation by itself cannot explain why OC_{fine} would exhibit a longitudinal increase along the river or why OC_{fine} overloading was higher downstream from the Alsea Valley.*

POM sources to overbank deposits

We used elemental composition (%C, %N, N:OC ratios) and carbon stable isotopes ($\delta^{13}C$) as first order proxies for the chemical characterization of the organic matter found in overbank deposits along the Alsea River (Table 3-3, Table 3-4). We also collected more than 100 soil samples from tributary areas within the basin, as soil organic matter have been identified as a prominent source material to the suspended load in the Alsea River¹⁰. The chemical characteristics of sediments (overbank and suspended) and soils from the Alsea River, collected after a storm in 2007 are shown in Figure 3.7.

The chemical composition of the organic matter found in overbank deposits was highly variable, matching a wide range of organic particles like those collected from surficial O-horizons, which receive large inputs of vascular plant material, to mineral soils (e.g. C-horizons), more depleted in biospheric carbon (Figure 3.7). OC_{coarse} exhibited a wide range of compositional variability with N/OC ratios that were as low as 0.036, corresponding to material typically found in O-horizons and as high as 0.11, typically found in OM stored in deep soil horizons in the watershed (Figure 3.7A). The lowest N/OC ratio was found at the Fall Creek confluence (T6a) and the highest at the rock slide sample from Blackberry park (C7c). OC_{coarse} had variable $\delta^{13}\text{C}$ ratios as well, covering a range from -27.3‰ to -25.1‰ (Figure 3.7B). The most ^{13}C depleted sample was collected at one of the deposit layers near the Tidewater gauging station (C8b) and the most enriched at a headwaters location (H2a). The range of $\delta^{13}\text{C}$ ratios observed in soil samples was wider than that in overbank deposits, going from -29.5‰ (O-horizons) to -25.3‰ (Bw horizons) (Figure 3.7B).

N/OC ratios in OC_{fine} covered a narrower range of values than that observed in OC_{coarse} or soil samples (Figure 3.7). The OC in the fine fraction had N/OC values mostly concentrated around 0.06 and falling between the endmembers of O-horizons and deep mineral soils (Figure 3.7A). Furthermore, there was considerable overlap between the chemical composition of OC_{fine} and that of intermediate soil horizons (i.e. A and B horizons) in the Alsea watershed (Figure 3.7A). In contrast, $\delta^{13}\text{C}$ ratios in OC_{fine} exhibited a similar range of variability to that observed in OC_{coarse} (-26.9 to -24.9‰), but still showed considerable overlap with the isotopic ratios observed in A and B horizons from soils in the Alsea watershed (Figure 3.7B).

To gain further resolution in the chemical characterization of the organic matter found in overbank deposits, we measured the concentration of specific biomarkers obtained from CuO oxidation (Table 3-4). CuO oxidation products include biomarkers for lignin, as well as markers that indicate the decomposition stage of the organic matter. Lignin phenols provided us with higher (chemical) resolution to separate contributions of vascular plant material from soil organic matter.

By using the normalized concentrations of lignin phenols from overbank deposits, we observed less overlap in the chemical composition of OC_{coarse} , OC_{fine} and OC_{soil} (Figure 3.8). OC_{coarse} samples were separated into two distinct groups of relatively high (6.5-12.6 mg LP/100mgOC) and relatively low (1.3-5.2 mg LP/100mgOC) concentrations of lignin phenols. While coarse fractions with higher yields of LP are typically associated with vascular plant debris^{1,36}, low lignin

yields are associated with soil organic matter³⁶, in this case, most likely, in the form of aggregates. In contrast, OC_{fine} samples had intermediate lignin phenols concentrations (3.4-5.4 mg LP/100mgOC). OC_{soil} samples seem to separate according to the contribution of potential sources with contrasting yields of lignin phenols like vascular plant material and (mineral-bound) soil organic matter.

Despite the contrasting chemical composition between OC_{coarse} and OC_{fine} , the normalized concentrations of these two fractions were strongly correlated. To illustrate how this association could have affected the chemical composition of fine and coarse OC, we matched OC_{coarse} and OC_{fine} across deposit layers, by assigning the same OC loadings (calculated from OC_{fine}) to both size fractions (Figure 3.8). Our results showed that in overloaded samples, both fractions, coarse and fine, tend to have higher concentrations of normalized lignin phenols than samples with OC loadings below 1.0 mg OC/m². Moreover, based on the OC loadings observed in soil samples (~1.3 mg OC/m²) it seems unlikely that material coming from these mixed soils could have contributed directly to the OC overloading found in the overbank deposits.

We also matched OC_{coarse} and OC_{fine} data in a theoretical mixing space, by connecting both types of samples using straight lines (Figure 3.9). We found that most of the lines ran in parallel to a theoretical mixing line, particularly those starting at samples with higher yield of lignin phenols (i.e. carrying a vascular plant signature) (Figure 3.9A). This alignment strongly suggests that OC_{coarse} was a direct source of OC to the fine fraction. In a random mixing scenario, connecting lines between OC_{coarse} and OC_{fine} would have gone in different directions (as it is the case for samples with lower lignin products yields). For this direct transfer to be the case, then a process of isotopic fractionation would be required, i.e. particles more enriched in ¹³C had to be transferred preferentially into the fine fraction. Furthermore, these particles were likely portions of plant material in a more advanced decomposition stage, which are more likely to be fragmented. To provide further evidence for this hypothesis, we plotted $\delta^{13}\text{C}$ data against the ratio of 3,5-dihydroxybenzoic acid and Vanillyl phenols (3,5-Bd/V). This ratio is used as an indicator of lignin degradation stage. Indeed, samples more enriched in ¹³C did have higher 3,5-Bd/V ratios, and therefore, were more degraded (Figure 3.9B).

*In summary, despite the strong correlation between the concentrations of $*OC_{\text{coarse}}$ and $*OC_{\text{fine}}$, these size fractions were composed of different types of organic matter particles. Many of these particles were co-deposited within heterogenous matrices of mineral grains with varying organic*

loadings (including the organic-poor-mineral rich sediments observed in suspension during high flows¹⁰). The specific details of the deposition of these sediments cannot be fully described by our small sample size though. Yet, we found general patterns that allow for the characterization of at least four types of particles carrying organic matter in those deposits:

In the coarsest deposits at headwater locations, we found OC with a soil organic signature (high N:OC ratios, lower lignin yields, enriched in $\delta^{13}\text{C}$ and with higher 3,5-Bd/VP ratios) in both coarse and fine fractions. We infer that at least two types of organic particles were present in those deposits: SOM-aggregates and their fragments.

In the finest deposits (including a suspected shallow landslide at Fall Creek (T6a), we found at least two types of plant residues: coarse and fresher plant material (low N:OC ratios, $\delta^{13}\text{C}$ -depleted, higher lignin yields, and lower 3,5-Bd/VP ratios) and fine and more degraded plant material (with intermediate values for the mentioned variables between fresh vascular plant material and SOM).

Discussion

We analyzed the granulometry and the chemical characteristics of event-associated overbank deposits along the Alsea River to better understand the processes involved in the downstream transport of POC along a SMRS during a storm. We found a downstream fining of mineral grains and an increase of both $\text{OC}_{\text{coarse}}$ and OC_{fine} along a small set of samples collected from headwaters to the estuary. The increase in OC_{fine} concentration could not be explained in terms of changes in SSA in fine particles and was significantly correlated to the availability of $\text{OC}_{\text{coarse}}$ in the overbank deposits. By combining information from elemental composition and lignin biomarkers we found that $\text{OC}_{\text{coarse}}$ could be a more likely source of OC_{fine} across the deposits. OC_{fine} was compositionally indistinguishable from the particles carried in suspension and the processes affecting its chemical characteristics were already happening during transport. The chemical characteristics of the organic matter deposited along overbank deposits in the Alsea River suggest that at least four types of particles were mobilized and deposited along the fluvial corridor: SOM aggregates, fragments of SOM aggregates, coarse and fresh plant debris, and fine and more degraded plant material. The relationships between these groups of particles as they were carried in suspension and deposited over the banks offered insights into the physical mechanisms affecting the distribution of POC in a SMRS in the Oregon Coast Range.

We found that after draining an upland alluvial valley, the Alsea River moves into a confined valley where the channel receives larger inputs from terrestrial vegetation that runs along the river until just a few kilometers before discharging into the ocean.

In these confined valley, substantial plant-derived OM inputs are likely generated by shallow landslides. These OM-rich particles add a temporary geochemical imprint that is further modulated by a sequence of deposition and resuspension events that promote the mixture of fragmented OM with in-transport FPOM.

Deposit layers were texturally heterogeneous due to the influences of an erosion-deposition gradient along the river and local hydrodynamics at the boat ramps.

The deposit layers sampled along the Alsea River were texturally heterogenous at larger and smaller spatial scales (i.e. longitudinal axis, boat ramps, respectively). Despite being dominated by sands, we observed a significant longitudinal decrease in the diameter of these coarser mineral particles. This decrease in particle diameter strongly suggests that the transport of sand-sized grains became more limited towards the estuary. Although our sampling scheme was not spatially exhaustive, it is notable to find evidence of this trend along the Alsea River. Furthermore, the increase in ^{137}Cs activity towards the estuary supports our inference about stronger transport limitation in the downstream direction. The longitudinal trend of this radioactive tracer of sediment mobility suggests that our samples were collected along a marked gradient of erosion-deposition^{31,32}, from headwaters to the estuary in the Alsea River.

Other studies of overbank deposition have not found fining trends along the river course^{11,45}. Researchers have attributed this lack of longitudinal gradients in grain size to small scale variability due to the hydraulics of the overbank flow^{15,47}. For instance, Walling & He (ref³⁵) modelled overbank sedimentation rates as a function of the distance from the channel, effective particle size, and microtopography. According to this model, even small changes in any of these factors would have a stronger effect on coarse particles ($>63\ \mu\text{m}$) with faster settling velocities, than on fine particles ($<63\ \mu\text{m}$) that remain suspended for longer times. Thus, particle sorting at the local scale can overrule other sources of variability. On the other hand, despite the drastic changes in sedimentation occurring during bankfull discharge, the structure of the deposited layers might still record valuable information about sediment transport processes⁴⁵. While the bottom layers of overbank deposits might reflect longitudinal gradients (e.g. changes in transport

capacity), top layers typically receive higher inputs of organic material, so recording the highest level of flooding attained. Yet top layers of overbank deposits are less structured and more variable with changes in channel width⁴⁵. The mixed influence of local and large-scale gradients likely affected the structure of sediment deposition across the boat ramps and hence, the variability in our sample set. For example, the boat ramps we sampled were oriented with varying angles with respect to the main stem. These changes in orientation could have influenced the deposition of particles at the local scale. Given that the longitudinal trend we found along our deposits explained between 40-60% of the variability in particle diameter, the role of small-scale processes in structuring these deposits must have been significant.

At larger spatial scales (e.g. along the longitudinal axis) downstream fining trends are more evident in the absence of tributaries or big obstructions along the channel⁴⁷. These two conditions were met by the Alsea River due to its low confluence density and its predominantly non-alluvial bedrock channel²⁶. Non-alluvial rivers with relatively simple geomorphological structure are commonly found along the Oregon Coast Range²⁶. Thus, these systems might offer an interesting opportunity to further investigate the physical controls of overbank deposition along SMRS.

Particle sorting strongly influenced the deposition of organic matter across overbank deposits.

During the GCG-2007, particle sorting exerted an overarching control on OC_{bulk} distribution along Alsea's overbank deposits. We found increasing concentrations of OC_{bulk} at locations where, most likely, 1) the river's transport capacity decreased to allow for a higher deposition of finer grains, or 2) the supply of sediments could have exceeded the ability of the flow to erode it (e.g. shallow landslide at Fall Creek, T6a or after the North-South Fork confluence, V3a-c). Although increases in organic matter content due to sediment fining are commonly attributed to a higher affinity of biogenic molecules to clay surfaces^{16,48}, our results suggest a different scenario.

Relatively high concentrations of both OC_{coarse} and OC_{fine} might have been co-deposited as the river flooded the boat ramps. In such a scenario hydrodynamic effects were more important than any potential mineralogical control by SSA. Carbon-enriched mineral grains are produced due to the higher affinity of biogenic molecules to clay surfaces^{16,48}. However, C-enriched mineral grains are not equivalent to overloaded fine sediments. In the first group most of the variability in the organic content is explained by changes in SSA⁴⁹. In the second group, SSA is a poor predictor of organic content because larger fragments of organic matter are not attached to the smaller mineral surfaces⁵⁰. In the overbank deposits created by The Great Coastal of 2007 along the

Alesea River, we found the largest amounts of organic associated to OC_{coarse} and not to OC_{fine} , contrary to what would be expected in the case of organic-loaded clays⁴⁵. Furthermore, we did not find evidence of SSA control on OC_{fine} ; mineral particles with large SSA were found at the coarsest deposit layers (at headwater locations), which had the lowest concentrations of organic matter. Since the amounts of OC_{fine} and OC_{coarse} were strongly and positively correlated, this co-deposition scenario suggests that both OC_{coarse} and OC_{fine} were transported as a relatively homogeneous mixture undergoing similar hydrodynamic controls over their deposition.

Muddled or mixed? The role of physical fragmentation

That OC_{coarse} and OC_{fine} were co-deposited as a homogeneous mixture does not mean that chemically they behave as such. On the contrary, our data suggest contrasting chemical characteristics for these two pools of organic matter. Thus, it results puzzling that the concentrations of OC_{coarse} and OC_{fine} were so strongly correlated and at the same time, these organic matter fractions were so chemically distinct. On one side, transport mechanisms affecting either fine or coarse particles in the river are expected to be different (supply limitation vs. transport limitation, respectively)⁵¹. However, the hydrodynamic behavior of organic matter particles is less predictable than what is generally assumed; they can either float and drift close to the water surface or be submerged and be closer to the river bed⁵². As this diverse array of organic particles travels through the water column, there is opportunity for mixing and co-deposition as the river interacts with its banks. On the other side, the hydrodynamic properties of organic matter particles depend on their shapes⁵³ and chemical composition⁵⁴; degraded, porous, and broken organic debris are more susceptible to be carried in suspension than water-logged woody debris that could be mobilized temporarily as part of the bedload⁵⁵. Thus, the transport of organic matter particles through the river channel can be complex and generate depositional patterns that are difficult to interpret.

Despite this complexity, our data suggest a consistent pattern of mass exchange between OC_{coarse} and OC_{fine} as they travel in suspension. We suggest that physical fragmentation of OC_{coarse} into OC_{fine} strongly influenced organic matter loading to overbank deposits along the Alesea River during the GCG-2007. We base this conclusion on several lines of evidence in our data: 1) the strong, significant, and positive correlation between OC_{coarse} and OC_{fine} ; 2) the power-law fit for the correlation between OC_{coarse} and OC_{fine} ; 3) the non-overlapping distribution of OC_{fine} and OC_{coarse} in the end-member mixing space and 4) the relative advanced degradation state of OC_{fine} compared to OC_{coarse} .

Correlation between OC_{coarse} and OC_{fine} could have resulted from the overarching control of particle sorting on both fractions (i.e. both were correlated with mean particle size). If this was the case, it still reinforces the fact that OC_{coarse} and OC_{fine} were traveling as a homogeneous mixture, but it does not explain why such a mixture would contain two chemically contrasting pools of organic matter. Also, if the correlation between OC_{coarse} and OC_{fine} was contingent on their correlation with mean grain size, their mutual correlation should be non-significant in a multiple regression model including both OC_{coarse} and mean grain size as predictors of OC_{fine} . We run such a model and found that after accounting for the significant effects of grain size ($p=0.02$), the correlation with OC_{coarse} was still significant ($p=0.02$) (model-adjusted $R^2=0.83$, $p<0.0001$). Thus, although our data set is too small to disentangle more specific transport mechanisms, the evidence suggests that a mixture of interconnected pools of OC_{coarse} and OC_{fine} were co-transported and co-deposited along the banks of the Alesa River during the GCG-2007.

A linear fit between OC_{coarse} and OC_{fine} on a log-log space is suggestive of a power law relationship between these two pools of organic matter. Recent evidence has shown that the mass distribution of coarse organic matter transported by mountain streams can be described by a single scaling exponent⁵². In turn, mass distributions that follow power laws are well known in the literature as examples of fragmentation processes of fractal nature⁵⁶⁻⁵⁸. Although the effects of physical fragmentation on carbon fluxes are poorly constrained in the literature¹¹ its fundamental role in the processing of organic matter in fluvial ecosystems have been recognized for decades^{59,60}.

Being co-transported and co-deposited as a homogeneous mixture, we found reasonable to hypothesize that OC_{coarse} and OC_{fine} would be derived from a common source (e.g. surface soils). However, our property-property plots (or end-member mixing space representation) showed that while OC_{coarse} covered a wide range of potential sources, OC_{fine} represented an apparently well-mixed pool of those sources. Furthermore, based on its elemental composition, OC_{fine} resembles a mixture of different soil horizons in the Alesa. However, this interpretation of the endmember mixing space could be misleading. Because our samples from different soil horizons also exhibited the characteristics of a mixture⁶¹ (Figure 3.7) that could be separated into specific contributions of other endmembers^{62,63} (like vascular plants and mineral associated SOM^{36,64} (Figure 3.8). Thus, the nature of the mixing process affecting the composition of OC_{fine} along the Alesa River must be fundamentally different or at least incorporate additional processes that does not occur in soils.

We argue that physical fragmentation implies a sort of “muddling” process as opposed of simple mixing. Theoretically, endmember mixing models are inspired in homogeneous mixtures that could be separated by a physical process (like water and salt), provided that the fundamental composition of the endmembers remains unaltered by the mixing process. We observed that the mass transfer from the OC_{coarse} pool to the OC_{fine} pool must results in isotopic fractionation, with OC_{fine} particles being more enriched in ^{13}C .

Isotopic fractionation might occur during the decomposition process because microbes discriminate less against ^{13}C than vascular plants do⁶⁴. Thus, because the distribution of microbes over detrital surfaces is patchy, decomposition also results in a patchy distribution of ^{13}C in larger pieces of organic matter undergoing degradation⁶⁴. This small-scale spatial heterogeneity of the decomposition process has fundamental implications on the physical fragmentation of vascular plant detritus due to mechanical reasons⁵⁴. Plant tissues are better described as pressurized cellular solids, i.e. materials whose mechanical strength depends critically on the integrity of the lignin and the hemicellulose on the cell walls⁵⁴. As cell wall components are attacked by microbes, the degraded tissues become more susceptible of fragmentation. The fragments produced would be enriched in ^{13}C , while their parent material would still be depleted in the same isotope. Indeed, OC_{fine} particles were more depleted in ^{13}C than OC_{coarse} and their lignin phenols showed a more advanced degradation stage supporting our argument in favor of physical fragmentation.

The biogeochemical signature of the GCG-2007

Event-associated overbank deposits provided testimonies of the POC mobilized and exported from the Alsea River during the GCG-2007. These deposits contained large-enough amounts of sediments that allowed for a detailed physical-chemical characterization that is difficult to achieve with suspended samples only⁶⁵. Despite the complexity of the depositional processes affecting these sediments, the properties of a heterogeneous mixture of particles carried in suspension were evident from the headwaters to the estuary. The immediate collection of these sediments deposited over previously rain-washed boat ramps, was essential for the preservation of the chemical composition of the samples. Based on these chemical characteristics, we inferred that physical fragmentation was an important driver of the mass transfer from the pool of coarse particulate organic matter to the pool of fine particulate organic matter. Thus, the biogeochemical signature of the GCG-2007 was imprinted along the fluvial channel due to the interaction of a strong erosion-deposition gradient, small-scale hydrodynamics and physical fragmentation. Our

results suggest that physical processing was an important modulator of the chemical characteristics of the POC exported from the Alsea River during the GCG-2007.

Since we analyzed a small set of samples from a single storm, we are aware that it is difficult to make broader generalizations to other SMRS from our data. Furthermore, because of the exceptionally high attrition rates reported for rivers running on sedimentary geology along the Oregon Coast Range²⁶, the role of physical fragmentation on POC processing could be enhanced in these SMRS.

Nonetheless, the chemical characteristics of the organic matter examined across Alsea's overbank deposits encompass the composition of the particles carried in suspension, not only by the Alsea, but also by other rivers along the Oregon's coast (e.g. Umpqua) over a wide range of discharges ($Q:Q_m:1.1-15.8$)⁵⁶(Figure 3.10). In that regard, we observed that the relationships between the chemical compositions of the coarse and the fine fractions in the Alsea's suspended load were similar to those observed along the river's overbank deposits (Figure 3.7 and Figure 3.8), except for the lack of coarse mineral grains carrying SOM signatures deposited along the upland valley. Notably, data from the Umpqua River are reported on bulk sediment samples⁵⁶ that contain a mixture of the coarse and fine sediment fractions. However, the Umpqua River's samples fit within the composition of fine particles from the Alsea River, highlighting the underrepresentation of the coarse fraction that is poorly sampled with the available methods^{2,55}. The underestimation of the export of coarse organic particles from SMRS could have important implications on constraining POC fluxes, as the coarse load could dominate POC export on a decadal time scale⁵⁵.

Further hydrodynamic sorting, mixing, and fragmentation (or "muddling") can exert control on the chemical characteristics of the POC exported off these mountainous rivers and buried in the coastal ocean (e.g. depocenters, Figure 3.10). Hydrodynamic sorting of the POC load has been documented for both SMRS in the Oregon Coast Range³⁶ and large river systems like the Mississippi-Atchafalaya⁴⁰. The more specific impacts of the routing of POC along fluvial systems on POC cycling across SMRS requires further research. We believe these future research efforts will be benefited from more detailed analysis that explicitly address the particulate character of POC and how the composition of these particulate loads evolves as it moves (rolls, deposits, and resuspends) on its way from headwaters to the ocean.

Conclusions

Along the steep channel of the Alsea River, characterized by high attrition rates and relatively simple geomorphology, we were able to obtain evidence of the important role of physical instream processing of organic matter in the export of particulate organic carbon from a small mountainous river system in the Oregon Coast range. We analyzed a sequence of overbank deposits longitudinally distributed following a strong gradient of erosion-deposition from headwaters to the estuary. We used the chemical characteristics of the organic matter found at these locations of transient storage for particulate material to describe different types of particles associated to OC_{coarse} and OC_{fine}. These particles included SOM aggregates, fragments from SOM aggregates, coarse and fine plant debris. While particle sorting played an important role in the mobilization and deposition of these particles during the GCG-2007, we provide evidence that extensive physical fragmentation of the coarse organic matter transported in the suspended load was a significant source of fine particulate organic matter in the river during this storm. Future research efforts will be required to constraint the role of POC routing through river channels on the fate and persistence of these carbon exports in long term sedimentary environment. Our data suggest that physical processing during floods must be an important driving force behind the imprinting of biogeochemical signatures in sedimentary records.

Bibliography

1. Hatten, J. A., Goñi, M. A. & Wheatcroft, R. A. Chemical characteristics of particulate organic matter from a small, mountainous river system in the Oregon Coast Range, USA. *Biogeochemistry* **107**, 43–66 (2012).
2. Goñi, M. A., Hatten, J. A., Wheatcroft, R. A. & Borgeld, J. C. Particulate organic matter export by two contrasting small mountainous rivers from the Pacific Northwest, U.S.A. *J. Geophys. Res. Biogeosciences* **118**, 112–134 (2013).
3. Leithold, E. L., Blair, N. E. & Wegmann, K. W. Source-to-sink sedimentary systems and global carbon burial: A river runs through it. *Earth-Sci. Rev.* **153**, 30–42 (2016).
4. Hilton, R. G. Climate regulates the erosional carbon export from the terrestrial biosphere. *Geomorphology* **277**, 118–132 (2017).
5. Benda, L. *et al.* The Network Dynamics Hypothesis: How Channel Networks Structure Riverine Habitats. *BioScience* **54**, 413 (2004).
6. Battin, T. J. *et al.* Biophysical controls on organic carbon fluxes in fluvial networks. *Nat. Geosci.* **1**, 95–100 (2008).
7. Montgomery, D. R. Process Domains and the River Continuum¹. *JAWRA J. Am. Water Resour. Assoc.* **35**, 397–410 (1999).
8. Wohl, E., Dwire, K., Sutfin, N., Polvi, L. & Bazan, R. Mechanisms of carbon storage in mountainous headwater rivers. *Nat. Commun.* **3**, 1263 (2012).
9. Rathburn, S. L. *et al.* The fate of sediment, wood, and organic carbon eroded during an extreme flood, Colorado Front Range, USA. *Geology* **45**, 499–502 (2017).
10. May, C. L. & Gresswell, R. E. Spatial and temporal patterns of debris-flow deposition in the Oregon Coast Range, USA. *Geomorphology* **57**, 135–149 (2004).

11. Walling, D. E. & He, Q. The spatial variability of overbank sedimentation on river floodplains. *Geomorphology* **24**, 209–223 (1998).
12. Nicholas, A. P. & Walling, D. E. The significance of particle aggregation in the overbank deposition of suspended sediment on river floodplains. *J. Hydrol.* **186**, 275–293 (1996).
13. Bølviken, B. *et al.* Overbank sediments: a natural bed blending sampling medium for large-scale geochemical mapping. *Chemom. Intell. Lab. Syst.* **74**, 183–199 (2004).
14. Bottrill, L. J., Walling, D. E. & Leeks, G. J. Geochemical characteristics of overbank deposits and their potential for determining suspended sediment provenance; an example from the River Severn, UK. *Geol. Soc. Lond. Spec. Publ.* **163**, 241–257 (1999).
15. Zwoliński, Z. Sedimentology and geomorphology of overbank flows on meandering river floodplains. *Geomorphology* **4**, 367–379 (1992).
16. Walling, D. E., Owens, P. N. & Leeks, G. J. L. The characteristics of overbank deposits associated with a major flood event in the catchment of the River Ouse, Yorkshire, UK. *CATENA* **31**, 53–75 (1997).
17. Cabezas, A., Angulo-Martínez, M., Gonzalez-Sanchis, M., Jimenez, J. J. & Comín, F. A. Spatial variability in floodplain sedimentation: the use of generalized linear mixed-effects models. *Hydrol Earth Syst Sci* **14**, 1655–1668 (2010).
18. Lovell, J. P. B. Tyee Formation: Undeformed Turbidites and their Lateral Equivalents: Mineralogy and Paleogeography. *GSA Bull.* **80**, 9–22 (1969).
19. Soil Survey Staff NRCS. Web Soil Survey, edited. United States Department of Agriculture. (2009).
20. Dietrich, W. E. & Dunne, T. Sediment budget for a small catchment in mountainous terrain. *Z. Geomorphol.* **29**, 191–206 (1978).
21. Benda, L. & Dunne, T. Stochastic forcing of sediment supply to channel networks from landsliding and debris flow. *Water Resour. Res.* **33**, 2849–2863 (1997).
22. Almond, P., Roering, J. & Hales, T. C. Using soil residence time to delineate spatial and temporal patterns of transient landscape response. *J. Geophys. Res. Earth Surf.* **112**, (2007).
23. Wheatcroft, R. A., Goñi, M. A., Hatten, J. A., Pasternack, G. B. & Warrick, J. A. The role of effective discharge in the ocean delivery of particulate organic carbon by small, mountainous river systems. *Limnol. Oceanogr.* **55**, 161–171 (2010).
24. Wheatcroft, R. A. & Sommerfield, C. K. River sediment flux and shelf sediment accumulation rates on the Pacific Northwest margin. *Cont. Shelf Res.* **25**, 311–332 (2005).
25. Snively Jr., P. D., MacLeod, N. S., Wagner, H. C. & Rau, W. W. *Geologic map of the Waldport and Tidewater quadrangles, Lincoln, Lane, and Benton counties, Oregon.* (1976).
26. O'Connor, J. E. *et al.* Geologic and physiographic controls on bed-material yield, transport, and channel morphology for alluvial and bedrock rivers, western Oregon. *Geol. Soc. Am. Bull.* B30831–1 (2014).
27. Gray, A. B., Pasternack, G. B. & Watson, E. B. Hydrogen peroxide treatment effects on the particle size distribution of alluvial and marsh sediments. *The Holocene* **20**, 293–301 (2010).
28. Folk, R. L. & Ward, W. C. Brazos River Bar: A Study in the Significance of Grain Size Parameters. *J. Sediment. Res.* **27**, (1957).
29. Blott Simon J. & Pye Kenneth. GRADISTAT: a grain size distribution and statistics package for the analysis of unconsolidated sediments. *Earth Surf. Process. Landf.* **26**, 1237–1248 (2001).
30. Richardson, K. N. D., Hatten, J. A. & Wheatcroft, R. A. 1500 years of lake sedimentation due to fire, earthquakes, floods and land clearance in the Oregon Coast Range: geomorphic sensitivity to floods during timber harvest period. *Earth Surf. Process. Landf.* **43**, 1496–1517 (2018).
31. Walling, D. E. & Quine, T. A. Use of ¹³⁷Cs measurements to investigate soil erosion on arable fields in the UK: potential applications and limitations. *J. Soil Sci.* **42**, 147–165 (1991).

32. Saç, M. M. & İçhedef, M. Application of ^{137}Cs technique for evaluation of erosion and deposition rates within cultivated fields of Salihli region, Western Turkey. *J. Radiat. Res. Appl. Sci.* **8**, 477–482 (2015).
33. Mayer, L. M. Relationships between mineral surfaces and organic carbon concentrations in soils and sediments. *Chem. Geol.* **114**, 347–363 (1994).
34. Goni, M. A., Cathey, M. W., Kim, Y. H. & Voulgaris, G. Fluxes and sources of suspended organic matter in an estuarine turbidity maximum region during low discharge conditions. *Estuar. Coast. Shelf Sci.* **63**, 683–700 (2005).
35. Perdue, E. M. & Koprivnjak, J.-F. Using the C/N ratio to estimate terrigenous inputs of organic matter to aquatic environments. *Estuar. Coast. Shelf Sci.* **73**, 65–72 (2007).
36. Hastings, R. H., Goñi, M. A., Wheatcroft, R. A. & Borgeld, J. C. A terrestrial organic matter depocenter on a high-energy margin: The Umpqua River system, Oregon. *Cont. Shelf Res.* **39**, 78–91 (2012).
37. Goñi, M. A. & Montgomery, S. Alkaline CuO Oxidation with a Microwave Digestion System: Lignin Analyses of Geochemical Samples. *Anal. Chem.* **72**, 3116–3121 (2000).
38. Goni, M. A. *et al.* Oceanographic and climatologic controls on the compositions and fluxes of biogenic materials in the water column and sediments of the Cariaco Basin over the Late Holocene. *Deep Sea Res. Part Oceanogr. Res. Pap.* **56**, 614–640 (2009).
39. Hedges, J. I. & Mann, D. C. The characterization of plant tissues by their lignin oxidation products. *Geochim. Cosmochim. Acta* **43**, 1803–1807 (1979).
40. Bianchi, T. S., Galler, J. J. & Allison, M. A. Hydrodynamic sorting and transport of terrestrially derived organic carbon in sediments of the Mississippi and Atchafalaya Rivers. *Estuar. Coast. Shelf Sci.* **73**, 211–222 (2007).
41. Prahl, F., Ertel, J., Goni, M., Sparrow, M. & Eversmeyer, B. Terrestrial organic carbon contributions to sediments on the Washington margin. *Geochim. Cosmochim. Acta* **58**, 3035–3048 (1994).
42. Dalzell, B. J., Filley, T. R. & Harbor, J. M. The role of hydrology in annual organic carbon loads and terrestrial organic matter export from a midwestern agricultural watershed. *Geochim. Cosmochim. Acta* **71**, 1448–1462 (2007).
43. Otto, A. & Simpson, M. J. Evaluation of CuO oxidation parameters for determining the source and stage of lignin degradation in soil. *Biogeochemistry* **80**, 121–142 (2006).
44. Goni, M. A. *et al.* Terrigenous organic matter in sediments from the Fly River delta-clinof orm system (Papua New Guinea). *J. Geophys. Res. Earth Surf.* **113**, (2008).
45. Sollins, P. *et al.* Sequential density fractionation across soils of contrasting mineralogy: evidence for both microbial- and mineral-controlled soil organic matter stabilization. *Biogeochemistry* **96**, 209–231 (2009).
46. Berges, J. A. Ratios, regression statistics, and “spurious” correlations. *Limnol. Oceanogr.* **42**, 1006–1007 (1997).
47. He, Q. & Walling, D. E. An investigation of the spatial variability of the grain size composition of floodplain sediments. *Hydrol. Process.* **12**, 1079–1094 (1998).
48. Pondell, C. R. & Canuel, E. A. The role of hydrodynamic sorting on the accumulation and distribution of organic carbon in an impoundment: Eglebright Lake, California, USA. *Biogeochemistry* **133**, 129–145 (2017).
49. Fisher, B. A., Aufdenkampe, A. K., Yoo, K., Aalto, R. E. & Marquard, J. Soil carbon redistribution and organo-mineral associations after lateral soil movement and mixing in a first-order forest watershed. *Geoderma* **319**, 142–155 (2018).
50. Fisher, B. Geomorphic controls on mineral weathering, elemental transport, carbon cycling, and production of mineral surface area in a schist bedrock weathering profile, Piedmont Pennsylvania. (2016).
51. Knighton, D. *Fluvial Forms and Processes: A New Perspective.* (Arnold, 1998).

52. Turowski, J. M. *et al.* The mass distribution of coarse particulate organic matter exported from an Alpine headwater stream. *Earth Surf. Dyn.* **1**, 1–11 (2013).
53. Atkinson, C. F., Aumen, N. G., Miller, G. L. & Ward, G. M. Influence of Particle Shapes and Size Distributions on Fine Particulate Organic Matter Surface Area in Streams. *J. North Am. Benthol. Soc.* **11**, 261–268 (1992).
54. Niklas, K. J. Mechanical Behavior of Plant Tissues as Inferred from the Theory of Pressurized Cellular Solids. *Am. J. Bot.* **76**, 929–937 (1989).
55. Turowski, J. M., Hilton, R. G. & Sparkes, R. Decadal carbon discharge by a mountain stream is dominated by coarse organic matter. *Geology* **44**, 27–30 (2016).
56. Turcotte, D. L. Fractals and fragmentation. *J. Geophys. Res. Solid Earth* **91**, 1921–1926 (1986).
57. Wohletz, K. H., Sheridan, M. F. & Brown, W. K. Particle size distributions and the sequential fragmentation/transport theory applied to volcanic ash. *J. Geophys. Res. Solid Earth* **94**, 15703–15721 (1989).
58. Kun, F. & Herrmann, H. J. Transition from damage to fragmentation in collision of solids. *Phys. Rev. E* **59**, 2623–2632 (1999).
59. Boling, R. H. *et al.* Toward A Model of Detritus Processing in a Woodland Stream. *Ecology* **56**, 141–151 (1975).
60. Yoshimura, C., Fujii, M., Omura, T. & Tockner, K. Instream release of dissolved organic matter from coarse and fine particulate organic matter of different origins. *Biogeochemistry* **100**, 151–165 (2010).
61. Weltje, G. J. End-member modeling of compositional data: Numerical-statistical algorithms for solving the explicit mixing problem. *Math. Geol.* **29**, 503–549 (1997).
62. Parnell, A. C., Inger, R., Bearhop, S. & Jackson, A. L. Source Partitioning Using Stable Isotopes: Coping with Too Much Variation. *PLOS ONE* **5**, e9672 (2010).
63. Phillips, D. L. & Gregg, J. W. Source partitioning using stable isotopes: coping with too many sources. *Oecologia* **136**, 261–269 (2003).
64. Acton, P., Fox, J., Campbell, E., Rowe, H. & Wilkinson, M. Carbon isotopes for estimating soil decomposition and physical mixing in well-drained forest soils: CARBON ISOTOPES FOR FOREST SOILS. *J. Geophys. Res. Biogeosciences* **118**, 1532–1545 (2013).
65. Johnson Erin R., Inamdar Shreeram, Kan Jinjun & Vargas Rodrigo. Particulate Organic Matter Composition in Stream Runoff Following Large Storms: Role of POM Sources, Particle Size, and Event Characteristics. *J. Geophys. Res. Biogeosciences* **123**, 660–675 (2018).

Figures and tables

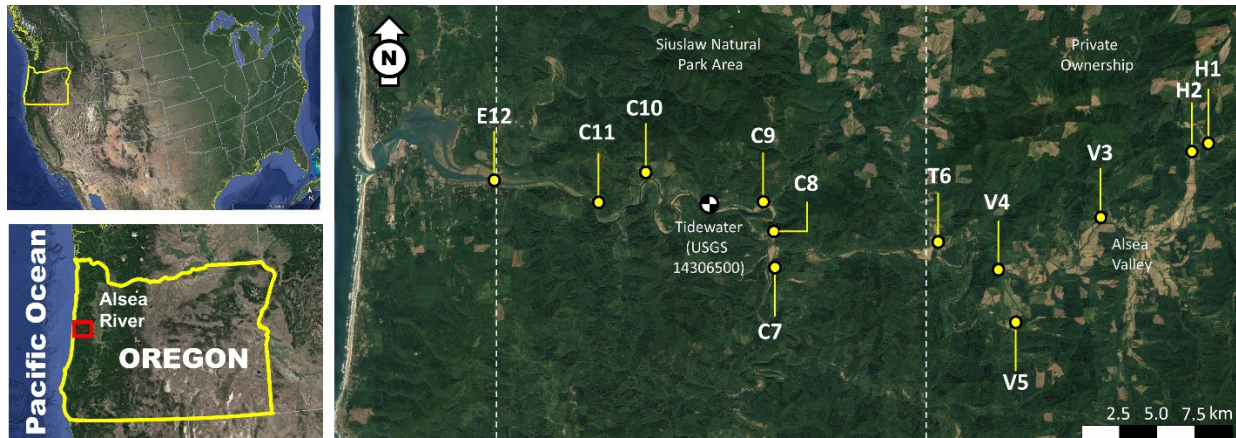


Figure 3.1. Study Area and sampling locations. Samples were collected along the main channel of the Alsea River, in the Oregon Coast Range, from headwaters to the estuary. Samples are numbered following flow direction (1-12) and the initial capital letter correspond to dominant fluvial feature (H= headwaters; V= Upland valley, T= tributary, C=Confined channel, E= Estuary). Source: Google earth pro V 7.3.1.4507 (December 13, 2015). United States of America. Eye alt(s): 4421.69 km (Contiguous US); 1286.29 km (State of Oregon); 51.01 km (Alsea River). US Department of State Geographer. 2018. Google. Image Landsat/Copernicus, Data SIO, NOAA, U.S. Navy, NGA, GEBCO (January 27, 2018). Suspended sediment samples were collected at Tidewater's gauging station and described in ref¹⁰.



Figure 3.2 Contrasting characteristics between flood deposits sampling locations along the Alsea River. Top panel: river channel at headwater (H) and upland valley (V) locations had a bedrock bottom with interspersed patches of gravel (black circle). Smaller boat ramps interrupt angiosperm/herbaceous-dominated riparian fringes. Flood deposits were thick and mainly composed of coarse grains. Bottom panel: river channel at confined (C) locations had bedrock bottom with no gravel patches (arrow). Larger boat ramps interrupted riparian fringes that were surrounded by conifers. Flood deposits had larger contribution of coarse plant-derived material.

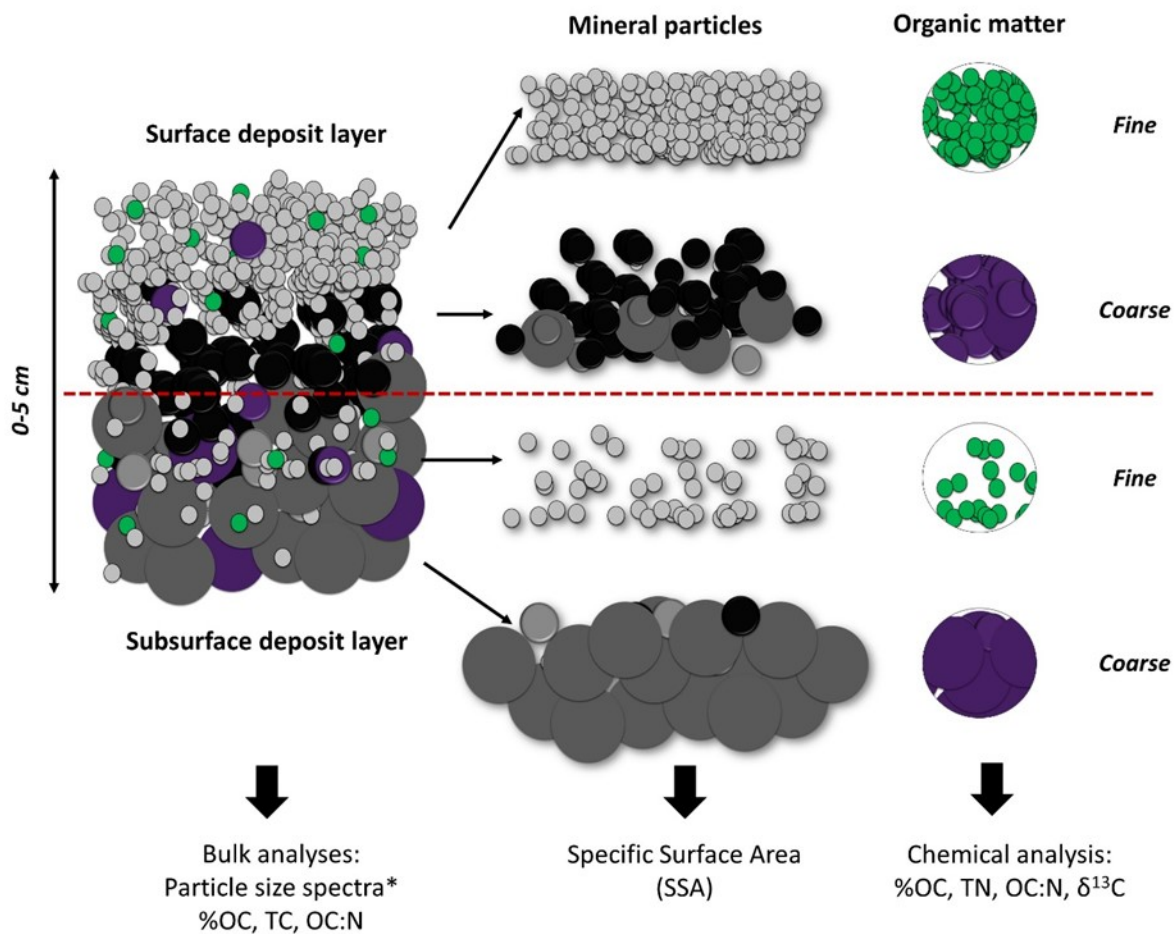


Figure 3.3. Deposit layers as sample units. Surficial samples were collected from all deposits (0-1cm). At 7 specific locations, where deposit depth was over 7 cm, subsurface samples were also collected (1-5cm). All samples underwent the same analytical procedure for physical (i.e. Specific Surface Area) and chemical characterization. Although surface samples were significantly finer than subsurface samples (Supplementary Figure 5), sampling depth did not affect the major trends observed in our data set (Supplementary Figure 6). Therefore, deposit layers, regardless their sampling depth, are treated as sample units.

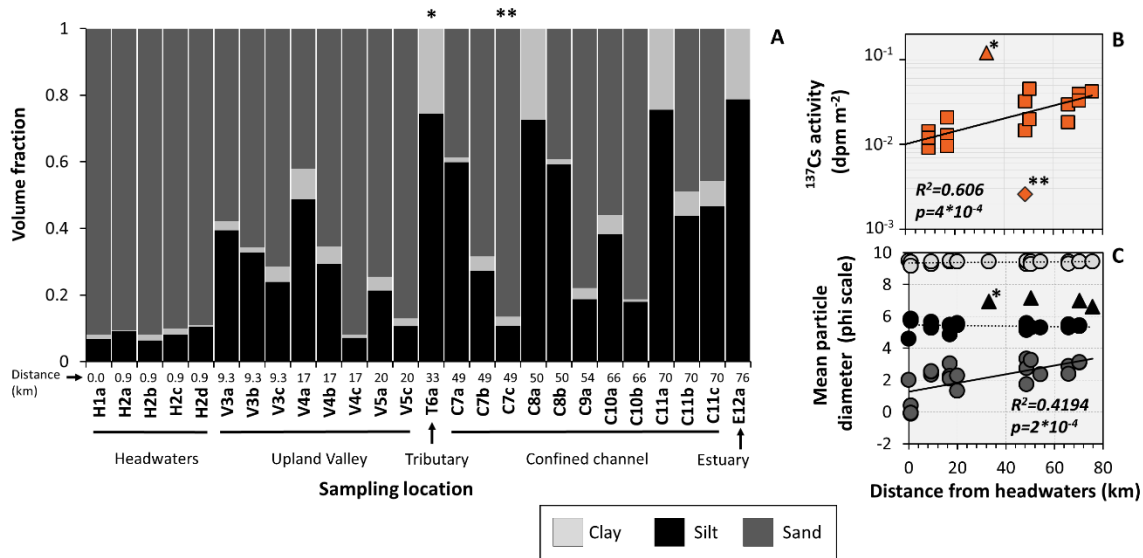


Figure 3.4. Physical properties of overbank deposits along the Alsea River after a flood event in December 2007. **A.** Textural composition as fractions of sand, silt, and clay across sampling locations (see Table 1, for location descriptions). Initial capital letters correspond to the type of fluvial landscape from headwaters to the estuary (H= headwaters, V= upland valley, C=confined channel, T= tributary, E= estuary). **B.** Activity of radioactive Cesium as an indicator of erosion/deposition of recent sediments along the stream channel. Samples from a suspected landslide deposit at T6a (Fall Creek) as well as from a rocky debris-like material at C7c (Blackberry park) are marked with (*) and (**) respectively. **C.** Changes in mean particle diameter within each size class plotted against distance from headwaters (km). A significant decrease in particle diameter (dark red trendline) was observed only in the sand fraction ($p=2*10^{-4}$). Particles in the silt fraction from a landslide deposit and other three similar samples were finer than the along-river average within the same fraction. A Sample collected from a landslide deposit at the confluence with Fall Creek, a major tributary, is marked with a star (*).

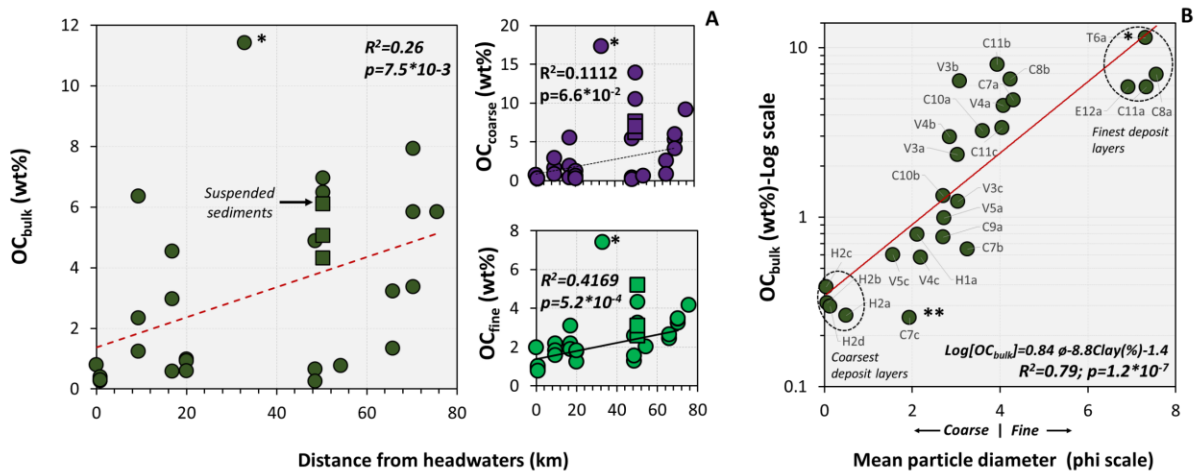


Figure 3.5. **A.** Longitudinal profiles of organic carbon concentrations (OC_{bulk} , $OC_{\text{coarse}} > 63 \mu\text{m}$, and $OC_{\text{fine}} < 63 \mu\text{m}$) in overbank deposits along the Alsea River after a flood in December 2007. Values for suspended sediment samples collected during the GCG-2007 by Hatten et al., (2012) are identified by squares ($n=3$). **B.** About 80% of the variability in OC_{bulk} concentrations is explained by changes in mean particle diameter (phi scale, larger values for finer grains) ($(D_{16}+D_{50}+D_{84})/3$) and the percentage of clays in the samples. After accounting for the effects of grain size, no longitudinal gradients in organic matter distribution are observed. A Sample collected from a deposit at a suspected shallow landslide location at the confluence with Fall Creek (T6a), a major tributary, is marked with a star (*, A and B). A sample collected from rocky debris at Blackberry (C7c) is marked with **, panel B only.

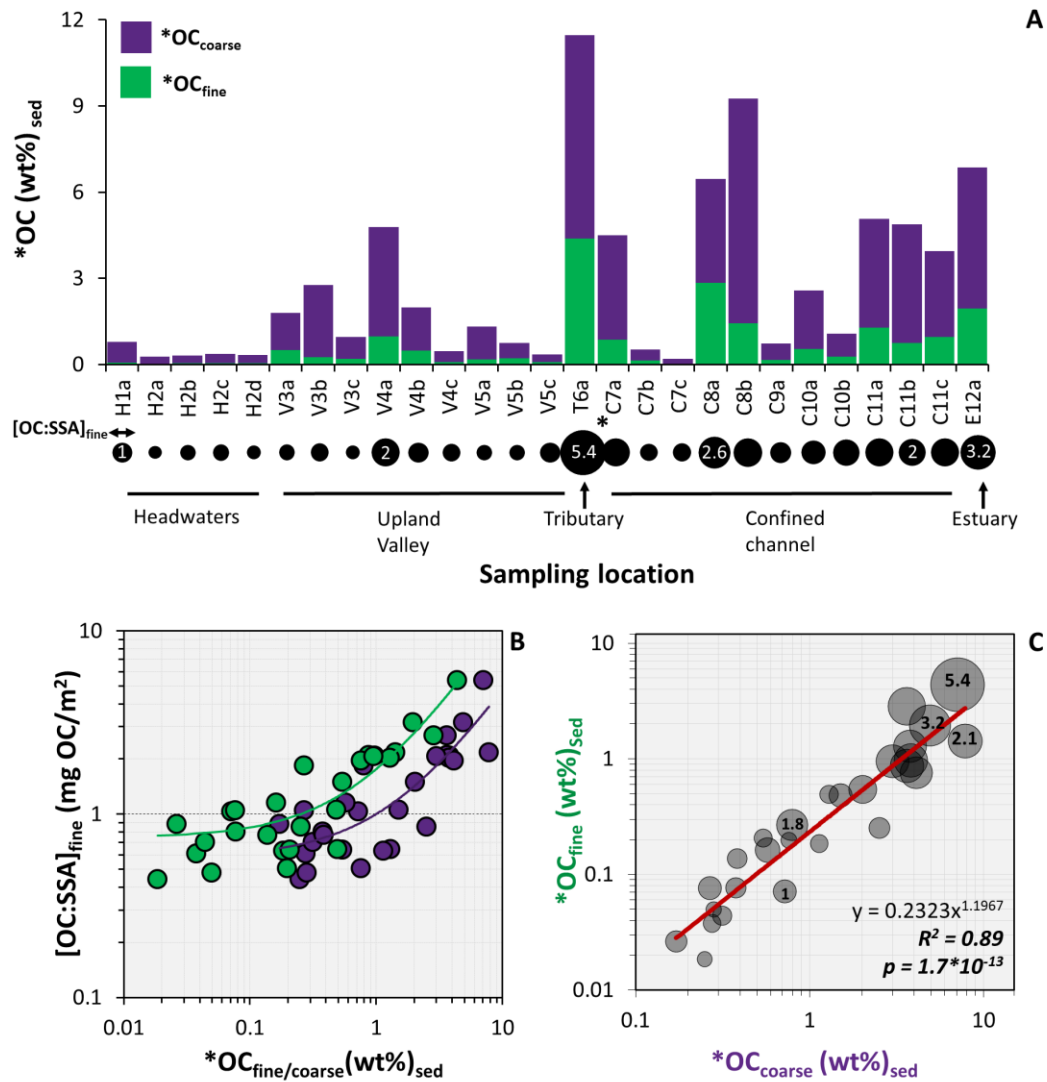


Figure 3.6. Total organic carbon content ($OC_{bulk} = *OC_{coarse} + *OC_{fine}$) and OC loaded to fine sediments in overbank deposits along the Alsea River after a flood in December 2007. Percentages are expressed over the total mass of sediments in the deposit layer ($wt\%_{sed}$) as opposed to Figure 5 in which percentages are calculated relative to the mass of fine or coarse sediments (see text for details). In panels A and C the area of the circles is proportional to OC loading [OC:SSA ($mg\ OC/m^2$)] (Values inside the circles are included for scaling). A. OC_{bulk} and its components, as well as OC loading showed higher values after the confluence with Fall Creek (T6), where a sample was collected from a landslide deposit (marked with a star (*)). B. For OC:SSA values above $1.0\ mg\ OC/m^2$, OC-loading correlates, in a similar fashion, with both OC_{fine} and OC_{coarse} . C. A power-law function fits the correlation between OC_{coarse} and OC_{fine} across the deposits but does not explain the patterns of OC loading into the fine fraction.

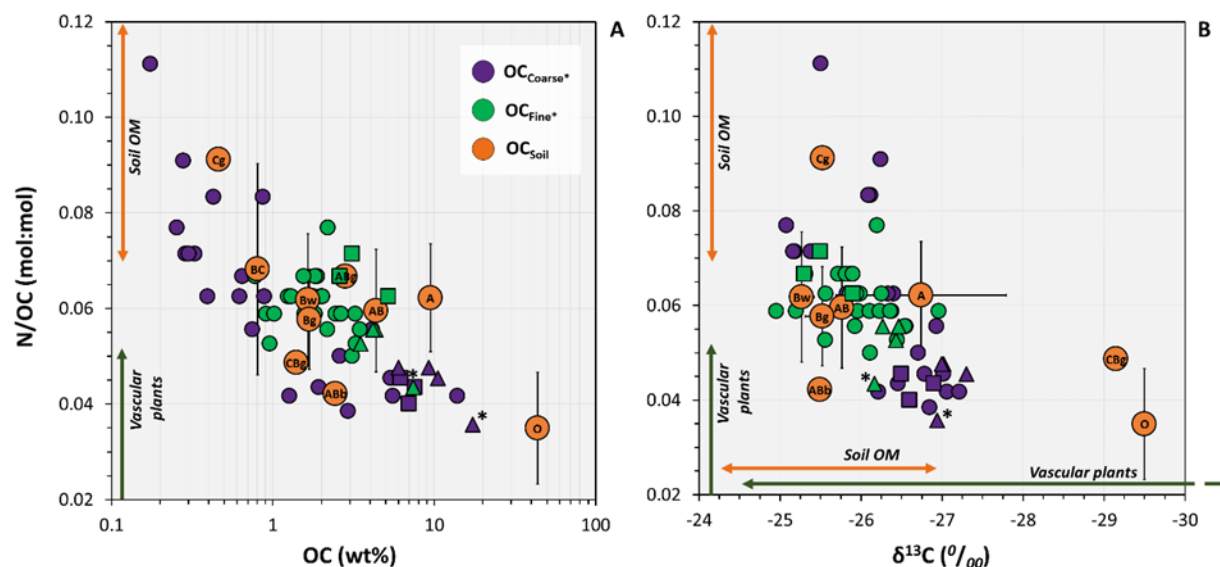


Figure 3.7. Elemental (A) and isotopic (B) composition of organic matter in sediments and soils in the Alsea River basin. Sediments collected from overbank deposits along the river channel after a flood in 2007 are represented by the smaller circles (green for OC_{fine} and dark purple for OC_{coarse}). Overbank deposits with landslide-like granulometry are represented by triangles. Samples collected from a landslide deposit at the confluence with Fall Creek, a major tributary, are identified with a star (*). December 2007's suspended sediments samples are represented by squares. Bulk soil samples were collected from hillslopes and other contributing areas in a watershed located in the lower portion of the Alsea River Basin (orange circles). Different sample sizes were used to characterize the elemental composition ($n=125$) and the isotopic content $\delta^{13}\text{C}$ ($n=60$) of soil organic matter. Error bars correspond to 1 s.d. around the mean value for each variable. For certain soil horizons (e.g. ABb, CBg, Cg) only one sample was available, and no error bars are shown. To aid the interpretation of the compositional characteristics in our samples, the expected ranges of compositional values for soil OM and vascular plant material are included (represented with double-headed arrows, except for N/OC for vascular plant material which could be as low as 0.005^{21}).

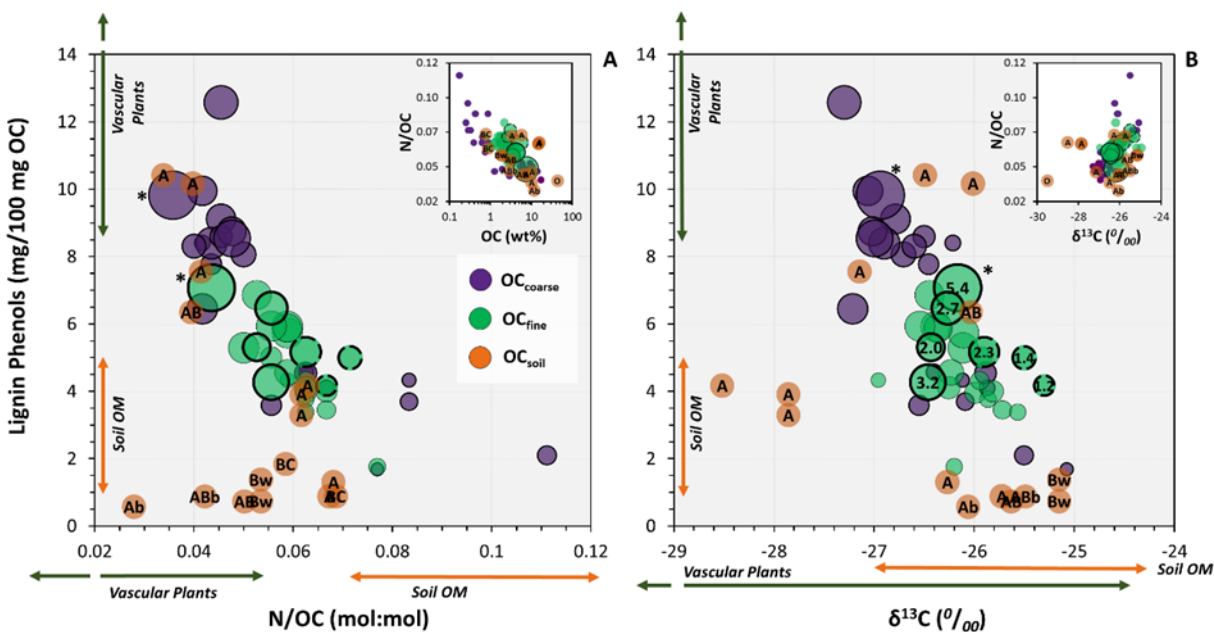


Figure 3.8. Lignin phenols, N/OC ratios (A) and $\delta^{13}\text{C}$ (B) composition of organic matter in sediments and soils in the Alesia River basin and its relationship with OC_{fine} loaded to overbank deposits along the river channel after a flood in 2007. OC_{fine} and OC_{soil} samples are represented by circles with an area that is proportional to OC loading [OC: SSA (mg OC/m²)] (Values inside the circles are included for scaling). To match $\text{OC}_{\text{coarse}}$ fractions with their corresponding fine fraction across samples, we assigned the same values of OC-loading to each set (Color key as in Figure 7). OC_{fine} from overbank deposits with landslide-like granulometry is represented by circles with thick and continuous outlines while OC_{fine} from suspended sediments collected during December 2007's flood is represented by circles with thick and discontinuous outlines (no distinction is made for $\text{OC}_{\text{coarse}}$ for clarity). A reduced amount of soil samples was analyzed for biomarker yields ($n=16$; see Figure 7) (A) and only 14 of those samples had $\delta^{13}\text{C}$ data available (B). To maintain comparability across our results, patterns shown in Figure 7 were reproduced with the reduced number of soil samples used in this figure (small panels, top right). To aid interpretation of compositional characteristics in our samples, the expected ranges of compositional values for soil OM and vascular plant material are included (represented with double-headed arrows²¹).

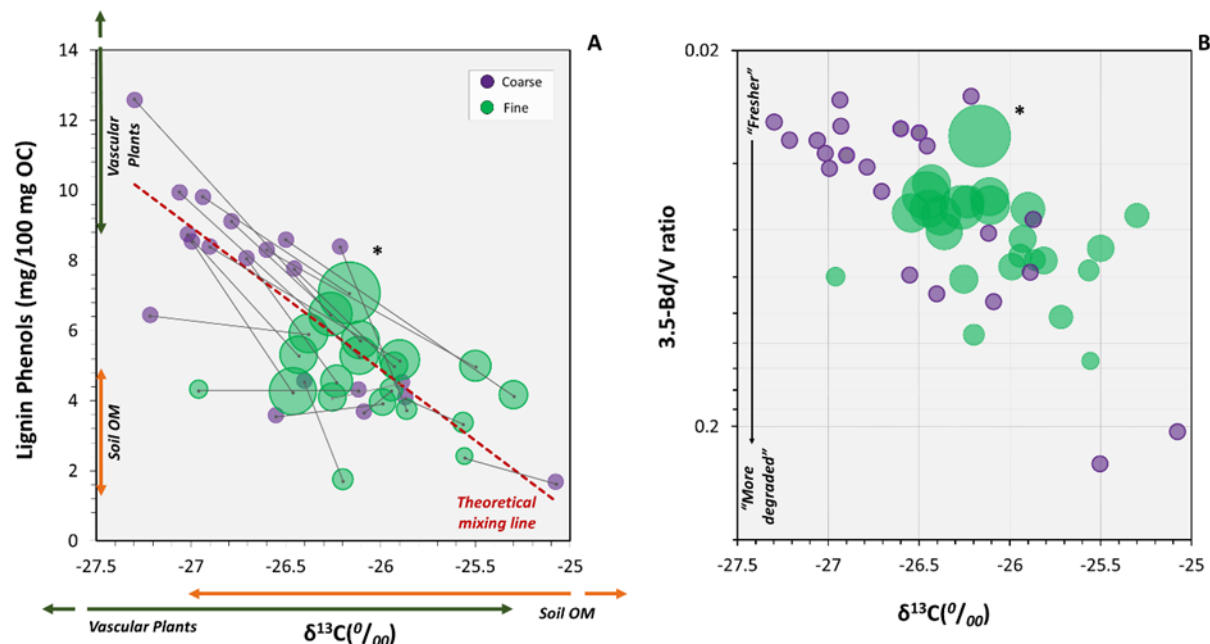


Figure 3.9. $\text{OC}_{\text{coarse}}$ as a proximal source of OC_{fine} in overbank deposits along the Alsea River after a storm in 2007. The incorporation of material resembling vascular plant fragments into a more homogeneous mixture represented by OC_{fine} seems to produce isotopic fractionation (A). The fragments being transferred from $\text{OC}_{\text{coarse}}$ to OC_{fine} have a higher 3.5-Bd/V ratio than the “parent” material, suggesting that particles with more advanced degradation stage are more likely to be fragmented.

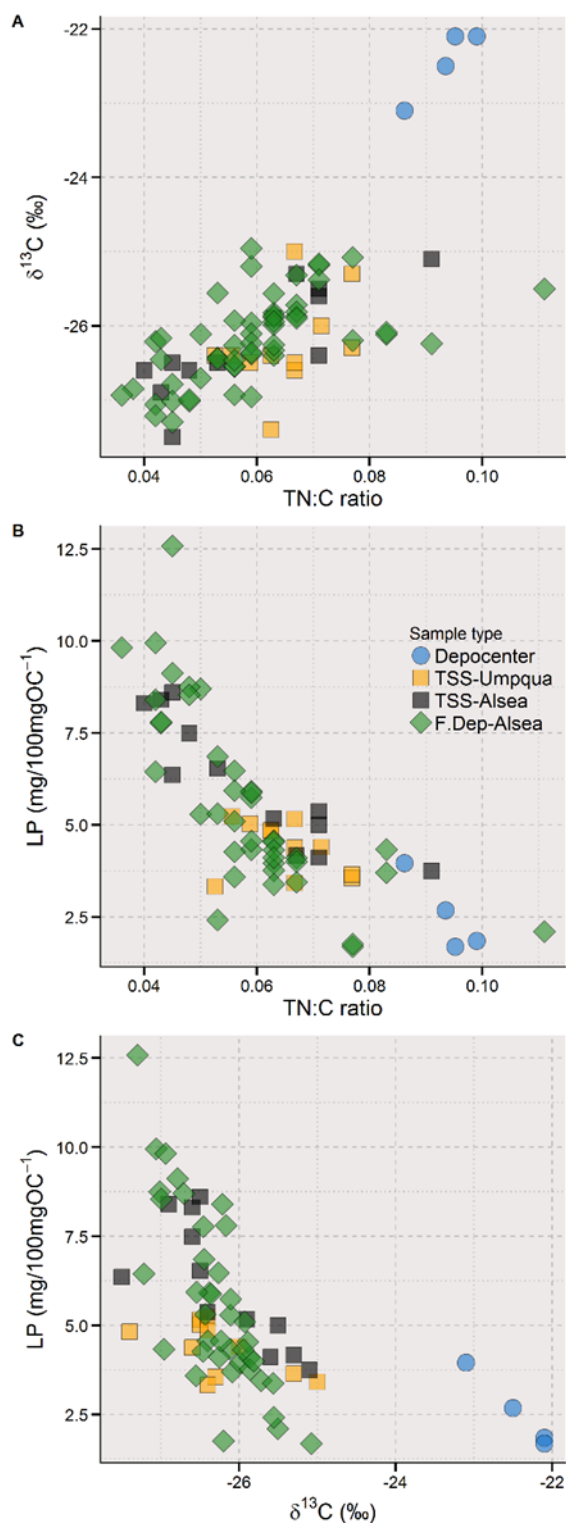


Figure 3.10. Chemical characteristics of overbank sediments deposited after the GCG-2007 along the Alesea River as compared to suspended sediments from the Alesea¹⁰ and Umpqua⁵⁶ Rivers. Also, the average chemical composition of a terrestrial organic matter depocenter off the Umpqua River mouth²⁵ are provided for reference

Table 3-1. Locations for the collection of overbank deposit samples along the Alsea River, Oregon Coast Range, after the Great Coastal Gale (December 2007). (*) Measurements from Google earth pro V 7.3.1.4507 (December 13, 2015)-eye alt:220; provided for relative comparison only.

River Stop	Fluvial landscape	Station code	Distance from headwaters*	Elevation (m)*	River gradient (m km⁻¹)*	Channel width (m)*	Location	Depth (cm)
Hwy-34	Headwaters	H1a	0	108.7	6	25	A	0-7
Clemens	Headwaters	H2a	0.91	103.3	4.6	23	A	0-5
Clemens	Headwaters	H2b	0.91	103.3	4.6	23	A	5-10
Clemens	Headwaters	H2c	0.91	103.3	4.6	23	A	10-15
Clemens	Headwaters	H2d	0.91	103.3	4.6	23	A	15-20
Mill Creek	Upland valley	V3a	9.34	76.1	0	24	A	0-3
Mill Creek	Upland valley	V3b	9.34	76.1	0	27	A	3-5
Mill Creek	Upland valley	V3c	9.34	76.1	0	27	B	0-3
Campbell	Upland valley	V4a	16.91	66	5.3	27	A	0-2
Campbell	Upland valley	V4b	16.91	66	5.3	27	B	0-1
Campbell	Upland valley	V4c	16.91	66	5.3	27	B	1-4
Salmon	Upland valley	V5a	20	62.7	1.3	27	A	0-3.5
Salmon	Upland valley	V5b	20	62.7	1.3	27	B	0-1
Salmon	Upland valley	V5c	20	62.7	1.3	27	B	1-5
Fall Creek	Tributary	T6a	32.92	42	1.8	27	A	0-4
Blackberry	Confined Channel	C7a	48.58	18.1	0	42	A	0-1
Blackberry	Confined Channel	C7b	48.58	18.1	0	42	B	0-3.5
Blackberry	Confined Channel	C7c	48.58	18.1	0	42	B	3.5-7
Tidewater	Confined Channel	C8a	50.28	16.8	0.7	42	A	0-5
Tidewater	Confined Channel	C8b	50.28	16.8	0.7	42	B	0-3
Random	Confined Channel	C9a	54.28	14.3	0.1	56	A	0-17
Kozy	Confined Channel	C10a	65.82	3.9	0	90	A	0-2
Kozy	Confined Channel	C10b	65.82	3.9	0	90	A	2-13
Risley	Confined Channel	C11a	70.3	3.5	0	100	A	0-1
Risley	Confined Channel	C11b	70.3	3.5	0	100	A	1-7
Risley	Confined Channel	C11c	70.3	3.5	0	100	B	0-7
RV Park	Estuary	E12a	75.64	3.5	0	250	A	0-1

Table 3-2. Textural characteristics of samples from overbank deposits after The Great Coastal Gale (December 2007) along the Alsea River, Oregon Coast Range.

<i>Fluvial landscape</i>	<i>Station code</i>	<i>Distance from headwaters</i>	<i>Estimated Texture</i>	<i>% Coarse</i>	<i>% Fine</i>	<i>Mean grain size (phi)</i>	<i>D₁₆ (μm)</i>	<i>D₅₀ (μm)</i>	<i>D₈₄(μm)</i>
Headwaters	H1a	0	Sandy	0.96	0.04	2.12	84.26	194.42	412.29
Headwaters	H2a	0.91	Sandy	0.98	0.02	0.50	375.64	681.67	1061.81
Headwaters	H2b	0.91	Sandy	0.95	0.04	0.06	478.35	968.57	1426.68
Headwaters	H2c	0.91	Sandy	0.95	0.04	0.04	374.51	1017.82	1519.65
Headwaters	H2d	0.91	Sandy	0.93	0.06	0.14	328.28	957.37	1444.41
Upland valley	V3a	9.34	Fine Sand-Silty	0.75	0.22	3.03	6.56	94.10	265.63
Upland valley	V3b	9.34	Fine Sand-Silty	0.84	0.13	3.08	13.03	104.60	236.47
Upland valley	V3c	9.34	Fine Sand	0.88	0.12	3.04	17.03	111.98	235.90
Upland valley	V4a	16.91	Fine Sand-Silty	0.66	0.30	4.08	3.98	42.71	131.27
Upland valley	V4b	16.91	Fine Sand-Silty	0.76	0.21	2.85	11.24	114.73	289.42
Upland valley	V4c	16.91	Sandy	0.95	0.04	2.20	99.03	212.48	343.04
Upland valley	V5a	20	Fine-Sand	0.86	0.10	2.72	19.61	144.21	290.31
Upland valley	V5b	20	Fine-Sand	0.82	0.16	N.D.	N.D.	N.D.	N.D.
Upland valley	V5c	20	Sandy	0.94	0.04	1.56	102.65	322.82	590.81
Tributary	T6a	32.92	Silty	0.40	0.57	7.32	1.12	4.99	12.70
Confined Channel	C7a	48.58	Silty	0.64	0.32	4.30	8.86	44.37	98.84
Confined Channel	C7b	48.58	Fine Sand	0.87	0.10	3.26	18.97	94.91	198.25
Confined Channel	C7c	48.58	Sandy	0.97	0.02	1.94	97.09	270.65	413.13
Confined Channel	C8a	50.28	Silty	0.33	0.63	7.56	1.09	4.13	10.67
Confined Channel	C8b	50.28	Silty	0.52	0.41	4.23	8.39	44.26	106.91
Confined Channel	C9a	54.28	Fine Sand	0.90	0.08	2.71	32.39	144.88	280.82
Confined Channel	C10a	65.82	Fine Sand-Silt	0.74	0.21	3.60	8.58	69.90	168.40
Confined Channel	C10b	65.82	Fine Sand	0.89	0.10	2.71	41.85	159.67	258.55
Confined Channel	C11a	70.3	Silty	0.59	0.34	7.34	1.21	4.85	12.50
Confined Channel	C11b	70.3	Silty	0.72	0.22	3.95	5.63	55.70	133.42
Confined Channel	C11c	70.3	Silty	0.69	0.26	4.05	5.02	48.85	127.17
Estuary	E12a	75.64	Silty	0.49	0.43	6.92	1.36	6.70	16.66

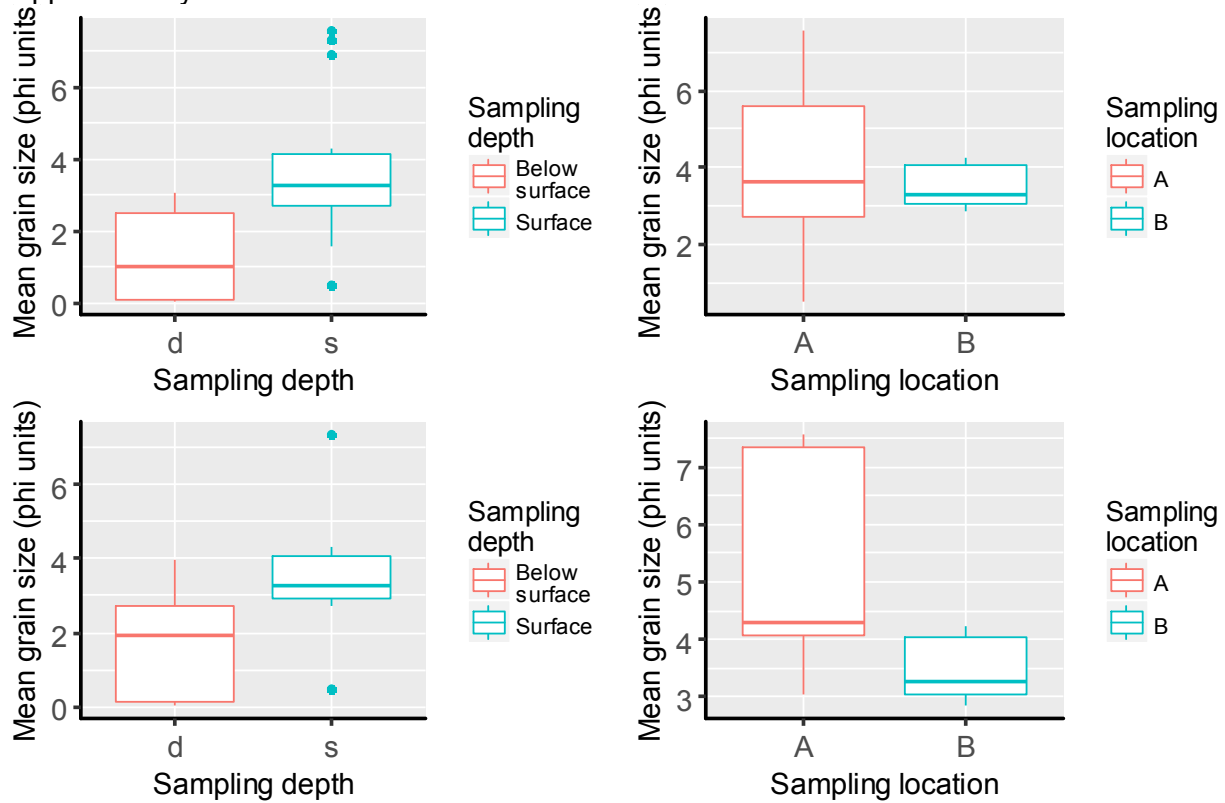
Table 3-3. Organic carbon, nitrogen to carbon ratio, specific surface area, and organic carbon loading ([OC:SSA]) in overbank deposits along the Alsea River, Oregon Coast Range. Samples were collected after the Great Coastal Gale (December 2007). The fraction of the sample analyzed is indicated by a subscript (Coarse >63 μm ; fine <63 μm). Percentages were calculated over the total mass sediment for that fraction. (*) Loadings calculated over corrected SSA values (see text for details).

<i>Fluvial landscape</i>	<i>Station code</i>	<i>Distance from headwaters</i>	<i>Mean grain size (phi)</i>	<i>OC_{bulk} (%wt)</i>	<i>N: OC_{bulk}</i>	<i>OC_{coarse} (%wt)</i>	<i>N: OC_{coarse}</i>	<i>SSA (m² mg⁻¹)</i>	<i>OC_{fine} (%wt)</i>	<i>N: OC_{fine}</i>	<i>[OC: SSA]_{fine}* (mg OC m⁻²)</i>
Headwaters	H1a	0	2.12	0.789	0.048	0.748	0.056	26	1.997	0.063	1.0
Headwaters	H2a	0.91	0.50	0.262	0.077	0.254	0.077	41	0.957	0.053	0.4
Headwaters	H2b	0.91	0.06	0.311	0.063	0.288	0.071	41	0.908	0.059	0.6
Headwaters	H2c	0.91	0.04	0.388	0.053	0.329	0.071	41	1.025	0.059	0.7
Headwaters	H2d	0.91	0.14	0.298	0.067	0.301	0.071	41	0.779	0.067	0.5
Upland valley	V3a	9.34	3.03	2.333	0.067	1.671	0.063	38	2.192	0.077	0.6
Upland valley	V3b	9.34	3.08	6.357	0.024	2.92	0.038	25	1.827	0.059	0.9
Upland valley	V3c	9.34	3.04	1.233	0.048	0.868	0.083	35	1.579	0.059	0.5
Upland valley	V4a	16.91	4.08	4.534	0.045	5.55	0.042	17	3.106	0.05	2.1
Upland valley	V4b	16.91	2.85	2.962	0.034	1.933	0.043	25	2.187	0.056	1.1
Upland valley	V4c	16.91	2.20	0.579	0.056	0.394	0.063	30	1.894	0.067	0.8
Upland valley	V5a	20	2.72	0.986	0.05	1.268	0.042	33	1.793	0.063	0.6
Upland valley	V5b	20	N.D.	0.926	0.056	0.649	0.067	25	1.244	0.063	0.6
Upland valley	V5c	20	1.56	0.599	0.067	0.279	0.091	27	1.833	0.067	1.0
Tributary	T6a	32.92	7.32	11.414	0.038	17.337	0.036	15	7.408	0.043	5.4
Confined Channel	C7a	48.58	4.30	4.888	0.042	5.466	0.045	14	2.586	0.059	2.1
Confined Channel	C7b	48.58	3.26	0.645	0.071	0.43	0.083	20	1.303	0.063	0.8
Confined Channel	C7c	48.58	1.94	0.255	0.077	0.174	0.111	25	1.556	0.067	0.9
Confined Channel	C8a	50.28	7.56	6.95	0.045	10.549	0.045	17	4.326	0.056	2.7
Confined Channel	C8b	50.28	4.23	6.483	0.042	13.935	0.042	17	3.26	0.059	2.2
Confined Channel	C9a	54.28	2.71	0.764	0.083	0.625	0.063	22	2.026	0.063	1.2
Confined Channel	C10a	65.82	3.60	3.23	0.05	2.603	0.05	19	2.45	0.059	1.5
Confined Channel	C10b	65.82	2.71	1.335	0.05	0.886	0.063	19	2.659	0.059	1.8
Confined Channel	C11a	70.3	7.34	5.844	0.045	5.992	0.048	18	3.488	0.053	2.0
Confined Channel	C11b	70.3	3.95	7.921	0.045	5.359	0.045	19	3.262	0.053	2.0
Confined Channel	C11c	70.3	4.05	3.364	0.048	4.139	0.056	19	3.465	0.056	2.1
Estuary	E12a	75.64	6.92	5.839	0.05	9.213	0.048	14	4.177	0.056	3.2

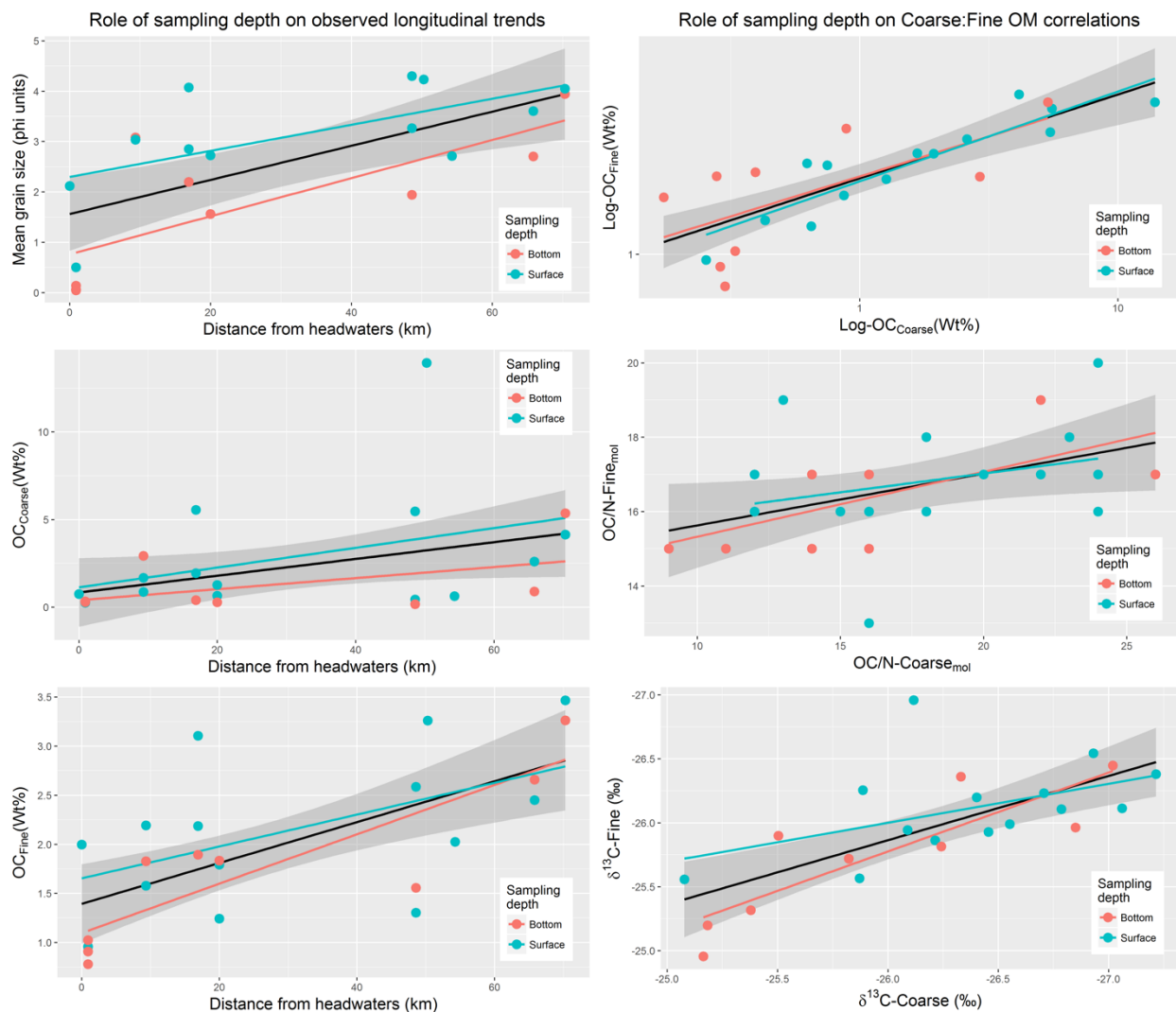
Table 3-4. $\delta^{13}\text{C}$ ratios and Carbon-normalized yields ($\text{mg } 100 \text{ mg OC}^{-1}$) of CuO product classes in fine $<63 \mu\text{m}$ and coarse $>63 \mu\text{m}$ particles overbank deposits along the Alsea River, Oregon Coast Range. VP vanillyl phenols, SP syringyl phenols, CP lignin-derived cinnamyl phenols, 3,5-Bd 3,5-Dihydroxybenzoic acid

<i>Fluvial landscape</i>	<i>Station code</i>	<i>Distance from headwaters</i>	$\delta^{13}\text{C}_{\text{coarse}}$ ($^{\circ}/_{\text{oo}}$)	$\text{VP}_{\text{coarse}}$	$\text{SP}_{\text{coarse}}$	$\text{CP}_{\text{coarse}}$	$3,5\text{-Bd}_{\text{coarse}}$	$\delta^{13}\text{C}_{\text{fine}}$ ($^{\circ}/_{\text{oo}}$)	VP_{fine}	SP_{fine}	CP_{fine}	$3,5\text{-Bd}_{\text{fine}}$
Headwaters	H1a	0	-26.552	2.770	0.660	0.160	0.220	-25.989	2.890	0.850	0.220	0.217
Headwaters	H2a	0.91	-25.078	1.300	0.320	0.070	0.269	-25.558	1.770	0.480	0.170	0.236
Headwaters	H2b	0.91	-25.183	N.D.	N.D.	N.D.	N.D.	-25.198	N.D.	N.D.	N.D.	N.D.
Headwaters	H2c	0.91	-25.164	N.D.	N.D.	N.D.	N.D.	-24.956	N.D.	N.D.	N.D.	N.D.
Headwaters	H2d	0.91	-25.379	N.D.	N.D.	N.D.	N.D.	-25.317	N.D.	N.D.	N.D.	N.D.
Upland valley	V3a	9.34	-26.402	3.190	1.060	0.320	0.283	-26.199	1.270	0.380	0.110	0.145
Upland valley	V3b	9.34	-26.85	N.D.	N.D.	N.D.	N.D.	-25.963	N.D.	N.D.	N.D.	N.D.
Upland valley	V3c	9.34	-26.117	3.100	1.050	0.180	0.190	-26.959	3.110	0.990	0.230	0.249
Upland valley	V4a	16.91	-27.061	6.720	2.740	0.490	0.233	-26.113	4.240	0.910	0.140	0.207
Upland valley	V4b	16.91	-26.456	5.910	1.560	0.300	0.212	-25.929	3.650	1.100	0.260	0.231
Upland valley	V4c	16.91	-25.823	N.D.	N.D.	N.D.	N.D.	-25.719	2.400	0.850	0.200	0.246
Upland valley	V5a	20	-26.214	7.180	0.950	0.270	0.190	-25.863	2.670	0.860	0.230	0.192
Upland valley	V5b	20	-25.871	3.200	0.700	0.200	0.180	-25.566	2.480	0.720	0.180	0.191
Upland valley	V5c	20	-26.242	N.D.	N.D.	N.D.	N.D.	-25.814	2.690	1.060	0.250	0.195
Tributary	T6a	32.92	-26.937	7.550	1.930	0.340	0.205	-26.166	5.860	1.000	0.220	0.190
Confined Channel	C7a	48.58	-26.786	6.500	2.250	0.370	0.265	-26.107	4.400	1.110	0.230	0.227
Confined Channel	C7b	48.58	-26.089	2.690	0.850	0.160	0.250	-25.944	3.240	0.880	0.200	0.227
Confined Channel	C7c	48.58	-25.504	1.430	0.560	0.110	0.358	-25.898	N.D.	N.D.	N.D.	N.D.
Confined Channel	C8a	50.28	-27.298	8.400	3.420	0.760	0.260	-26.264	5.080	1.210	0.180	0.265
Confined Channel	C8b	50.28	-27.215	4.530	1.620	0.300	0.157	-26.38	4.650	1.110	0.160	0.256
Confined Channel	C9a	54.28	-25.887	3.380	0.850	0.310	0.263	-26.255	2.950	0.960	0.200	0.239
Confined Channel	C10a	65.82	-26.707	6.030	1.740	0.300	0.286	-26.232	3.560	0.840	0.160	0.180
Confined Channel	C10b	65.82	-26.331	N.D.	N.D.	N.D.	N.D.	-26.361	4.210	1.400	0.270	0.255
Confined Channel	C11a	70.3	-27.016	6.110	2.210	0.430	0.229	-26.432	4.180	0.950	0.180	0.189
Confined Channel	C11b	70.3	-27.019	N.D.	N.D.	N.D.	N.D.	-26.448	5.290	1.310	0.260	0.279
Confined Channel	C11c	70.3	-26.931	N.D.	N.D.	N.D.	0.172	-26.544	4.360	1.290	0.280	0.236
Estuary	E12a	75.64	-26.994	5.960	2.240	0.340	0.246	-26.463	3.290	0.840	0.140	0.172

Supplementary material



Supplementary Figure 5. Differences in mean grain size between deposit layers from the Aalsea's overbank deposits. Samples were collected at different depths and locations. Upper panels include all samples; therefore, categories have unequal sample sizes. Bottom panels include paired samples (comparing same deposits when they were sampled at different depths or locations) As expected, surficial samples had lower mean grain sizes because of the rapid deposition of coarse material (phi units). Samples collected from different locations are assumed to belong to different populations as shown by unequal variances between A and B locations.



Supplementary Figure 6. Role of sampling depth on observed longitudinal trends and correlations between biogeochemical proxies in overbank deposits from the Alesja River. Although surface samples were significantly finer than subsurface samples, sampling depth did not affect the major trends observed in our data set. Therefore, deposit layers, regardless their sampling depth, are treated as sample units.

Specific surface area (SSA) along overbank deposits in the Alsea River

The longitudinal trends observed in overbank deposits along the Alsea River indicated increasing deposition of fine sediments from headwaters to the estuary. Furthermore, these fine sediments became more enriched in organic matter in the downstream direction. As % OC_{fine} implies a normalization of organic matter content over the available amount of fine sediments, increasing deposition of fine materials should not influence OC concentration values. Thus, a first possible explanation for these results could be related to changes in the specific surface area of mineral particles within the fine fraction. This is because finer particles with larger surface areas will carry higher amounts of OC per gram of sediment. Although this hypothesis was at odds with the virtually constant mean particle diameters in the silt and clay fractions, we tested for any longitudinal trend in SSA data.

Contrary to our expectations, Specific Surface Area (SSA) in the fine sediment fraction decreased significantly in the downstream direction ($R^2=0.5764$, $p=1.6 \times 10^{-5}$; Supplementary Figure 7). Particles with the highest SSA, 41 m²/g, were found along the entire depth profile at headwaters (H2a-d, with the coarsest deposit layers). The lowest SSA, 14 m²/g, was measured in a surficial deposit layer at Blackberry park (C7a), within the confined valley segment. Both landslide-like deposit layers (SSA, 14-18 m²/g), and suspended sediments had SSA values within the longitudinal trend (30.6 ± 1.15 m²/g; Supplementary Figure 7A). However, we did not include SSA from suspended sediments in our regression analysis.

The longitudinal trend in SSA suggested that particles with large surface areas were mostly associated with coarse sand deposits. Moreover, since mean particle diameter in the sand fraction exhibited a significant decreasing longitudinal trend, we tested for a correlation between mean particle diameter in the sand fraction and SSA. We found that SSA increased in 6.94 ± 0.99 s.d. m² per phi-unit change in the diameter of sand particles ($R^2=0.69$, $p=8.9 \times 10^{-7}$).

Specific surface area measurements in heterogeneous sediment mixtures

The relationship between specific surface area (SSA) and mean grain size changed across the size fractions analyzed. In bulk samples, SSA values ranged from 10 to 31 m²/g. In these unfractionated samples, we identified three groups encompassing distinct ranges of mean grain size and surface area (Supplementary Figure 8). The first group consisted of the coarsest samples with an average surface area of 30.5 ± 0.5 m²/g and with mean grain size between 0-2 phi units (1000-250µm). The second group, with a wider range in S.A. values (10 – 27 m²/g), had mean grain sizes between 2.1 and 4.2 phi units (233-54µm). The third group, corresponding to

those samples with only silt and clay, and a mean grain size diameter of 7.3 ± 0.32 phi units ($\sim 6\mu\text{m}$), had S.A. values in the range of 12- 17 m^2/g . Contrary to our expectations, we observed an overall trend of decreasing surface area with decreasing grain size. This trend was also evident in the coarse fraction isolated by sieving (Supplementary Figure 8). In these sand-sized sediments, only samples corresponding to the first two groups observed in the bulk samples were measured. Again, in the coarsest samples SSA ranged from 28 to 31 m^2/g while the mean grain size ranged from -0.11 to 1.73 phi units (1079-301 μm). In the remaining samples -i.e. second group-SSA ranged from 8 to 18 m^2/g and the mean grain size was in the range of 2.01 to 3.34 phi units (248-99 μm). There were no consistent relationships between mean grain size and SSA within the groups observed in both bulk and coarse samples. These findings contrasted with our observations from the fine fraction of these sediments.

Within the fine fraction, SSA increased proportionally to decreasing mean grain size. Furthermore, the samples clustered in a distinctive fashion in comparison to bulk sediments and their coarse fraction (Supplementary Figure 8). We assigned numbers to these groups to differentiate them from the description above. Group 1 was formed by a pair of samples collected at Highway 34 (first sampling location) and at Campbell Park (fourth sampling location in the downstream direction). This group had intermediate values of SSA (26 and 30 m^2/g respectively) and were the coarsest samples within the fine fraction (mean grain size 5.16-5.02 phi units, 31-28 μm). Group 2, the largest cluster of samples, exhibited a sharp gradient of increasing SSA with decreasing grain size. Within a narrow range of grain sizes (5.3-6.3 phi units or 13-25 μm) we observed a three-fold increase in SSA from 14 to 41 m^2/g . A significant linear trend with mean grain size as predictor ($p=9.1 \times 10^{-5}$, $n=21$) explained 60% of the observed variability in SSA. Group 3 was formed by samples from deposits dominated by silt and clay, as in the case of bulk sediments. Because of the small sample size ($n=4$) we did not attempt a linear regression within this group. However, higher values of SSA did correspond to smaller grain sizes.

The distinctive clustering of samples within the fine fraction were related to the shapes of their grain size distributions (Supplementary Figure 9). We observed three types of average cumulative distributions (curves) for particle sizes (Supplementary Figure 9A and B). Following the numerals used above, Curve 1 had two points of curvature located at 4 (D_{20}) and 33 μm (D_{50}). The first point showed convexity, while the second point showed concavity suggesting a smoother rate of accumulation for particle sizes on a wide range of diameters around the median grain size (10-50 μm). Curve 2 had one convex point of curvature at 13 μm (D_{50}). This averaged curve

encompassed the largest group of cumulative distributions. In this group of samples SSA values increased in proportion to the overall curvature in the distribution, suggesting a complex, but predictable textural effect. For curve 3, we found a single convex point of curvature at $17\ \mu\text{m}$ (D_{95}) also pointing toward rapid accumulation of particles with smaller diameters than D_{95} . Because of these differences in location for points of curvature, the largest distances between cumulative curves, a proxy for the distance between clusters of samples, were found approximately at D_{50} and at D_{84} . This is also shown by plotting SSA values against D_{50} and D_{84} (Supplementary Figure 9C and D).

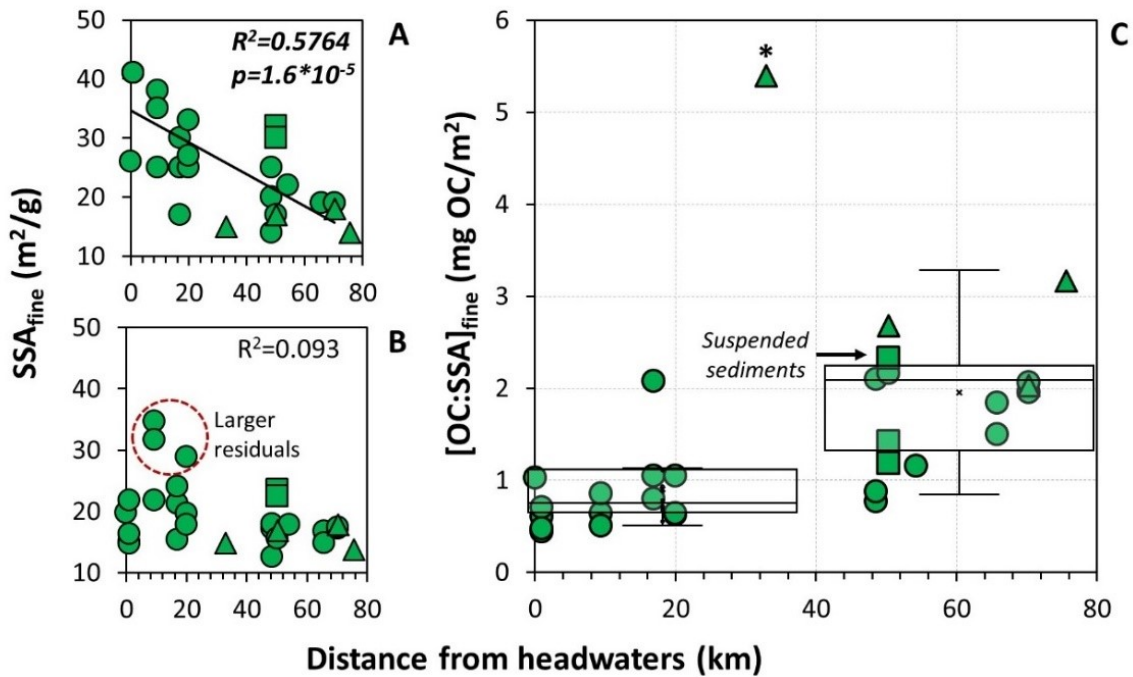
In summary, the relationship between surface area and mean grain size is influenced by the shape of underlying grain size distribution in our dataset.

Why did the coarsest samples have particles with the largest SSA?

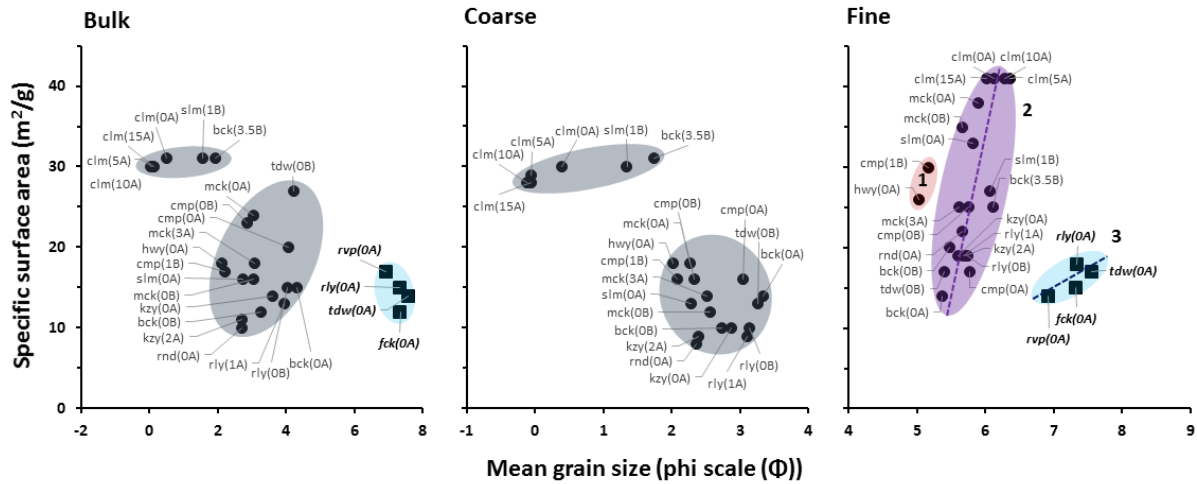
The average stream power decreases longitudinally. Thus, larger particles eroded in headwaters have limited transport rate. Once mobilized, the coarse fraction is more susceptible to deposition than to transport. However, the finest particles across the deposits, carriers of large surface areas, were co-deposited with sand-sized sediments instead of being transported. Furthermore, these finer sediments should not make any contribution to surface area measurements in the coarse fraction (separated by sieving). So, why are these fine silts being deposited altogether with sands and retained in the coarse fraction? We argue that these fine sediments are originally found forming cohesive aggregates. Cohesive sediments might exhibit different stability to water breakage and while many of them can be broken and mobilized, other particles remain as aggregates to be co-deposited within the sand fraction. Since the combustion treatment prior to SSA measurements was procedures were done after sieving, we believe that many of these aggregates were originally retained in the $63\ \mu\text{m}$ sieve, while a small number of them ended up in the fine fraction. Indeed, less than 10% of sediment mass/volume is represented by large surface area carriers.

Thus, these particles seem to make a disproportionate contribution to surface area compared to their abundance. For instance, 1g of bulk sediments from Clemens produces a total surface area of $\sim 30\text{m}^2$. If we attribute these large surface areas solely to small particles representing 10% of the total mass, then their actual surface area would be an order of magnitude larger (i.e. $300\ \text{m}^2\ \text{g}^{-1}$). These values cannot be observed directly because the shape of the particle size distribution introduces a dilution effect as we discussed earlier.

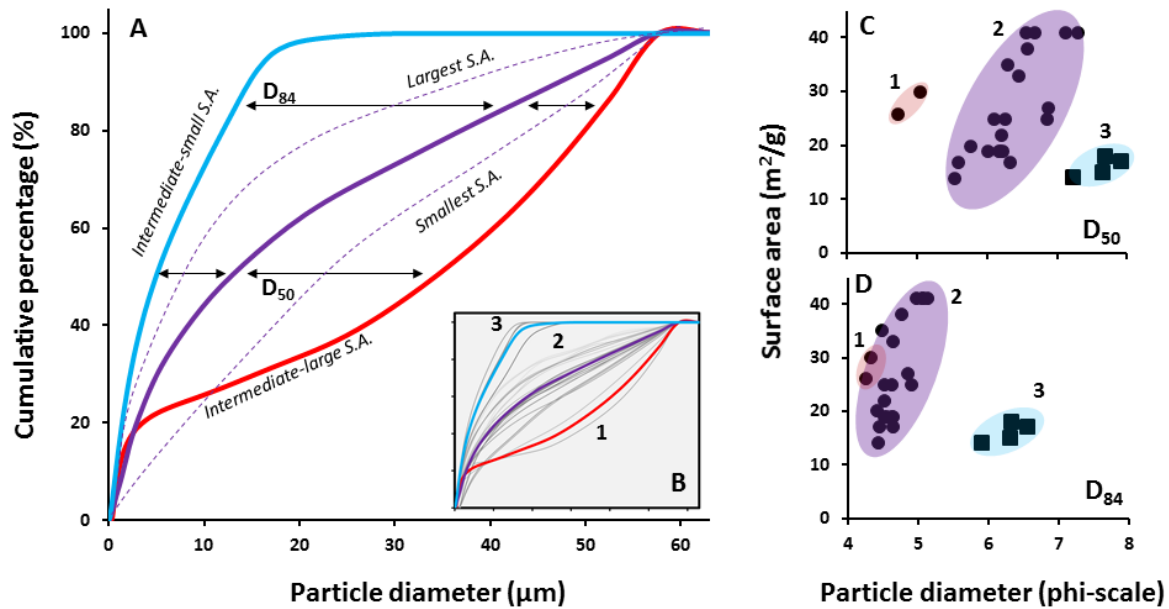
Given that less than 10% of sediment mass in the samples with largest surface area is less than 10% and that surface area from fine suspended sediments in the Alsea River is in the range of $31 \text{ m}^2 \text{ g}^{-1}$, we conclude that large surface area carriers are indeed found mostly in suspension. Thus, sediment transport and the river's longitudinal profile control the availability of mineral surface area across flood deposits.



Supplementary Figure 7. Longitudinal profiles of Specific Surface Area (SSA) and organic carbon loading $[OC:SSA]_{fine}$ in fine sediments, across overbank deposits along the Alesia River after a flood in December 2007. A. SSA decreased significantly in the downstream direction ($p < 0.0001$). B. No longitudinal trend in SSA_{fine} is observed after accounting for the input of coarse sands to each deposit ($SSA_{fine} = \beta_0 + \beta_1 \cdot \phi_{sand}$; $R^2=0.69$, $p=8.9 \times 10^{-7}$) (deposit layers with large residuals were excluded from trend fitting). C. Corrected organic carbon loadings show a significant contrast between deposits located upstream and downstream the confluence with Fall Creek (Landslide sample). Deposits with landslide-like granulometry are identified by triangles (see below). Values for suspended sediment samples collected during the storm by Hatten et al (ref¹⁰) are identified by squares ($n=3$). A sample collected from a landslide deposit at the confluence with Fall Creek, a major tributary, is marked with a star (*).



Supplementary Figure 8. The relationship between surface area (S.A.) and mean grain size changes between and within the size fractions analyzed. Coarse fraction defined as grains $<4\Phi$ or $>63\ \mu\text{m}$. Fine fraction is $>4\Phi$ or $<63\ \mu\text{m}$. Shaded areas represent distinct groups according to the observed relationship between mean grain size and S.A. Only groups in the fine fraction were numbered (1-3). Linear trends plotted across fine-sediment samples are for descriptive purposes. However, an $R^2=0.6034$, $p=9.1 \times 10^{-5}$ was obtained for the linear trend across group 2.



Supplementary Figure 9. Textural influence on the relationship between mean grain size and surface area in fine sediments (clay + silt) from the Alesja River. **A.** Averaged cumulative particle size distributions across groups identified in figure 2. The distance between distributions have maximums at D_{50} (group 1 vs. group 2) and at D_{84} (group 2 vs group 3). Cumulative distributions for samples with the largest and the smallest SSA are also shown. In comparison, samples in group 1 have intermediate to large SSA whereas samples in group 3 have intermediate to small SSA. **B.** Cumulative distribution for particle size across samples and averaged by groups are shown in panel A. Panels **C** and **D** show group separations obtained by using a single parameter from size distribution (either D_{50} or D_{84}) instead of the overall mean grain size distribution used in Supplementary Figure 8.

Chapter 4 Disentangling signals of watershed responses to disturbance from the information content of particle size spectra: An analysis of a 1500-year sedimentary archive from Loon Lake, Umpqua River Basin, Oregon.

Introduction

Fluvial sediments are a dynamic biogeophysical fabric connecting terrestrial and aquatic ecosystems across the earth's surface (Figure 4.1). The erosion mechanisms that mobilize particulate matter across the landscape are complex, ranging from suspended sediment transport to massive movements of the soil mantle, particularly in landscapes dominated by steep slopes¹. In mountainous watersheds, climatic and tectonic forcings (i.e. storms, earthquakes) trigger sediment mobilization and transport, resulting in a highly episodic and intermittent inputs of particles to stream channels². Sediment routing and storage across the fluvial network is also stochastic³. From the complex interactions of the mechanisms of sediment supply and transport that occur at varying spatial and temporal scales emerges a pattern of sediment availability within the watershed described as the natural sediment regime⁴. In the modern era, the accelerated transformation of mountainous landscapes due to human activities have altered the natural sediment regime in many areas around the globe via soil erosion⁵. Although the negative effects of an altered sediment regime propagate across the terrestrial-aquatic continuum, from hillslopes to the ocean⁵, due to the multiplicity of processes involved in fluvial sediment transport, these effects can be easily masked becoming insidious and chronic⁶.

The measurement of sediment yields have been one of the most common approaches to assess alterations in the natural sediment regime¹ because it is viewed as an environmental signal of response to disturbances⁷. However, evidence compiled over the last few decades suggests that inferring characteristics of a watershed's sediment regime from time series of sediment yields could be misleading^{8,9}. Researchers have shown that neither a constant sediment yield implies no alteration of the sediment regime⁸, nor changes in sediment yields imply an univocal watershed's response to such an alteration¹⁰. Even the validity of long-term sedimentary records (e.g. sediment cores) as sources of information for the reconstruction of past environmental conditions have been called into question¹⁰. At the center of these criticisms there is the idea that self-organized processes of sediment routing within the watershed modulate the variability of sediment yields making them insensitive to external forces including human impacts¹⁰⁻¹².

A lack of understanding of sediment routing processes further complicates the interpretation of the particulate load as a watershed's signal of response to disturbances⁷. Since constraining

sediment budgets have been a priority in the last few decades^{7,9}, other aspects of the suspended sediment yield that could offer insights into sediment routing have received less attention. One of those aspects is the distribution of particle sizes in the suspended load⁷. Several studies have suggested that sediment transport processes could modulate the textural composition of the suspended load^{13–19}. The distribution of particle sizes are highly sensitive to the mechanisms of entrainment, transport, and deposition, which are ultimately reflected in the degree of sorting of the deposited sediment mixtures^{13,20–22}. Yet, classical approaches to the study of particle size of suspended and deposited sediments use conventional univariate statistics that mask the polymodal nature of these particle size distributions^{13,23–25}. Moreover, since particle size distributions result from the superposition of different routing mechanisms within the fluvial network, the statistical structure of these distributions is better described by the concept of spectra^{23,26}.

In practical terms, the spectral nature of particle size distributions means that the peaks and the multiple modes observed on a histogram of particle size classes are not random deviations from a smoother density function but have specific relevance in terms of the interpretation of the textural composition (like spectral peaks). Unfortunately, classical statistical summaries can hardly capture the complexity of particle size spectra or allow for the recognition and separation of spectral peaks.

The deconvolution of peaks from particle size spectra (PSS) offers the possibility of identifying transport mechanisms involved in sediment routing^{13,23,24}. By analyzing the spectral characteristics of long-term sediment records, it could be possible to reconstruct fundamental aspects of the sediment regime^{15,23} and set the basis for a better assessment of natural and human-induced changes in a watershed's sediment regime.

Here, we take advantage of a high-resolution sediment archive encompassing 1500 years of sedimentation due to fire, earthquakes, floods, and land clearance in the Oregon Coast Range²⁷. We further develop an existing method based on the principles of information theory²⁸ (entropy analysis, see below) to allow for the deconvolution of peaks from particle size spectra and asked the following questions:

- What kind of signals of watershed response to disturbance can we identify from the information content of particle size spectra?

- Can we use the information content of the PSS to identify different spectral peaks and identify their relationship with physical and chemical process during long-term sedimentation in a lake environment?
- How can we use the information content of PSS to gain insights into the analysis of sedimentary archives not offered by other traditional methods?

Background: Entropy and the analysis of particle size spectra

The concept of entropy in Shannon's information theory

Heterogeneous environments and signals produce uncertainty that can be quantified using the mathematics of information theory²⁹. A particle size spectrum can be described as an heterogeneous set in which the relative proportions of its components contain information about the underlying physical process generating such heterogeneity¹³. Shannon's entropy is a generalized measurement of uncertainty, or variability³⁰ that can also be extended to the analysis of spectral variability^{31,32}. The general application of Shannon's entropy as a measurement of uncertainty in natural systems was suggested several decades ago by Vistelius (ref.³³) by applying entropy as a measurement of variability in geochemical properties. A fundamental insight in Vistelius's work was that "[...] *entropy reflects the behavior of frequencies in compliance with the (geochemical) process generating the distribution*". This idea has gained support from evidence accumulated over the following years in the geosciences³⁴ and Shannon's entropy is at the center of applications related to signal analysis³⁵, model diagnostics³⁶ and pattern discovery³⁷.

The properties of the Shannon's entropy as an uncertainty measure have been extensively studied^{30,38} and summarized in terms of the following axioms also described in the original formulation of the concept of information entropy²⁸:

1. Continuity

Shannon's entropy (H) is a continuous function of a set of probabilities p_i . Small changes in the values of p_i would produce small changes in H . The implication of this axiom is that H is an integrative measure that detects changes in probability distributions as changes in the uncertainty represented by such a distribution. Whether these changes are produced by deterministic causes or by random processes cannot be determined solely by the calculation of H . Therefore, H is sensitive to environmental noise.

2. Maximum entropy

H reaches a maximum value when all the probabilities have the same value ($p_n = 1/n$). Given a fix number of probability components (n), only a uniform distribution, corresponding to a highly heterogeneous system, maximizes the uncertainty. Any other probability distribution will have less entropy compared with the uniform distribution. This simple fact imposes a limit to the amount of entropy that could be generated from any system, particularly if probability distributions of a given property are changing in response to external forces, like disturbances.

3. Composition Law^{30,39}

The composition law is perhaps the most important axiom for the analysis of heterogeneity in environmental signals. The composition law establishes that entropy is an extensive property, like physical entropy. According to the composition law, the total entropy of a probability distribution remains the same regardless the way in which the probability values could be grouped. The implications of this axiom are less direct than in the previous cases, but more fundamental:

For the total entropy of a probability distribution to remain constant, the entropies of any subgroup of probabilities must be lower than the total entropy. This is the equivalent of breaking down a choice among 100 alternatives into a sequence of choices between two groups of 50, and then among 5 groups of 10, and so on. Although the total uncertainty for the process remain constant, the uncertainty experienced at each step along the sequence is lower, with the potential advantage of speeding up the selection among the alternatives offered. Then by grouping probabilities local reductions of uncertainty can be achieved. If these probabilities describe a completely independent and identically distributed random variable (i.i.d.) there is no grouping that should be preferred. However, if these probabilities describe events that are correlated, there will be a finite set of groupings that maximize local reductions in uncertainty. Finding those sets is mathematically equivalent to finding patterns in the data. Therefore, one of the most striking implications of the composition law is the potential for pattern recognition.

Entropy of particle size spectra

Entropy analysis^{26,40,41} was originally designed as a classification algorithm based on Shannon's information theory²⁸. This algorithm assumes that the combination of particle sizes in a sediment

layer is equivalent to a long string of characters playing different roles. Some characters contain information about specific events or transport mechanisms (e.g. floods, landslides, earthquakes, etc.)⁵, others are redundant (as a byproduct of the event or transport mode)¹³ and other are just random noise. Thus, the aim of an entropy analysis is two-fold: 1) To quantify the amount of information contained within and between the layers (i.e. to separate patterns from noise) and 2) to find the minimum number of characters that is required to encode such patterns (i.e. to get rid of apparently redundant characters).

The analysis of particle size in sediments by using the principles of information theory was proposed several decades ago³³. Yet, applications of entropy analysis in sedimentological studies have been intermittent in the scientific literature. This is because this information theory -based algorithm is not as popular among scientists as other techniques like end member mixing models¹³, curve fitting analysis (CFA)²³, and principal component analysis (PCA)^{19,42}. But to understand the advantages of the entropy analysis, it is necessary to put it in the context of these other existing approaches.

In some way, EMMA, CFA and PCA are restricted versions of the entropy approach. By using the analogy of particle sizes as string characters, we could say that EMMA models assume that only certain words can be found in the strings (i.e. only a reduced number of particle size spectra, the so-called end members, can represent different patterns of sediment transport and deposition)²⁴. CFA assumes that sequences are made of a set of fixed characters (i.e. specific combinations of particle sizes or log-normally distributed subpopulations, can represent a given pattern of transport deposition conditions)²³. Lastly, on a more radical variant, PCA abandons the original language and represents the string of characters as sequences of real numbers (i.e. the samples are no longer represented in the physical domain of the particle size space but in the new dimensions or components provided by the algorithm)¹⁹.

Entropy analysis makes no assumptions about the number of words or characters per word. Instead, the algorithm looks for predictability along the string of characters (or particle size classes). Whether this predictability comes from individual particles sizes or from the entire spectra is an outcome from the algorithm and not a pre-requisite. Entropy analysis are done on the original domain of the data, i.e., particle size.

More formally, EMMA and CFA try to highlight a specific aspect of the particle size spectra. EMMA focuses on the overall shape of the end-member spectra, and CFA on the decomposition of spectral shapes in terms of linear combinations of log-normal distributions. The solutions obtained from these approaches suffer from some sort of indeterminacy or non-uniqueness¹³. On one hand, with more than three end-members in (any EMMA) model, the determination of their contributions to a given mixture becomes highly uncertain (as it has been mathematically proved in mixing models with stable isotopes in ecology)^{43,44}. On the other hand, the number of linear combinations of log-normal distributions that could result in a given spectra is infinite^{13,23}. Either the number of end-members or the number of subpopulations must be hand-picked by the researcher¹³.

PCA is not well suited for the compositional nature of particle size spectra⁴⁵. Compositional data are expressed as percentages or fractions, which constrains their values to a non-negative constant sum (1 or 100%). Thus, researchers using PCA for particle size analysis argue for the need of transformations to remove such a constraint from the dataset^{19,42}. Log-ratio transformations are used to represent the data in the real space and to minimize the probability of spurious correlations⁴⁵. However, these transformations might obscure the physical interpretation of PCA results in the context of sediment transport processes¹³. This loss of interpretability is because sediment mixtures must be described in terms of their compositional structure^{46–48}; sediment transport occurs as a multiphase flow and the mechanical properties of these mixtures depend on the relative proportions of their components. Therefore, the removal of the compositional structure from the dataset could be, at best, unnecessary, and at worst, a significant loss of physical consistency.

Entropy analysis is suited for compositional data typical of sediment mixtures, allows for identifying changes in the overall shape of the particle size spectra, and reduces the dimensionality of the dataset without forcing the variability to be condensed into a single specific component (like in PCA).

Materials and Methods

Setting

Loon Lake is a 4-km long clastic-rich throughflow lake (landslide-dammed) in the southern Oregon Coast Range (OCR) (Umpqua River Basin, 43.585°N, 123.839 °W, 128 m.a.s.l.; Figure 4.2). A detailed description of the study area can be found in ref.²⁷. Briefly, Loon Lake catchment is

characterized by an active geomorphic regime with sediment production dominated by mass movements (deep-seated landslides, shallow landslides and debris flows)^{49,50}. Average annual precipitation is ~2000 mm falling mostly as low intensity rain between November and April, with an annual hydrological cycle following closely the distribution of the precipitation and affected by summertime droughts. Hydrology in the region is influenced by the Pacific Decadal Oscillation (PDO) as shown by the magnitude of peak flows within the larger Umpqua River basin⁵¹.

Disturbance history in the last 1500 years in Loon Lake's catchment was reconstructed by Richardson et al., (ref.²⁷). This history is recorded in the bottom of the lake as a sequence of event beds deposited in sharp contrast within a matrix of background sedimentation. At least 7 out of the 23 event beds identified by Richardson et al., (ref.²⁷) were associated with >8.2 magnitude earthquakes (including the 9.0 megathrust earthquake in 1700, as shown by cross-dating with turbidites records from the Cascadia subduction zone⁵²). Seismic activity was recorded as post-seismic sediment delivery via hyperpycnal flows. Forest fires in 1770 and 1890 were also recorded as event beds. After 1939, event beds record the impacts of landscape destabilization due to the interaction between intense storms and timber harvesting. High-intensity precipitation events described as "atmospheric rivers" producing large flooding events has been part of the recent history in the watershed (water years (WY) 1965, 1982, 1996, and 1997).

Lake sedimentation rates have changed over the last 1500 years reaching a maximum of 0.79 g cm⁻² y⁻¹ during the timber harvesting peak (1939-1978) that also coincided with the cool phase of the PDO. Sedimentation rates during the "Early-period" (514-1671) were significantly lower than those during the timber harvesting peak (average 0.38 g cm⁻² y⁻¹)

Core 02aN

We selected the longest core (~7m) out of 20 collected in Loon Lake in 2013 for the analysis in this study. Bulk sediment samples were obtained from Core 02aN at 1 cm resolution for grain size and elemental analysis. Sample pre-treatment before grain size analyses followed the methods described in ref.⁵³ and particle size spectra were obtained from a Malvern Masterizer 2000 following the methods described in ref.⁵⁴. Elemental composition (%TC, %TN, TN:C ratios) was determined on 10-20 mg aliquots combusted at high temperature in a Flash EA1112 Elemental Analyzer. The stable isotopic composition of OC ($\delta^{13}\text{C}$, $\delta^{15}\text{N}$) in our samples was determined by isotope ratio mass spectrometry after high-temperature combustion of pre-acidified samples.

Precision in the $\delta^{13}\text{C}$ measurements was $\sim 0.1\%$, and the analyses of reference materials showed accuracies that were within 5% of measured values.

Core chronology was established by a combination of measurements of ^{137}Cs and ^{210}Pb activities for the recent past (>1963) and radiocarbon dating of terrestrial macrofossils (leaves, needles and cone-bracts) collected throughout the core. ^{14}C dates were calibrated with Oxcal program with the IntCal13 atmospheric curve dataset (see ref.²⁷ and references therein).

Entropy analysis of particle size spectra

Most applications of information theory to the analysis of particle size spectra have targeted classification of spatially distributed sediment samples^{26,41}. To the best of our knowledge, this is the first application of the entropy analysis to the study of sediment cores. The full classification algorithm is explained elsewhere^{26,40,41} and a summary of the equations and steps is presented in Figure 4.3. Our method consists in two general steps:

1. Entropy of sediment layers

We calculated the entropy of each sediment layer. Entropy values from particle size spectra are seldom reported in the literature. Earlier work by Sharp and Fan (ref.²⁰) showed that entropy can be used as a sorting index. Sorting indices based in univariate statistics seem to correlate with flooding stages within a single event layer^{55,56}. Thus, a time series of entropies along the core could assist in the separation of event layers from background sedimentation. The entropy of a particle size spectra is calculated as:

$$H = \sum_{i=1}^s p_i \log_2 p_i$$

Where, p_i is the proportion of particles in size class “ i ”^{28,40}. Entropies calculated with base 2 logarithms are expressed in “bits”. Entropy values for a given layer can be normalized by the total entropy that would be expected if all grain size classes were equally represented in the sample (i.e. $\log_2 N$, where N is the total number of size classes considered). This “relative entropy” (H_{Rel}) ranges between 0 and 1 and compares a given distribution with an uniform distribution of values among the classes analyzed²⁸. An H_{Rel} value of zero (0) indicates the layer only contain particles of a single size class (well sorted), while an H_{Rel} value of one (1) indicates that the layer contains

particles of all size classes in equal proportions (poorly sorted). All entropy values for Loon Lake's core are expressed as relative entropies unless indicated otherwise.

2. Estimation of Information contribution by each particle size class.

To gain further insights into the physical mechanisms behind the compositional variability of event beds and background sedimentation, it was necessary to narrow the range of particle size classes considered for the analysis. This is because not all the particle sizes contribute in the same way to the changes observed in the entropy signal. For instance, both coarsening or fining of the sediments can increase or decrease H_{Rel} . Also, full consideration of the 82 particle size classes makes H_{Rel} highly sensitive to small random changes and not all those changes might be critical to separate event layers from background sedimentation. Thus, to reduce the dimensions of the signal space without sacrificing physical consistency or resolution, it is necessary to identify the particle size classes that exhibit the most significant changes along the entire record. In the context of the entropy analysis, this means to estimate the contribution of each particle size to the overall pattern of variability contained in the record, i.e. the information contribution from each particle size class.

Because information is additive, particle size classes with similar contributions can be added together if the grouping criteria based on their information contributions is respected. In this way, the dimensionality of the data can be reduced without significantly altering the integrity of the record (e.g., the possibility to separate events from background sedimentation). After the aggregation, H_{Rel} can be recalculated over the reduced number of size classes. Aggregation effects are theoretically predicted from the composition law^{28,30,39} (Figure 4.3):

$$H_T = H_G + H_{IG}$$

Where H_T is the entropy calculated over the entire dataset without any grouping, H_G is the entropy calculated between the groups and H_{IG} is the intragroup entropy. It follows that by grouping grain size classes into larger and more encompassing categories, the entropy calculated over this dimensionally reduced dataset is always lower than the total entropy. The difference, which is equal to H_{IG} , is equivalent to the information gained about the dataset by using a given grouping scheme (Figure 4.3).

Information contribution for a given grain size could vary throughout the core if deposition of those particles changes over time. We have no indications of dramatic shifts in the depositional regime of Loon Lake during the last 1500 years. Yet, we used a Monte Carlo simulation with 10,000 iterations to calculate information contributions on groups of a 100 sediment layers randomly drawn from the sample set. In this way, we could establish if the contributions to information for a given particle size was consistent through the entire depth of the core.

Information content analysis estimate the average information contribution of a given grain size to the pattern observed through the sediment core. To illustrate how the pattern of information contribution from a depositional environment diverges from random noise, we created “noisy” version of a sediment core by assigning a uniform distribution to the volumetric concentrations for the same range of particles sizes analyzed in core 02aN. And we performed an identical information content analysis to this surrogate sediment core.

Results

Long-term depositional processes

For the last 1500 years, the deepest part of Loon Lake has systematically accumulated particles in the range of clays and fine silts. Yet, in the early period of record (510-1370 A.D.), finer sediments were more common, as shown by the high frequency of particles between 5-10 μm between the bottom of the core and ~350 cm depth (Figure 4.4). Between 1370-1770 A.D. the frequency of clays and fine silts decreased noticeably (Figure 4.4). It would be premature to attribute this change in the composition of the sediments to a specific factor from these data only. This is because, post-depositional reworking could have affected the structure of the sediments deposited after 1370 A.D.²⁷. Fine silts and clays became more frequent with the advent of the timber harvesting era in 1946 (Figure 4.4).

The contrasting textural characteristics of the event beds in Loon Lake were evident in their particle size spectra. Two broad categories of event beds were immediately recognized throughout the core (Figure 4.4): i) deposits that significantly deviated from the long-term sedimentation trend due to inputs of coarser grains (e.g. events at 630 A.D., 920 A.D., 1770 A.D. and 1890 A.D.) and ii) deposits that exhibited an intensification in the deposition of fine particles (~5-10 μm). This second group of deposits showed high variability of particle sizes towards both large and small diameters and was the most common along the record. Because of its thickness, the deposit formed c.a. 510 A.D. offers a detailed picture of the structure of the second group of

event beds (Figure 4.4). Thus, the textural characteristics of Loon Lake's core suggest that for the last 1500 years, the most common record of disturbances were changes in particle size variability.

Entropy analysis of particle size spectra

Entropy changes and disturbances along the sediment core

We used particle size entropy (H_{Rel}) as a distribution-free measure of variability due to the multimodality and compositional nature of particle size spectra²⁶. H_{Rel} changed consistently throughout the core matching the occurrence of events (Figure 4.5). H_{Rel} values were relatively high with an average of 0.75 and ranging between 0.59-0.87 ($H_{Rel} = 1$ for a random signal). H_{Rel} decreased during the first ~600 years of the record (until 1150 A.D.), coinciding with the high abundance of fine silts and clays deposited in the bottom of the lake. Being an indicator of overall particle size variability, H_{Rel} could also have been affected by post-depositional reworking between 1370 A.D. and 1770 A.D. A slight decreasing trend in H_{Rel} is observed after 1770 A.D.

Most of the events could be separated from background deposition according to the range of their H_{Rel} values (Figure 4.5). Event beds seemed to have recorded high-resolution imprints of the changes occurring during short periods of intense sedimentation. By interpreting H_{Rel} as a sorting index^{20,57} we interpreted its behavior as suggestive of the hydrodynamic conditions conducive to the deposition of thick event beds⁵⁵. We found that the entropy signal from single events exhibited a recurrent wave-like shape. This pattern was more evident in the deposit formed around 510 A.D. (Figure 4.5). During this event, particle sorting decreased at the beginning due to sediment coarsening. This initial phase was followed by an extraordinary fining as shown by the highest concentration of fine silts and clays recorded throughout the core. Two more phases of alternating coarsening and fining completed the cycle of this event. Such a non-monotonic behavior of H_{Rel} during events, suggests a record of the waning and waxing phases of river flow during the formation of hyperpynites⁵⁵, as reported from a previous analysis of the sedimentation rates in Loon Lake²⁷.

Information contribution from different particle sizes to entropy changes: Mode-Peak equivalents (MP_{eq})

We used calculated information contributions from the particle size spectra to identify specific grain size classes responsible for the observed changes in entropy along the core (i.e. to identify different grain size subpopulations^{13,23}). Information contribution was unevenly distributed among particle size classes as expected from a relatively ordered depositional process (Figure 4.6). A completely random depositional pattern would have resulted in a noisy record, in which particles

of all sizes were equiprobable in a given layer (Figure 4.6 A, B). In depositional environments, particles settle at a rate proportional to their size (e.g. Stokes' law). Thus, because of such a strong physical constraint, ordering the size classes in an increasing fashion, resulted in a consistent grouping criterion (Figure 4.6C, D). We found three large groups of particles sizes based to their contribution to information along the sediment core: sands and coarse silts, fine silts and clay, and colloids and aggregates (groups I, II, and III, Figure 4.6C). It is worth noting that these groups are not bounded by the commonly used thresholds for sand, silt, and clay. Moreover, within these groups information contribution reaches maximum values around specific size classes (i.e. 0.2, 0.6, 4.3, 79, 275 and 1260 μm) (Figure 4.6C). Whether or not these grain sizes are at the center of true subpopulations could be debatable. So, we treat them as "Mode-Peak Equivalent" (MP_{eq}), that is, if true subpopulations do exist, these MP_{eq} would correspond to their modes. Otherwise, they would just represent specific size classes that maximize the information content along the core (i.e. peaks along the overall spectrum of information contribution). In this way, entropy analysis does not require initial assumptions about the underlying probability structure of the data.

To facilitate the interpretation of the MP_{eq} we assigned them to the closest particle size category they could represent. In that sense, the six MP_{eq} identified by their information contribution would correspond to colloids ($\sim 0.2 \mu\text{m}$), aggregates ($\sim 0.6 \mu\text{m}$), clay ($\sim 4.3 \mu\text{m}$), fine sands ($\sim 79 \mu\text{m}$), medium sands ($\sim 275 \mu\text{m}$) and coarse sands ($\sim 1260 \mu\text{m}$). We observed large variability in the information contribution from fine and medium sands. A separate analysis (data not shown) indicated that this was an effect of the type of event being recorded. On one hand, sand-sized grains were involved in the coarsening of the sediments that accompanied the most common event type along the core. On the other hand, these coarser fractions were also highly informative of large departures from the long-term depositional patterns, that are also recorded as larger inputs of coarser materials (e.g. 630 A.D., 920 A.D., 1770 A.D. and 1890 A.D.). When the events with the highest proportions of coarse grains were included in the calculation of information contributions, fine and medium sands had their maximum values of information content (Figure 4.6C). When these events were removed from the record, (or when just a few layers from these events were randomly sampled as part of our Monte Carlo simulation) information contribution from medium sands reached a minimum value (Figure 4.6C, D).

Entropy signal processing and event detection

The effects of different levels of aggregation on the integrity of the entropy signal are shown in Figure 4.7. We also show the effect of imposing a pre-establish aggregation scheme (e.g. Sand-Silt-Clay) on the entropy signal derived from such a classification.

We first calculated H_{Rel} over the six groups separated by visually identified local minima along the distribution of information contributions. The result of this aggregation was an overall uncertainty reduction (or information gain) as much of the variability was lumped within the groups, conducting to a sharpening of the signal. Compression of the signal was equivalent to an average 80% reduction in the overall uncertainty. This allowed for a wider range of H_{Rel} values, which in turn facilitates the separation of event beds from background sedimentation (Figure 4.7A). Further signal sharpening was achieved by calculating H_{Rel} after aggregating the data into groups I, II, and III (Figure 4.6C, Figure 4.7B). However, this sharpening came at the expense of an overall increase in uncertainty. These results were expected because a smaller number of groups implies that each one of them must account for a larger amount of variability. In these circumstances the intra group entropy (H_{IG}) becomes larger and group behavior will appear more random. Despite these differences, all the entropy signals calculated in this way, still preserved the fundamental structure that separated event beds from background sedimentation. In contrast, when we used the sand-silt-clay classification scheme as an aggregation criterium, the entropy signal was highly distorted (Figure 4.7C).

To prevent information loss and to have more resolution into the details of deposit layers, we used the six MP_{eq} identified according to their information contributions and the corresponding values $H_{\text{Rel}}(6)$ for further analysis.

Textural characterization of event layers using $MP_{\text{eq}}(s)$

The composition of both event and background sedimentation layers was highly heterogenous throughout the core (Figure 4.8). We observed a noticeable decrease in the clay-sized material throughout the record. Nonetheless, MP_{eq} -clay was the dominant size class in Loon Lake's sediment core. Based on the textural characteristics showed in Figure 4.8, the six $MP_{\text{eq}}(s)$ selected represented a summarized version of the depositional patterns observed along the sediment core. Thus, longitudinal changes of these $MP_{\text{eq}}(s)$ should capture the basic sedimentation mechanisms operating during different events. To gain further insights into these

mechanisms, we selected examples of the two types of events found along the core to examine textural and chemical changes in the sediments deposited in Loon Lake (Figure 4.9).

Because of the wave-like pattern in the entropy signal that characterized individual events, these deposits are internally heterogeneous as well (Figure 4.9). Yet, the overall structure seems to be consistent with the transport mechanisms depositing these sediments in the bottom of the lake. For instance, the deposit in 1996 A.D. was created after massive debris flows and landslides in the Umpqua River basin⁵⁸. Given its textural similarity to the deposit at 510 A.D., we inferred that at least these sediments were transported in similar fashion. Furthermore, based on the structure of the earlier deposit, the associated event could have had a higher magnitude. It is unlikely that this event occurred closer to the lake, due to the extreme level of sorting we observed in the internal layers of the 510 A.D. deposit (with some layers exhibiting H_{Rel} values close to 0). Thus, such a relatively large volume of well-sorted fine sediments, must have been deposited during an extreme event. Another distinctive feature of these landslide-like deposits is the deposition of a colloid-aggregate cap. We observed that deposits with >0.5% volume represented in colloids and aggregates, would have a colloidal fraction. The colloid-aggregate cap would also be accompanied by a small number of coarser particles towards the end of the event. Such an association suggests that these particles were likely forming flocs of different sizes but with lower density and relatively slow settling velocities⁵⁹. Although the number of layers with this colloid-aggregate structure throughout the core is small to allow for conclusive correlation analyses, this observation points towards a physical link between these two types of particles.

Event layers at 920 and 1890 A.D. illustrate events with higher inputs of coarse and poorly sorted material to the lake. These events had higher carbon content compared to other sediment layers. These two attributes strongly suggest that at least some of the sediments deposited within these event beds were mobilized from the area immediately surrounding the lake. MP_{eq} -clay changed abruptly at both the beginning and the end of the event, and the textural characteristics of these coarser deposits, particularly the event bed from 1890 A.D. show no signs of the waning and waxing phases in river flow.

Shifts in MP_{eq} dominance affected the amount and type of organic matter that was buried within event layers (Figure 4.9). As mentioned above, event deposits dominated by coarser grains (i.e. fine sands, e.g. 920 and 1890 A.D.) showed a higher carbon concentration than fine-dominated event layers (i.e. clays, e.g. 510 and 1996 A.D.). Also, the organic matter associated with fine

sands in these deposits had lower TN:C ratios, was intermediately depleted in $\delta^{13}\text{C}$ (~ -26.5 ‰), within a range between -25 and -29 ‰), and depleted in $\delta^{15}\text{N}$. In contrast, organic matter associated to clay-sized material had higher TN:C ratios, was either enriched or depleted in $\delta^{13}\text{C}$, and enriched in $\delta^{15}\text{N}$ (Figure 4.9).

These results suggest that both H_{Rel} (calculated as H_{G}) as well changes in the proportions of the $\text{MP}_{\text{eq}}(\text{s})$ identified based on their information contributions, summarize the essential depositional characteristics determining the structure of the event beds in Loon Lake's sediments.

Residual MP_{eq} or $r\text{MP}_{\text{eq}}(\text{s})$

Because of the "Composition Law"³⁹, calculating H_{Rel} by using groups centered around the $\text{MP}_{\text{eq}}(\text{s})$ (Figure 4.3) is the equivalent to splitting the total entropy signal into two variability components. A first component is related to the compression of the textural characteristics represented along the sediment core (i.e. the reduction in the number of bits required to encode the information in the core, $\sim 80\%$ with six groups). The effect of this compression on the entropy signal is represented by the series of inter-group entropies (H_{G}), for whose calculation we used the original values of each MP_{eq} from the PSS. The second component is related to the changes in variability in the PSS not accounted by H_{G} . This "residual" variability must be evaluated by calculating intra-groups entropies (H_{IG}). For the calculation of $H_{\text{IG}}(\text{s})$, the original values of the $\text{MP}_{\text{eq}}(\text{s})$ need to be adjusted and expressed as a ratio to the total volume of each group that contain such an MP_{eq} . This step produces a new set of *residual $\text{MP}_{\text{eq}}(\text{s})$* whose changes along the core must be mostly uncorrelated with the patterns captured by H_{G} . As mentioned above, changes in H_{G} were representative of the depositional processes that structure sediment layers in Loon Lake. Thus, changes in H_{IG} and its components might capture other sources of variability that remain represented in the sedimentary record after accounting for depositional effects. The changes in $r\text{MP}_{\text{eq}}$ throughout Loon Lake's sediment core are presented in Figure 4.10.

The volumes for $r\text{MP}_{\text{eq}}(\text{s})$ differed dramatically from those of $\text{MP}_{\text{eq}}(\text{s})$ in terms of their contribution to the variability in particle size (Figure 4.10). $r\text{MP}_{\text{eq}}$ -clay and $r\text{MP}_{\text{eq}}$ -fine sands were the less dominant fractions. Instead, most of the variability was captured by changes in coarse and medium sands, and colloids and aggregates. Since establishing the provenance of sediments is typically complicated by depositional effects^{13,16,17}, we took advantage of the observed trends in $r\text{MP}_{\text{eq}}(\text{s})$ to use them as predictors of several proxies of organic matter provenance to the lake (%TC, TN:C ratios, $\delta^{13}\text{C}$ and $\delta^{15}\text{N}$). We observed that the $r\text{MP}_{\text{eq}}(\text{s})$ were mostly orthogonal

between them and thus, uncorrelated (Supplementary Figure 10), suggesting that their changes along the core could offer additional and non-redundant insights into sediment routing across the watershed. We adjusted a Generalized Least Squares Multiple Regression model to test for the significance of the correlation between the $MP_{eq}(s)$ and the mentioned geochemical proxies after accounting for other influential factors including historical changes in land-use or the occurrence of events (see supplementary methods).

Bulk chemical composition and “Pseudo” property-property plots for $rMP_{eq}(s)$

We found that colloids and aggregates as well as clays, and fine sands, were significantly correlated with at least one geochemical proxy (Table 4-1). In some cases, two different $rMP_{eq}(s)$ had opposite correlations with the same proxy. For instance, while rMP_{eq} -clay was negatively correlated with %TC, rMP_{eq} -fine sands had a positive correlation with the carbon concentration in the sediments. The correlations between rMP_{eq} -clay and rMP_{eq} -fine sands with TN:C ratios were inverted. We used the matrix of signs for the correlation coefficients from the regression model to qualitatively represent the chemical characteristics of Loon Lake sediments and their association with different MP_{eq} by means of pseudo-property-property plots (see supplementary methods) (Figure 4.11).

Although there was overlap between our sample points, we did observe separation of layers dominated by different grain size classes in terms of their elemental and isotopic composition (Figure 4.11). Colloids, aggregates, and clays were associated with chemical compositions resembling degraded organic matter, i.e. %TC < 0.5% (not shown) higher TN:C ratios (>0.75), and enriched $\delta^{13}C$ and $\delta^{15}N$ (>-26 ‰, >2‰, respectively) (Figure 4.11). This type of organic matter is commonly found in deep soil horizons and floodplains. In turn, fine to medium sand sized particles carry a signature that resembles surficial soil horizons or riverine fine particulate organic matter (FPOM): %TC > 0.5% (not shown) lower TN:C ratios (<0.65), and $\delta^{13}C$ and $\delta^{15}N$ depleted (<-26 ‰, <1‰, respectively) (Figure 4.11).

We used chemical data from suspended sediment samples collected over a wide range of winter discharges in the Umpqua⁶⁰ and Alsea⁶¹ rivers (Q:Q_m ranging from 1.1 to >15) as an extended pool of riverine end-members from small mountainous river systems in the Pacific Northwest. We also used data from the literature to provide an average composition for mixed lacustrine plankton⁶². Our data suggest that the chemical composition of Loon Lake sediments is strongly dominated by terrestrial inputs associated to fluvial transport (Figure 4.11). Furthermore, our

samples could be separated into two larger groups with contrasting amount of fluvial influence. While sediment layers with chemical signatures close to those observed in riverine suspended sediments had a more heterogeneous composition in terms of $MP_{eq}(s)$, sediment layers dominated by medium and coarse sands appeared to be derived from a different terrestrial source likely mixed with organic matter of aquatic origin (Figure 4.11). We interpreted this gradient of fluvial influence on the chemical composition of Loon Lake sediments as an indication of impacts of changes in the hydrological regime, most likely linked to climate. We will explore this scenario in the discussion section.

Discussion

Synthesis of the approach

We analyzed the information content of a sediment core collected in Loon Lake's catchment, in the OCR. These sedimentary archives span more than 1500 years of sedimentation due to earthquakes, fires, floods and land clearance²⁷. We used entropy analysis of the PSS as this mathematical approach is suited for compositional data. Given the robust age model available for Loon Lake sediments²⁷ and the correspondence of the disturbance history recorded in the core (02aN) with other regional records, we were able to test the ability of our approach to identify events and their different textural characteristics. By using an algorithm based on information theory, we identified grain size classes with the largest contributions to variability in particle size throughout the core. Further developments of the algorithm are needed to establish whether these grain size classes are true grain subpopulation modes or just peaks along a spectra of information contributions. Thus, we used the term "Mode-Peak Equivalents" to refer to those grain size classes that maximizes the information content of the sediment core. By grouping the data into six classes centered around the $MP_{eq}(s)$, we achieved a compression of ~80% (bits/bits) of the data represented in the sediment core while preserving essential textural information. This textural information allowed for a better understanding of sedimentation processes in Loon Lake's bottom.

By applying the "composition law", also derived from information theory, we were able to separate the effect of the depositional regime from other potential sources of variability affecting the characteristics of the PSS along Loon Lake's history. The effect of the depositional regime on particle size variability was captured by the entropy signal and the long-term changes in the $MP_{eq}(s)$. We found support for this conclusion by exploring the behavior the $MP_{eq}(s)$ using event windows also defined by the entropy signal. Our results corroborated the role of hyperpycnal flows

in structuring many of the event beds, but we also found evidence of reduced sorting and therefore, direct inputs of poorly sorted sediments into the bottom of the lake. We suspect these inputs were eroded from surrounding areas in the lake (besides the event in 630 A.D.) (Supplementary Figure 11).

When we analyzed the signals corresponding to $rMP_{eq}(s)$ (those required to calculate intra-group entropies) we found that components typically associated to changes in sedimentation rates (clays and fine sands) had lower adjusted volumes than other $rMP_{eq}(s)$ including colloids and coarse sands. These results suggested that the long-term trends of $rMP_{eq}(s)$ were less affected by the processes related to the deposition of the sediments in the bottom of the lake and more likely contained information about additional sources of variability of PSS.

We used pseudo-property-property plots to identify potential sources of sediments to Loon Lake by matching the bulk chemical composition of our samples with the abundances of $rMP_{eq}(s)$. We found a strong terrestrial signature imprinted in these sediment layers as evidenced by elemental and isotopic composition resembling inputs from terrestrially-derived particulate organic matter carried by rivers. Yet, the data exhibited two contrasting patterns of fluvial influence. Layers with higher adjusted volumes of medium and coarse sands had a weaker terrestrial signature when compared to layers with more heterogeneous composition and including fine sands and clays.

Modeling particle size variability with Entropy

Our results suggest that together, the entropy signal and the $MP_{eq}(s)$ were the equivalent to a very simple data-driven model (in the sense of data representation) of the depositional processes occurring in Loon Lake. Likewise, the $rMP_{eq}(s)$ resembled the residual variability in the data after accounting for the effects of lake sedimentation on the structure of the PSS. This entropy model made no assumptions about the underlying probabilistic structure of the data (e.g. specific grain size subpopulations vs. spectral end-members) and started with a single constraint to explain the pattern across the layers: a gravitationally driven settling process requiring the representation of the grain size classes in an ascending order. This organization scheme for the size classes allowed for immediate recognition of a reduced number of groups that would be required to capture the most important details depicted in the graphic representation of the data (e.g. PSS stacked raster, Figure 4.4). Thus, the entropy analysis used here to represent the data follows closely the fundamental principles of data compression and it is reminiscent of Bayesian methods of inference³⁴.

We compared the general characteristics of the entropy analysis with other available methods commonly used to analyze particle size spectra (e.g. EMMA, CFA, PCA) in the background section. In the light of our results a few additional comments are in order. Flood et al., (ref.⁴²) argued that the effectiveness of a multivariate entropy analysis of particle size distribution was suboptimal due to the compositional structure of the original dataset. Our analysis do not support such a criticism, at least for entropy analysis.

The ultimate objective of PCA is to represent the data along orthogonal axis that maximize the ability to discriminate any pair of samples. To do so, compositional data are transformed to reduce any possibility of spurious correlations. Entropy analysis detected both correlated and uncorrelated structures in the dataset. The correlated structure was reflected in the strong divergence of the information contributions of entire groups of particle sizes from the pattern depicted by our noise model (being the noise model the extreme version of uncorrelated particle sizes, Figure 4.6). This correlated structure between our $MP_{eq}(s)$ reflected the patterns expected to occur in a depositional process, i.e., coarser grains settle faster than finer grains, therefore, this pair of size classes might behave as mutually exclusive in a given layer and appear negatively correlated throughout the core. On the other hand, $rMP_{eq}(s)$ appeared almost perfectly orthogonal (Supplementary Figure 10) indicating the presence of an underlying uncorrelated structure in the dataset. Further analysis suggest that the behavior of these uncorrelated fractions could be linked to the dynamic of contributing sediment sources to the Lake. This corroborates our initial argument about the role of the compositional structure of the data in preserving the physical connection of PSS with processes occurring in the lake.

Further analyses are required to validate the general applicability of our method to the reconstruction of sedimentation processes in other geographical locations. Nonetheless, since our method is guided by fundamental first principles of information theory³⁴ and make no other assumptions than particle settling under gravitational forces, we anticipate it would be useful in understanding particle size variability in long-term sedimentary records of more dynamic environments. In that regard, we did not see evidence of a drastic change in the depositional regime in Loon Lake over the last 1500 years (that would have appeared as a long-term sustained excursion in the overall particle size distribution towards coarsening or fining, shifts in $MP_{eq}(s)$ and H_{Rel}). This type of changes, typically referred to as regime shifts between alternative states⁶³ would be captured in our model by temporal changes in the information contribution of particle

sizes. A first indication of such temporal trends would be wider confidence intervals in around the information contributions of the grain size classes involved in the shift (Figure 4.6).

Disentangling signals of watershed response to disturbance

rMP_{eq}(s) and climate

An apparent shift in the fluvial influence on the chemical composition of Loon Lake sediments was suggested by our pseudo-property-property plots (Figure 4.11). A closer inspection of Figure 4.10 reveals long-term trends in the rMP_{eq}-coarse and medium sands, apparently related with a lower influence of fluvial inputs to the lake. Together, those sandy fractions appear slightly more predominant towards the middle section of the sediment core (inverted U-shape). At the same time, a rMP_{eq}-colloids and aggregates became less prominent in the record (U-shape). Also, the overall frequency (over time) of rMP_{eq}-colloids and aggregates decreased, particularly after 920 A.D. Because of these long-term trends and since gradients of fluvial influence could be affected by climate, as peak flows in the region are affected by the PDO⁵¹, we investigated long-term records of climatic proxies for the region. Much of the climatic variability in the Pacific Northwest is linked to changes in El Niño Southern Oscillation (ENSO) and its interaction with the Pacific Decadal Oscillation (PDO). Thus, we used an available 13,000-year long record of ENSO variability⁶⁴ to provide an even longer-term context to our observations, particularly for the period preceding our sediment record (i.e. last 2,000 years).

We observed a close match between the long-term pattern of rMP_{eq}-Colloidal-Aggregates and, coarse and medium sands and the ENSO proxy (Figure 4.12). During the warmer periods, particularly during the Medieval Climatic Anomaly (MCA) (900-1300 AD)⁶⁵⁻⁶⁷, there was an apparent reduction in the supply of colloids-aggregates to the lake and an increase in the relative supply of medium and coarse sands. Meanwhile, sedimentation related variables (e.g. clays and fine sands) remained constant.

Changes in the relative proportions of particles with diameters >250µm has been associated to active topsets (first part of the delta in the stream flow direction) in lacustrine environments^{15,68,69}. In those cases, coarser particles deposited during peak flood flows on lake channels and onto topsets can be subsequently transported by traction currents to the deepest part of the lake. On the other hand, the largest accumulations of colloidal and aggregates in the lake followed widespread land sliding in 1996 AD and likely in 510 AD. We found similar particles carrying a SOM signature in overbank deposits in the headwaters of the Alsea River (Chapter 3). The possibility that these particles could be a proxy for land sliding activity in Loon Lake's catchment

is intriguing. If so, these signals could be pointing towards changes in sediment supply within the catchment driven by climatic variability. A possible explanation for these changes in the composition of particles in the lake bottom could be that during the MCA there was erosion of the topset of the lake likely due to lower sediment concentrations supplied from the catchment. This was probably due to a shift in the winter precipitation regime with a decrease in the frequency of rain-on-snow events and excess of soil moisture, important triggers of landslides in the region. Different lines of evidence suggest that although the temperatures were higher during the MCA, the Pacific Northwest experienced exceptional wetness in winter⁶⁶ (Figure 4.13). Thus, it is likely that high flows relatively depleted in sediments could mobilize these grains to the bottom parts of the lake. Although highly encouraging, these are very preliminary results that would require further analysis.

Conclusions

We analyzed the information content of a high-resolution sedimentary archive encompassing more than 1500 year of history in a Small Mountainous River System in the OCR. Our approach allowed for the identification of two major group of signals recorded in Loon Lake sediments: an average signal depicting depositional processes associated with event and background sedimentation and a residual signal that showed a potential connection with long-term fluctuations in the regional climate. We identified at least six Mode-Peak equivalents within the particle size classes that accounted by more than 80% of the variability in particle size represented in the sediment core. The temporal dynamics of these $MP_{eq}(s)$ provided further insights into the depositional mechanisms operating in the lake for the last 15 centuries. We showed that when other grouping criteria are used to explain variability in grain size, most of the signal associated with the structure of the core can be significantly distorted. These results suggest that an incomplete understanding of changes in particle size variability could lead to wrong conclusions about internal “shredding” of a watershed’s signals of response to disturbance.

Bibliography

1. Hinderer, M. From gullies to mountain belts: A review of sediment budgets at various scales. *Sedimentary Geology* **280**, 21–59 (2012).
2. Benda, L. & Dunne, T. Stochastic forcing of sediment supply to channel networks from landsliding and debris flow. *Water Resources Research* **33**, 2849–2863 (1997).
3. Benda, L. & Dunne, T. Stochastic forcing of sediment routing and storage in channel networks. *Water Resources Research* **33**, 2865–2880 (1997).
4. Wohl, E. *et al.* The Natural Sediment Regime in Rivers: Broadening the Foundation for Ecosystem Management. *BioScience* **65**, 358–371 (2015).
5. Syvitski, J. P. M., Vörösmarty, C. J., Kettner, A. J. & Green, P. Impact of Humans on the Flux of Terrestrial Sediment to the Global Coastal Ocean. *Science* **308**, 376–380 (2005).

6. Naden, P. S. The Fine-Sediment Cascade. in *Sediment Cascades* (eds. Burt, essor T. P. & Allison, essor R. J.) 271–305 (John Wiley & Sons, Ltd, 2010). doi:10.1002/9780470682876.ch10
7. Romans, B. W., Castelltort, S., Covault, J. A., Fildani, A. & Walsh, J. P. Environmental signal propagation in sedimentary systems across timescales. *Earth-Science Reviews* **153**, 7–29 (2016).
8. Trimble, S. W. Decreased Rates of Alluvial Sediment Storage in the Coon Creek Basin, Wisconsin, 1975–93. *Science* **285**, 1244–1246 (1999).
9. Warrick, J. A. Eel River margin source-to-sink sediment budgets: Revisited. *Marine Geology* **351**, 25–37 (2014).
10. Wiel, M. J. V. D. & Coulthard, T. J. Self-organized criticality in river basins: Challenging sedimentary records of environmental change. *Geology* **38**, 87–90 (2010).
11. Colombaroli, D., Gavin, D. G., Morey, A. E. & Thorndycraft, V. R. High resolution lake sediment record reveals self-organized criticality in erosion processes regulated by internal feedbacks. *Earth Surface Processes and Landforms* **43**, 2181–2192 (2018).
12. Coulthard, T. J. & Van de Wiel, M. J. Climate, tectonics or morphology: what signals can we see in drainage basin sediment yields? *Earth Surface Dynamics* **1**, 13–27 (2013).
13. Weltje, G. J. & Prins, M. A. Muddled or mixed? Inferring palaeoclimate from size distributions of deep-sea clastics. *Sedimentary Geology* **162**, 39–62 (2003).
14. Bloemsmas, M. R. *et al.* Modelling the joint variability of grain size and chemical composition in sediments. *Sedimentary Geology* **280**, 135–148 (2012).
15. Xiao, J. *et al.* The link between grain-size components and depositional processes in a modern clastic lake. *Sedimentology* **59**, 1050–1062 (2012).
16. Koiter, A. J., Owens, P. N., Peticrew, E. L. & Lobb, D. A. The behavioural characteristics of sediment properties and their implications for sediment fingerprinting as an approach for identifying sediment sources in river basins. *Earth-Science Reviews* **125**, 24–42 (2013).
17. Laceby, J. P. *et al.* The challenges and opportunities of addressing particle size effects in sediment source fingerprinting: A review. *Earth-Science Reviews* **169**, 85–103 (2017).
18. Sklar, L. S. *et al.* The problem of predicting the size distribution of sediment supplied by hillslopes to rivers. *Geomorphology* **277**, 31–49 (2017).
19. Flood, R. P. *et al.* Compositional data analysis of Holocene sediments from the West Bengal Sundarbans, India: Geochemical proxies for grain-size variability in a delta environment. *Applied Geochemistry* **75**, 222–235 (2016).
20. Sharp, W. E. & Fan, P.-F. A Sorting Index. *The Journal of Geology* **71**, 76–84 (1963).
21. Malmon, D. V., Reneau, S. L. & Dunne, T. Sediment sorting and transport by flash floods. *J. Geophys. Res.* **109**, F02005 (2004).
22. Law, B. A. *et al.* Size sorting of fine-grained sediments during erosion: Results from the western Gulf of Lions. *Continental Shelf Research* **28**, 1935–1946 (2008).
23. Gammon, P. R., Neville, L. A., Patterson, R. T., Savard, M. M. & Swindles, G. T. A log-normal spectral analysis of inorganic grain-size distributions from a Canadian boreal lake core: Towards refining depositional process proxy data from high latitude lakes. *Sedimentology* **64**, (2017).
24. Weltje, G. J. End-member modeling of compositional data: Numerical-statistical algorithms for solving the explicit mixing problem. *Math Geol* **29**, 503–549 (1997).
25. Ashley, G. *Interpretation of Polymodal Sediments*. **86**, (1978).
26. Mikkelsen, O. A., Curran, K. J., Hill, P. S. & Milligan, T. G. Entropy analysis of in situ particle size spectra. *Estuarine, Coastal and Shelf Science* **72**, 615–625 (2007).
27. Richardson, K. N. D., Hatten, J. A. & Wheatcroft, R. A. 1500 years of lake sedimentation due to fire, earthquakes, floods and land clearance in the Oregon Coast Range: geomorphic sensitivity to floods during timber harvest period. *Earth Surface Processes and Landforms* **43**, 1496–1517 (2018).

28. Shannon, C. E. A Mathematical Theory of Communication. *Bell System Technical Journal* **27**, 379–423 (1948).
29. *Adaptability: The Significance of Variability from Molecule to Ecosystem*. (Springer US, 1983).
30. Bialynicki-Birula, I. & Rudnicki, L. Entropic Uncertainty Relations in Quantum Physics. *arXiv:1001.4668 [quant-ph]* 1–34 (2011). doi:10.1007/978-90-481-3890-6_1
31. Powell, G. E. & Percival, I. C. A spectral entropy method for distinguishing regular and irregular motion of Hamiltonian systems. *J. Phys. A: Math. Gen.* **12**, 2053 (1979).
32. Zurlini, G., Li, B.-L., Zaccarelli, N. & Petrosillo, I. Spectral entropy, ecological resilience, and adaptive capacity for understanding, evaluating, and managing ecosystem stability and change. *Glob Change Biol* **21**, 1377–1378 (2015).
33. Vistelius, A. B. Informational Characteristic of Frequency Distributions in Geochemistry. *Nature* **202**, 1206 (1964).
34. Ruddell, B. L., Brunzell, N. A. & Stoy, P. Applying Information Theory in the Geosciences to Quantify Process Uncertainty, Feedback, Scale. *Eos, Transactions American Geophysical Union* **94**, 56–56 (2013).
35. Brunzell, N. A. A multiscale information theory approach to assess spatial–temporal variability of daily precipitation. *Journal of Hydrology* **385**, 165–172 (2010).
36. Weijs, S. V., Giesen, N. van de & Parlange, M. B. Data compression to define information content of hydrological time series. *Hydrology and Earth System Sciences* **17**, 3171–3187 (2013).
37. Wellmann, J. & Wellmann, J. F. Information Theory for Correlation Analysis and Estimation of Uncertainty Reduction in Maps and Models. *Entropy* **15**, 1464–1485 (2013).
38. Kullback, S. & Leibler, R. A. On Information and Sufficiency. *The Annals of Mathematical Statistics* **22**, 79–86 (1951).
39. Jaynes, E. T. Information Theory and Statistical Mechanics. *Phys. Rev.* **106**, 620–630 (1957).
40. Johnston, R. J. & Semple, R. K. *Classification using information statistics*. (Geo Books, 1983).
41. Forrest, J. & Clark, N. R. Characterizing grain size distributions: evaluation of a new approach using a multivariate extension of entropy analysis. *Sedimentology* **36**, 711–722 (1989).
42. Flood, R. P., Orford, J. D., McKinley, J. M. & Roberson, S. Effective grain size distribution analysis for interpretation of tidal–deltaic facies: West Bengal Sundarbans. *Sedimentary Geology* **318**, 58–74 (2015).
43. Phillips, D. L. & Gregg, J. W. Source partitioning using stable isotopes: coping with too many sources. *Oecologia* **136**, 261–269 (2003).
44. Parnell, A. C., Inger, R., Bearhop, S. & Jackson, A. L. Source Partitioning Using Stable Isotopes: Coping with Too Much Variation. *PLOS ONE* **5**, e9672 (2010).
45. Aitchison, J. *The Statistical Analysis of Compositional Data*. (Chapman & Hall, Ltd., 1986).
46. Brennen, C. E. & Brennen, C. E. *Fundamentals of Multiphase Flow*. (Cambridge University Press, 2005).
47. Jha, S. K. & Bombardelli, F. A. Two-phase modeling of turbulence in dilute sediment-laden, open-channel flows. *Environ Fluid Mech* **9**, 237 (2009).
48. Jha, S. K. & Bombardelli, F. A. Toward two-phase flow modeling of nondilute sediment transport in open channels. *Journal of Geophysical Research: Earth Surface* **115**, (2010).
49. Dietrich, W. E. & Dunne, T. Sediment budget for a small catchment in mountainous terrain. *Zeitschrift für Geomorphologie* **29**, 191–206 (1978).
50. Roering, J. J., Kirchner, J. W. & Dietrich, W. E. Characterizing structural and lithologic controls on deep-seated landsliding: Implications for topographic relief and landscape evolution in the Oregon Coast Range, USA. *Geological Society of America Bulletin* **117**, 654–668 (2005).
51. Wheatcroft, R. A., Goñi, M. A., Richardson, K. N. & Borgeld, J. C. Natural and human impacts on centennial sediment accumulation patterns on the Umpqua River margin, Oregon. *Marine Geology* **339**, 44–56 (2013).

52. Goldfinger, C. *et al.* *Turbidite Event History--Methods and Implications for Holocene Paleoseismicity of the Cascadia Subduction Zone.* (2012).
53. Gray, A. B., Pasternack, G. B. & Watson, E. B. Hydrogen peroxide treatment effects on the particle size distribution of alluvial and marsh sediments. *The Holocene* **20**, 293–301 (2010).
54. Sperazza, M., Moore, J. N. & Hendrix, M. S. High-Resolution Particle Size Analysis of Naturally Occurring Very Fine-Grained Sediment Through Laser Diffraction. *Journal of Sedimentary Research* **74**, 736–743 (2004).
55. Schillereff, D. N., Chiverrell, R. C., Macdonald, N. & Hooke, J. M. Flood stratigraphies in lake sediments: A review. *Earth-Science Reviews* **135**, 17–37 (2014).
56. Vasskog, K. *et al.* A Holocene record of snow-avalanche and flood activity reconstructed from a lacustrine sedimentary sequence in Oldevatnet, western Norway. *The Holocene* **21**, 597–614 (2011).
57. Martín, M. A. & Rey, J.-M. On the role of Shannon's entropy as a measure of heterogeneity. *Geoderma* **98**, 1–3 (2000).
58. Risley, J. C. Floods of November 1996 through January 1997 in the Umpqua River Basin, Oregon. *USGS Fact Sheet FS-2004-3134* 5 (2004).
59. Nicholas, A. P. & Walling, D. E. The significance of particle aggregation in the overbank deposition of suspended sediment on river floodplains. *Journal of Hydrology* **186**, 275–293 (1996).
60. Goñi, M. A., Hatten, J. A., Wheatcroft, R. A. & Borgeld, J. C. Particulate organic matter export by two contrasting small mountainous rivers from the Pacific Northwest, U.S.A. *J. Geophys. Res. Biogeosci.* **118**, 112–134 (2013).
61. Hatten, J. A., Goñi, M. A. & Wheatcroft, R. A. Chemical characteristics of particulate organic matter from a small, mountainous river system in the Oregon Coast Range, USA. *Biogeochemistry* **107**, 43–66 (2012).
62. Meyers, P. A. & Lallier-vergés, E. Lacustrine Sedimentary Organic Matter Records of Late Quaternary Paleoclimates. *Journal of Paleolimnology* **21**, 345–372 (1999).
63. Livers, B., Wohl, E., Jackson, K. J. & Sutfin, N. A. Historical land use as a driver of alternative states for stream form and function in forested mountain watersheds of the Southern Rocky Mountains. *Earth Surf. Process. Landforms* n/a-n/a doi:10.1002/esp.4275
64. Moy, C. M., Seltzer, G. O., Rodbell, D. T. & Anderson, D. M. Variability of El Niño/Southern Oscillation activity at millennial timescales during the Holocene epoch. *Nature* **420**, 162–165 (2002).
65. Ersek, V., Clark, P. U., Mix, A. C., Cheng, H. & Edwards, R. L. Holocene winter climate variability in mid-latitude western North America. *Nature Communications* **3**, 1219 (2012).
66. Steinman, B. A., Abbott, M. B., Mann, M. E., Stansell, N. D. & Finney, B. P. 1,500 year quantitative reconstruction of winter precipitation in the Pacific Northwest. *PNAS* **109**, 11619–11623 (2012).
67. Cook, B. I., Smerdon, J. E., Seager, R. & Cook, E. R. Pan-Continental Droughts in North America over the Last Millennium. *J. Climate* **27**, 383–397 (2013).
68. Ashley, G. M. Interpretation of Polymodal Sediments. *The Journal of Geology* **86**, 411–421 (1978).
69. Pondell, C. R. & Canuel, E. A. The role of hydrodynamic sorting on the accumulation and distribution of organic carbon in an impoundment: Eglebright Lake, California, USA. *Biogeochemistry* **133**, 129–145 (2017).
70. Pinheiro, J., Bates, D., DebRoy, S., Heisterkamp, S. & Van Willigen, B. Package 'nlme'. (2018). Available at: <https://cran.r-project.org/web/packages/nlme/nlme.pdf>. (Accessed: 30th October 2018)
71. Meyers, P. A. Organic geochemical proxies of paleoceanographic, paleolimnologic, and paleoclimatic processes. *Organic Geochemistry* **27**, 213–250 (1997).

Figures and tables

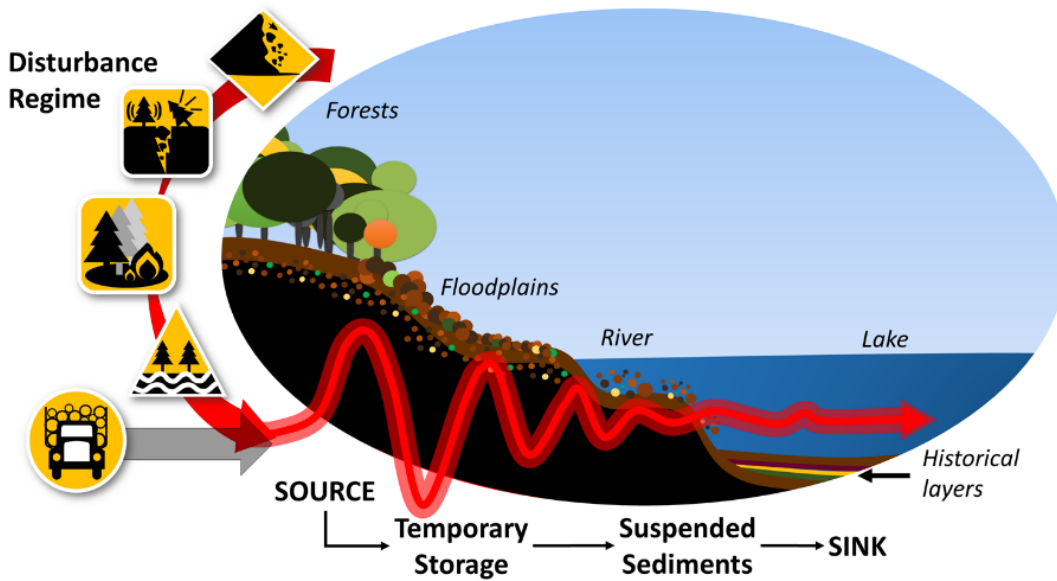


Figure 4.1. Conceptual model. Disturbance signals propagate like ripples across the biogeophysical fabric that connect forests soils, through rivers and sediments, to lake bottoms. Along its path from source to sink, temporary storage, mixing, and selective transport strongly attenuate signal propagation producing confounding effects.

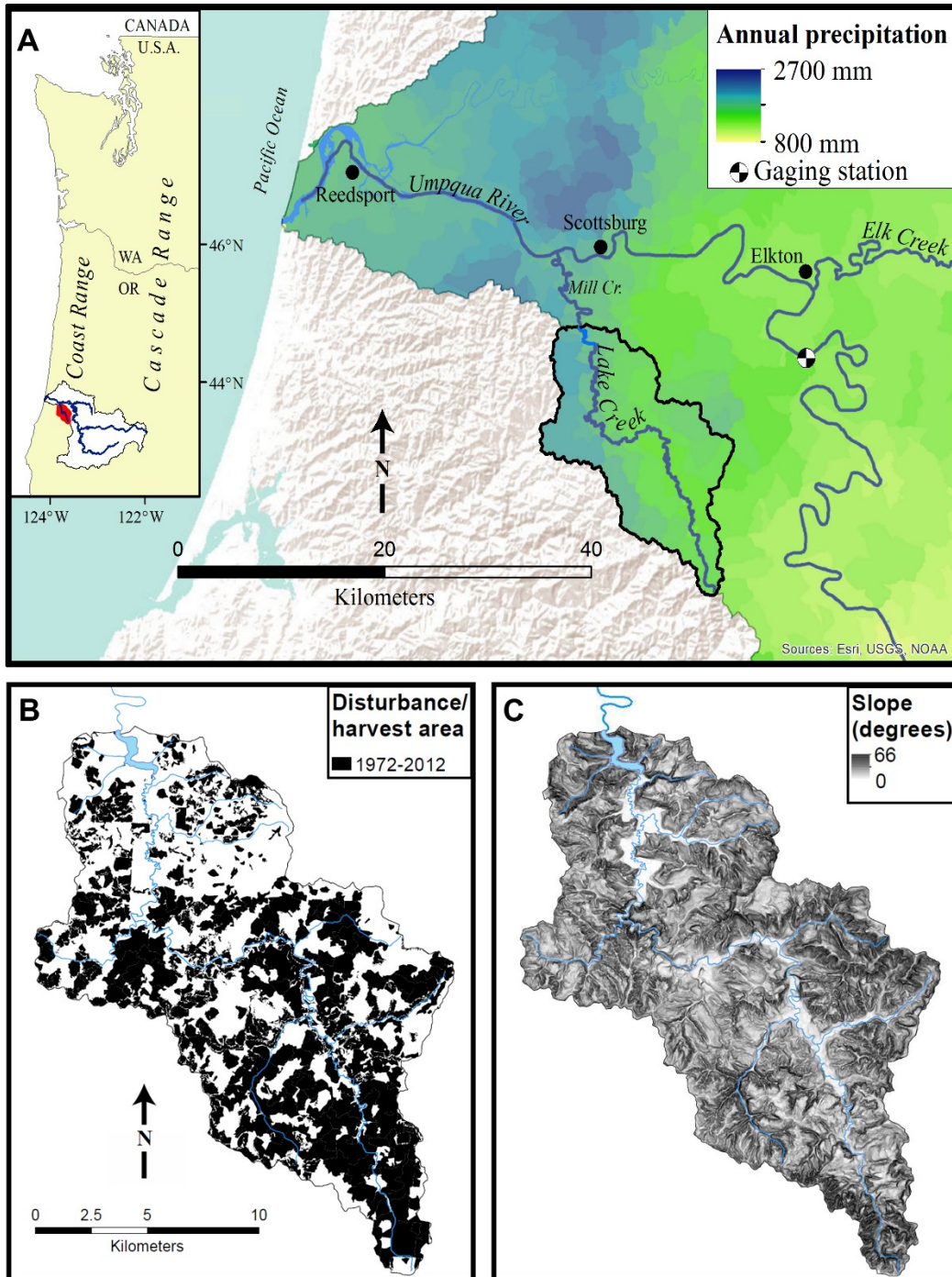


Figure 4.2. Study area. A. Loon Lake catchment location within the Umpqua River basin. The study area is filled with red on the left insert and outlined with black on the enlarged area showing the spatial distribution of the precipitation in the lower Umpqua River basin. B. Harvested area within the catchment between 1972-2012 and C. A rugged topography with slopes >50 degrees is characteristic representative of small mountainous river systems in the Oregon Coast Range. Modified from ref.²⁹

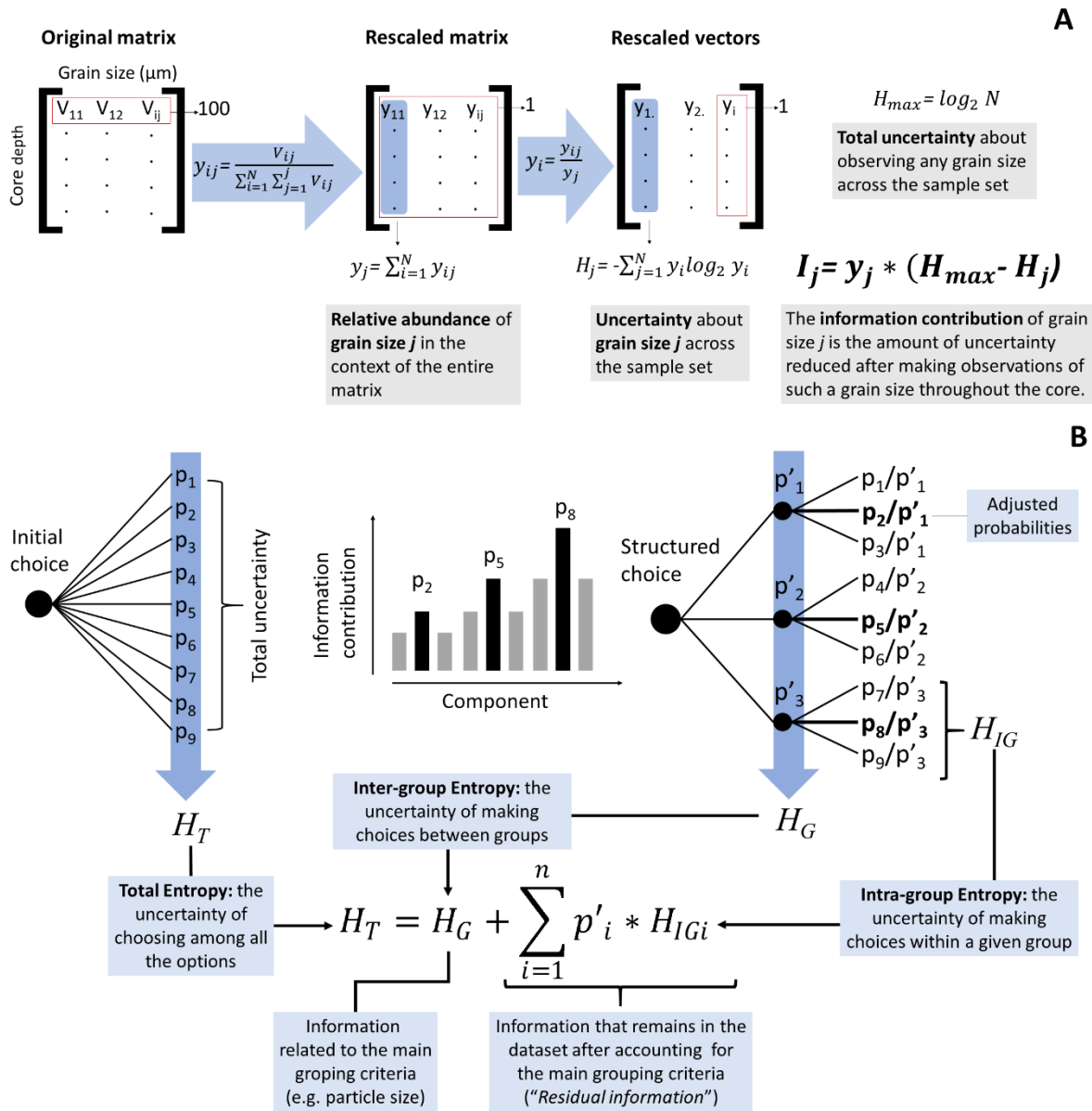


Figure 4.3. An information theory approach to the analysis of particle size spectra (PSS). **A.** Information contribution calculations from a matrix of PSS following ref.³⁰. **B.** Entropy and “Residual information”. According to the “Composition Law”^{28,59} the total uncertainty experienced by making the initial choice (H_T) can be broken down into sequential steps of choosing between groups (H_G) and then within groups (H_{IG}). Because the total uncertainty must be conserved regardless how the options are presented²⁸, once the choices are grouped, the probabilities within each group must be adjusted from p_i to p_i / p'_i . The information carried by these adjusted probabilities is the information that remains after reducing the uncertainty in the dataset by means of grouping. If we assume the process of grouping as the equivalent to developing an (Entropy) model for the dataset, then, H_G represent the “simulated values” and, H_{IG} is a measurement of “Residual information”.

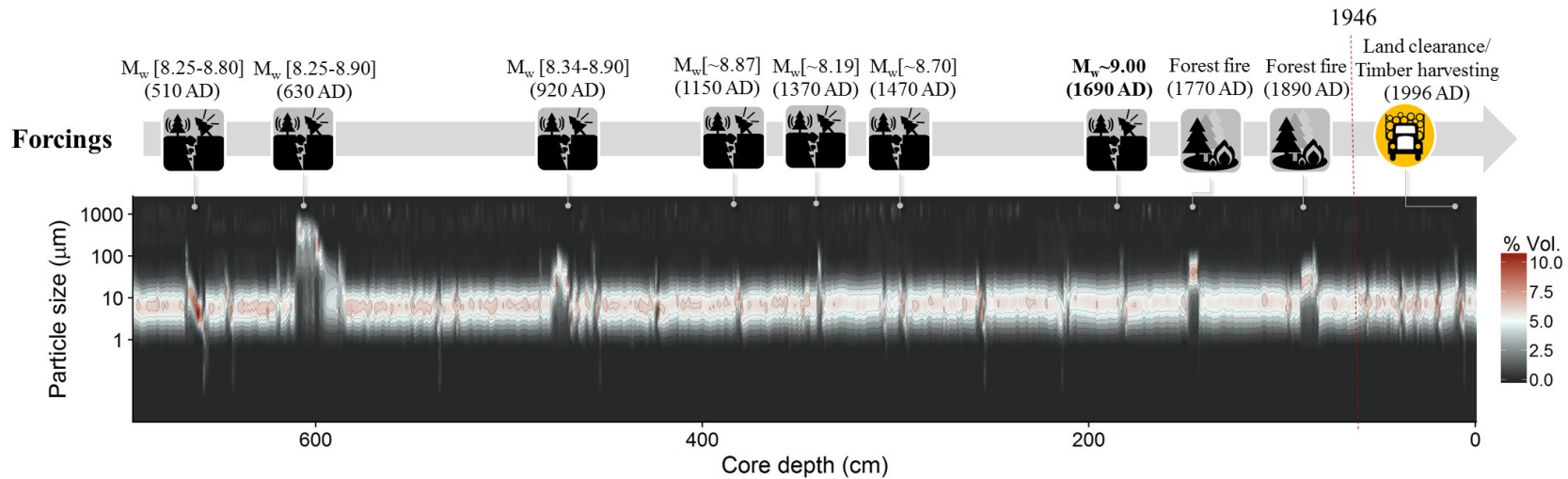


Figure 4.4. Disturbance history of Loon Lake's catchment as recorded by sediment core 02aN. Grain size contour plot (particle size spectra along the 695 cm-long sedimentary archives are stacked horizontally with volumetric contributions per size class distributed vertically). Event layers associated with the occurrence of earthquakes with magnitudes (M_w) >8.2 are indicated. ^{14}C calibrated dates in parenthesis and estimated magnitude of quake in brackets²⁹. The 9.0 megathrust earthquake in 1700 is highlighted in bold. Other disturbances include forest fires and, in the second half of the 20th century, timber harvesting. Landslides and floods are assumed to be common along the record and to interact with other disturbances in lake sedimentation processes.

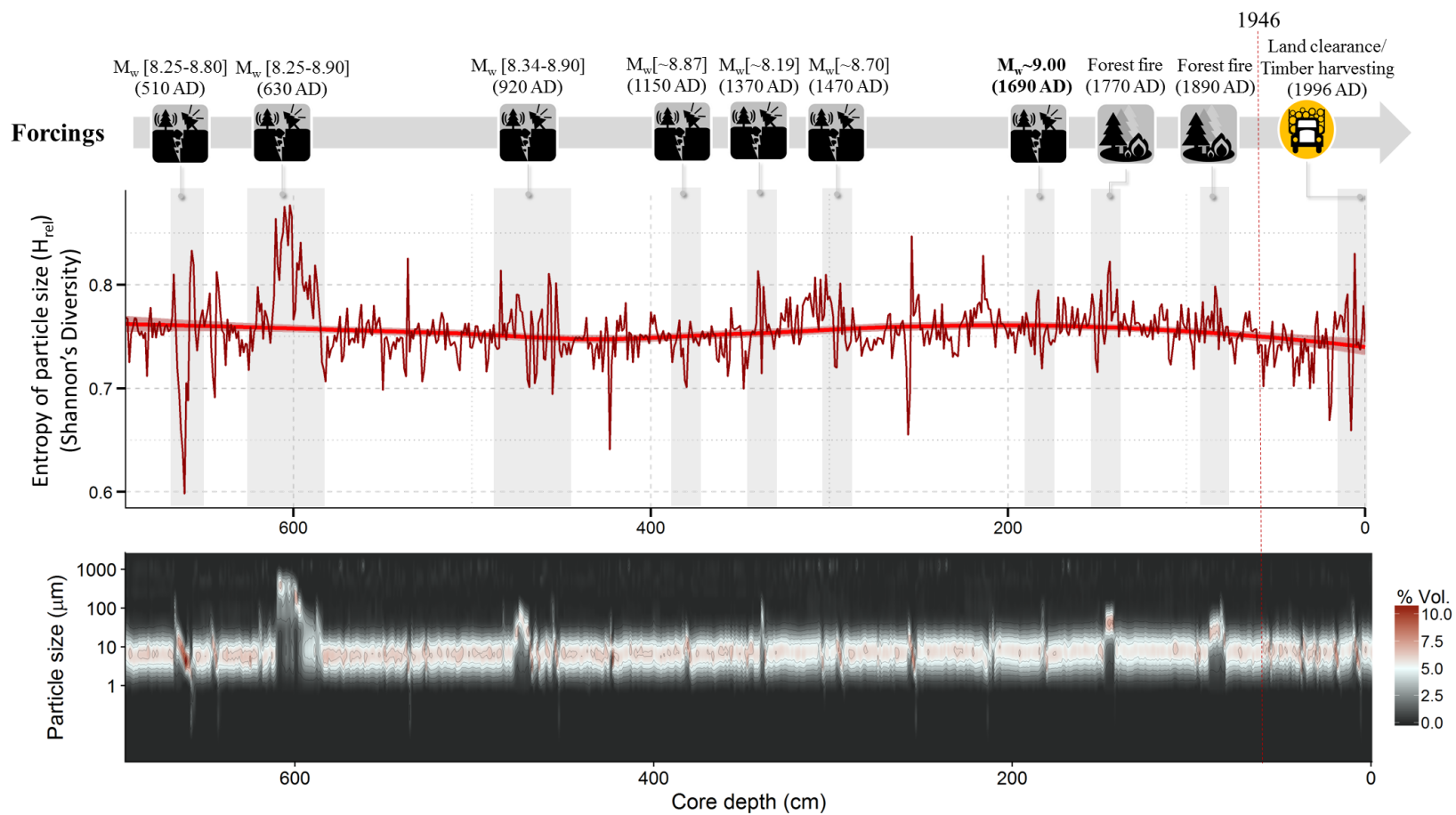


Figure 4.5. The diversity of particle sizes shows the extremely dynamic deposition that takes place in Loon Lake in response to disturbances (forcings as in Figure 4.4). Event layers are characterized by abrupt changes in particle size variability. (Diversity of particle sizes measured as Shannon's Entropy over the total size classes (82) ranging from 0.03-2000 μm).

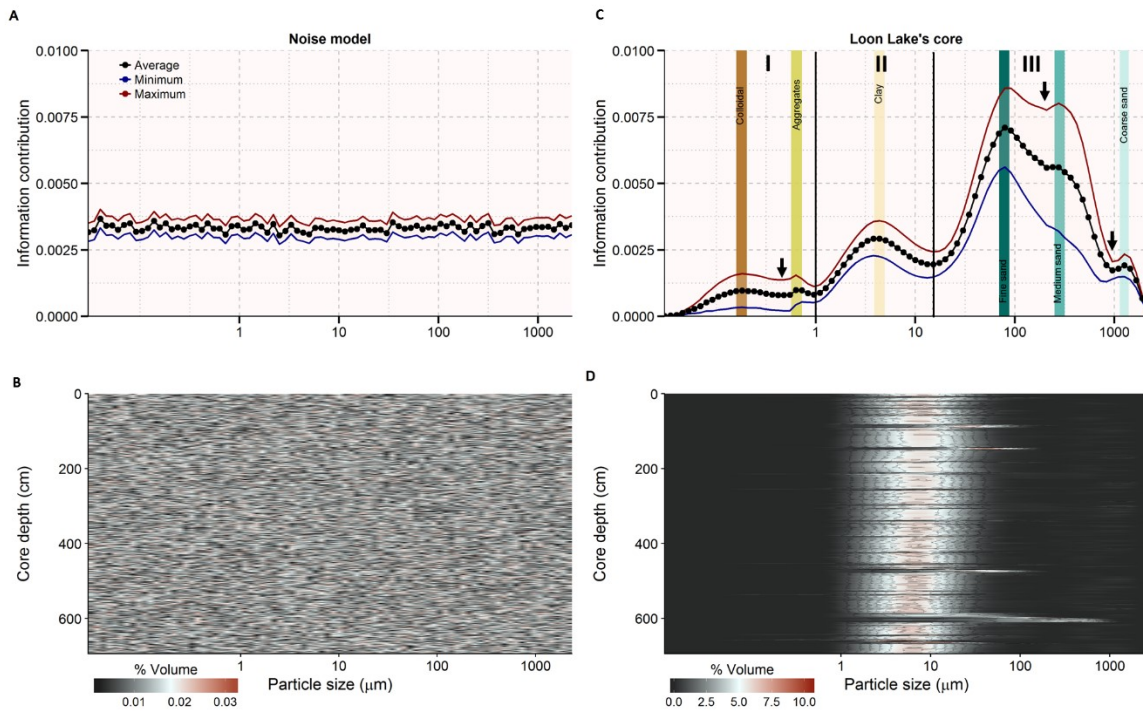


Figure 4.6. Information spectra for a “Noisy” core (simulation) and a real sediment core (Loon Lake, 02aN). The ranges of information content were estimated by Monte Carlo simulation with 10,000 iterations. A flat information spectrum is obtained from the noise model. An asymmetric contribution to information (or regions) characterizes Loon Lake’s information spectra. The peaks within each region (or Mode-Peak equivalents- MP_{eq}) are labeled according to the closest particle size in granulometric classifications (i.e. clay, silt, sand, etc.).

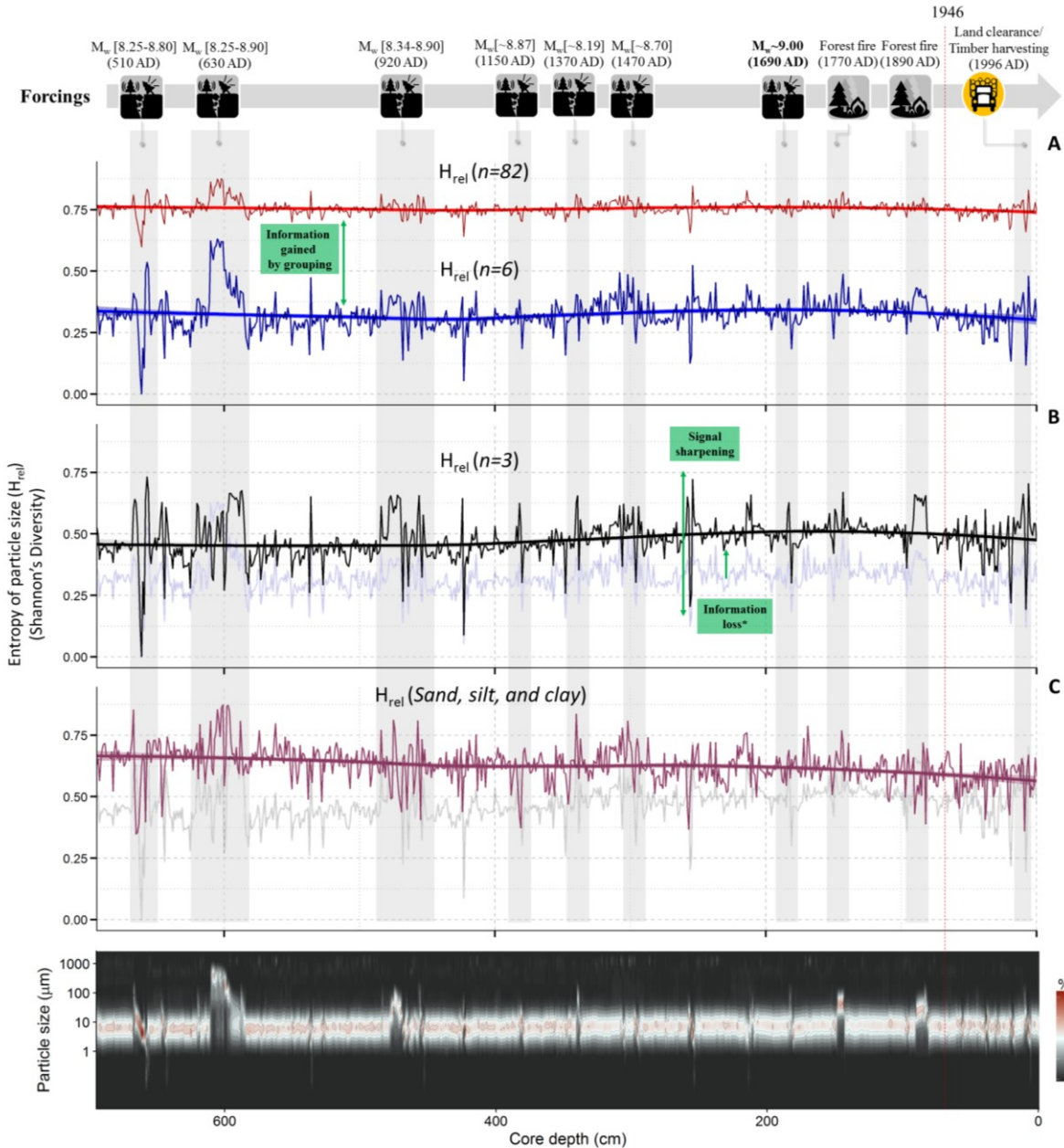


Figure 4.7. Effects of data aggregation on the characteristics of the entropy signal derived from particle size spectra from Loon Lake core 02aN. These effects include information gain (or uncertainty reduction), signal sharpening, and information loss (or increases in uncertainty). In A and B, grouping follows the information contribution criterium. In C, entropies were calculated on the proportion of sand, silt, and clay in the sample. In the background of panels B and C $H_{Rel}(6)$ and $H_{Rel}(3)$ respectively are represented with a lighter color for comparison.

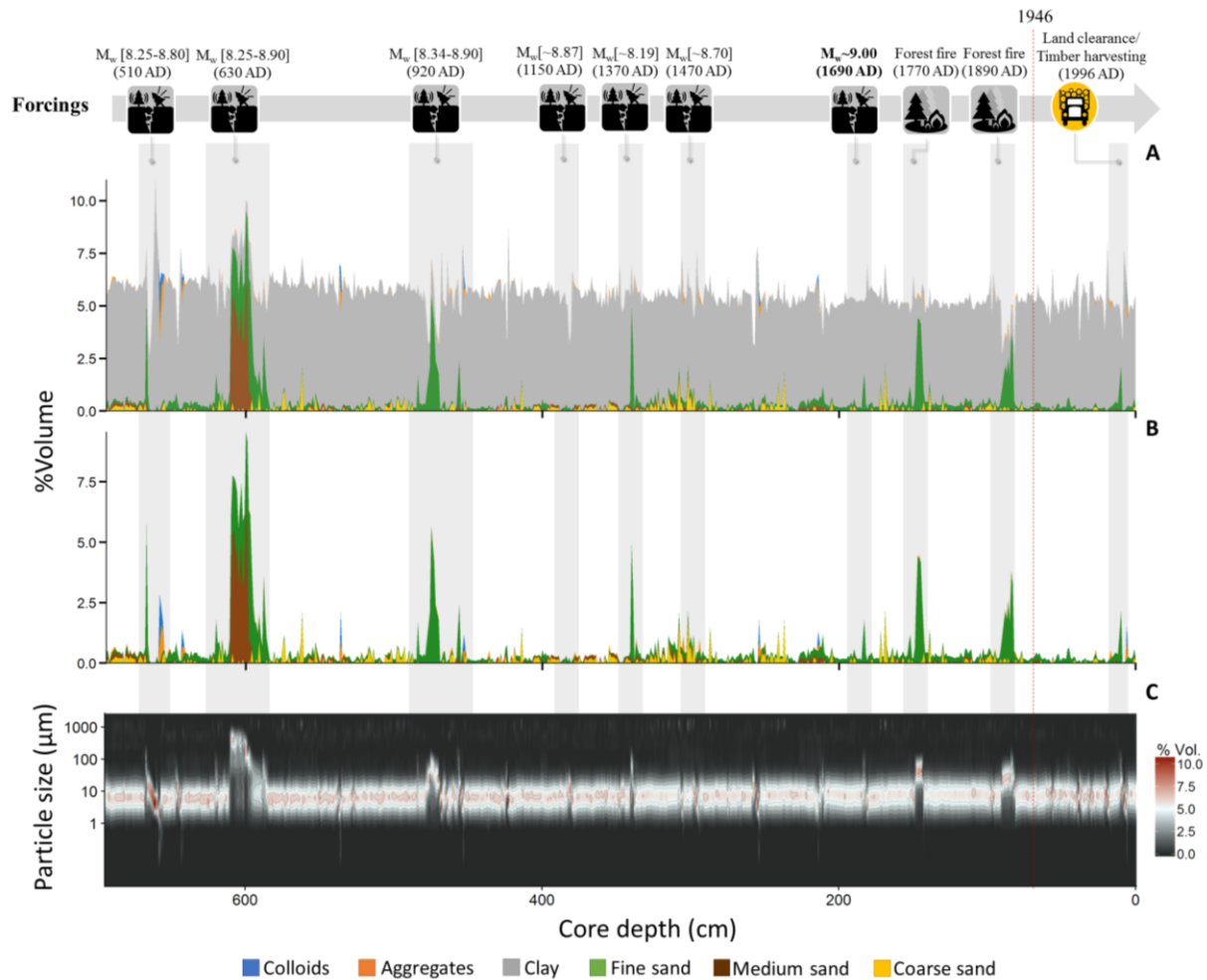


Figure 4.8. Long-term trends of Modal-Peak equivalents (MP_{eq}) along the sediment core 02aN (Loon Lake, Oregon). MP_{eq} were labeled according to the closest particle size represented by their diameters (Colloids, aggregates, clay, fine sand, medium sand, and coarse sand). A. Absolute volumes for all MP_{eq} . B. All MP_{eq} excluding clays.

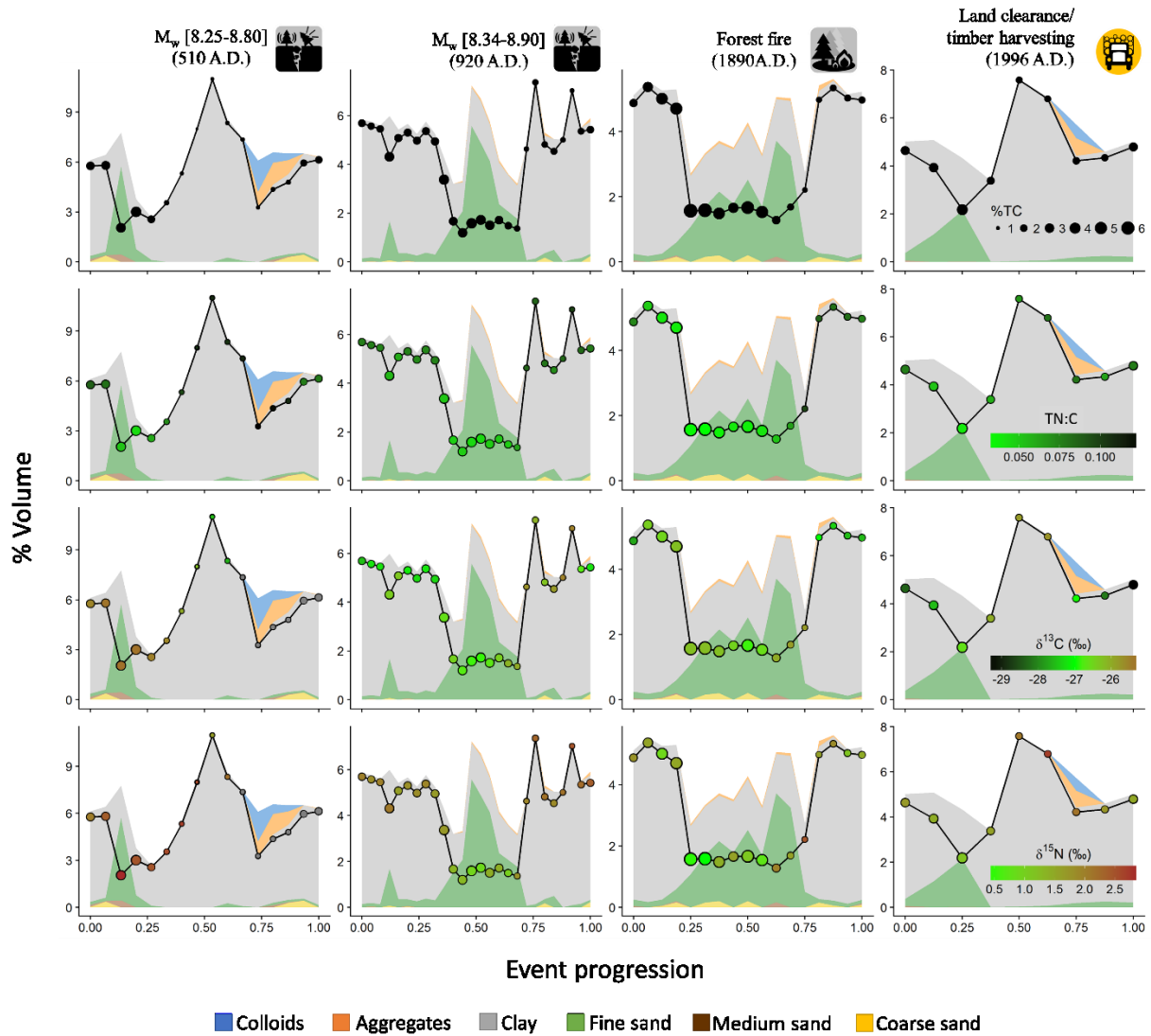


Figure 4.9. Elemental composition of organic matter deposited within selected event layers from Loon Lake sediment core 02aN. MP_{eq} composition in the background. Lines and dots representing the absolute trend in MP_{eq} -clay during the event. Sizes and colors representing the bulk chemical composition of each layer.

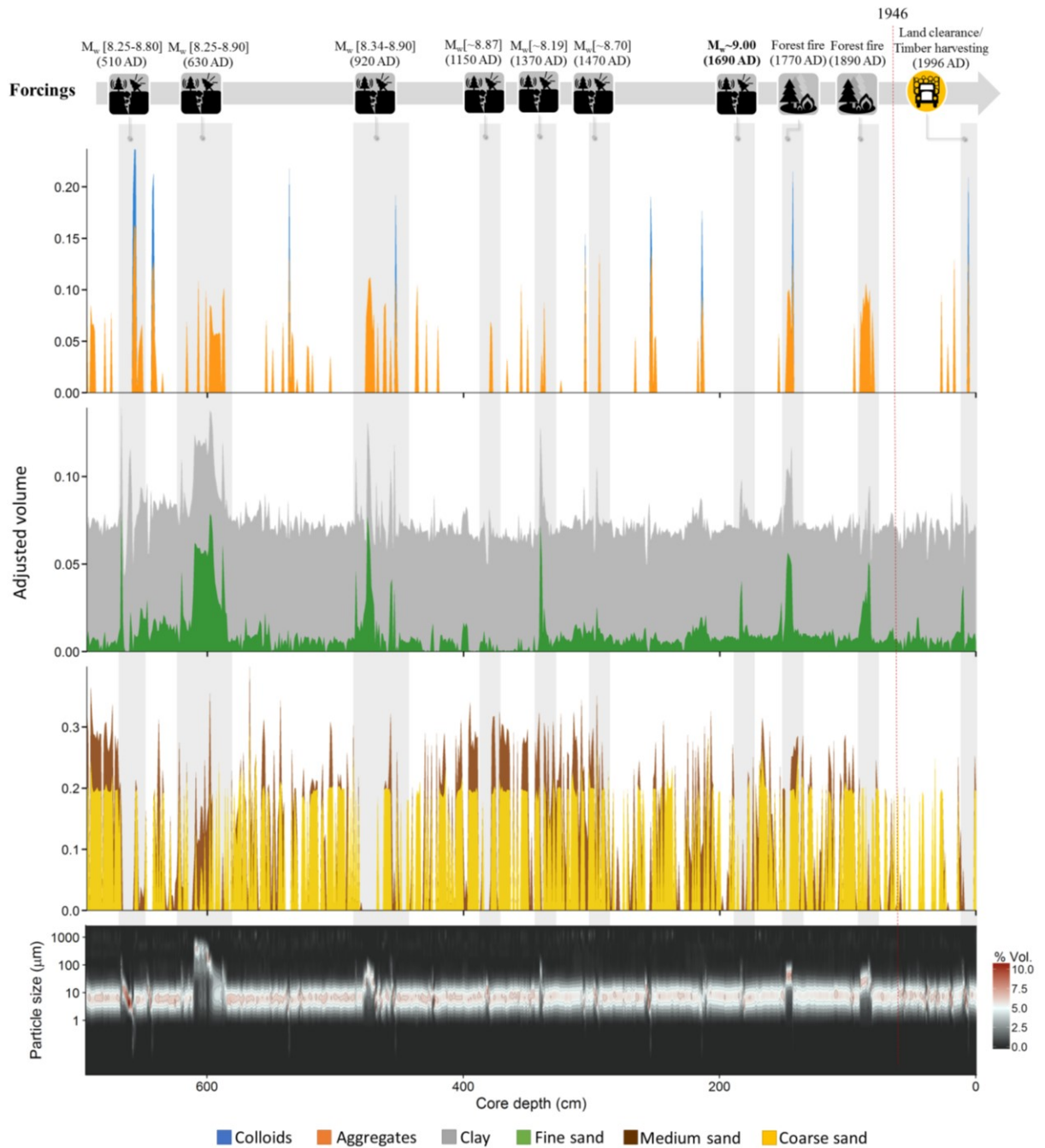


Figure 4.10. Long-term trends of residual Mode-Peak equivalentents (rMP_{eq}) along the sediment core 02aN (Loon Lake, Oregon). MP_{eq} were labeled according to the closest particle size represented by their diameters (color scale). Note the difference in the adjusted volumes of clay and fine sands in comparison to other $rMP_{eq}(s)$.

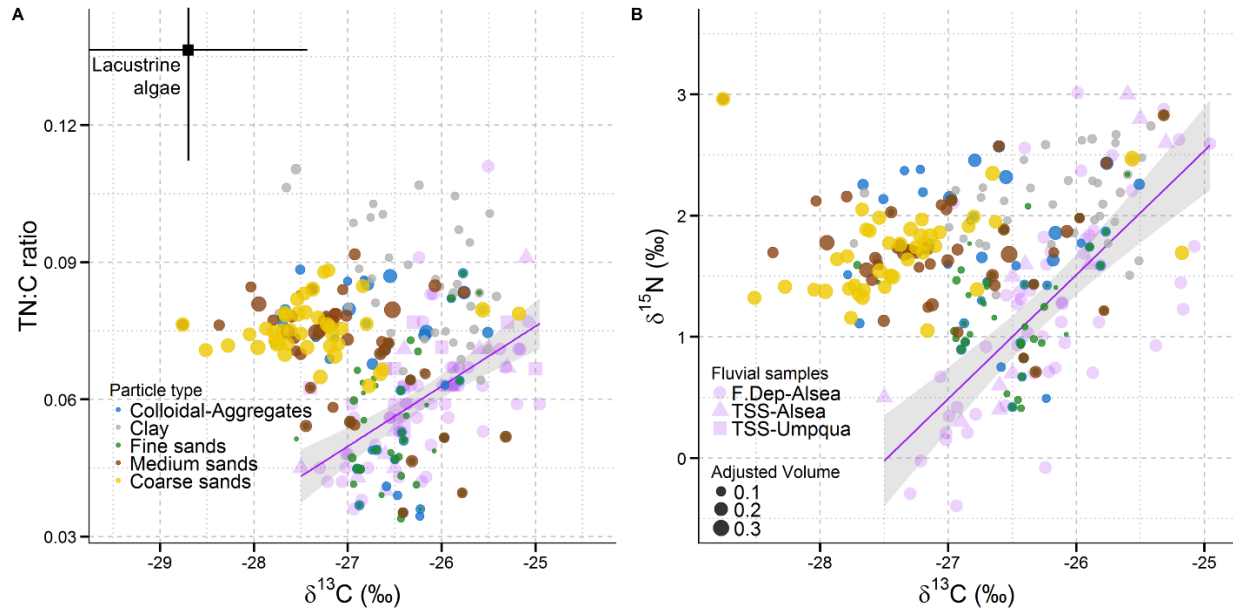


Figure 4.11. Pseudo-property-property plots using $rMP_{eq}(s)$ from Loon Lake sediment core 02aN. Color scale representing particle types and point size is proportional to the adjusted volume of a given particle type in a sediment layer. Fluvial samples from 2008's water year (excluding summer) from the Umpqua and Alsea rivers in light purple. Samples include overbank flood deposits and suspended sediments (Alsea data from ref.⁵⁷ and chapter 2, $n=66$; Umpqua's data from ref.⁵⁸, $n=11$). Samples were collected over a wide range of discharges- Q ($Q: Q_{mean}, 1.1-15.6$) $\delta^{15}\text{N}$ data was available from and Alsea River only ($n= 66$) (B). A linear trend connecting the suspended samples and its 95% confidence interval is shown with a dotted line and the light purple shade. Lacustrine data from ref.⁵⁹. Error bars (upper and left) for lacustrine algae TN:C data point extend beyond the plot dimensions.

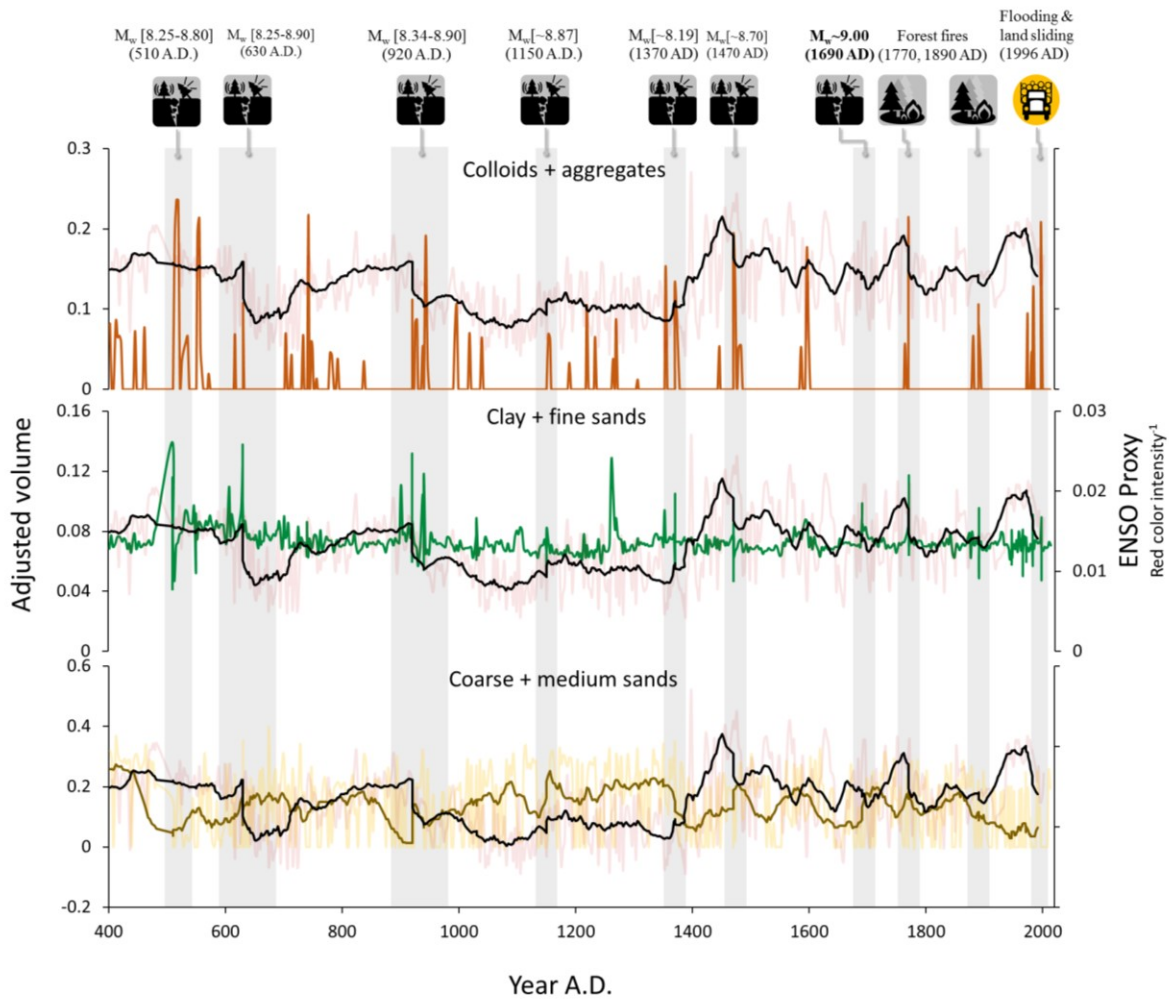


Figure 4.12. Climatic variability in the last 1500 years and as potentially recorded by the textural characteristics of the sediments in the core 02aN, Loon Lake (OCR). A and B Long-term trends of adjusted volumes of the rMP_{eq} colloids and aggregates (A) and fine sands (B). C. Long-term trends of the relative volumes of the rMP_{eq} coarse and medium sands. Variability in El Niño Southern Oscillation (ENSO) is superimposed by using proxy data from Laguna Palcacocha in the southern Ecuadorian Andes⁶⁴; raw data in red, moving average over a time window (~30 years) in black.

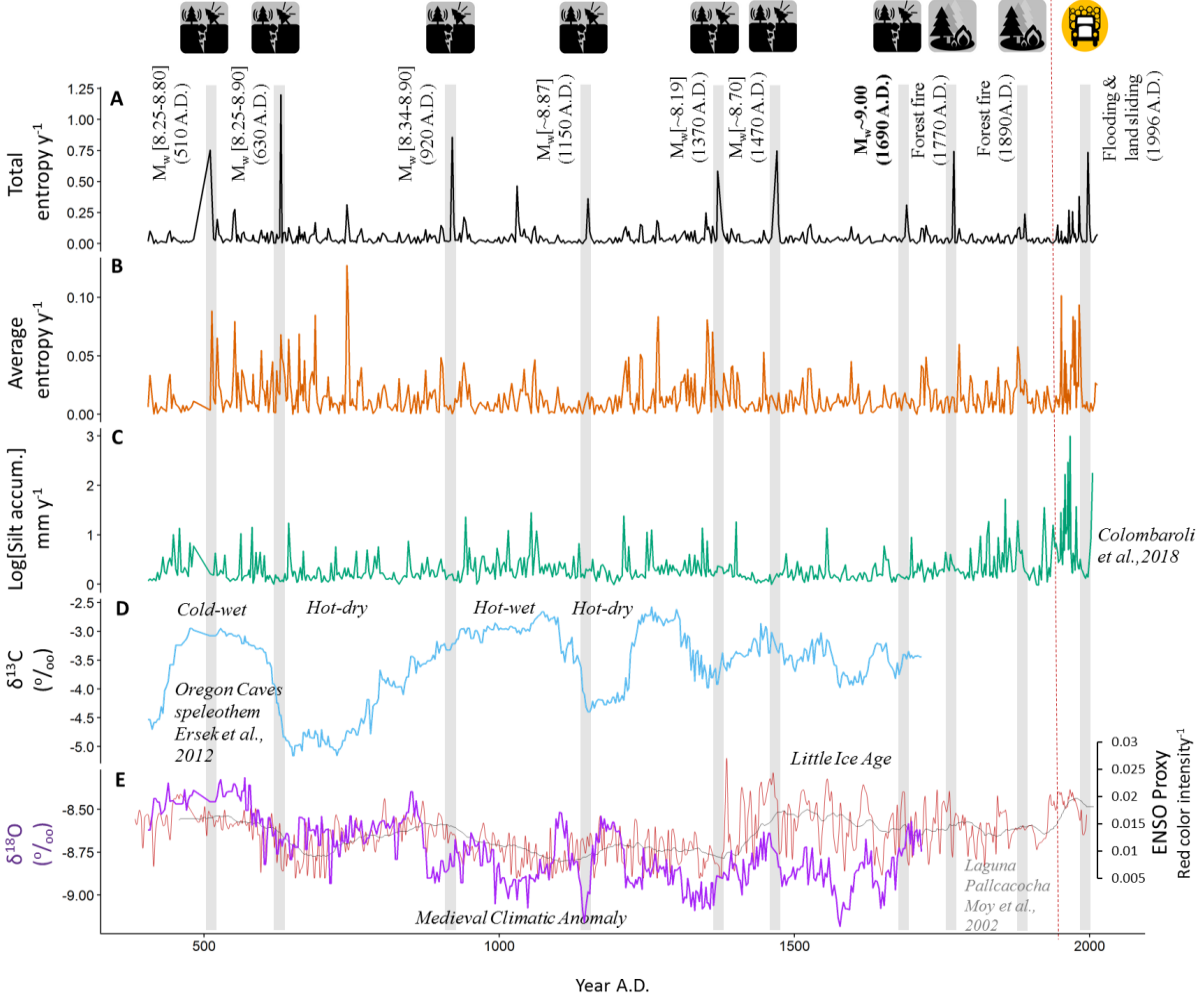
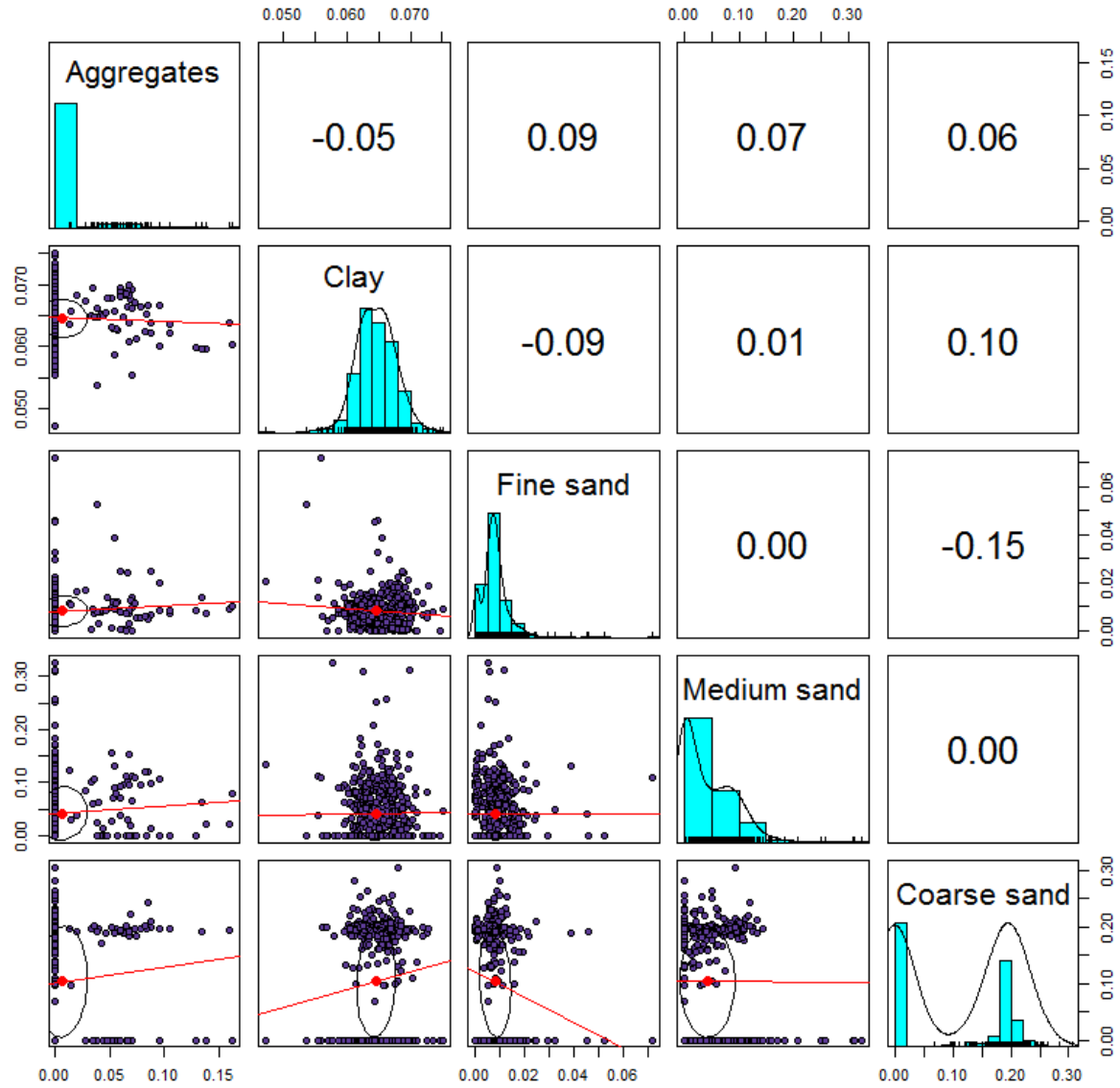


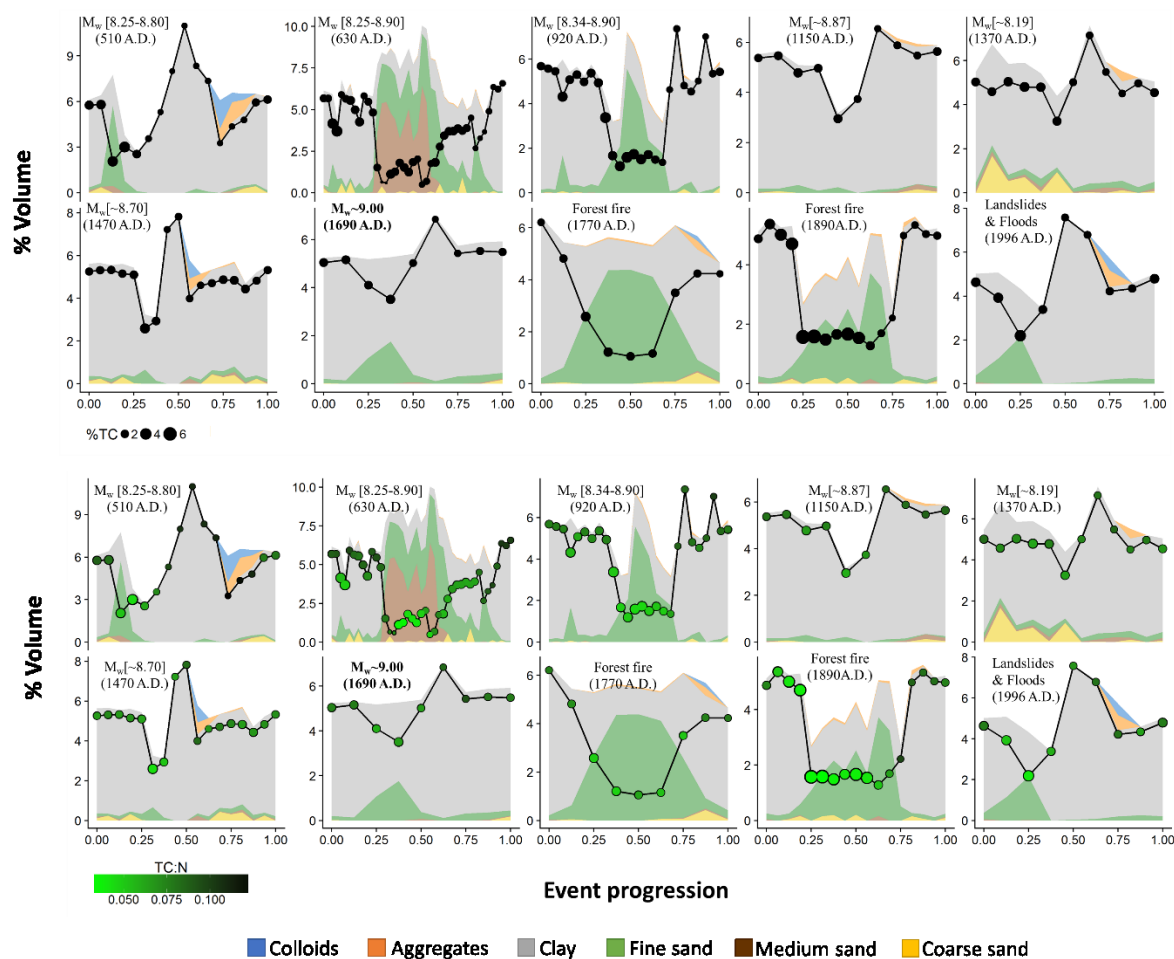
Figure 4.13. Proxies for sediment accumulation rates and their relationship with long-term trends in regional climate in the Pacific Northwest. A and B. Entropy data from Loon Lake. C. Data from Upper Squaw Lake⁴⁰. D and E. Isotopic data from Oregon Caves speleothem⁶⁵. Also trends in ENSO variability reconstructed from the Laguna Pallcacocha⁶² are superimposed over the temperature record reconstructed from $\delta^{18}O$.

Table 4-1. General Least Squares Regression of biogeochemical proxies on modal peak equivalents (MP_{eq}) for Loon Lake sediment core 02aN.

Coefficient	Biogeochemical proxy				p-values			
	%TC	TN:C	$\delta^{13}C$	$\delta^{15}N$	%TC	TN:C	$\delta^{13}C$	$\delta^{15}N$
Intercept	3.16	0.04	-25.53	1.53	0.000	0.000	0.000	0.000
MP_{eq} -Colloidal-Aggregates	-0.06	0.04	0.92	1.44	0.906	0.000	0.196	0.002
MP_{eq} -Clay	- 12.50	0.52	-12.24	6.57	0.001	0.000	0.017	0.030
MP_{eq} -Fine sand	13.69	-0.37	4.22	-6.63	0.000	0.000	0.107	0.000
MP_{eq} -Medium sand	-0.02	0.00	-0.76	0.33	0.949	0.688	0.068	0.225
MP_{eq} -Coarse sand	0.02	0.00	0.14	0.16	0.919	0.960	0.555	0.297
Bulk Density	-0.88	0.01	1.43	0.39	0.000	0.001	0.000	0.010
Historical period	0.04	0.00	-1.28	-0.18	0.837	0.996	0.058	0.023
Post-OFPA	0.15	0.00	-0.46	0.13	0.539	0.168	0.547	0.255
Entropy	0.44	0.00	-5.75	-0.91	0.361	0.868	0.009	0.019
Event	-0.15	0.00	-2.17	-0.09	0.476	0.640	0.084	0.618
Entropy*Event	0.77	0.01	5.70	0.11	0.225	0.634	0.163	0.848
OFPA*Event	N.D.	N.D.	5.62	N.D.	N.D.	N.D.	0.011	N.D.
OFPA*Event*Entropy	N.D.	N.D.	-17.15	N.D.	N.D.	N.D.	0.012	N.D.
Pseudo-R2	0.22	0.45	0.32	0.28				



Supplementary Figure 10. Scatterplots and correlation coefficients between pairs of residuals Mode-Peak equivalents (rMP_{eq}) from sediment core 02aN, Loon Lake, Oregon.



Supplementary Figure 11. Elemental composition of organic matter deposited within selected event layers from Loon Lake sediment core 02aN. MP_{eq} composition in the background. Lines and dots representing the absolute trend in MP_{eq} -clay during the event. Sizes and colors representing the bulk chemical composition of each layer.

Supplementary method: building “pseudo-property-property” plots

We tested for the significance of the correlation between OM chemistry and the MP_{eq} throughout the entire record by means of a Generalized Least Squares multiple regression model. We selected a GLS model structure because we found significant autocorrelation in both the predictor (e.g. rMP_{eq}) and response variables (e.g. %TC, TN:C ratios, $\delta^{13}C$, etc.) at (spatial) lags > 3. Although deposition rates changed over time and the lags could have represented different time scales, we found that an autoregressive model (order 1) controlled for most of the autocorrelations. Also, since the most important changes in sedimentation rates occurred in the contemporary period²⁹ we include predictor variables related to the beginning of the timber harvesting era and the implementation of the Oregon Forest Practices Act (OFPA). We also included a categorical variable to separate event from non-event layers. We estimated a pseudo- R^2 for the model's predictions by linear regression between predicted and observed data. All analyses were run using function “glS” from the package “nlme”⁶² R version 3.5.0.

The coefficients and p-values obtained from our GLS multiple regression model are presented in Table 4-1. Most rMP_{eq} were significantly correlated with at least one biogeochemical proxy (except $MP_{eq}(s)$ medium and coarse sands). Although we could use our model coefficients to predict the chemistry of Loon Lake sediments as driven by changes in particle size, we decided to use our regression model in a different way: to infer the potential chemical characteristics of each rMP_{eq} . Since we did not have enough independent chemical proxies to run an inverse model (i.e. MP_{eq} as a function of biogeochemistry), we used the overall structure of our regression model to build an approximated graphical representation of the chemical characteristics of each of our MP_{eq} . We called this representation a “pseudo-property-property plot”. Property-property plots are commonly used in biogeochemistry^{46–48,52}. In them, each sediment sample is plotted in the chemical space with coordinates corresponding to the bulk elemental composition (e.g. TN:C vs %TC, $\delta^{15}N$ vs $\delta^{13}C$). Unless samples are separated into different size fractions, there is no way to associate chemical properties to specific grain size classes like clays or fine sands. In our pseudo-property-property plots we represent our data points in the exact same way in which is done conventionally. The only difference is that we assign to each point a color corresponding to the dominant MP_{eq} in the sample to link a specific combination of chemical properties to a particle size class. In our case, the prefix “pseudo” means that we did not have a formal test for this specific assignment, beyond the significant correlation structure found in our GLS model.

The reasoning behind our pseudo-property-property plots is as follows. First, by using the sign of those regression coefficients that were significant for a given biogeochemical proxy (i.e. $\%TC = \pm\beta \cdot MP_{eq}$), it is possible to make basic graphical representation of the gross chemical makeup of the organic matter being deposited in association with different particle sizes. For instance, MP_{eq} -clay was negatively correlated with $\%TC$ and positively correlated with $TN:C$ (Table 4-1). On the other hand, MP_{eq} -Fine sand, was positively correlated with $\%TC$ and negatively correlated with $TN:C$ (Table 4-1). Thus, if we build a plot of $TN:C$ vs. $\%TC$ with qualitative axis related to the signs of the regression coefficients ($-/+$), MP_{eq} -clay will plot on the upper left quadrant ($+TN:C/-\%TC$) and MP_{eq} -Fine sand will plot on the opposite one ($-TN:C/+ \%TC$).

Second, because of the strong orthogonality observed between $rMP_{eq}(s)$ -(Supplementary Figure 10) sediment layers dominated by a given MP_{eq} would not coincide in location when plotted on property-property plots (e.g. $\%TC$ vs $TN:C$ or $\delta^{13}C$ vs $\delta^{15}N$), unless they have similar chemical characteristics. If most of the samples dominated by a given MP_{eq} are consistently plotted around the same location, and if these samples do not overlap with any other(s) MP_{eq} , then, the probability that their location in the plot is closer to their true chemical composition is higher. In our example, if most of the samples loaded with fine sands plot in the high $\%TC$ -low $TN:C$ corner, it is more likely that they carry a plant-like chemical signature.

Third, since we built our regression model by using $rMP_{eq}(s)$ as predictors, correlation coefficients should reflect the relationship between the $rMP_{eq}(s)$ and the geochemical proxies independently of the conditions of deposition. Thus, we assumed that our pseudo-property-property plots were indicative of the compositional characteristics of the sediments from Loon Lake as related to sediment sources within the watershed.

We built pseudo-property-property plots for our $rMP_{eq}(s)$ by repeatedly ranking all samples according to the % volume of each grain size class. In each iteration, we selected the top 50 values, to minimize overlapping, labeled these samples with their corresponding name of rMP_{eq} , and plotted all the layers on the same chemical space (Figure 4.11).

Chapter 5 . Conclusions

In this dissertation we explored the origin, evolution and fate of biogeochemical signals of mountainous watersheds' response to disturbances in three different locations in the Pacific Northwest of the U.S. We reconstructed a 30-year long record of particulate organic carbon exports from headwaters streams in the Oregon Cascades. We found that temporal changes in the variability of POC yields were indicative of the long-term impacts of both natural and anthropogenic-induced disturbances. We also found that the headwaters examined exhibited a switching behavior from short-term POC storage compartments to long-term POC sources driven by the disturbance regime. In the logged watershed, a channel-scouring debris flow dragging logging residues through the channel, transformed WS-10, in the H. J. Andrews in a long-term source of chemically heterogenous POC. Interestingly, a large flooding event in the winter of 1996 produced a strong episode of hydro-geomorphic convergence between WS-10 and its natural counterpart (WS-09). The specific mechanisms behind the convergence episode will be subject of further investigation.

We also studied the chemical characteristics of overbank deposits created along the Alsea River to demonstrate their utility as testimonies of the POC mobilized by the Great Coastal Gale of 2007. By having access to relatively large amounts of sediments (compared to typically low-volumes of suspended sediment samples) we were able to unravel a series of mechanisms involved in the evolution of the particulate load as it moves from headwaters to oceans. We showed how mineral specific surface area exerted a marginal control on the concentrations of organic matter founds along these deposits. But perhaps, the most surprising result was to find evidence of physical fragmentation as a major control linking the coarse and fine fractions of the particulate organic matter exported by the Alsea River. Contrary to what is typically assumed, physical processing in small mountainous river systems might have the potential to modulate the chemical characteristics of the organic matter exported from the terrestrial biosphere to the ocean.

Lastly, we analyzed the information content of particle size spectra from a high resolution sedimentary archive spanning more than 1500-years of natural history. We found that particle size variability not only contain information pertaining to specific depositional processes, but also it has the potential to record climatic changes. Although this second conclusion is highly speculative, our results show the potential to disentangle biogeochemical signals of watersheds' response to disturbances by applying the principles of information theory.

An overarching conclusion from this dissertation is the extraordinary heterogeneity that characterizes the biogeochemical signals of watershed's response to disturbances which is in startling contrast with the availability of conceptual approaches to understand such a heterogeneity. Thus, I will use the last paragraphs of these section to outline an approach that I consider will be fruitful in the coming years in understanding ecosystem's responses to changes in the disturbance regime.

I must start arguing for the integrative nature of these hydro-biogeochemical signals as they emerge from the fundamental coupling of water, sediments and organic matter in forested watershed ecosystems^{1,2}. Because of these coupling, hydro-biogeochemical signals reflect integrated responses to climate- and human-induced disturbances. Although the evidence of the impacts of these disturbances on watershed ecosystems is increasing^{2,3}, the potential trajectories of watershed ecosystems under these pressures is unknown and difficult to predict⁴. In this context, long-term records of hydro-biogeochemical signals and their integrated interpretation, are essential to understand watershed responses to disturbances, and to gain predictive capabilities on future scenarios^{5,6}.

Watershed responses to disturbances are also complex due to the inherent heterogeneity in disturbance characteristics (e.g. variable precipitation inputs) and ecosystem processes (e.g. biogeochemical cycles)⁷. This heterogeneity in the disturbance regime is produced by the interaction between natural and anthropogenic drivers of landscape patterns³, multi-scale ecosystem response mechanisms⁸ and non-linear interactions among hydrological, geomorphological and biogeochemical processes (e.g. discharge-sediment-particulate organic matter transport)³. The increasing complexity of watersheds responses to disturbances will demand variables sensitive enough to provide diagnostic value in terms of disturbance effects as well as conceptual frameworks that allow the understanding of the heterogeneity and complexity associated with the responses to those disturbances. As part of this dissertation, we explored different approaches based on the theory of information as the initial steps towards the development of a framework and diagnostic approach.

For many years, scientists have used Shannon's entropy, as a measure of *complexity*^{9,10}. Several information-derived indexes have been developed to characterize complexity in hydro-biogeochemical signals like soil water fluxes and hydrological time series¹¹. Even digital images from forests have been considered as subject of these analysis⁹. However, the most elemental

behavior of Shannon's entropy, as a measure of uncertainty in ecosystem properties, have been completely overlooked.

Interpreting Shannon's entropy as uncertainty in hydro-biogeochemical signals, might have profound implications in understanding their responses to disturbances. The analysis of entropy allows the study of *changes in variability as an ecosystem response*. This is an aspect that have been overlooked for decades by analyzing changes in mean values with tools that requires homogeneity of variances like ANOVA or ANCOVA¹². These analyses are among the most common statistical approaches to study the impacts of harvesting practices on hydrological regimes in watershed ecosystems, although multiple regression is becoming increasingly used to account for other sources of variability¹³.

Bibliography

1. Aufdenkampe, A. K. *et al.* Riverine coupling of biogeochemical cycles between land, oceans, and atmosphere. *Front. Ecol. Environ.* **9**, 53–60 (2011).
2. Leithold, E. L., Blair, N. E. & Wegmann, K. W. Source-to-sink sedimentary systems and global carbon burial: A river runs through it. *Earth-Sci. Rev.* **153**, 30–42 (2016).
3. Wheatcroft, R. A., Goñi, M. A., Richardson, K. N. & Borgeld, J. C. Natural and human impacts on centennial sediment accumulation patterns on the Umpqua River margin, Oregon. *Mar. Geol.* **339**, 44–56 (2013).
4. Allan, J. D. Landscapes and Riverscapes: The Influence of Land Use on Stream Ecosystems. *Annu. Rev. Ecol. Evol. Syst.* **35**, 257–284 (2004).
5. Meyers, P. A. & Teranes, J. L. Sediment organic matter. (2001).
6. McLauchlan, K. K. *et al.* Reconstructing Disturbances and Their Biogeochemical Consequences over Multiple Timescales. *BioScience* **64**, 105–116 (2014).
7. Swanson, F. J., Johnson, S. L., Gregory, S. V. & Acker, S. A. Flood Disturbance in a Forested Mountain Landscape. *BioScience* **48**, 681–689 (1998).
8. Webster, J., Benfield, E. J., Golladay, S. W. & McTammany, M. E. Recovery of particulate organic matter dynamics in a stream draining a logged watershed. *Swank Wayne T Webster Jackson R Comps Eds Long-Term Response For. Watershed Ecosyst. Clear. South. Appalach. Oxf. Univ. Press 156-176* 156–176 (2014).
9. Proulx, R. & Parrott, L. Measures of structural complexity in digital images for monitoring the ecological signature of an old-growth forest ecosystem. *Ecol. Indic.* **8**, 270–284 (2008).
10. Vranken, I., Baudry, J., Aubinet, M., Visser, M. & Bogaert, J. A review on the use of entropy in landscape ecology: heterogeneity, unpredictability, scale dependence and their links with thermodynamics. *Landsc. Ecol.* **30**, 51–65 (2015).
11. Ruddell, B. L., Brunsell, N. A. & Stoy, P. Applying Information Theory in the Geosciences to Quantify Process Uncertainty, Feedback, Scale. *Eos Trans. Am. Geophys. Union* **94**, 56–56 (2013).
12. Alila Younes, Kuraś Piotr K., Schnorbus Markus & Hudson Robert. Forests and floods: A new paradigm sheds light on age-old controversies. *Water Resour. Res.* **45**, (2009).
13. Hatten, J. A. *et al.* Effects of contemporary forest harvesting on suspended sediment in the Oregon Coast Range: Alsea Watershed Study Revisited. *For. Ecol. Manag.* **408**, 238–248 (2018).